Alma Mater Studiorum – Università di Bologna

DOTTORATO DI RICERCA
IN
MECCANICA DELLE STRUTTURE

Ciclo XXII

DYNAMIC IDENTIFICATION OF STRUCTURES: EXPERIMENTAL ASSESSMENT OF MODAL PARAMETERS THROUGH METHODS IN FREQUENCY DOMAIN, IN TIME-FREQUENCY DOMAIN AND MODEL UPDATING

Settore scientifico disciplinare di afferenza: ICAR/09 – Tecnica delle Costruzioni

Redatta da: Claudia Belmonte

Coordinatore Dottorato
Prof. E. Viola

Relatore
Prof. P.P. Diotallevi

Correlatori
Prof. E. Caetano
Dr. L. Landi

Esame finale anno 2010

KEYWORDS

- Dynamic identification
- Experimental test
- Wavelet transforms
- FE model

PREFAZIONE

Tra i metodi sperimentali solitamente utilizzati per definire il comportamento di un sistema in scala reale, le prove dinamiche costituiscono la procedura più completa ed affidabile. Una prova dinamica è una procedura sperimentale atta a determinare un insieme di parametri caratteristici del comportamento dinamico del sistema, quali le frequenze naturali della struttura, le deformate modali corrispondenti ed i valori di smorzamento associati. La conoscenza di queste grandezze modali può essere utilizzata sia per verificare le assunzioni teoriche di progetto, che per controllare le prestazioni del sistema strutturale durante la sua fase di esercizio.

La tesi di dottorato sarà strutturata nelle seguenti sezioni:

- Il primo capitolo, di carattere introduttivo, richiama alcune nozioni di base della Dinamica delle Strutture, focalizzando il discorso sul problemi di sistemi a più gradi di libertà, quali possono essere i sistemi reali oggetto di studio, se eccitati con forzanti di tipo armonico o in vibrazioni libere.
- Il secondo capitolo è interamente dedicato al problema dell'identificazione dinamica di una struttura, se sottoposta ad una prova in sito in vibrazioni forzate. Si descrive dapprima il classico metodo, tramite FFT del segnale registrato, che premette di risalire alla FRF e da questa ai parametri modali della struttura. Successivamente viene introdotta una diversa metodologia, anch'essa nel dominio delle frequenze, che consente di descrivere puntualmente la FRF, sfruttando le caratteristiche geometriche dell'ellisse che rappresenta il diretto confronto input-output. I due metodi sono quindi confrontati e si pone particolare attenzione su alcuni vantaggi che la metodologia proposta possiede.
- Il terzo capitolo è incentrato sullo studio di strutture reali se soggette a prove in sito in cui la forzante non è nota, eccitazioni di tipo ambientale e prove d'urto o rilascio. In questo tipo di analisi si è scelto di utilizzare la CWT, che permette uno studio contemporaneo nel

dominio del tempo e delle frequenze di un generico segnale x(t). La CWT è stata dapprima applicata ad una prova in oscillazioni libere, ottenendo ottimi risultati sia in termini di frequenze proprie che di smorzamenti che di modi di vibrare. L'applicazione nel caso di vibrazioni ambientali ha definito ancora in modo sufficientemente accurato i parametri modali del sistema, anche se sullo smorzamento occorre fare alcune interessanti considerazioni.

- Il quinto capitolo tratta ancora il problema di post processing di dati acquisiti a seguito di una prova in vibrazioni ambientali, ma questa volta attraverso l'applicazione della trasformata discreta di Wavelet (DWT). In una prima parte i risultati ottenuti tramite la DWT sono confrontati con quelli relativi all'applicazione della CWT.

  Particolare attenzione viene data all'utilizzo della DWT come strumento di filtraggio del segnale registrato, che in caso di vibrazioni ambientali è spesso affetto dalla presenza di un'importante quota di rumore.
- Il quinto capitolo analizza un'altra importante fase del processo di identificazione: il model updating. In questo capitolo, partendo dai parametri modali ottenuti da alcune prove in vibrazioni ambientali, eseguite dall'università di Porto nel 2008 e dall'università di Sheffild nel 1994 sul ponte Humber in Inghilterra, si vuole definire un modello FEM del ponte in acciaio, al fine di stabilire quale sia il tipo di modellazione che permetta di cogliere in modo più vicino il reale comportamento dinamico del ponte.
- Il sesto capitolo riporta le necessarie conclusioni dell'intero lavoro. Esse riguardano l'applicazione di una metodologia nel dominio delle frequenze al fine di valutare i parametri modali di una struttura ed i suoi vantaggi, i vantaggi nell'applicazione di una procedura basata sull'utilizzo delle trasformate di Wavelet nel processo di identificazione dinamica nel caso di prove con input non noto ed infine il problema della modellazione 3D di sistemi a molti gradi di libertà e con diversi tipi di incertezze (nello specifico nel caso di un ponte sospeso modellazione collegamento torre-impalcato, scelta elemento FEM per

l'impalcato, interazioni cavo impalcato e possibile presenza di modi di vibrare locali).

PREFACE

Among the experimental methods commonly used to define the behaviour of a full scale system, dynamic tests are the most complete and efficient procedures. A dynamic test is an experimental process, which would define a set of characteristic parameters of the dynamic behaviour of the system, such as natural frequencies of the structure, mode shapes and the corresponding modal damping values associated. An assessment of these modal characteristics can be used both to verify the theoretical assumptions of the project, to monitor the performance of the structural system during its operational use.

The thesis is structured in the following chapters:

- The first introductive chapter recalls some basic notions of dynamics of structure, focusing the discussion on the problem of systems with multiply degrees of freedom (MDOF), which can represent a generic real system under study, when it is excited with harmonic force or in free vibration.
- The second chapter is entirely centred on to the problem of dynamic identification process of a structure, if it is subjected to an experimental test in forced vibrations. It first describes the construction of FRF through classical FFT of the recorded signal. A different method, also in the frequency domain, is subsequently introduced; it allows accurately to compute the FRF using the geometric characteristics of the ellipse that represents the direct input-output comparison. The two methods are compared and then the attention is focused on some advantages of the proposed methodology.
- The third chapter focuses on the study of real structures when they are subjected to experimental test, where the force is not known, like in an

ambient or impact test. In this analysis we decided to use the CWT, which allows a simultaneous investigation in the time and frequency domain of a generic signal x(t). The CWT is first introduced to process free oscillations, with excellent results both in terms of frequencies, dampings and vibration modes. The application in the case of ambient vibrations defines accurate modal parameters of the system, although on the damping some important observations should be made.

- The fourth chapter is still on the problem of post processing data acquired after a vibration test, but this time through the application of discrete wavelet transform (DWT). In the first part the results obtained by the DWT are compared with those obtained by the application of CWT. Particular attention is given to the use of DWT as a tool for filtering the recorded signal, in fact in case of ambient vibrations the signals are often affected by the presence of a significant level of noise.
- The fifth chapter focuses on another important aspect of the identification process: the model updating. In this chapter, starting from the modal parameters obtained from some environmental vibration tests, performed by the University of Porto in 2008 and the University of Sheffild on the Humber Bridge in England, a FE model of the bridge is defined, in order to define what type of model is able to capture more accurately the real dynamic behaviour of the bridge.
- The sixth chapter outlines the necessary conclusions of the presented research. They concern the application of a method in the frequency domain in order to evaluate the modal parameters of a structure and its advantages, the advantages in applying a procedure based on the use of wavelet transforms in the process of identification in tests with unknown input and finally the problem of 3D modeling of systems with many degrees of freedom and with different types of uncertainty.

CONTENTS

INTRODUZIONE

Le vibrazioni fanno parte della vita di ogni giorno, esse sono tuttavia sempre considerati come fenomeni sgradevoli ed indesiderati, che possono comportare semplici disagi o malfunzionamenti, o nel caso più estremo il collasso della struttura. Gli effetti indotti dai terremoti rappresentano forse la manifestazione più spaventosa e distruttiva di come un fenomeno di vibrazione dinamica possa compromettere, anche irreversibilmente, la possibilità di utilizzo di una generica struttura.

Negli ultimi decenni, un'attenzione sempre maggiore è stata data alla necessità di classificare efficientemente il comportamento dinamico di un edificio. L'utilizzo di tecniche di progettazione sempre più sofisticate insieme allo sviluppo di materiali innovativi hanno permesso la costruzione di strutture sempre più leggere, ma parallelamente sempre più flessibili, quindi più soggette a fenomeni di vibrazione. Conseguentemente sono aumentati drammaticamente i problemi dinamici in termini di vibrazioni, rumore e fatica.

Pertanto, strumenti di analisi delle vibrazioni, che siano al contempo semplici ed affidabili, sono una necessità di base della moderna ingegneria. L'analisi modale è uno di questi strumenti, in grado di fornire una classificazione delle caratteristiche strutturali, delle sue condizioni di funzionamento, che consentono di progettare una struttura in vista di un suo ottimale comportamento dinamico.

In generale, le applicazioni dell'analisi modale sperimentale oggi coprono una vasta gamma di obiettivi, come: individuazione e valutazione dei fenomeni di vibrazione; validazione, correzione e aggiornamento dei modelli dinamici di analisi; sviluppo di modelli dinamici basati su indagini sperimentali; valutazione dell'integrità strutturale e di rilevamento dei danni; definizione di criteri e specifiche per la progettazione, qualificazione e certificazione. In altre parole, l'analisi modale mira a sviluppare dei modelli affidabili del comportamento dinamico di una struttura.

L'analisi modale sperimentale parte dall'elaborazione dei dati acquisiti durante una prova dinamica in sito, realizzata su una struttura esistente. Il segnale registrato può essere la risposta della struttura ad una eccitazione nota (prova di vibrazione forzata) o ad una eccitazione sconosciuta (prova d'urto o prove in vibrazioni ambientali). Nella tesi i due tipi di test sono stati elaborati con algoritmi diversi: il primo è stato analizzato attraverso metodi nel dominio delle frequenze (in quanto coinvolgono segnali di tipo stazionario) il secondo invece ha previsto l'applicazione di una procedura che lavora nel dominio tempo-frequenza (in questo caso si registrano segnali non stazionari, quindi il comportamento nel dominio del tempo diventa importante).

Le procedure nel dominio della frequenza sono di solito applicate quando la struttura è soggetta a una forzante di tipo sinusoidale, ad esempio generata da una classica vibrodina. In questo caso la risposta della struttura è registrata come accelerazione e si considera solo la parte a regime della risposta acquisita. Lo studio del segnale ed il suo confronto con la forzante che eccita viene riassunto tramite la FRF. Essa è definita puntualmente in modulo dal rapporto della FFT della accelerazione del sistema e la FFT della forzante che lo eccita. La stessa FRF è in particolare calcolata anche attraverso un'altra metodologia che permette di risalire ancora puntualmente ad essa, ma tramite le caratteristiche geometriche di un ellisse che rappresenta il confronto diretto tra input-output, registrati durante la prova.

Nota la FRF, le frequenze naturali sono definite attraverso il metodo Peak Picking, che individua le frequenze naturali in corrispondenza dei picchi della stessa [Bendat & Piersol, 1993]. Limite principale di questo metodo, sebbene molto semplice ed intuitivo, è che esso si basa sull'ipotesi che il sistema analizzato sia caratterizzato da modi di vibrare ben distinti, cioè che ogni picco non sia di fatto influenzato dai restanti, e che il sistema non sia poco smorzato.

Il metodo Circle-Fit (Kennedy & Pancu, 1947; Klosterman, 1971) si basa invece sulla possibilità di rappresentare la FRF nel piano di Nyquist o Argard. Se infatti

si considerano i punti della FRF prossimi alla risonanza e si rappresentano in un piano parte reale-immaginaria, si ottiene nel caso ideale un cerchio. Attraverso le caratteristiche geometriche di detto cerchio è in particolare possibile risalire allo smorzamento relativo alla frequenza di risonanza considerata.

L'utilizzo di vibrazioni forzate, tuttavia, comporta alcuni svantaggi. Innanzitutto esso diventa di difficile applicazione per alcune strutture, quali ponti o dighe; in questi casi risulta complesso eccitare con sufficiente energia ed in modo controllato dette strutture talvolta caratterizzate da modi significativi in una gamma di frequenze molto basse (si ricorda che in vibrazioni forzate lo shaker introduce una forzante il cui modulo è direttamente proporzionale alla frequenza di eccitazione). Nelle strutture molto grandi e flessibili, come ponti strallati o sospesi, in particolare, l'eccitazione forzata richiede attrezzature molto pesanti e costose, raramente disponibili nella maggior parte dei laboratori di dinamica. Queste problematiche sono state accompagnate da notevoli sviluppi tecnologici nel settore dei trasduttori e convertitori A/D negli ultimi anni che hanno reso possibile la misurazione in modo molto preciso, dei segnali anche per livelli molto bassi di eccitazione, quale quella indotta da forzanti ambientali come vento e traffico. Si è quindi sviluppato notevolmente l'utilizzo di metodi di identificazioni modale basata su prove di vibrazione output-only, in cui la forzante non è nota ed è di tipo ambientale. Pertanto, l'utilizzazione di prove dinamiche output-only è diventata un'alternativa di straordinaria importanza nel campo dell'ingegneria civile, essa permette l'identificazione accurata delle proprietà modali di grandi strutture nella fase di messa in opera o durante la vita utile della struttura, evitando in generale l'interruzione del suo esercizio e con un abbattimento dei costi notevole. Solitamente la forzante non nota in ingresso viene assunta come un rumore bianco.

Esistono due metodi per identificare i parametri modali di una struttura a seguito di una prova in vibrazione ambientale e si distinguono in metodi non parametrici,

sviluppati nel dominio delle frequenze e metodi parametrici, che utilizzano invece la rappresentazione nel dominio del tempo.

La prima applicazione di una metodologia nel dominio delle frequenza per questo tipo di prove nasce da un opportuno riadattamento del metodo Peak-picking, già applicato a qualche decennio fa nell'identificazione modale di edifici [Crawford and Ward, 1964; Trifunac, 1962] e ponti [Lamore et al, 1971; Abdel-Ghaffar, 1978], convenientemente modificato da Felber [Felber, 1993]. L'approccio nel dominio della frequenza è stato successivamente migliorato [Prevosto, 1982; Corrêa & Campos Costa, 1992] attraverso una procedura di diagonalizzazione della matrice di densità spettrale tramite la tecnica del SVD, in modo da separare i modi accoppiati e ottenere da un sistema a N gradi di libertà (GDL), N sistemi ognuno ad un singolo GDL. Questo metodo (Frequency Domain Decomposition (FDD)) è stato sviluppato e curato da Brincker et al. [Brincker et al., 2001]; esso è stato poi potenziato [Brincker et al., 2000] al fine di estrarre i valori di smorzamento modale. In questo ultimo approccio (EFDD), queste stime sono ottenute considerando il decadimento delle funzioni di auto-correlazione.
I metodi nel dominio del tempo nascono dalla scelta iniziale di un appropriato modello matematico, in grado di definire il comportamento dinamico di una struttura (si utilizzano di solito i modelli ARMAV e ARV). Il metodo ARMA, ad esempio, è caratterizzato dal fatto che si descrive l'uscita del modello (ovvero il segnale acquisito) tramite la combinazione lineare dei suoi valori assunti in istanti precedenti (parte Auto- Regressiva) e la combinazione lineare dei valori assunti dalla forzante nei medesimi istanti (parte a Media Mobile).

I metodi finora accennati, come detto, lavorano o nel dominio delle frequenze o nel dominio del tempo; alla luce di questa contestualizzazione si è scelto in questa tesi di applicare una metodologia in grado di lavorare congiuntamente nel dominio del tempo e delle frequenze, in modo da caratterizzare un segnale non stazionario completamente in entrambi i domini. Questa utile e interessante possibilità è offerta dall'applicazione delle Trasformate Continue di Wavelet (CWT); in un'unica trasformata, quindi in un'unica computazione e rappresentazione, è possibile leggere come il segnale si comporti nel tempo per ciascuna frequenza del range di interesse. La procedura è applicata ai segnali acquisiti durante prove di vibrazioni libere ed ambientali. I risultati, in termini di

parametri modali, sono confrontati con quelli ottenuti da alcuni dei metodi precedentemente introdotti. Si sono in generale riscontranti risultati molto simili. Al fine di abbattere i tempi computazionali si è poi provato ad applicare la Trasformata Discreta di Wavelet (DWT). In questo caso, la notevole approssimazione introdotta dalla discretizzazione ha portato a preferire, ai fine dell'estrazione dei parametri modali, la CWT. La DWT è stata tuttavia implementata al fine di filtrare segnali, caratterizzati da un'elevata quota di rumore e disturbi.

Nell'ultima parte della tesi è stato discusso un ultimo ma importante aspetto dell'identificazione dinamica: il model updating. Esso in pratica consiste nella definizione di un modello FEM, che sia in grado di riprodurre i reali parametri modali di una struttura esistente, sottoposta ad una prova di vibrazione dinamica in sito. Sicuramente data la crescente complessità delle strutture realizzate, la modellazione FEM diventa uno strumento indispensabile per definire il comportamento di una struttura e modellarne la sua componente dinamica. Spesso tuttavia, per problemi computazionali, o per incertezze legate al comportamento di materiali o condizioni di vincolo, i modelli possono discostarsi in modo importante dal reale comportamento del costruito. Il problema è la definizione di un modello che davvero sia in grado di rappresentare quanto realizzato. Ciò quindi può essere fatto ad esempio definendo le frequenze naturali di un sistema attraverso una prova sperimentale a monte e producendo a valle un modello FEM che sia caratterizzato da frequenze naturali con un errore minimo, rispetto a quelle sperimentali. Questa procedura è stata applicata ad un ponte sospeso, interamente in acciaio e di grande luce, sottoposto quindi ad una prova di tipo ambientale e modellato sulla base delle frequenze naturali sperimentali ottenute dal post-processing dei dati acquisiti.

INTRODUCTION

Vibrations, or dynamic motion, are inherent to life though generally mankind regards them as unpleasant and unwanted phenomena causing such undesirable consequences as discomfort, noise, malfunctioning, wear, fatigue and even

destruction. Earthquakes are perhaps the most frightening manifestations of dynamic motion, caused by forces generated in the earth's crust, and their destructive effect upon the environment and man-made structures is well known.
In the last few decades, technology developments have created an increasing need for reliable dynamic analysis. The sophistication of modern design methods together with the development of improved materials instilled a trend towards lighter structures. At the same time, there is a constant demand for larger structures, capable of carrying more loads at higher speeds under increasing drive power. The consequences of all these trends are dramatic increases in dynamic problems in terms of vibration, noise and fatigue, at the same time as requirements for improved environmental factors are being defined and enforced.
Therefore, strong and reliable vibration analysis tools are a basic need of modern engineering. Modal analysis is just one of those tools, providing an understanding of structural characteristics, operating conditions and performance criteria that enables designing for optimal dynamic behaviour or solving structural dynamics problems in existing designs.
Modal analysis is primarily a tool for deriving reliable models to represent the dynamics of structures. In general, it can be said that the applications of modal analysis today cover a broad range of objectives, namely: identification and evaluation of vibration phenomena; validation, correction and updating of analytical dynamic models; development of experimentally based dynamic models; structural integrity assessment, structural modification and damage detection; model integration with other areas of dynamics such as acoustics, fatigue, etc.; establishment of criteria and specifications for design, test, qualification and certification. In short, modal analysis aims to develop reliable dynamic models that may be used with confidence in further analysis.

Experimental modal analysis is the processing of data acquired during a dynamic test, performer on a generic structure. The response of the structure can be the

dynamic result of a known excitation (forced vibration test) or unknown excitation (impact test or ambient test). In the thesis the two types of tests are processed with different algorithms: frequency domain and time-frequency domain procedures are applied respectively.

The frequency domain procedures are usually applied when the structure is subject to a sinusoidal force, carried out on it by an electromechanical shaker for example. In this case the response of the structure is recorded as acceleration and only its stationary part is considered. An FRF is constructed point by point and from it all the modal parameters of the system are extracted: natural frequencies. modal dampings and mode shapes. The FRF is in particular computed by classical FFT on one hand and by the Lissajous Diagrams on the other hand.

From the FRF the natural frequencies are defined through the Peak Peaking method, which indentifies the natural frequencies in correspondence of the peaks of the FRF [Bendat & Piersol, 1980]. An important aspect concerning the Peak Peaking method is that all the estimates concerning a mode shape are based only on three points from each FRF estimate. It is evident that this method is very sensitive to noise and also to the level of damping present in the system. On the other hand, very low modal damping originates extremely sharp FRF peaks and consequently a very low precision in the damping estimates. A final difficulty can be expected in the application of the Peak Peaking method when mode shapes are very closely spaced in frequency, as the significant modal interference may then prevent the accurate identification of resonances.

The Circle-Fit method (Kennedy & Pancu, 1947; Klosterman, 1971) employs another interesting property of the SDOF FRF approach, the fact, the Mobility, the Inertance or Receptance function describes a circle in the Nyquist diagram (i.e. real part versus imaginary part), the influence of the other modes being approximated by a complex constant.

Note that the SDOF approach is only valid in the neighbourhood of a resonance, hence the complete FRF will not be a complete circle around each resonance, but will be constituted by sections of near-circular arcs around those frequencies.

The main problem associated to the performance of forced vibration tests in bridges, buildings or dams stems from the difficulty to excite, with sufficient energy and in controlled manner, their most significant modes of vibration in a low range of frequencies. In very large and flexible structures, like cable-stayed or suspension bridges, in particular, the forced excitation requires extremely heavy and expensive equipment very seldom available in most dynamic labs.

However, the technological developments registered in the fields of transducers and A/D converters during the last years made feasible the very accurate measurement of very low levels of dynamic response induced by ambient excitations, like wind or traffic, strongly stimulating the development of output-only modal identification methods. Therefore, the performance of output-only modal identification tests became an alternative of extraordinary importance in the field of Civil Engineering, allowing the accurate identification of modal properties of large structures at the commissioning stage or during the structure life time, in a much more comfortable way and avoiding any type of interruption of normal traffic in bridges.

The ambient excitation has commonly a multiple input nature and wide band frequency content, stimulating a significant number of modes of vibration. For simplicity, output-only modal identification methods assume the excitation input as a zero mean Gaussian white noise [Garibaldi et al. 2003], which means that the real excitation can be interpreted as the output of a suitable filter excited with that white noise input.

There are two main groups of output-only modal identification methods: nonparametric methods essentially developed in frequency domain and parametric methods in time domain. The basic frequency domain method (Peak-Picking), though already applied some decades ago to the modal identification of buildings [Crawford and Ward, 1964; Trifunac, 1962] and bridges [Lamore et al, 1971;

Abdel-Ghaffar, 1978], was only conveniently systematized by Felber [Felber, 1993] about twelve years ago. The frequency domain approach was subsequently improved [Prevosto, 1982; Corrêa & Campos Costa, 1992] by performing a single value decomposition of the matrix of response spectra, so as to obtain power spectral densities of a set of SDOF systems. This method (Frequency Domain Decomposition (FDD)) was better detailed and systematized by Brincker et al. [Brincker et al., 2001], and subsequently enhanced [Brincker et al., 2000] in order to extract modal damping factors estimates. In this last approach (EFDD) these estimates are obtained through inspection of the decay of auto-correlation functions, evaluated by performing the inverse Fourier transform of the SDOF systems' power spectral densities.

The time domain parametric methods involve the choice of an appropriate mathematical model to idealize the dynamic structural behaviour (usually time discrete state space stochastic models, ARMAV or ARV models, [Andersen, 1997, Larbi & Lardies, 2000]) and the identification of the values of the modal parameters so as that model fits as much as possible the experimental data, following some appropriate criterion. These methods can be directly applied to discrete response time series or, alternatively, to response correlation functions. The evaluation of these functions can be made based on their definition, using the FFT algorithm [Brincker et al., 1992] or applying the Random Decrement method (RD) [Asmussen, 1997].

All the methods introduced work or in time domain or in frequency domain. In this thesis we have decided to introduce the Continuous Wavelet Transforms [Garibaldi et al., 1997; Huang & Su, 2007], able to define the behaviour of the signal in time and frequency domain at the same time. The procedure is applied to the signal acquired during free and ambient vibration tests [Gouttebroze & Lardies, 2001] and the results are compared to that one obtained by the methods previously briefly described. The Discrete Wavelet Transform is also used in this kind of investigation [Lotfollahi-Yaghin & Hesari, 2008]; in this thesis the powerful of DWT is analyses principally in the important problem of signal filtering [Strang & Nguyen, 1996].

Another important aspect of the experimental modal analysis, discussed in this thesis, is the model updating [Friswell & Mottershead, 1995]. In order to obtain a FE model, able to define the real behaviour of a complex structure, a dynamic test is performed on the building, object of study. The experimental modal parameters are then extracted and a FE model, characterized by very similar modal parameters, is after implement. The FE model of a structure is constructed on the basis of highly idealized engineering blueprints and designs that may or may not truly represent all the physical aspects of an actual structure. When field dynamic tests are performed to validate the analytical model, inevitably their results, commonly natural frequencies and mode shapes, do not coincide with the expected results from the analytical model. These discrepancies originate from the uncertainties in simplifying assumptions of structural geometry, materials, as well as inaccurate boundary conditions. The problem of how to modify the analytical model from the dynamic measurements is known as the model updating in structural dynamics [Link, 1999]. This procedure is applied on a suspended bridge, subject to an ambient test.

CHAPTER ONE

Dynamic of a vibrant system: fundamentals of modal analysis

1.1. Basic concepts of dynamic system

All dynamic properties of mechanical system are distributed in space. These properties are mass, stiffness and damping, responsible respectively for inertia, elastic and dissipative forced (Maia & Silva, 1998). Modelling a real mechanical system is therefore a very complex or even impossible task if one tries to describe how all features of the system interact with one other. However, in most case, satisfactory results may be achieved if the basic properties are considered as separated into simple discrete elements which, properly combined, can represent the dynamic properties of the system to sufficient accuracy.

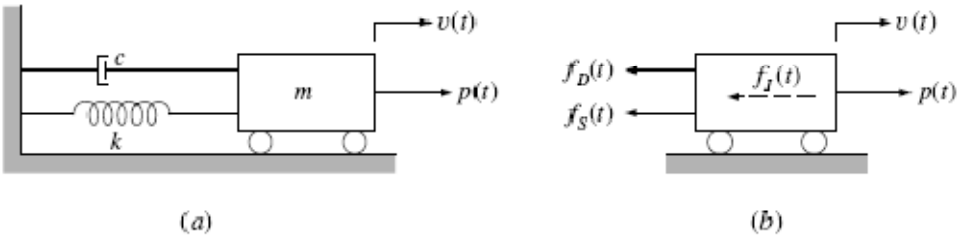

Figure 1.1 Idealized SDOF system, (a) basic components; (b) forced in equilibribium

The simplest possible discretization is a considering a system as a just a single degree-of-freedom (SDOF), whose properties are represented by figure 1.1 (Clough and Penzien) . However, most real mechanical systems and structure cannot be modelled successfully by assuming a single-degree-of-freedom, i.e. a single coordinate to describe their vibratory motion.

Real structures are continuous and nonhomogeneous elastic systems which have an infinite number of degree of freedom. Therefore, their analysis entails an approximation which consist of describing their behaviour through the use of a finite number of degree of freedom, as many as necessary to ensure enough accuracy. Adequate choice of the motion coordinates corresponds therefore to an

initial decision that the analysis must take, which is of paramount importance as the success of the subsequent analysis depends on this choice.

Usually, continuous and nonhomogeneous structures are described as lumped-mass multiple degree-of freedom (MDOF) systems. For example we consider the system in figure 1.2, representing a viscously damped system described by its spatial mass, stiffness and damping properties. A total of N coordinates xi(t) are required to describe the position of the N masses relative to their static equilibrium positions.

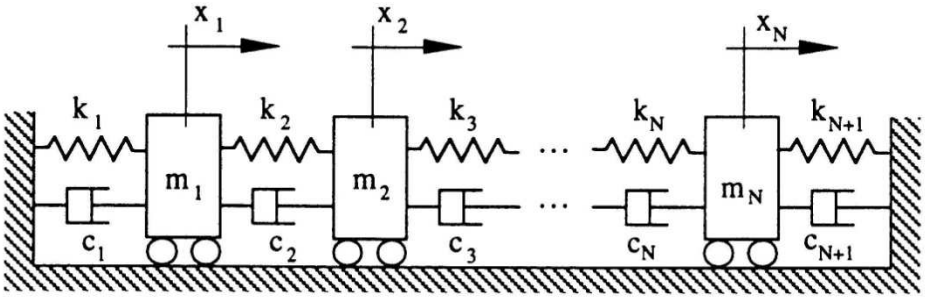

Figure 1.2 Idealized MDOF system, example of a model with N degrees of freedom.

Assuming that each mass may be forced to move by an external force fi(t) and establishing the equilibrium of the forces acting on them, the motion of the system is found to be governed by the following compact equation

$$\mathbf{M}\ddot{\mathbf{x}}\left(t\right)+\mathbf{C}\dot{\mathbf{x}}\left(t\right)+\mathbf{K}\mathbf{x}\left(t\right)=\mathbf{f}\left(t\right) \tag{1.1}$$

where **M**, **C** and K are the NxN mass, damping and stiffness symmetric matrices respectively, describing the spatial properties of the system. The column matrices $\ddot{\mathbf{x}}\left(t\right)$, $\dot{\mathbf{x}}\left(t\right)$ *and* $\mathbf{x}\left(t\right)$ are Nx1 vectors of time varying acceleration, velocity and displacement response and f (t) is an Nx1 vector of time varying external excitation forces.

1.2. Modal parameters of system

In general when a SDOF is subjected to an initial perturbation and subsequently left free to move, it oscillates around the static equilibrium position. Dynamically, the system was fully charactirezed through an unique property described by its free vibration natural frequency. The same procedure is applied for a MDOF system, then the modal parameters are obtained through its free vibration, expressed through the following equation [Chopra, 1995]

$$\mathbf{M}\ddot{\mathbf{x}}\left(t\right)+\mathbf{C}\dot{\mathbf{x}}\left(t\right)+\mathbf{K}\mathbf{x}\left(t\right)=0 \tag{1.2}$$

A general solution of eq. (1.2) is

$$\mathbf{x}=\overline{\mathbf{X}}e^{st} \tag{1.3}$$

substituting into (1.2) we obtain

$$\left[s^2\mathbf{M}+s\mathbf{C}+\mathbf{K}\right]\overline{\mathbf{X}}=0 \tag{1.4}$$

which constitutes a complex eigenproblem. A more convenient way of solving (1.4) is to define a complex state vector $\mathbf{u}(t)$ as

$$\mathbf{u}(t)=\begin{Bmatrix}\mathbf{x}\left(t\right)\\ \dot{\mathbf{x}}\left(t\right)\end{Bmatrix} \tag{1.5}$$

Rewriting (1.2) in terms of this new variable we obtain

$$\begin{bmatrix}\mathbf{C} & \mathbf{M}\\ \mathbf{M} & \mathbf{0}\end{bmatrix}\dot{\mathbf{u}}\left(t\right)+\begin{bmatrix}\mathbf{K} & \mathbf{0}\\ \mathbf{0} & \mathbf{-M}\end{bmatrix}\mathbf{u}\left(t\right)=0 \tag{1.6}$$

or, more simply

$$\mathbf{A}\dot{\mathbf{u}}\left(t\right)+\mathbf{B}\mathbf{u}\left(t\right)=0 \tag{1.7}$$

This formulation is often called the state-space analysis, by contrast with the usual vector-spaced analysis. **A** and **B** are 2Nx2N real symmetric matrices. Substituting eq. (1.3) in (1.5) the vector **u**(t) becomes

$$\mathbf{u}\left(t\right) = \begin{Bmatrix} \overline{\mathbf{X}} \\ s\overline{\mathbf{X}} \end{Bmatrix} e^{st} = \overline{\mathbf{U}} e^{st} \tag{1.8}$$

and

$$\dot{\mathbf{u}}\left(t\right) = \begin{Bmatrix} s\overline{\mathbf{X}} \\ s^2\overline{\mathbf{X}} \end{Bmatrix} e^{st} = s\overline{\mathbf{U}} e^{st} \tag{1.9}$$

Then, substituting (1.8) and (1.9) into (1.7), for all time we obtain

$$\left[s\mathbf{A} + \mathbf{B}\right]\overline{\mathbf{U}} = 0 \tag{1.10}$$

representing a generalised eigenproblem whose solution comprises of 2N eigenvalues that are real or exist in complex conjugate pairs (in the case of undamped system, easier situation). Calling the eigenvalues by sr and s*r and the eigenvectors ψ_r and ψ_r^* and using the orthogonality properties of an undamped or proportionally system, we can write the eigenvalues in the known form

$$s_r = -\omega_r \xi_r + i\omega_r \sqrt{1 - \xi_r^2} \tag{1.11}$$

where ω_r *and* ξ are the undamped natural frequency and damping ratio of r vibration mode, respectively. The eigenvectors are related to the system properties by the following equations

$$\frac{\left[\psi_r^*\right]^T \mathbf{C}\psi_r}{\left[\psi_r^*\right]^T \mathbf{M}\psi_r} = \frac{c_r}{m} = 2\boldsymbol{\omega}_r \boldsymbol{\xi}_r \tag{1.12}$$

$$\frac{\left[\psi_r^*\right]^T \mathbf{K}\psi_r}{\left[\psi_r^*\right]^T \mathbf{M}\psi_r} = \frac{k_r}{m} = \boldsymbol{\omega}_r^2 \tag{1.13}$$

Thus we end up, for a generic viscously damped MDOF system, in analogy with the undamped and with the proportionally damped MDOF system, a modal mass mr, a modal damping cr and a modal stiffness kr. Also, ω_r *and* ξ, may be taken as the undamped natural frequency and the damping ratio associated with mode r.

1.3. Signal analysis

Over the years, measurement techniques have been developed continuously to improve the accuracy of measured frequency response functions and to reduce testing time, and therefore the cost of modal testing [Ewins, 2000]. In this chapter and in the following one, the attention is focused on the analysis of time signals corresponding to an applied force, which are recorded and processed to obtain frequency response functions (FRFs) or impulse response functions (IRFs), which are better analysed by appropriate curve-fitting techniques to yield the modal properties of the structure. The treatment of the signal involves quite number of precautions, techniques and procedures that justify a closer look at the area, known as Signal Processing.

In the past three decades, the introduction of the Fast Fourier Transform (FFT) algorithm [Cooley & Tukey, 1965], the availability of digital data processing equipment and powerful micro-computers have led to the development of test procedures that makes the process easier and accurate. These procedures are usually applied in the case of a forced vibrations test and free vibration tests; the modal properties are obtained through the analysis of a signal recorded as response of a generic structure subject to a sinusoidal excitation, carried out by an electromechanical shaker, or an impulsive force using an instrumented hummer. The measured data are then digitally processed to yield estimates of the FRFs or IRFs. In the following sections the basic concepts of Fourier Analysis are presented.

1.3.1. Fourier transforms for deterministic signals

The complete solution of the motion equation is available only when the forces vector f(t) assumes particular time-varying expression. For example it is definable when the f(t) is an harmonic function. However, excitations may be of many

different types other than harmonic. In fact if one considers real excitation sources such as, for example, earthquakes, wind, sea waves, and all types of machinery, it is easy to understand that the forcing functions are of many different types and may be harmonic only in very particular cases. Therefore the response of a generic structure, acquired during a real test, is not perfectly harmonic, even if the exciting force is perfectly sinusoidal.

Dynamic signals may be generally classified as deterministic or random; in the first case the former can be described as an analytical expression of their magnitude, random signal, instead, cannot. Deterministic signals may be periodic or transient; periodic signal as one that repeats itself after a period T. A transient signal is one that occurs only in a short period of time. If a certain function is periodic and satisfies certain conditions then it can be represented of a summation of harmonic functions, know as Fourier series.

Considering a generic periodic signal x(t), its Fourier series is expressed by the following equation

$$x\left(t\right)=\sum_{-\infty}^{\infty}X_{k}\left(\boldsymbol{\omega}\right)e^{ik\boldsymbol{\omega}t} \tag{1.14}$$

with

$$X_{k}\left(\boldsymbol{\omega}\right)=\frac{1}{T_{0}}\int_{-\frac{T_{0}}{2}}^{\frac{T_{0}}{2}}x\left(t\right)e^{-ik\frac{2\pi}{T_{0}}t}\,dt \tag{1.15}$$

Considering now that x(t) is sampled at regular time represented by the discrete series $\left\{x(k)\right\},\ k=0,1,2,...N-1$ where t = kT/N. In this case the eq. (1.15) can be expressed by the following relation

$$X\left(j\right)=\frac{1}{N\boldsymbol{\Delta}t}\sum_{k=0}^{N-1}x(k)e^{-2\pi ijk/N}\boldsymbol{\Delta}t=\frac{1}{N}\sum_{k=0}^{N-1}x(k)e^{-2\pi ijk/N} \tag{1.16}$$

And (1.14) becomes

$$x\left(k\right)=\sum_{j=0}^{N-1}X(j)e^{-2\pi ijk/N} \tag{1.17}$$

For j = 1,2,..., N-1 and k =1,2,...,N-1. A direct evalutation of (1.16) would require nearly N^2 complex multiply and add operation. For large value of N, this can be prohibitive. A sophisticated algorithm, the Fast Fourier Transform (FTT) proposed by Cooley and Tukey in 1965, being much faster. These kind of reduction are applicable to more general case of $N = 2^m$, where m is any positive integer, reducing the computation from N^2 operation to $(N/2)\log_2 N$ multiplication, additions and subtraction. For N = 1024, this represents a computational reduction more than 200 to 1.

When the time functions are non periodic (transient), they cannot be handled directly using Fourier series. However, it is not difficult to accept that a transient signal may be viewed as a periodic signal with period $T = \infty$. By considering the limit which is approached by a Fourier series as the period becomes infinite, it will be found that, under certain condition, an arbitrary function x(t) can be described by an integral X(w) given by

$$X(\omega) = \int_{-\infty}^{\infty} x(t) e^{-i\omega t} dt \tag{1.18}$$

Where $X(\omega)$ is known as the Fourier transform of x(t). Conversely, the time dependent function x(t) can always be obtained from $X(\omega)$ through the inverse Fourier transform

$$x(t) = \frac{1}{2\pi} \int_{-\infty}^{\infty} X(\omega) e^{i\omega t} d\omega \tag{1.19}$$

These integrals are very important because they allow a time domain signal to be transformed to and from a frequency domain signal.

1.3.2. Random excitation

Random signals cannot be treated in the same way as the deterministic signals so far discussed. By nature they are not periodic and it might be thought they could be analysed assuming a periodicity of infinite period. However this is not possible

because they do not obey to the Dirichelet condition which states the Fourier transforms can only be used if the following condition is satisfied:

$$\int_{-\infty}^{\infty} \left| x\left(t\right) \right| dt < \infty \tag{1.20}$$

Given their inherent properties, the analysis of random signals entails the use of probabilistic concepts. Considering a generic random signal x(t) the so-called random autocorrelation function is defined through the following equation

$$R_{xx} = \lim_{T\to\infty} \frac{1}{T} \int_{-\frac{T}{2}}^{\frac{T}{2}} x\left(t\right) x(t+\boldsymbol{\tau}) dt \tag{1.21}$$

where x(t) is the magnitude of our function at an instant t of time and $x(t+\boldsymbol{\tau})$ designates the magnitude of the same signal observed after a time delay $\boldsymbol{\tau}$ has elapsed. In physical terms, the auto-correlation function expresses how a particular instantaneous amplitude value of a generic random signal depends upon previously occurring instantaneous amplitude values. The auto-correlation function can be Fourier transformed, applying (1.18)

$$S_{xx}\left(\boldsymbol{\omega}\right) = \int_{-\infty}^{\infty} R_{xx}\left(\boldsymbol{\tau}\right) e^{-i\boldsymbol{\omega}\boldsymbol{\tau}} d\boldsymbol{\tau} \tag{1.22}$$

known as the auto-spectral density (ASD) or power spectrum (PSD), which is also a real and even function of frequency. The ASD provides a frequency description of our random signal. These concepts can be extended considering simultaneously the random force x(t) and the random response y(t) functions (more generic case). Thus may define

$$R_{xy} = \lim_{T\to\infty} \frac{1}{T} \int_{-\frac{T}{2}}^{\frac{T}{2}} x\left(t\right) y(t+\boldsymbol{\tau}) dt = \frac{1}{2\boldsymbol{\pi}} \int_{-\infty}^{\infty} S_{xy}\left(\boldsymbol{\omega}\right) e^{i\boldsymbol{\omega}\boldsymbol{\tau}} d\boldsymbol{\omega} \tag{1.23}$$

$$S_{xy}\left(\boldsymbol{\omega}\right) = \int_{-\infty}^{\infty} R_{xy}\left(\boldsymbol{\tau}\right) e^{-i\boldsymbol{\omega}\boldsymbol{\tau}} d\boldsymbol{\tau} \tag{1.24}$$

and, conversely

$$R_{yx} = \lim_{T\to\infty} \frac{1}{T} \int_{-\frac{T}{2}}^{\frac{T}{2}} y\left(t\right)x(t+\boldsymbol{\tau})dt = \frac{1}{2\boldsymbol{\pi}} \int_{-\infty}^{\infty} S_{yx}\left(\boldsymbol{\omega}\right)e^{i\boldsymbol{\omega}\boldsymbol{\tau}}d\boldsymbol{\omega} \tag{1.25}$$

$$S_{yx}\left(\boldsymbol{\omega}\right) = \int_{-\infty}^{\infty} R_{yx}\left(\boldsymbol{\tau}\right)e^{-i\boldsymbol{\omega}\boldsymbol{\tau}}d\boldsymbol{\tau} \tag{1.26}$$

as the cross-correlation and the cross-spectral density functions, respectively. It is important to note that the cross-spectral densities are complex frequency spectra, containing real and imaginary parts (or magnitude and phase information) whereas the PSD is a real function containing only magnitude (squared) information. At least the autocorrelation function is correlated to the Fourier transform of the signal x(t) through this expression

$$S_{xx}\left(\boldsymbol{\omega}\right) = X\left(\boldsymbol{\omega}\right)^{*} X\left(\boldsymbol{\omega}\right) \tag{1.27}$$

where $X\left(\boldsymbol{\omega}\right)^{*}$ indicates the complex conjugate of $X\left(\boldsymbol{\omega}\right)$. The same reasoning can be applied to the cross-correlation function; $S_{yx}\left(\boldsymbol{\omega}\right)$is correlated to the Fourier transform of x(t) and y(t) through this equation

$$S_{xy} = X\left(\boldsymbol{\omega}\right)^{*} Y\left(\boldsymbol{\omega}\right) \tag{1.28}$$

1.3.3. Time domain. Impulse response function

An alternative to the Fourier analysis is the use of a time domain approach for estimating a system's response to an arbitrary impulse. The simplest form of a non periodic time function is the unit impulse of Dirac

$$x\left(t\right) = \boldsymbol{\delta}\left(t-\boldsymbol{\tau}\right) \tag{1.29}$$

which is zero for all values except for $t = \boldsymbol{\tau}$ where

$$\lim_{\boldsymbol{\Delta}t\to\infty} \int_{\boldsymbol{\tau}}^{\boldsymbol{\tau}+\boldsymbol{\Delta}t} x\left(t\right)dt = 1 \tag{1.30}$$

The response to an arbitrary input f(t) may be taken as the superposition of the responses to a series of impulses which represent the original forcing function. This is true given the fact that we are considering linear systems, hence

$$x\left(t\right) \approx \sum_{\tau} f\left(\boldsymbol{\tau}\right) h\left(t-\boldsymbol{\tau}\right) \boldsymbol{\Delta\tau} \qquad for\ t > \boldsymbol{\tau} \tag{1.31}$$

Letting $\boldsymbol{\Delta\tau} \to 0$ the summation becomes an integral, and therefore

$$x\left(t\right) = \int_{0}^{t} f\left(\boldsymbol{\tau}\right) h\left(t-\boldsymbol{\tau}\right) d\boldsymbol{\tau} \qquad for\ t > \boldsymbol{\tau} \tag{1.32}$$

The integral in eq.(1.32) is called the convolution Duhamel's integral.

Changing the variable of integration to ϑ using the relationship $\tau = t - \vartheta$, we obtain

$$x\left(t\right) = -\int_{\infty}^{0} f\left(t-\vartheta\right) h\left(\vartheta\right) d\vartheta = \int_{0}^{\infty} f\left(t-\vartheta\right) h\left(\vartheta\right) d\vartheta \tag{1.33}$$

Standing that $h(t-\tau) = 0$ for all $t < \tau$ is equivalent to write $h(\vartheta) = 0$ for all $\vartheta < 0$ the second integral of (1.33) can also be extended to minus infinity, i.e.

$$x\left(t\right) = \int_{-\infty}^{\infty} f\left(t-\vartheta\right) h\left(\vartheta\right) d\vartheta \tag{1.34}$$

Eq. (1.34) is the convolution of the forcing function and the impulse function, then it is possible to write

$$x\left(t\right) = h\left(t\right) * f\left(t\right) \tag{1.35}$$

or in other words

$$X\left(\omega\right) = H\left(\omega\right) F\left(\omega\right) \tag{1.36}$$

$F\left(\omega\right)$ is in particular the Fourier transform of the Dirac function, so it is equal to 1. Then considering it in eq. (1.19) we have at least

$$x\left(t\right) = \frac{1}{2\boldsymbol{\pi}} \int_{-\infty}^{\infty} H\left(\boldsymbol{\omega}\right) e^{i\omega t} d\boldsymbol{\omega} \tag{1.37}$$

which, by definition, must be identical to h(t) and with

$$H\left(\omega\right)=\int_{0}^{\infty}h\left(t\right)e^{-i2\pi\omega\tau}d\tau \tag{1.38}$$

Thus, it may be concluded that the frequency response function (FRF) $H\left(\boldsymbol{\omega}\right)$ and the impulse response function h(t) constitute a Fourier pair. Then the FRF can be computed just by taking the Fourier transform of its impulse response function.

1.3.4. Frequency response functions

The frequency response function (FRF) assumes a relevant importance in the field of structural identification [Ewins, 2000]. Its construction allows the definition of all the modal parameters of a generic system, i.e. natural frequencies, modal damping and modes shape. It is the Fourier transform of the unit impulse and it is expressed by eq. (1.38). If y(t) is the structure response and f(t) its excitation the eq.(1.36) allows to define the following relationship

$$H\left(\omega\right)=\frac{Y\left(\omega\right)}{F\left(\omega\right)} \tag{1.39}$$

where $Y\left(\omega\right)$and $F\left(\omega\right)$are respectively the Fourier transform of response and force applied on structure. Dynamic properties of a system may be expressed in terms of any convenient response characteristics, and not necessarily in terms of displacement as we have doing until now.

Usually vibration is measured in term of motion and therefore the corresponding FRF may be represented in terms of displacement, velocity or acceleration. Then we have the following different expression and definition of FRF

$$\alpha\left(\omega\right)=\frac{displacement\ response}{force\ excitation}=RECEPTANCE$$

$$Y\left(\omega\right)=\frac{velocity\ response}{force\ excitation}=MOBILITY$$

$$A(\omega) = \frac{acceleration\ response}{force\ excitation} = INERTANCE\ or\ \ ACCELERANCE$$

In particular the Inertance is correlated to the Receptance through the following expression

$$A(\omega) = -\omega^2 \alpha(\omega) \tag{1.40}$$

In the following sections always the Inertance is considered, because in the dynamic tests considered always the structure acceleration is acquired through some sensors. Considering now a MDOF subject to a generic excitation f(t), the motion equation is, as already expressed in eq. (1.1)

$$\mathbf{M}\ddot{\mathbf{x}}(t) + \mathbf{C}\dot{\mathbf{x}}(t) + \mathbf{K}\mathbf{x}(t) = \mathbf{f}(t) \tag{1.41}$$

A Fourier transform of the left and right term of eq. (1.41) is performed and the results is written in the equation below

$$\int_{-\infty}^{\infty} \mathbf{M}\ddot{\mathbf{x}} + \mathbf{C}\dot{\mathbf{x}} + \mathbf{K}\mathbf{x}\, e^{-i\omega t} dt = \int_{-\infty}^{\infty} \mathbf{f} e^{-i\omega t} dt \tag{1.42}$$

The eq. (1.42) can be rewritten as

$$\left(-\omega^2 \mathbf{M} + i\omega \mathbf{C} + \mathbf{K}\right) \mathbf{X}(\omega) = \mathbf{F}(\omega) \tag{1.43}$$

where $\mathbf{X}(\omega)$ *and* $\mathbf{F}(\omega)$ are respectively the Fourier transform of displacement **X** and exciting force **f**. The receptance can be expressed as

$$\boldsymbol{\alpha}(\omega) = \frac{\mathbf{F}(\omega)}{\mathbf{X}(\omega)} = \frac{1}{\left(-\omega^2 \mathbf{M} + i\omega \mathbf{C} + \mathbf{K}\right)} \tag{1.44}$$

Considering the modal matrix $\boldsymbol{\psi}$ and the orthogonality properties of modes shape, we can use the following relationship

$$\boldsymbol{\psi}^T \mathbf{K} \boldsymbol{\psi} = \mathbf{diag}\left(\omega_r^2\right) \tag{1.45}$$

$$\boldsymbol{\psi}^T \mathbf{M} \boldsymbol{\psi} = \mathbf{I} \tag{1.46}$$

$$\boldsymbol{\psi}^T \mathbf{C} \boldsymbol{\psi} = \mathbf{diag}\left(2\xi_r \omega_r\right) \tag{1.47}$$

Using eqs. (1.45), (1.46) and (1.47) the eq. (1.44) can be rewritten in this way:

$$\boldsymbol{\psi}^T \left(-\omega^2 \mathbf{M} + i\omega \mathbf{C} + \mathbf{K}\right) \boldsymbol{\psi} = \boldsymbol{\psi}^T \boldsymbol{\alpha}\left(\omega\right)^{-1} \boldsymbol{\psi} = \mathbf{diag}\left(\omega_r^2 - \omega^2 + 2i\xi_r \omega_r \omega\right) \tag{1.48}$$

Then the Receptance can be expressed as

$$\boldsymbol{\alpha}\left(\omega\right) = \boldsymbol{\psi}^T \mathbf{diag}\left(\omega_r^2 - \omega^2 + 2i\xi_r \omega_r \omega\right) \boldsymbol{\psi} \tag{1.49}$$

or

$$\alpha_{jk}\left(\omega\right) = \sum_{r=1}^{N} \frac{\psi_{rj} \psi_{rk}}{\left(\omega_r^2 - \omega^2 + 2i\xi_r \omega_r \omega\right)} \tag{1.50}$$

Using eq. (1.40), the Inertance is equal to

$$A_{jk}\left(\omega\right) = -\sum_{r=1}^{N} \frac{\omega^2 \psi_{rj} \psi_{rk}}{\left(\omega_r^2 - \omega^2 + 2i\xi_r \omega_r \omega\right)} \tag{1.51}$$

Eq. (1.51) can be defined in the following way

$$A_{jk}\left(\omega\right) = -\sum_{r=1}^{N} \frac{\omega^2 \left(R_{jk}\right)_r}{\left(\omega_r^2 - \omega^2 + 2i\xi_r \omega_r \omega\right)} \tag{1.52}$$

where the residue $\left(R_{jk}\right)_r$ is obtained by the product between the autovectors.

1.3.5. MDOF FRF graphical representation

A generic system with N degree of freedom is described by a modal model with N natural frequencies and N mode shapes. Also, it is clear that the corresponding FRF may be written under the form of a series of terms, each of which refers to the contribution to the total response of each mode of vibration, as stated by eq. (1.52). In particular we consider for an example the FRF of an undamped system with 3 degree of freedom system. Figure 4 and 5 display the magnitude and the phase, respectively, using a linear scale, of a direct point receptance.

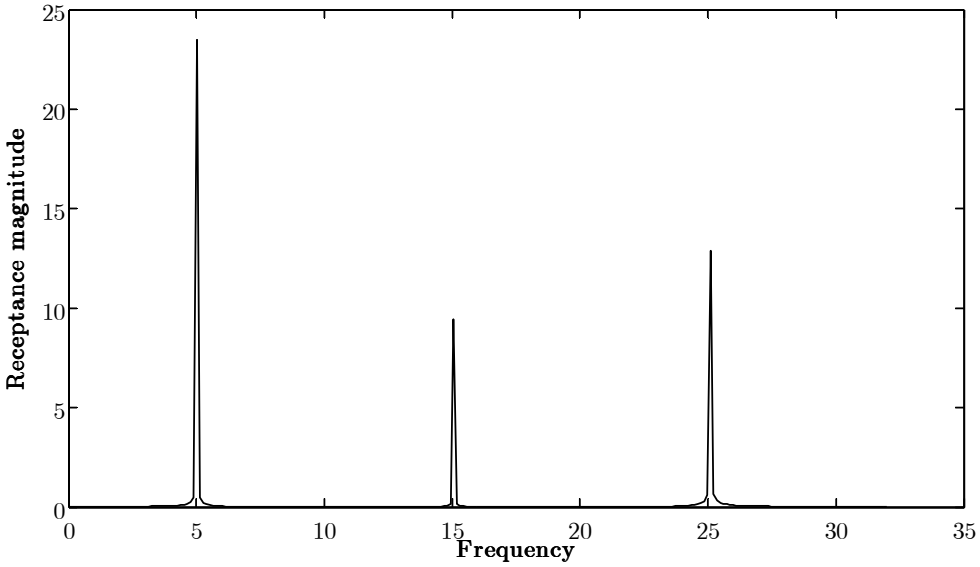

Figure 1.3 Magnitude of receptance plotted versus frequency, example of a MDOF

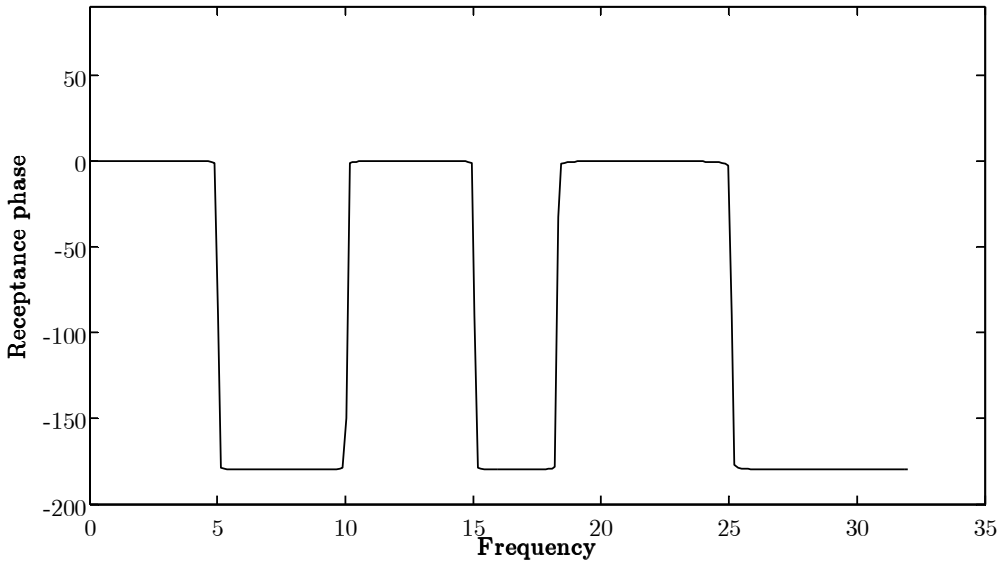

Figure 1.4 Phase of receptance plotted versus frequency, MDOF undamped system

What is immediately obvious, from the magnitude plot, is that there are three peak amplitudes, corresponding to the three natural frequencies of the system. The meaning of this is that one is now confronted with three different resonances. In analogy with what happens for SDOF systems, it is to be expected that, for

each resonance, there will be a 180° phase shift. The real and imaginary part of FRF are represented in the figures below

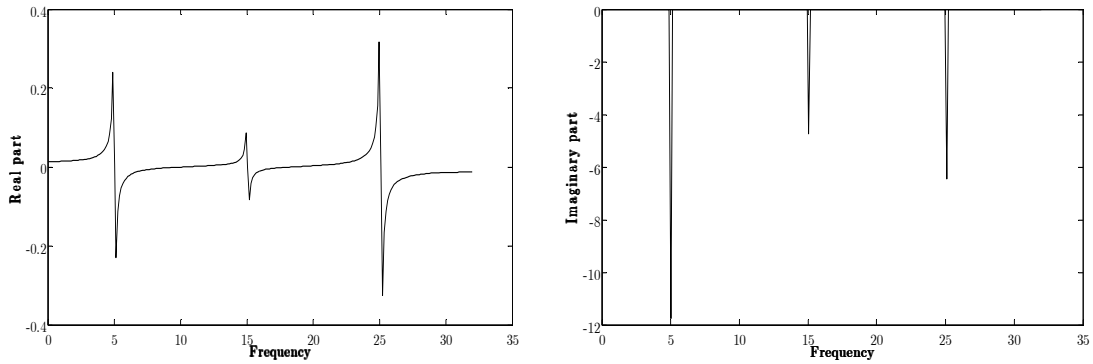

Figure 1.5 Real and imaginary part of FRF (receptance)

Taking for example eq. (1.52) for zero damping it becomes

$$\alpha_{jk}\left(\omega\right) = -\sum_{r=1}^{N} \frac{\left(R_{jk}\right)_r}{\left(\omega_r^2 - \omega^2\right)} \tag{1.53}$$

Where $\left(R_{jk}\right)_r$ is now a real quantity. If we consider a direct point, for example α_{kk}, the modal constant $\left(R_{kk}\right)_r$ is always positive due to it being the product of element k of the eigenvector for mode r, by itself.

What eq. (1.53) states is that the total receptance FRF is the sum of the contributions of "SDOF" terms corresponding to each of the system modes of vibration. For a direct point receptance:

$$\alpha_{kk} = \frac{\left(R_{kk}\right)_1}{\omega_1^2 - \omega^2} + \frac{\left(R_{kk}\right)_2}{\omega_2^2 - \omega^2} + \ldots + \frac{\left(R_{kk}\right)_N}{\omega_N^2 - \omega^2} \tag{1.54}$$

Thus, in the lower frequency region, all terms in the summation are positive and the receptance value is positive and dominated by the first mode (r=1), for which the denominator $\omega_1^2 - \omega^2$ is smaller than for the other terms in the summation. After the first resonance, $\omega_1^2 - \omega^2$ becomes negative and therefore the first term in the series becomes negative. This change of sign corresponds to a phase shift from 0° to -180°.

Now taking into consideration damped systems, the magnitude of FRF is very similar to that one describes in figure 2.3. The peaks are less sharp, due to the presence of a defined level of damping for each mode.

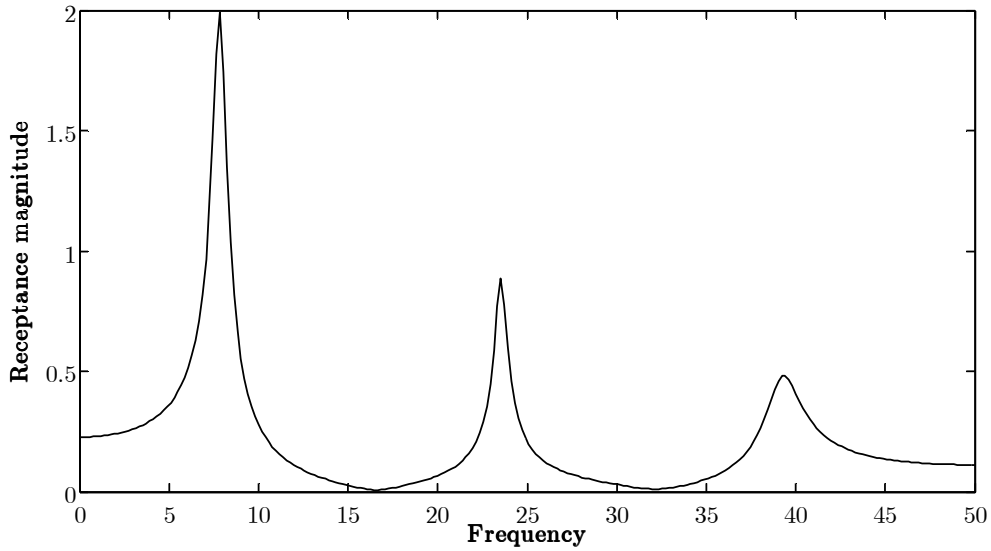

Figure 1.6 Magnitude of FRF for a proportionally damped MDOF system

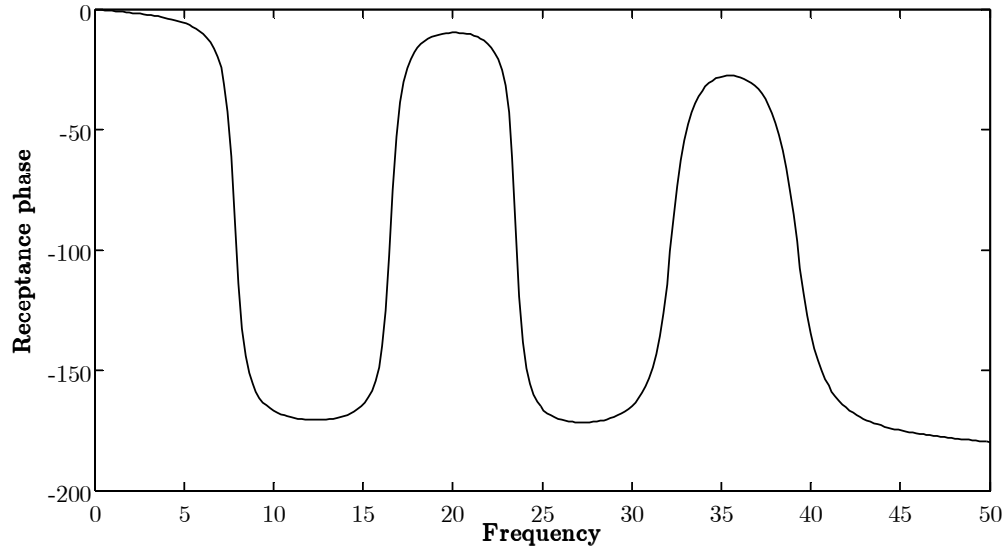

Figure 1.7 Phase of FRF for a proportionally damped MDOF system

The differences are due to the resonances being less sharp and the phase angle being no longer exactly 0° or -180°. The following figures represent real and imaginary part of the FRF. Due to the use of a linear scale and the fact that, in general, the receptance amplitude decays with frequency, the higher modes tend

not to show in the plot. Thus does not happen in this case, because we consider three modes with light dampings. This problem is characteristic of the receptance plot; it is not evident in the inertance plot, used in the next chapter.

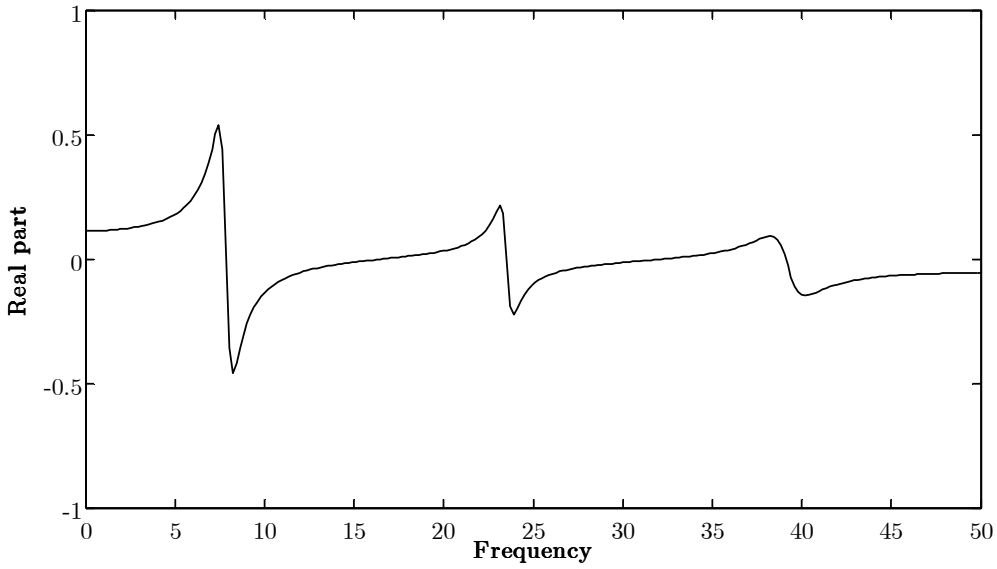

Figure 1.8 Real part of FRF for a proportionally damped MDOF system

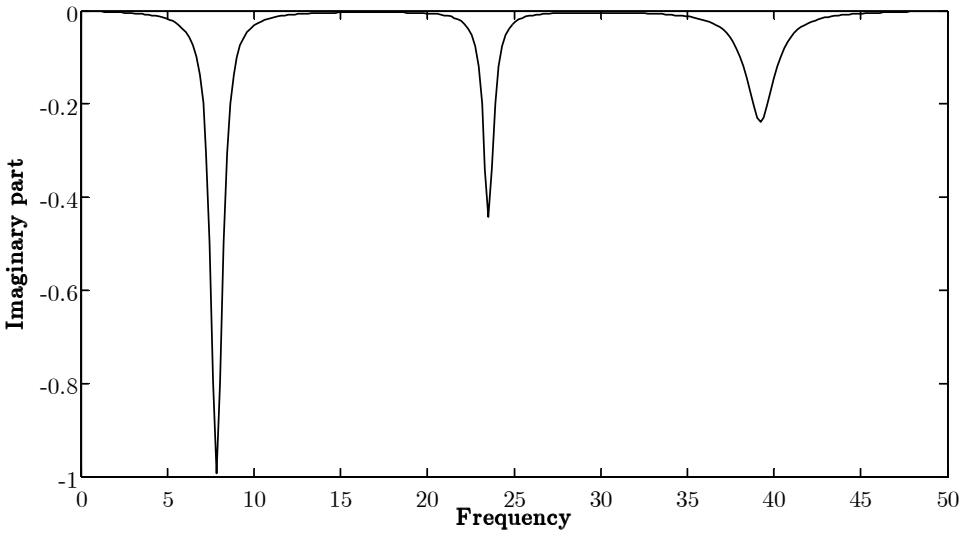

Figure 1.9 Imaginary part of FRF for a proportionally damped MDOF system

At this point it is possible to introduce another kind of representation of the FRF, when it is plotted in the Nyquist or Argand plane, or in a plane real versus imaginary part. If the points of FRF close to the peak of its magnitude plot are

considered, a perfect and centred circle is obtained. The FRF of the three degrees of freedom system before considered is plotted in the Nyquist plane and its trend is represented in the figure below

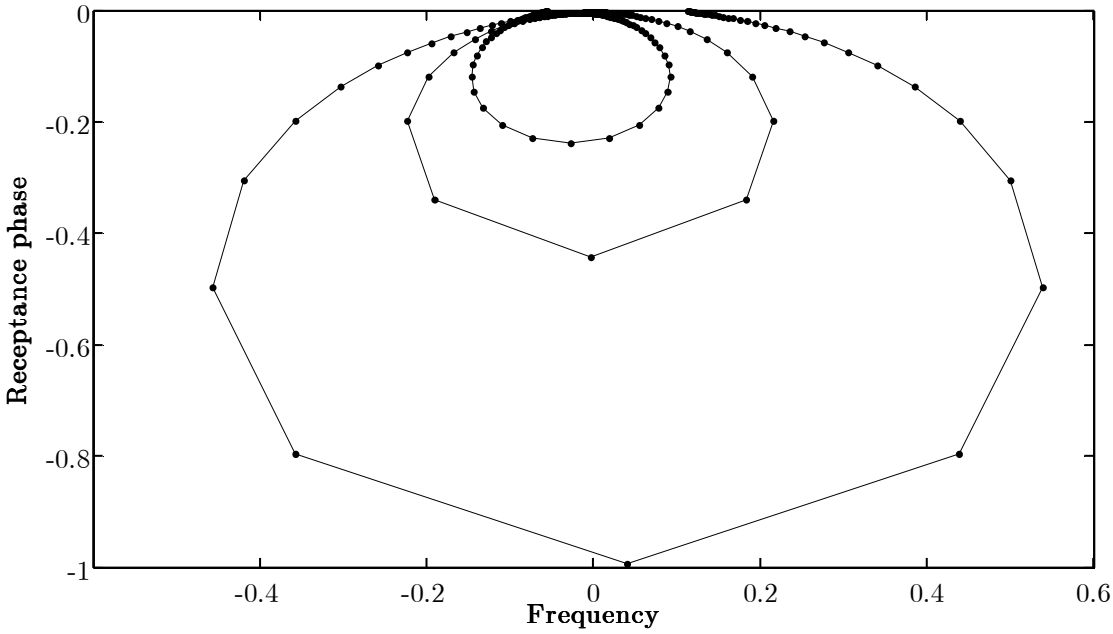

Figure 1.10 Nyquist plot of FRF for a proportionally damped MDOF system

As expected, the natural frequency regions plot as circular loops. However, it can be seen that the loops are not exactly centred with respect to the imaginary axis as in the case of a SDOF system (see chapter 2). This can be easily explained if we recall eq. (1.52) and rewrite it for a direct point receptance of a 3 DOF system with proportional damping.

$$\begin{aligned}\alpha_{kk}\left(\omega\right) &= \sum_{r=1}^{3}\frac{\left(R_{kk}\right)_r}{\left(\omega_r^2-\omega^2+2i\xi_r\omega_r\omega\right)} = \\ &= \frac{\left(R_{kk}\right)_1}{\left(\omega_1^2-\omega^2+2i\xi_1\omega_1\omega\right)}+\frac{\left(R_{kk}\right)_2}{\left(\omega_2^2-\omega^2+2i\xi_2\omega_2\omega\right)}+\frac{\left(R_{kk}\right)_3}{\left(\omega_3^2-\omega^2+2i\xi_3\omega_3\omega\right)}\end{aligned} \tag{1.55}$$

Where $\left(R_{kk}\right)_r$ are real quantities due to the fact that the damping is assumed to be proportional. Consider, for example, the first loop in figure 1.10. Recalling that each loop occurs for a frequency region close to the corresponding natural

frequency, then it may be assumed that, for a particular frequency range (1.55) can be approximated by

$$\alpha_{kk}(\omega) = \frac{\left(R_{kk}\right)_1}{\left(\omega_1^2 - \omega^2 + 2i\xi_1\omega_1\omega\right)} + B_{kk} \tag{1.56}$$

where B_{kk} is a complex quantity accounting for the contribution of the remaining modes to the total receptance value, which is dominated by the first mode. The first term of the summation plots as a circle with its centre on the imaginary axis, just like the receptance of a SDOF system. The only difference from a SDOF system is the fact that there is a real scaling factor (which alters the circle diameter), due to the existence of the modal constant $\left(R_{kk}\right)_1$ in the numerator. Summing a complex quantity B_{kk} will be produce a translation of the circle, displacing it from the original position. It is important to underlaine that this circle defines, through its geometrical characteristics, the modal damping of the MDOF. How it is possible to compute this modal parameter from the Nyquist plot is explained in the following chapter.

If we consider the situation where damping is non-proportional, it is not difficult to predict what is going to happen. The difference now is the fact that the modal constants become complex quantities, i. e., they have a magnitude and a phase. Thus, the circular loop displacement and scaling effect remain and are due to the contribution of the off-resonant modes and to the magnitude of the modal constant, respectively. In addition to the previous effects, the phase of the modal constants produces rotation of the modal loops which are no longer in the "upright" position, as illustrated in figure 1.10.

At least, the scaling problem we found when plotting the real and imaginary part of receptance versus frequency will also present here and make it difficult to understand a Nyquist plot of receptance covering the total frequency range of interest. The solution is use separate Nyquist plots, one for each natural frequency region. This is indeed performed when taking advantage of the

particular features of the Nyquist plots for the purpose of identifying system modal properties (see chapter 2).

CHAPTER TWO

Dynamic identification through methods in frequency domain

2.1 Introduction

The Forced Vibration Testing techniques, employed in Civil Engineering structures, constitute straight applications of the so-called Modal Analysis Techniques, which were born in the areas of Mechanical and Aeronautic Engineering some decades ago [Caetano, 2000]. These techniques are based on the application of a controlled and known excitation, and measurement of the response at a set of locations. Usually the excitation is a sinusoidal force, produced by an electromechanical shaker, and the response of the structure is recorded as acceleration through a set of accelerometers, dislocated on the building. From the set of excitation and response time histories, estimates of Frequency Response Functions (FRF's) can be obtained, in order to extract the most relevant dynamic parameters of the structure, i.e., the natural frequencies, modal shapes and damping coefficients [Balmes, 1997]. The definition of the modal parameters from the FRF is obtained by the following super position: all the response can be attributed to the local mode and any effect due to the other modes can be ignored [Inman, 1994]. In other words, in correspondence of every peak of the FRF a single degree of freedom system can be identified and it is not influenced from the other peaks. This kind of assumption can be used only when the structures exhibit well-separated modes which are not so lightly-damped that accurate measurement at resonance are difficult to obtain, on the other hand, are not so heavily damped that the response at the resonance is strongly influenced by more than one mode. This may be a limitation in very flexible structures, as cable-stayed bridge, that are characterized by very closely spaced in frequency mode shapes; in this case the required resolution is increased and frequency domain methods may be no longer efficient.

In this chapter the Peak-Picking method (PP), the circle-fit method and another method always in the frequency domain based on the construction of the Lissajous Diagram are described.

2.2 Peak-Picking method

The Peak Peaking or Peak Amplitude method (Pendered & Bishop, 1963) is based on the fact that the magnitude of the FRF (Receptance, Inertance or Mobility) has peaks at the resonant frequencies (in reality very close, but not exactly at these frequencies). The natural frequencies are then the frequencies that are associated with the peaks of the FRF magnitude. In particular the PP method is applied as follows:

(i) Individual resonance peaks are present on the FRF plot, each peak is a natural frequency of the system (ω_r).

(ii) The local maximum value of the FRF is noted $\left|\hat{H}\right|$ and the frequency bandwidth (Half-Power Bandwidth) for a response level equal to $\left|\hat{H}/\sqrt{2}\right|$ is defined ($\Delta\omega$). The two points thus identified as ω_b and ω_a are the half power points (see Figure 2.2.1 *Trend of FRF of a generic MDOF System* and Figure 2.2.2).

(iii) The damping for each natural frequency can be estimated by one of the following expression :

$$\eta_r = \frac{\omega_a^2 - \omega_b^2}{2\omega_r^2} \cong \frac{\Delta\omega}{\omega_r} \tag{2.1}$$

$$2\zeta_r = \eta_r \tag{2.2}$$

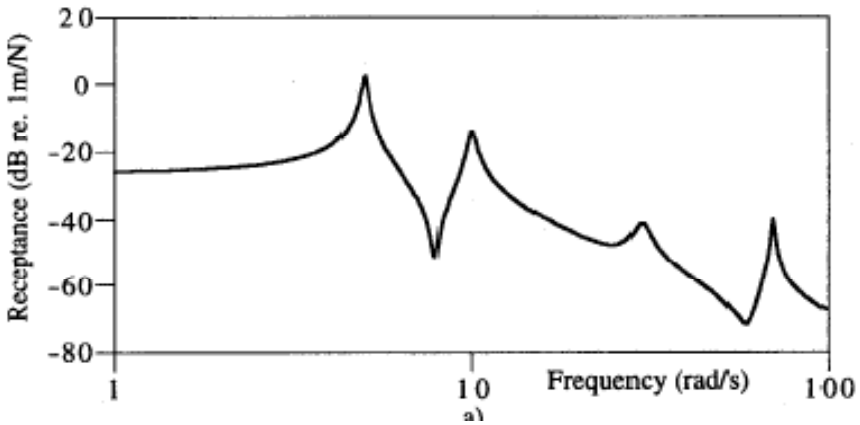

Figure 2.2.1 Trend of FRF of a generic MDOF System

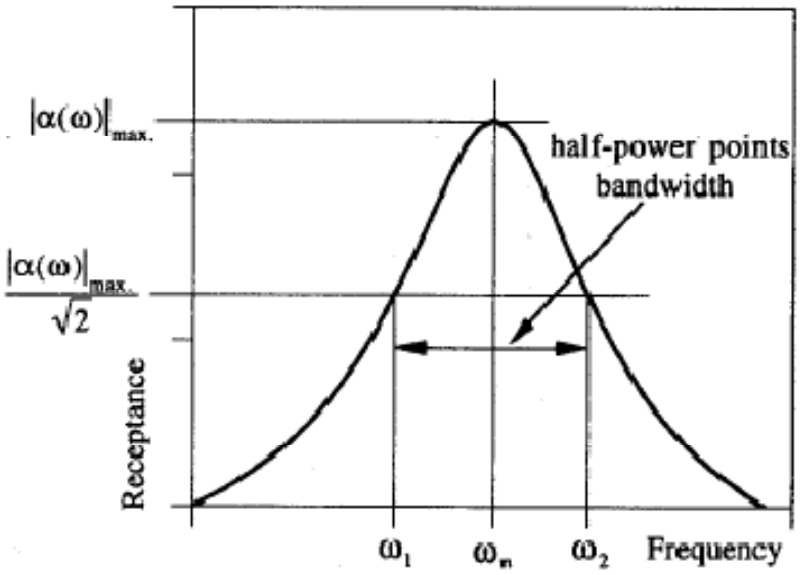

Figure 2.2.2 Half Power bandwidth

The modal components can now be estimated for the set of FRFs, taking the peak values of those functions at resonance. These are given, according to eq. 1.50, by

$$\left|\alpha_{ij}\left(\omega_r\right)\right| \cong \frac{\phi_{ir}\phi_{jr}}{2\zeta_r\omega_r^2} \tag{2.3}$$

So, starting with the diagonal terms, i.e., with the FRFs relating input and response measured at the same location, the following components are obtained

$$\begin{aligned} \phi_{ir} &= \sqrt{2\zeta_r\omega_r^2\left|\alpha_{ij}\left(\omega_r\right)\right|} \\ \phi_{jr} &= \sqrt{2\zeta_r\omega_r^2\left|\alpha_{ij}\left(\omega_r\right)\right|}\Big/\phi_{ir} \end{aligned} \tag{2.4}$$

Recalling that the mode shapes were assumed to be real, the phase of the components can only be 0° or 180° (positive or negative components, respectively). The sign is then determined comparing the phase of each FRF at resonance with the corresponding phase of the diagonal FRF.

An important aspect concerning the Peak Peaking method is that all the estimates concerning a mode shape are based only on three points from each FRF estimate. It is evident that this method is very sensitive to noise and also to the

level of damping present in the system. On the other hand, very low modal damping originates extremely sharp FRF peaks and consequently a very low precision in the damping estimates. A final difficulty can be expected in the application of the Peak Peaking method when mode shapes are very closely spaced in frequency, as the significant modal interference may then prevent the accurate identification of resonances.

Several procedures can be followed in order to obtain higher quality estimates of the modal parameters, such as the separation of signal components (torsion and bending, for example) or the successive elimination of the identified modal components.

2.3 Circlefit-method

The Circle-Fit method (Kennedy & Pancu, 1947; Klosterman, 1971) employs another interesting property of the SDOF FRF approach, which is the fact that the Mobility, as the Inertance or Receptance function describes a circle in the Nyquist diagram (i.e. real part versus imaginary part), the influence of the other modes being approximated by a complex constant.

Note that the SDOF approach is only valid in the neighbourhood of a resonance, hence the complete FRF will not be a complete circle around each resonance, but will be constituted by sections of near-circular arcs around those frequencies as shown in Figure 2.3.1(Maia & Silva, 1997).

To understand how this method works, it is possible to start from an ideal case, where a SDOF is considered. If the points in the neighbourhood of the resonance are plotted on a plane real part of FRF versus imaginary part a perfect circle is obtained, as it is possible to see in the Figure 2.3.2.

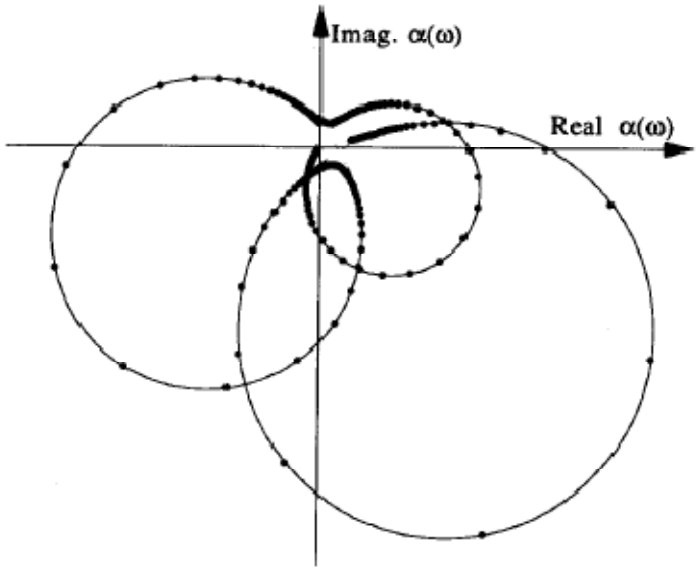

Figure 2.3.1 Nyquist plot of Receptance for a non-proportionally damped 3 DOF System

From this circle the modal damping of the system can be obtained by the following steps.

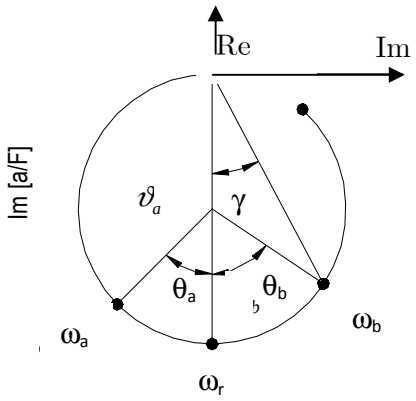

Figure 2.3.2 Nyquist plot for a single degree of freedom system

As it was previously said, this method starts from the assumption that in the vicinity of a generic resonance, the behaviour of most system is dominated by a single mode (the SDOF assumption). This can be expressed algebraically by the following formulae; for a generic MDOF the Inertance can be defines as follows

$$\mathrm{A_j}\left(\omega\right)=-\sum_{s=1}^{N}\frac{\omega^2\left(\mathrm{R_j}\right)_s}{\omega_s^2-\omega^2+2i\zeta_s\omega\omega_s} \tag{2.5}$$

The r-term, corresponding to a generic vibration mode r of the system, of the series can be extract and the inertance results represented

$$A_j\left(\omega\right)=-\frac{\omega^2\left(R_j\right)_r}{\omega_r^2-\omega^2+2i\zeta_r\omega\omega_r}-\sum_{s=1}^{N}\frac{\omega^2\left(R_j\right)_s}{\omega_s^2-\omega^2+2i\zeta_s\omega\omega_s} \tag{2.6}$$

Then, for the SDOF assumption, in a small range of the frequency, very close to natural frequency r of the system, the second term of the expression can be considered indipendent from the frequency and the equation can be written as

$$A_j\left(\omega\right)=-\frac{\omega^2\left(R_j\right)_r}{\omega_r^2-\omega^2+2i\zeta_r\omega\omega_r}-\left(R_j\right)_s \tag{2.7}$$

At this point to investigate on the modal properties of the Nyquist circle it is possible to start from the expression of the Inertance:

$$A_j\left(\omega\right)\cong-\frac{\omega^2}{\omega_r^2-\omega^2+2i\zeta_r\omega\omega_r} \tag{2.8}$$

As it can see from the comparison between eqs. (2.6) and (2.7), considering the eq. (2.8), the only effect of the modal constant $\left(R_j\right)_r$,which scales the size of the circle by $\left|\left(R_j\right)_r\right|$ and rotates it by its phase, is neglected.

The real and imaginary part of the Inertance function are represented from these equations:

$$\mathrm{Re}\left(A\right)=\frac{-\frac{\omega_k^2}{\omega_r^2}\left[1-\left(\frac{\omega_k}{\omega_r}\right)^2\right]}{\left[1-\left(\frac{\omega_k}{\omega_r}\right)^2\right]^2+4\zeta_r^2\frac{\omega_k}{\omega_r}} \tag{2.9}$$

$$\mathrm{Im}\left(A\right) = \frac{2\zeta_r \dfrac{\omega_k^3}{\omega_r^3}}{\left[1-\left(\dfrac{\omega_k}{\omega_r}\right)^2\right]^2 + 4\zeta_r^2 \dfrac{\omega_k}{\omega_r}} \tag{2.10}$$

Now, it may be seen that for any frequency ω, it is possible to write the following relationships:

$$\tan\gamma = \frac{2\zeta_r \left(\dfrac{\omega_k}{\omega_r}\right)}{\left[1-\left(\dfrac{\omega_k}{\omega_r}\right)^2\right]} \tag{2.11}$$

$$\tan\left(90-\gamma\right) = \tan\frac{\theta_k}{2} = \frac{1-\left(\dfrac{\omega_k}{\omega_r}\right)^2}{2\zeta_r \left(\dfrac{\omega_k}{\omega_r}\right)} \tag{2.12}$$

At this point we can select two different points on the Nyquist plot, before and after the natural frequency, respectively ω_b and ω_a. From the Figure 2.3.2 the following expressions are defined immediately:

$$\tan\frac{\theta_a}{2} = \frac{1-\left(\dfrac{\omega_a}{\omega_r}\right)^2}{2\zeta_r \left(\dfrac{\omega_a}{\omega_r}\right)} \tag{2.13}$$

$$\tan\frac{\theta_b}{2} = \frac{1-\left(\dfrac{\omega_b}{\omega_r}\right)^2}{2\zeta_r \left(\dfrac{\omega_b}{\omega_r}\right)} \tag{2.14}$$

These expressions yield:

$$\zeta_r = \frac{\omega_b^2 - \omega_a^2}{2\omega_r \left(\omega_b \tan\frac{\theta_b}{2} + \omega_a \tan\frac{\theta_a}{2} \right)} \tag{2.15}$$

or for lightly damping

$$\zeta_r \cong \frac{\omega_b - \omega_a}{\omega_r \left(\tan\frac{\theta_b}{2} + \tan\frac{\theta_a}{2} \right)} \tag{2.16}$$

It is interesting to note that selecting the half power point are those frequencies for which $\theta_a = \theta_b = 90^\circ$, we have

$$\zeta = \frac{\omega_a - \omega_b}{2\omega_r} \tag{2.17}$$

2.4 Lissajous diagram

The method described in this chapter can be used to analyze signals acquired during a forced vibration test in situ. In fact this methodology can be applied only when the input of the structure is known. To explain this, we consider at the beginning an ideal case, where the signal input, expressed in eq. (2.18), and the signal output, defined in eq. (2.19), are two perfect sine functions.

$$\mathrm{x(t)=Asin(wt+f_1)} \tag{2.18}$$

$$\mathrm{y(t)=Bsin(wt+\varphi_2)} \tag{2.19}$$

Initially, an input and output with the same frequency equal to $\omega=2\pi f_v$ are considered, also each signal is defined by a sample step $\Delta t = 4/(N f_v)$ and a number of sample points equal to N = 256.

If a curve where the x value are the point of the sine function 1 and the y value are the points of the sine function 2 is plotted, a perfect ellipse is obtain because the frequencies of the two compared signals are the same. In fact the eqs. (2.18)

and (2.19) are exactly the parametric equations of a generic ellipse, centred in the origin of the reference system. A generic case, defined by the eq. (2.20), is considered

$$\begin{aligned} x(t)&=10\sin(2\pi f_v t+\pi/6) \\ y(t)&=7.5\sin(2\pi f_v t-\pi/4) \end{aligned} \tag{2.21}$$

with $f_v = 1.3$ Hz.

Plotting the graph XY, as previously described, the following Lissajous diagram is obtained.

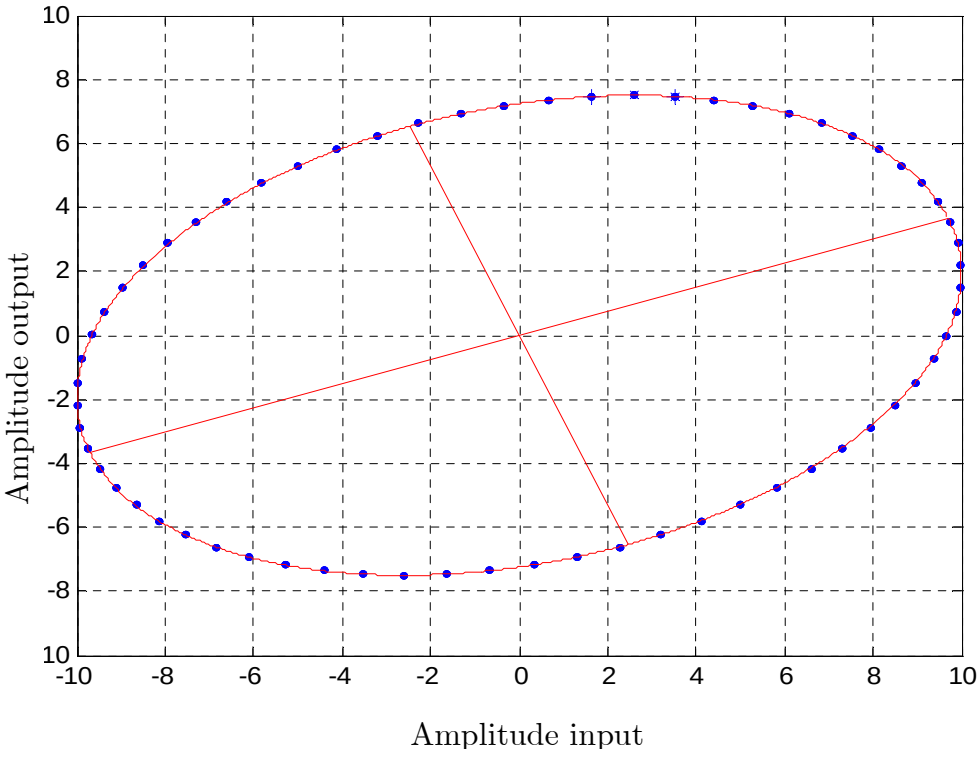

Figure 2.4.1 Trend of ellipse in the ideal case

From this ellipse it is possible to define the ratio between the amplitude of the two signals and their phase displacement [Heath, 2000]. In particular the amplitude ratio, as it is noticeable from eq. (2.22), is defined by the ratio between the length of the two semi axis, the phase displacement depends on the inclination of the major axis and its module is obtained from the arcsine of the ratio between the maximum y-value of the points of the ellipse (A) and the y-

value corresponding to the zero x-value (B), as it is represented in the following figure [Su et al., 2004; Su et al., 2005].

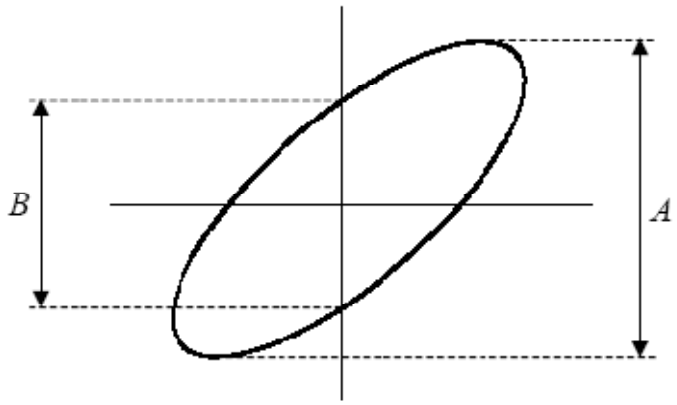

Figure 2.4.2 Definition of phase displacement

The limit of this representation is the impossibility determining the sign of the phase displacement. To obtain it, it is necessary to verify on the one hand if the points which describe the ellipse rotate clockwise or counter clockwise, and on the other hand which quadrant cuts the major axis. In particular the following four cases can happen:

(i) Case 1 major axis cuts the first and third quadrant and the points rotate counterclockwise $0 < \Delta\varphi' < 90 \rightarrow \Delta\varphi = \Delta\varphi'$

(ii) Case 2 major axis cuts the first and third quadrant and the points rotate clockwise $0 < \Delta\varphi' < -90 \rightarrow \Delta\varphi = 2\pi - \Delta\varphi'$

(iii) Case 3 major axis cuts the second and fourth quadrant and the points rotate counterclockwise $90 < \Delta\varphi' < 180 \rightarrow \Delta\varphi = \pi - \Delta\varphi'$

(iv) Case 4 major axis cuts the first and third quadrant and the points rotate clockwise $-90 < \Delta\varphi' < -180 \rightarrow \Delta\varphi = \pi + \Delta\varphi'$

When $\Delta\varphi = 90°, 270°, 360°$, the ellipse has the semi-axis coincident with the axis of the reference system. In particular the ellipse becomes a circle, centred in the system origin.

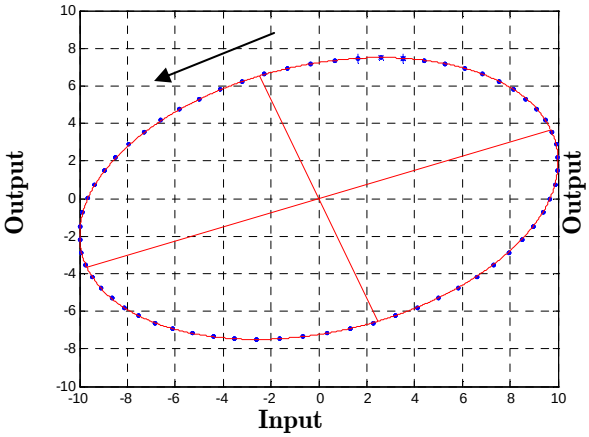

Figure 2.4.3 Case (i)

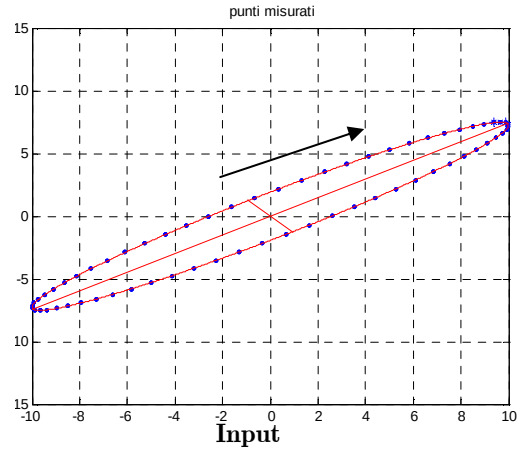

Figure 2.4.4 Case (ii)

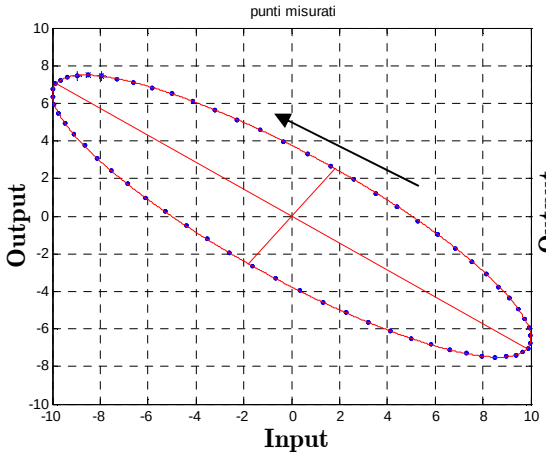

Figure 2.4.5 Case (iii)

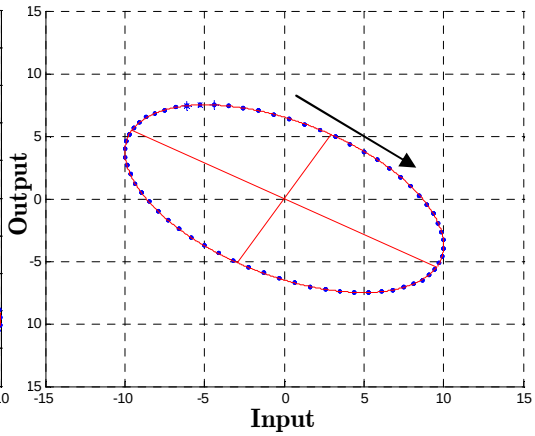

Figure 2.4.6 Case (iv)

At this point it is important to see what happens when the two signals are expressed by the following relation

$$\begin{aligned} x(t) &= X_0 + A\sin(wt + \varphi_1) \\ y(t) &= Y_0 + B\sin(wt + \varphi_2) \end{aligned} \tag{2.23}$$

Until now always a centres ellipse is considered, where $X_0 = Y_0 = 0$. Through eq. (2.23) an ellipse, shifted from the origin, is considered. As Figure 2.4.7 shows, this condition does not modify the amplitude ratio and the phase displacement.

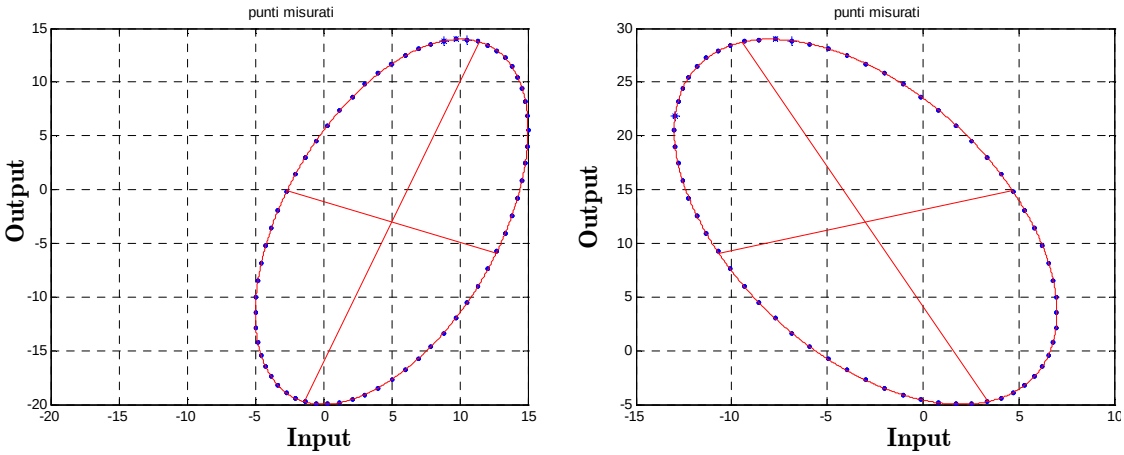

Figure 2.4.7 Ellipse not centred with different axis orientation

The last particular case is obtained when $\Delta\varphi = 0$, the ellipse becomes a straight line and its inclination defines the amplitude ratio between the two signals compared.

Now it is important to understand what happens when the two signals have different frequencies. At the beginning the simpler case, where the input frequency is a multiple of the output one, is considered. In the following figures the Lissajous Diagrams are represented when the natural frequency of the output is twice than the natural frequency of input. In the first graph the two signals have the same phase and amplitude, in the second graph there is a phase displacement between the two signals equal to 30° and they do not have the same amplitude. The graphs are very different from the ellipse and for this reason it is not able to define the amplitude ratio or the phase displacement, as illustrated before.

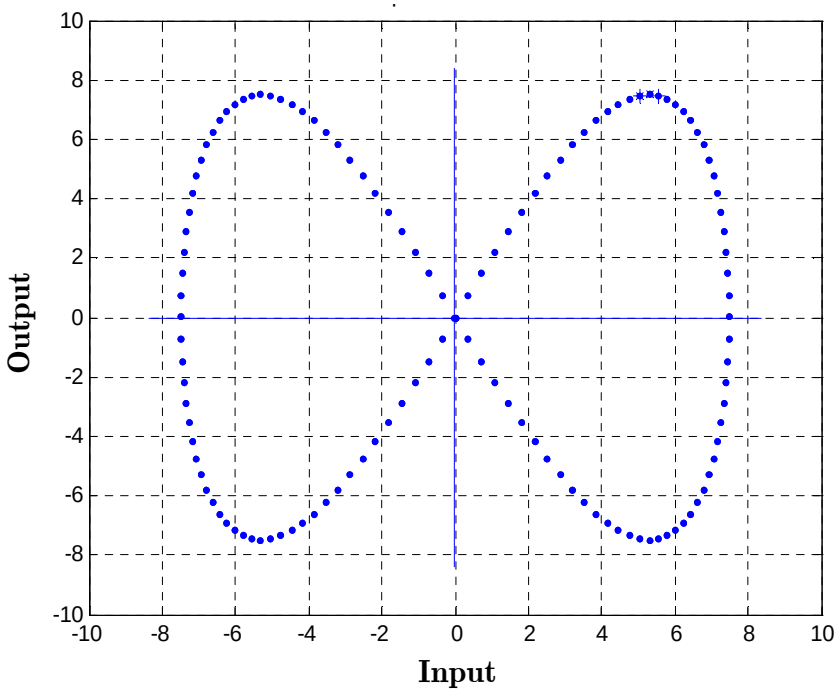

Figure 2.4.8 Lissajous Diagram; frequency output is twice frequency input, no phase displacement

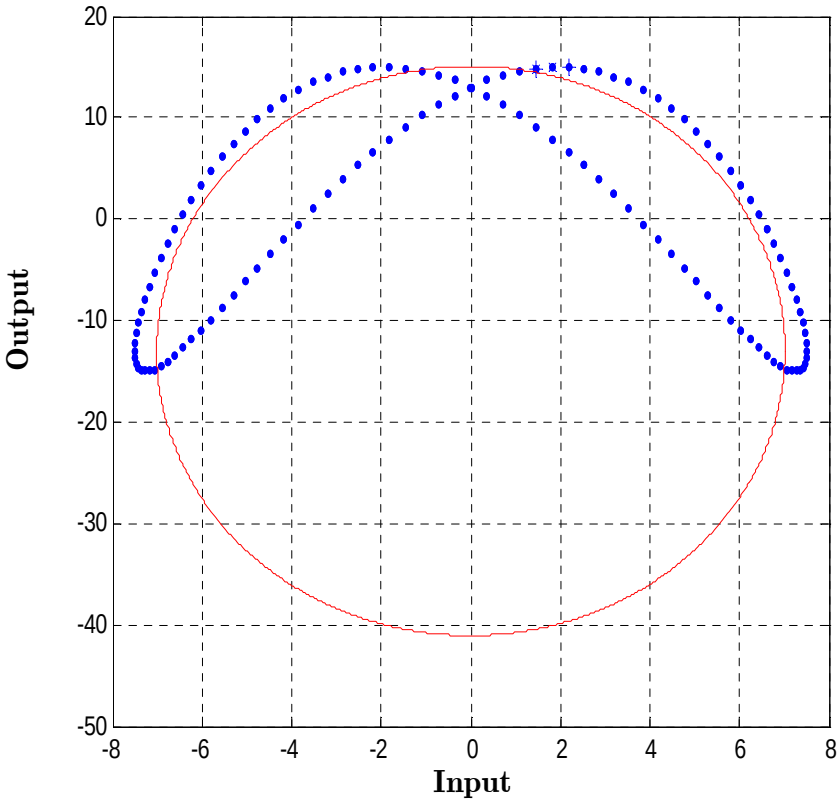

Figure 2.4.9 Lissajous Diagram; frequency output is twice frequency input, phase displacement equal to 30°

Below some Lissajous Diagrams for different frequencies ratio between the two signals are reported.

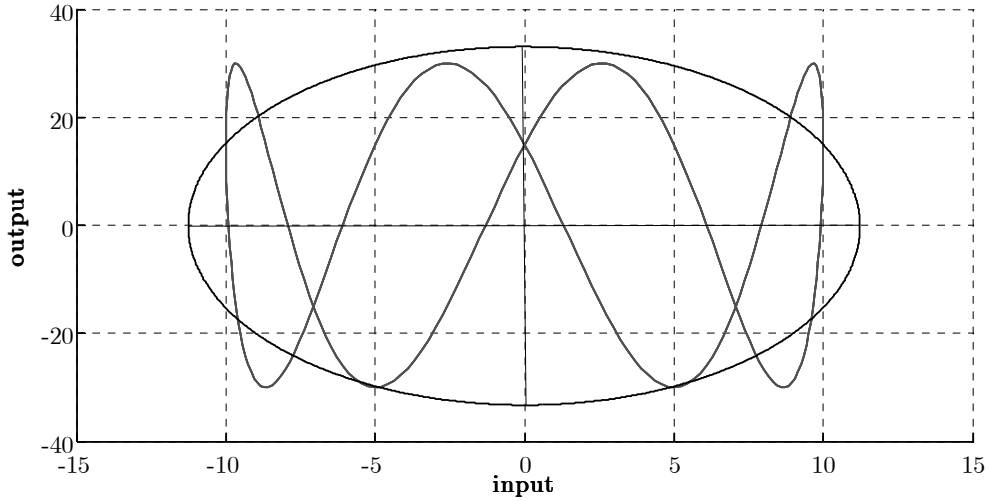

Figure 2.4.10 Lissajous Diagram, frequency ratio equal to 0.25, phase displacement equal to 30°

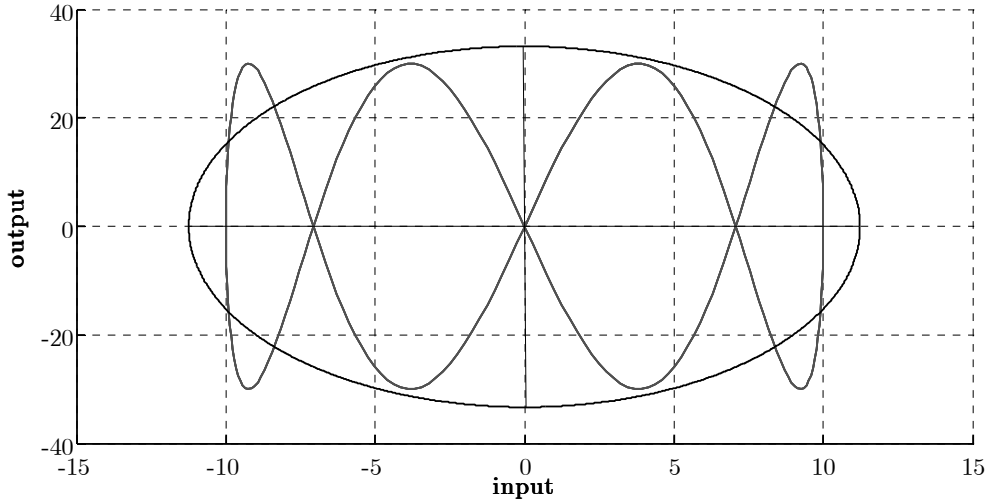

Figure 2.4.11 Lissajous Diagram, frequency ratio equal to 0.25, no phase displacement

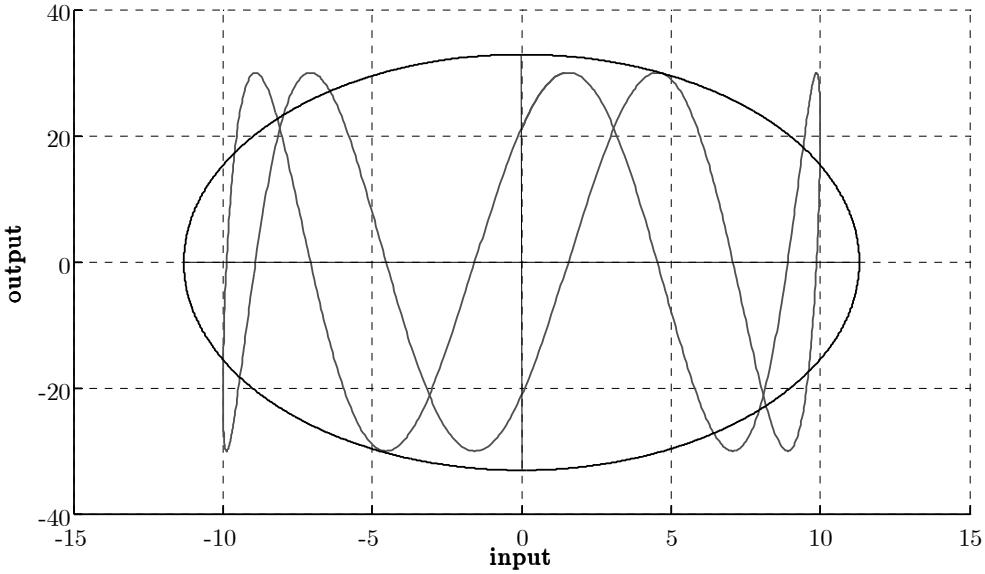

Figure 2.4.12 Lissajous Diagram, frequency ratio equal to 0.2, phase displacement equal to 45°

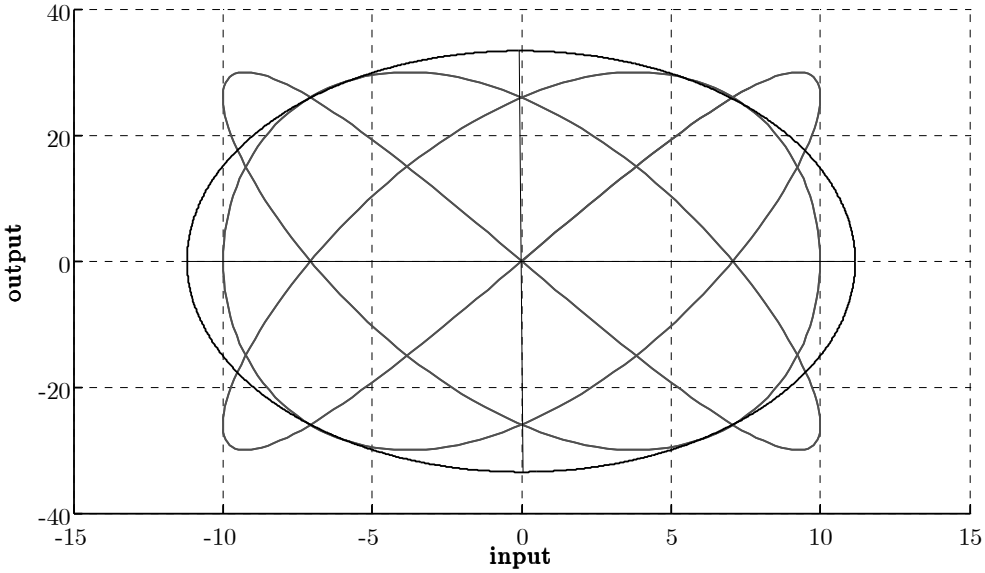

Figure 2.4.13 Lissajous Diagram, frequency ratio equal to 6:8, no phase displacement

From these figures it is noticeable that the frequencies ratio is equal to the ratio between the number of points with maximum y-value (factor frequency output) and the number of points with maximum x-value (factor frequency input). Moreover the amplitude ratio is obtained from the ratio between the major and minor sides of the rectangle that circumscribes the curve. The principal difficulty

is the computation of phase displacement, really complicated to define from this kind of curve. For this reason we take a step back and we try to define a theory that consider the possibility, with of course some necessary approximations, to define the parameter before described always from an ellipse.

2.4.1 Application in a real case

In this paragraph, considering what has been highlighted up to this point, the method is developed investigating a real case, as the signal acquired during a forced vibration test carried out on an existing structure. Under this circumstance the input signal is a perfect sine function that can be expressed by the following equation

$$F = 1.026\, f_v^2 \cos\frac{\alpha}{2} \sin\left(2\pi f_v + \gamma + \frac{\alpha}{2} - 86.9°\right) \tag{2.24}$$

Then its amplitude is $1.026\, f_v^2 \cos\frac{\alpha}{2}$ and its phase is $\left(\gamma + \frac{\alpha}{2} - 86.9°\right)$.The output is the response of the structure (see Figure 2.4.14), recorded as acceleration thought some accelerometers. So we have tried to define the Lissajous diagrams for this kind of signal. We start to consider what happens near the resonance, where the response of the structure is clearer and similar to a sine function.

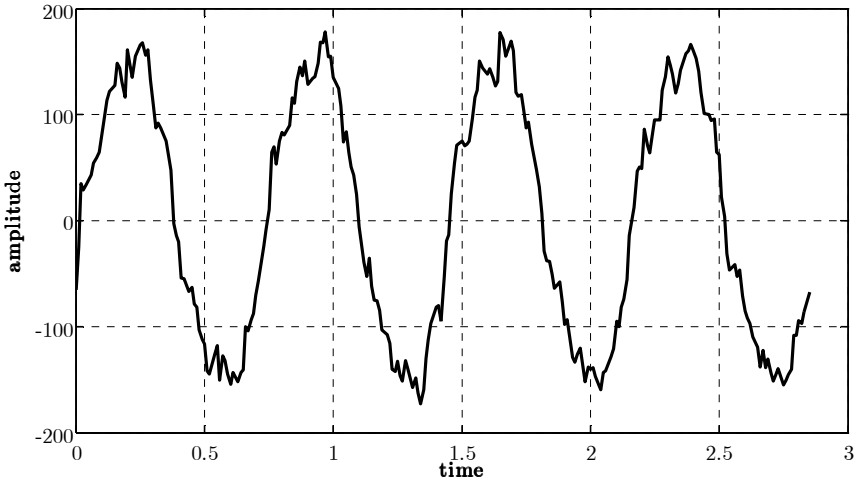

Figure 2.4.15 Example of acquired signal

In the real case the output signal is not a harmonic signal, then the points that define the Lissajous diagram does not describe a perfect ellipse and they tend to move away the perfect ellipse all the more the signal acquired is different from an harmonic response. To define the parameters which allow comparing the two signals, we decide to fit these points with the ellipse that better approaches its trend. Obviously this kind of approximation is valid when we are near the resonance; it becomes really strong far from it. In the next figures the comparison between the results obtained near the resonance and far from it are illustrated.

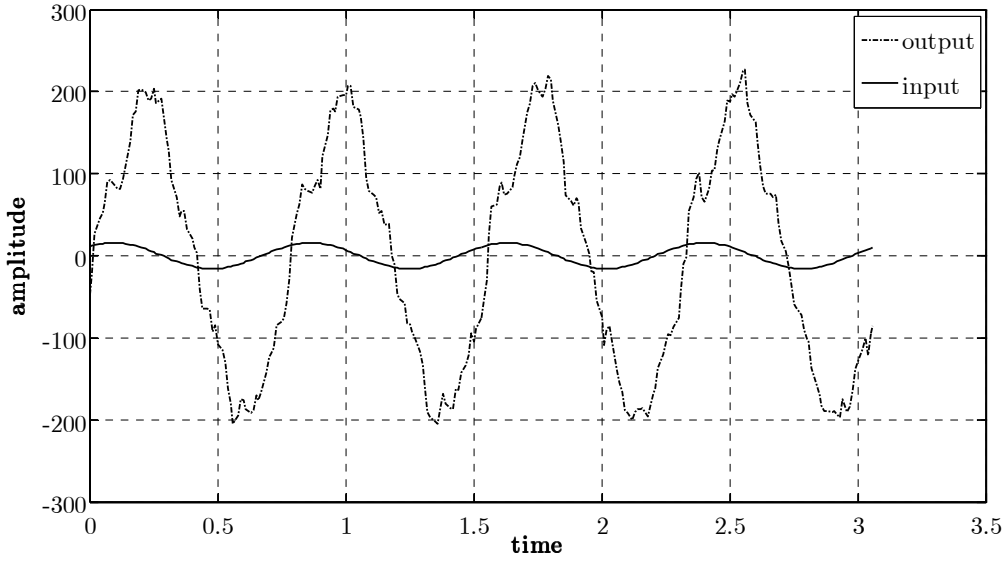

Figure 2.4.16 Trend of input and acceleration acquired from an accelerometer at frequency near the resonance

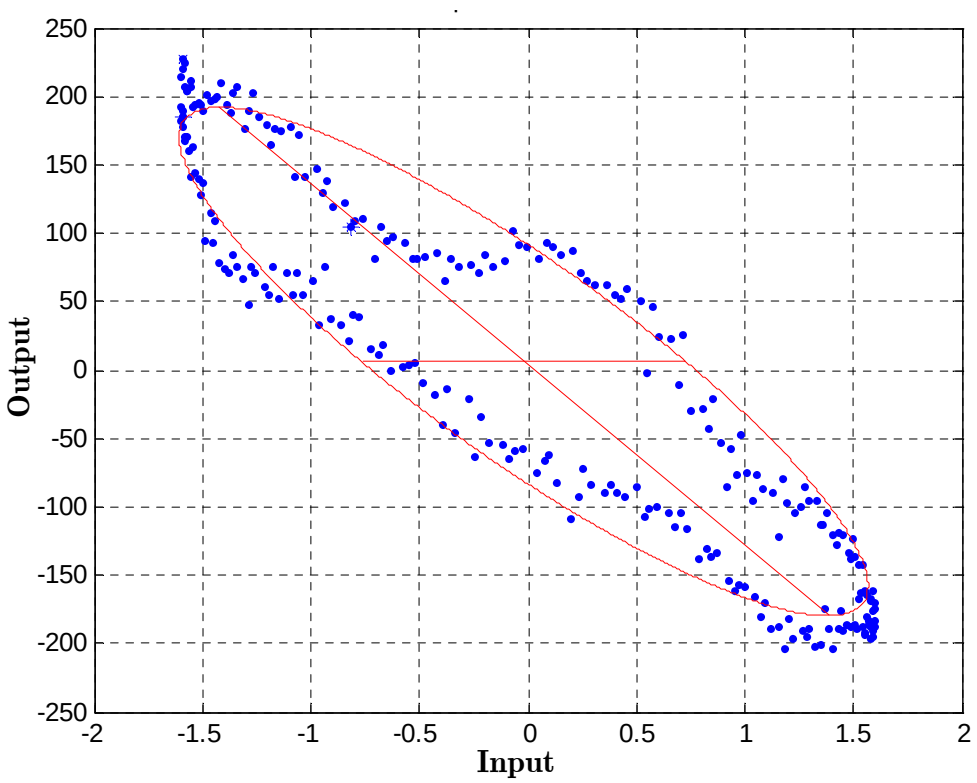

Figure 2.4.17 Representation of the two signals in the plane input-output; corresponding ellipse

Far from the resonance the sample points that describe the signals acquired, are distribute almost randomly, below an example is reported.

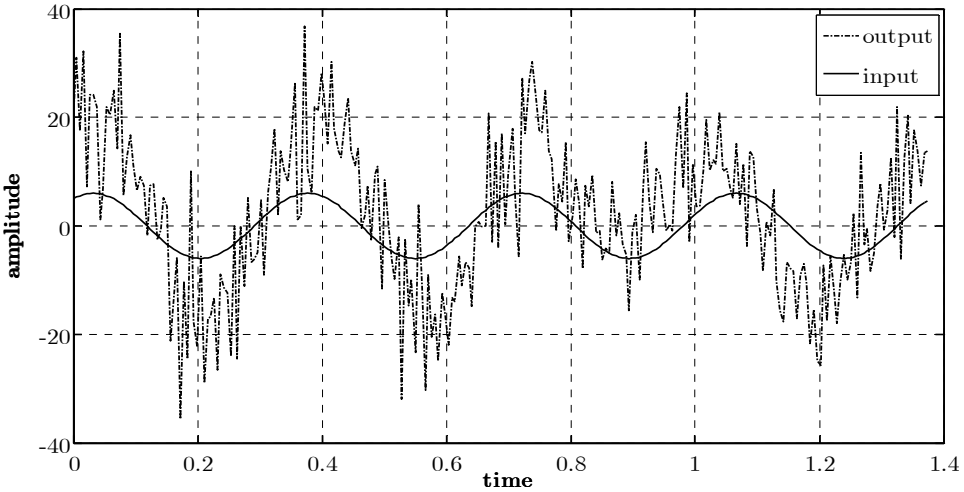

Figure 2.4.18 Trend of input and acceleration acquired from an accelerometer at frequency far from the resonance

In the plane input-output the points are very far from the ellipse that better approach it, as it is illustrated in the following figure.

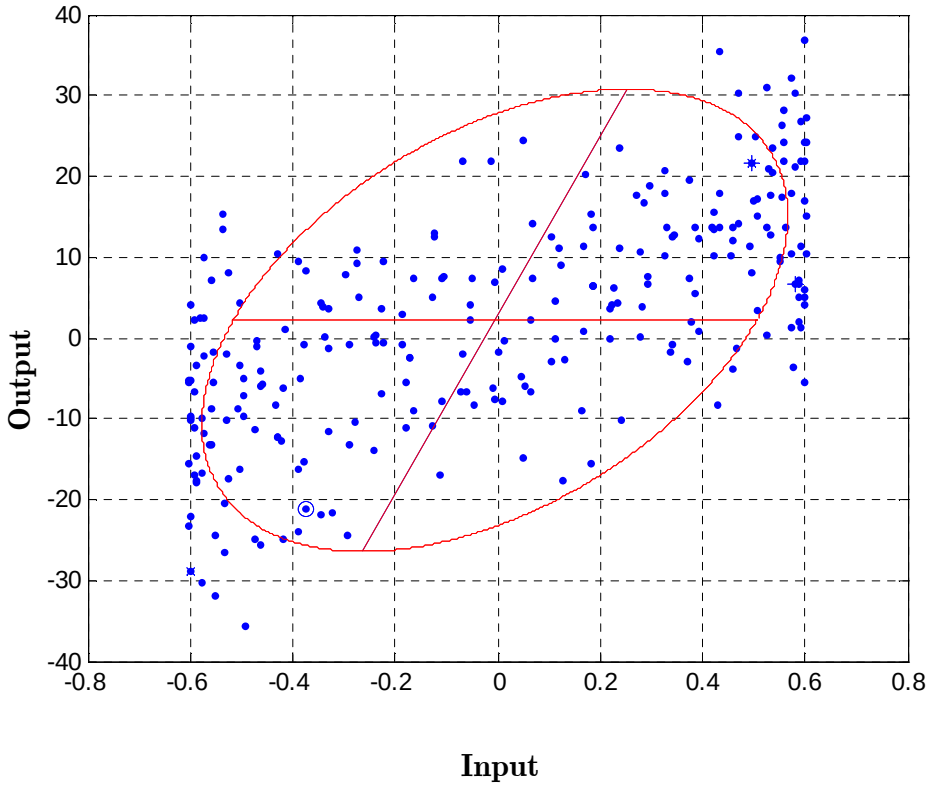

Figure 2.4.19 Representation in plane input-output

We would like to underline that almost the same problem occurs with the classical computation of the FFT. As the figure below illustrates, for a signal acquired at a generic frequency not close to the natural frequency the FFT plot is very irregular, and the amplitude of the of the different cosine functions, which decomposed the original signal, are important for different value of the frequency. When we define a point of FRF only the peak corresponding to the input frequency is considered, the other components are completely ignored. The consequent error is always neglected.

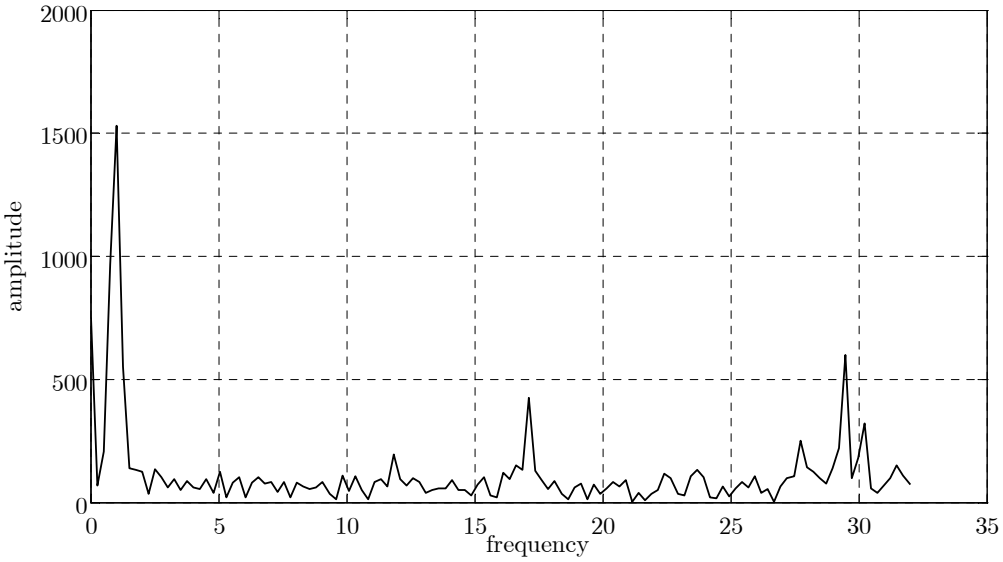

Figure 2.4.20 FFT of a signal with noise

2.5 Procedures applications

The aim of this chapter concerns the analysis and comparison of those modal parameters which are obtained by assessing two forced vibration tests, experienced on a laminated timber footbridge. The two tests were carried out five years apart to verify if the dynamic characteristics of the structure change considerably during its use. In particular, modal damping of the footbridge increases (that means an effective structural deterioration), whereas modal frequencies are substantially constant. It is noticeable that the analysis of the first test [Diotallevi et al., 2000] highlighted that the natural frequencies of the structure were included in the range between 1 and 2 Hz, more similar to the frequency of the human step. This can entail possible amplifications of the oscillations of the structure during the passing of pedestrians (low comfort level for users). The analysis of the structural durability is necessary because the ordinary maintenance of the footbridge is not usually made, although the structure is subject to hard weather condition.

In particular to both the data, acquired from the two forced test, the procedures previously described are applied and a comparison between the results, in terms of FRFs, are illustrated.

2.5.1 Introduction

Over the last thirty years timber bridge and footbridge have found considerable use especially by their versatility, good durability and pleasing aesthetic view. First the development of new technology and materials, as the laminated timber, second the use of innovative buildings, assembling and connection techniques and third the expansion of efficient, certain and inexpensive products for timber protection, have allowed the employ of this type of building.

The objective of this paper is on the one hand the definition of the dynamic behavior of an arc footbridge, constituted by laminated timber, to estimate its response to dynamic action, as wind, pedestrian action order seismic action which can affect the structure during its using; on the other hand to trace the possible structural damage by the analysis of its dynamic parameters in different periods of the life-time of the structure. The footbridge is realized mainly in laminated timber to satisfy the following requirement: unfavourable weather conditions, high exposure to the sun, limited aesthetical impact. The durability and the resistance to weather conditions are natural characteristics of the laminated timber, this behaviour is improved by several and specific treatments to which the material is subject during the manufacturing process. The laminated timber is completely immune from mildews and mushrooms trough specific impregnated products and periodic maintenance and it is able to resist to hard weather conditions. The laminated timber was used with good results in very wet environments, in places near the sea, so in marine ambient (as in this case), on the upper mountain and in places characterized by considerable temperature range. Furthermore, it was necessary to build the footbridge with a high span, because the river, that the structure crosses, is very dangerous. The Marecchia river is extremely irregular and is often subjected to flash flood, then the structure is bounded far from the dock of the river. The footbridge reaches a span

of 93 meters about in order to satisfy the requirement of safeguard the life of the users and to avoid that possible flood of the river can compromise the structural functionality. In this context the laminated timber was chosen first of all for its lightness (the specific weight of the laminated timber is 1/5 of that of RC) and was preferred to the steel because this material resist better in extern ambient than the steel and is not as deformable as the steel (its thermal expansivity is 1/3 of that of the steel) and its resistance to fire is better than the remaining materials. Finally, the footbridge is part of a naturalistic cycle-pedestrian route and constitutes the entrance on the inside of the Marecchia park and the use of the timber permits a correct integration of the structure in the context where was built and minimizes the impact assessment.

The peculiarity of the structure and the uncertainty about the mechanical characteristics of the main material used, involves the necessity to investigate about its dynamic behavior by dynamic tests. To this purpose, the University of Bologna performed a dynamic test by vibrodyne on the footbridge immediately after the lunch of the structure. Trough this test the assumptions about the structural dynamic behavior at the planning phase were compared with the real behavior of the footbridge. In particular, a good correspondence between the experimental results and the results relating to a fem modellation of the structure is achieved, in fact similar natural periods are obtain (see table 1).

e deck

The University of Bologna carried out after five years a second dynamic test, very similar to the previous one (the first test was replicated both by the same setting and positioning of the recording sensors of the structural response, both by the definition of the same exciting forces), to study the variation of the dynamic behaviour in the meantime. In general, the knowledge of the response of structural system, subject to sinusoidal forces, yields useful indications both for an improvement of the design quality of new structures, both to investigate on the behaviour of existing building. In this paper the dynamic identification was used trough both its functions.

2.5.2 Footbridge description

The footbridge is represented by one-span arch of about 93 m, crossing a river in the city of Rimini; more precisely the main structure consists of a twin arch of section 22x182 cm which bears the lower horizontal deck by means of vertical ties. The trampling level, made in timber, leans on two laminated timber truss of section 22x200 cm. The maximum height of the arc is about 13 meters and its radius of curvature in the vertical plane is 95 meters. The width of the footbridge is about 12 m. Steel cables, constituted by bars of diameter of 50 mm, connect the two arcs to contrast the horizontal loads. Furthermore, under the trampling level is located a steel reticular, of which the upper and lower elements are the laminated timber trusses previously described. The entire bridge is made with laminated timber, with the exception of the connectors (plates and bolts of zinc

coated steel) and of the whole frame beneath the walking floor aimed to increase the lateral stiffness.

The bridge is conceived for people walking and also for electrical and water transportation. If the electrical cables do not interact with the structural performance of the bridge, water pipes represent a considerable amount of the total load of the structure as shown in table 1. Each part of the bridge was pre-manufactured (in particular the laminated timber trusses were impregnated before its installation by specific chemicals, which protect it from the attack by atmospheric conditions), then shipped and assembled in the final place. Finally specific varnishes were put on the elements by painting to protect the timber from the attack by mildews, mushrooms and humidity. One day was required to erect the bridge and to put it on the concrete basement by using two cranes.

Table 1 Footbridge weights

Deck weight	Wooden floor 500x0,04	0,20 kN/m2
	Main deck beam 475/(4,0x5,14)	0,231 kN/m2
	Secondary deck beam 0,16x0,2x500x5/5,14	0,1556 kN/m2
	Hand-rail 0,12x0,15x500/5,14	0,0175 kN/m2
	Lower steel beams (IPE 160) 3x15,8/4,00	0,1185 kN/m2
	TOTAL	0,7226 kN/m2
Plant weight	Tube 500x6 (empty) 78,2/5,14	0,1521 kN/m2
	Tube 300x6 (empty) 46,2/5,14	0,0899 kN/m2
	Enel cables 12,7x(6+10+2,0+0,5)/5,14	0,1726 kN/m2
	TOTAL	0,4146 kN/m2
Water weight	Water weight (tube 500)	0,3637 kN/m2
Total weight		1,5009 kN/m2

2.5.3 Experimental set up

In both tests, the footbridge was subjected to horizontal and vertical forces, time dependent by a sinusoidal law, with the mechanical shaker, which is available at

the Laboratory of the Structural Engineering Department (Distart) of the University of Bologna. In the first test the instrumentation used to measure the footbridge response, recorded as acceleration, that was constituted by seven piezoelectric accelerometers PCB/393B12 whose voltage sensitivity is 10 V/g and three piezoelectric accelerometers PCB/393B12 whose voltage sensitivity is 1 V/g. In the second test the instrumentation was constituted by eight piezoelectric accelerometers PCB/393B12 and two piezoelectric accelerometers PCB/393B12 . The instruments were connected, through a signal conditioning unit, to a computer for data processing and recording (the data acquisition and processing were obtained by Labview).

The mechanical shaker (see is Figure 2.5.3) a device that, firmly attached to the construction, allows the application of sinusoidal time varying forces. It is constituted by masses mounted eccentrically on two disks rotating in opposite directions at the same phase and frequency of rotation fv; each disk has two eccentric masses, whose relative angle may be changed from 46° to 180°.

Figure 2.5.3 The electromechanical shaker

In this manner, the magnitude of the applied force F(t) can be varied to achieve various force capabilities, up to the maximum value of 20 kN. The amplitude and the phase of the sinusoidal generated force depend on some characteristic

parameters of the machine; relating to the shaker ISMES of Bergamo the applied force F(t) can be written by the following relation:

$$\begin{aligned} F(t) &= 1.026\, f_v^2 \cos \alpha/2 \; sen\left(2\pi f_v t + \alpha/2 - 86.9^{\circ} + \gamma\right) = \\ &= 1.026\, f_v^2 \cos \alpha/2 \; sen\left(2\pi f_v t + \varphi\right) \end{aligned} \tag{2.25}$$

where ø is the phase angle of the phasemeter signal and 86.9° is the phase displacement between the fixed mass and the position of the phasemeter. With reference to the axis linking the counter-rotating disks centers, whose positive direction is oriented towards the disk on which the phasemeter is mounted, the applied force phase angle $\varphi = \alpha/2 - 86.9^{\circ} + \gamma$ is measured counter clockwise looking from above the shaker. The shaker (Figure 2.5.3) has been placed on the footbridge deck to furnish both horizontal forces having transversal direction with respect to the footbridge axis (position 1 in Figure 2.5.4) and vertical forces (position 2 in Figure 2.5.4). The locations of the instruments and shaker are depicted in figures 3a for position 1 and 2 of the shaker, relating 2000 test, and in fig 3b for position 1 and 2 of the shaker, relating to 2005 test. The accelerometers are marked with labels A1, A2, …, A10. For example, for the first test in position 1, the accelerometers measure transverse movements with the exception of accelerometer A10, which is mounted in vertical direction, whereas in position 2, all accelerometers are placed vertically. It is noticeable that only the accelerometers A3 A4, A6 and A9 with horizontal shaker and A1, A3, A4, A5, A6, A7, A8 end A9 with vertical shaker are located in the same position in the two tests. In particular, in 2005 every accelerometer was placed on the arcs, because during the test there was a high wind. In particular in Figure 2.5.4 and Figure 2.5.5 the accelerometers, placed on the arcs, are highlighted by red colour.

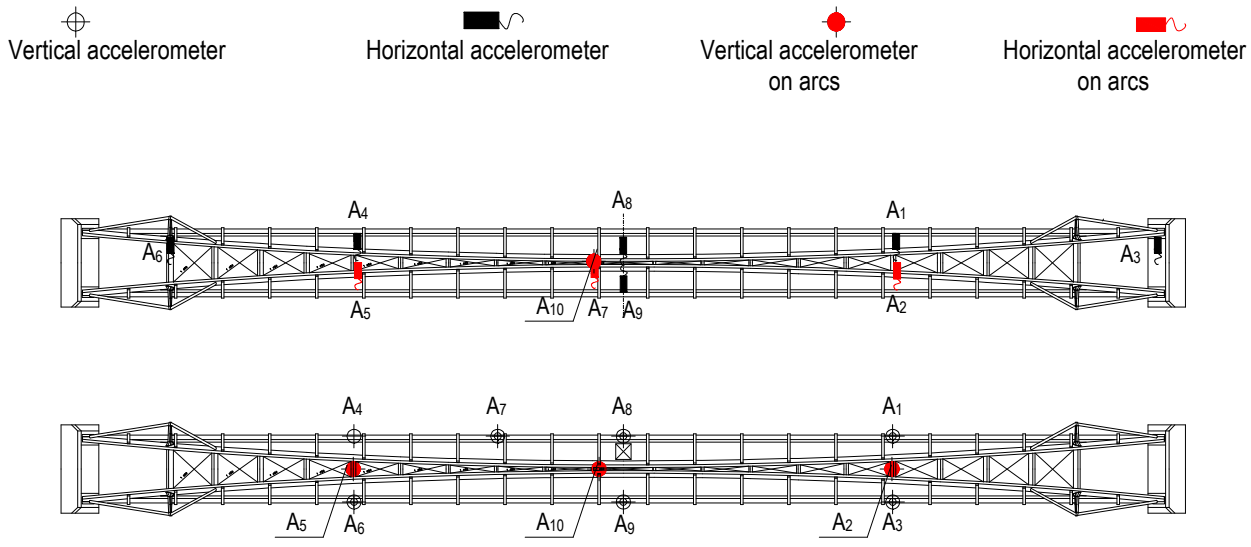

Figure 2.5.4 First test: instruments and shaker layout for position 1 and 2, respectively.

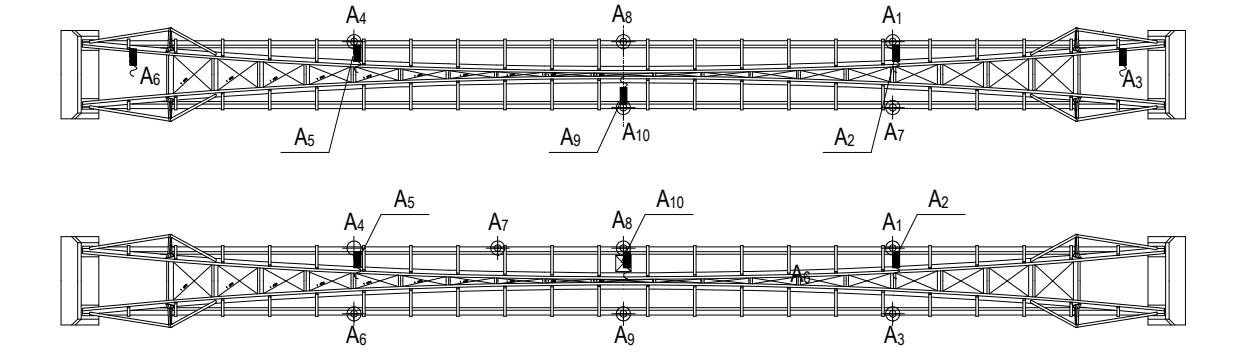

Figure 2.5.5 Second test: instruments and shaker layout for position 1 and 2, respectively.

In the first test the frequencies in the 0.7 – 7 Hz range were considered, whereas in the second test the frequencies in the 0.6 – 8 Hz range were analyzed, with different values of the angle α between the two masses. The frequency step is 0.1 Hz and becomes 0.05 Hz only by the resonance. The latest difference between the two trials is the number of sample points (N); in the first test were sample for each acquired signal a number of point N = 256 , equal to four cycles of the force, in the 2005 test N is 1024 , corresponding to sixteen cycles. An example of the different acquired signals is showed in fig 4. The theorem of Shannon or Nyquist is respected in the choose of the samples number for either cases.

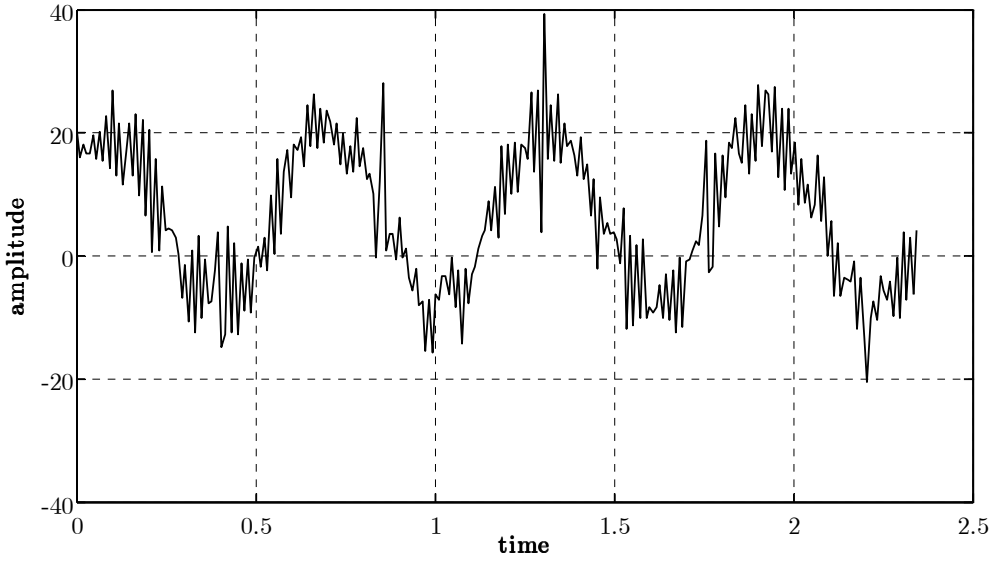

Figure 2.5.6 Sample signals in the first test

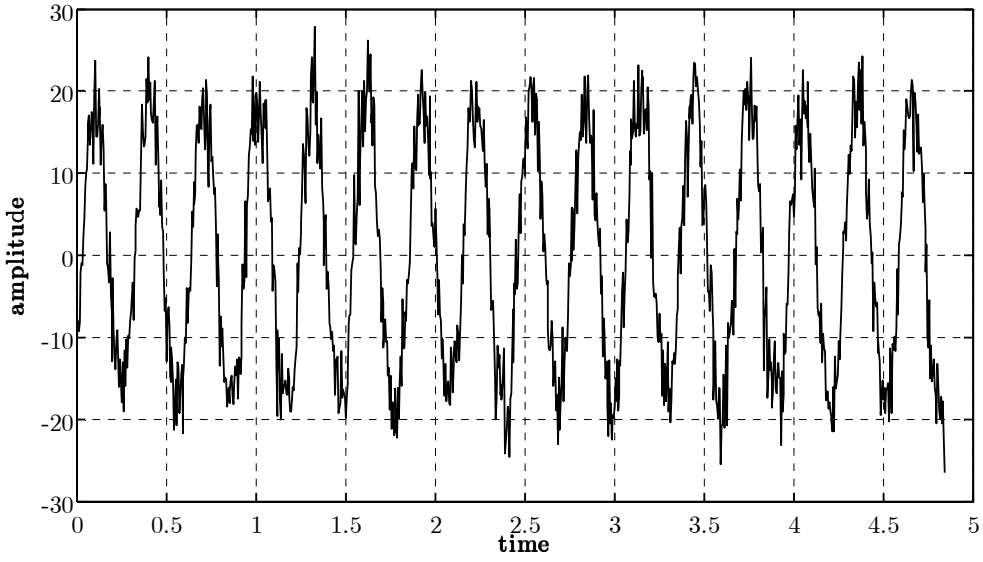

Figure 2.5.7 Sample signals in the second test

2.5.4 Extraction of modal parameter through FFT

The goal of this section is the comparison between the modal parameters, extracted from forced vibration test, that are obtained by two methods both in the frequency domain. A forced vibration test is carried out on a laminated

timber footbridge, whose span is about 93 meters, crossing the river Marecchia in Rimini.

The first method is based on the construction point by point of the FRF (inertance) through the computation of the Fast Fourier Transform (FFT) of the output signal, acquired as acceleration. When the FRF is defined, the modal parameters of the system are extracted through the classical Peak Picking method or circle-fit.

For the same structure, afterwards, the FRF is defined not by the FFT but by a direct comparison between the signal acquired in output and the signal in input. The amplitude of the sampled points, that represent the output signal, is represented along the y-axis and the amplitude of the input (perfectly sinusoidal in a forced vibration test) is represented along the x-axis in a generic plane input-output. In the plane the two signals are evaluated at the same frequency. These points tend to trace an ellipse in resonance and the geometrical characteristics (length of major axis and its inclination) of the ellipse that better approaches this trend can define the module and the phase of the FRF.

The correlation between the structure reply registered in correspondence of each accelerometer and the perfectly sinusoidal force applied by the vibrodyna can be observed for both the tests. The assumption is that, in the real resonance frequency, the structure reply will be almost sinusoidal and will be greater than the applied force. The computation of r^2 defines the distance between the points, relating to the real case, and the ellipse that better approaches their distribution. Then r^2 can be an index, that estimates the quality of the signal acquired, and can be used to define which is more probable natural frequency of the system when the FRF is constituted by very proximal peaks.

Computation of natural frequencies

The extraction of the modal parameters of the studied structure was done trough a method in the frequencies domain. In detail, to describe the points, a FRF is computed (the inertance, because only accelerations are considered): it represents

how the ratio between the structure behaviour (registered by some accelerometers) and the related force applied by the vibrodyna changes with the frequency variations. If there are many different vibration modes and if the damping factor is low, then the natural frequencies of the structure are found in correspondence to the inertance peaks.

Because, as already said before, the structure was forced by sinusoidal forces, for each exciting frequency fv, the ratio is, more in detail, between the amplitude of the acceleration harmonic part a(t) and the greatest intensity of the force F(t) described in the equation (2.25).

The computation of the sinusoidal force amplitude and phase is easy using the equation (2.25), while to define the a(t) amplitude and phase its Fourier transforms are computed. Thus is possible because in both the dynamic tests the points number is raised to the power of two, for computing the discrete Fourier transform the Fast Fourier Transform algorithm (FFT) is applied, that allows a great time-saving because it significantly reduces the number of the computations (for N= 1024 a computation that is 102 times faster than the standard one can be obtained). Therefore, the inertance is computed in module as the ratio between the fast Fourier transform of the accelerometer registration a(t) and the force amplitude, both considered at the same exciting frequency f_v. Because the FFT is a complex function (defined by both a real and a imaginary part or, instead, by a module and a phase), the FRF are represented both in module and in phase; the FRF phases diagram represents how the angle phase displacement between the structural behaviour and the applied force varies with the frequency variation, or, in other words, it represents the difference between the phase of the FFT of the acceleration and the force phase. Below the inertance trend is shown; it is represented in module by the ratio a/F and the phase φ[a/F], computed for the accelerometer 4 with the vibrodyna set in position 1, both for the 2000 test and for the 2005 one, and the accelerometer 3 with the shaker position 2.

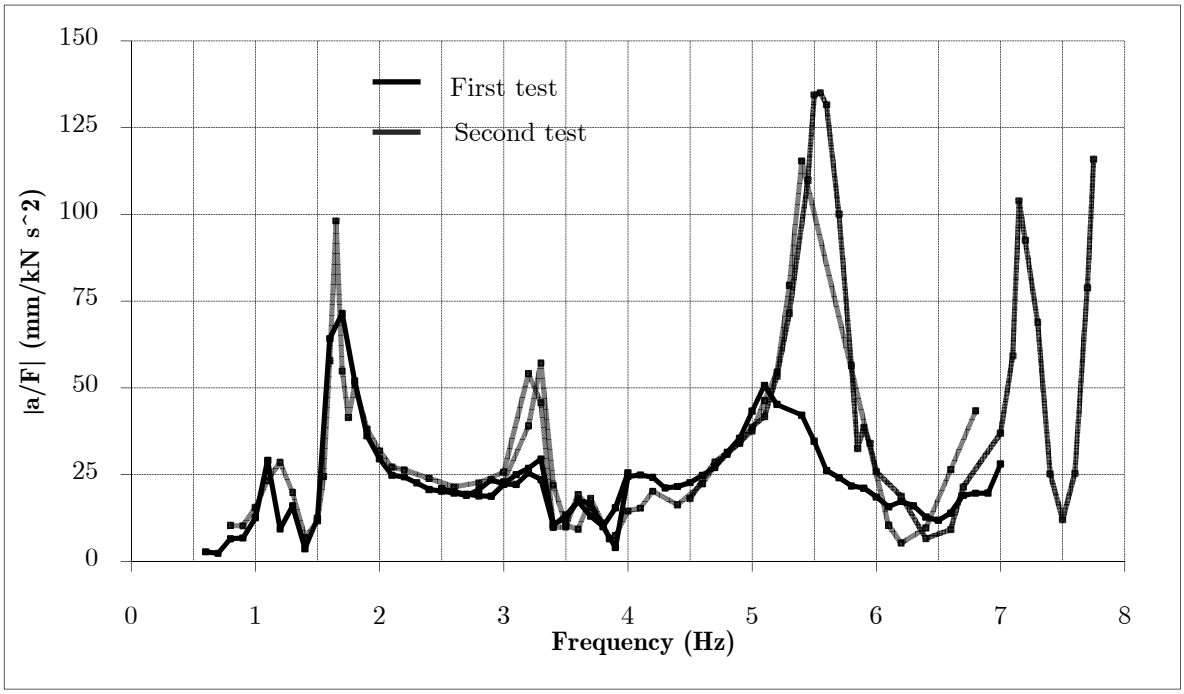

Figure 2.5.8 Comparisons between module inertance diagraphs for the first test (shaker in position 1)

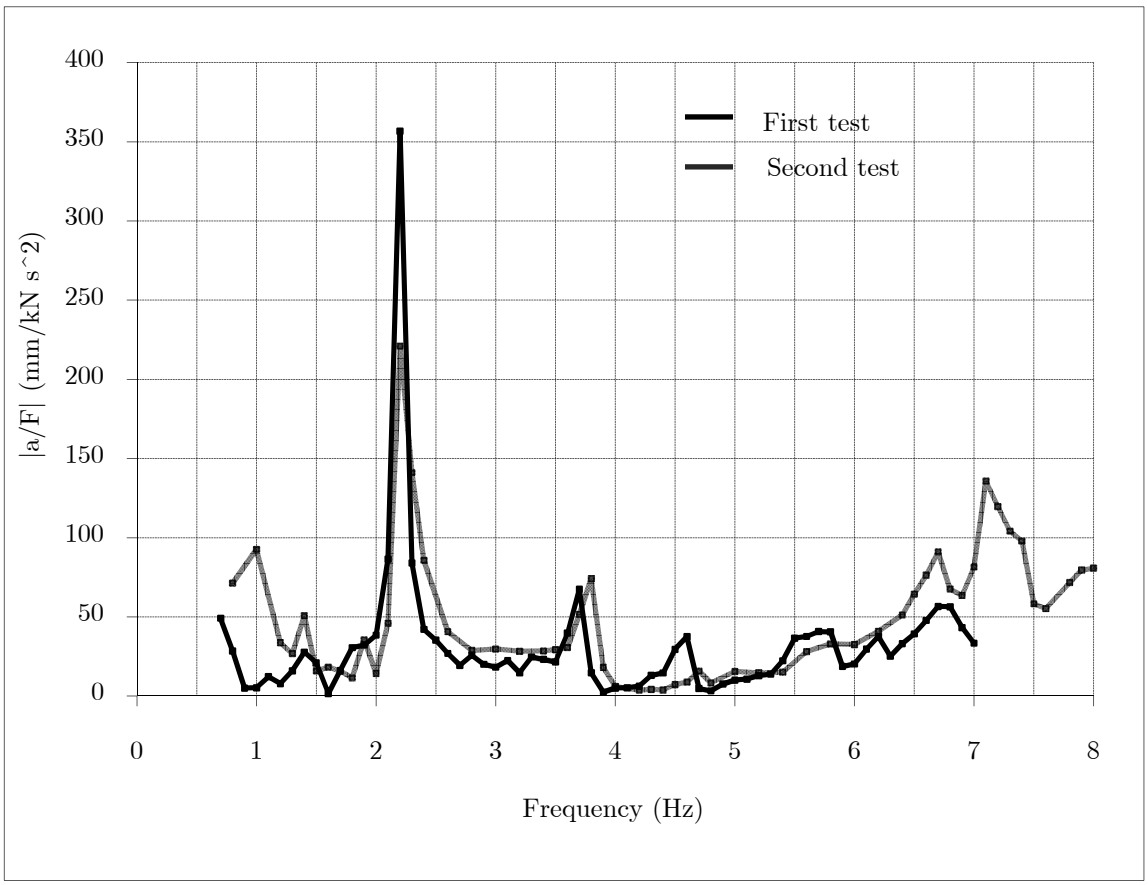

Figure 2.5.9 Comparisons between module inertance diagraphs for the second test (shaker in position 2)

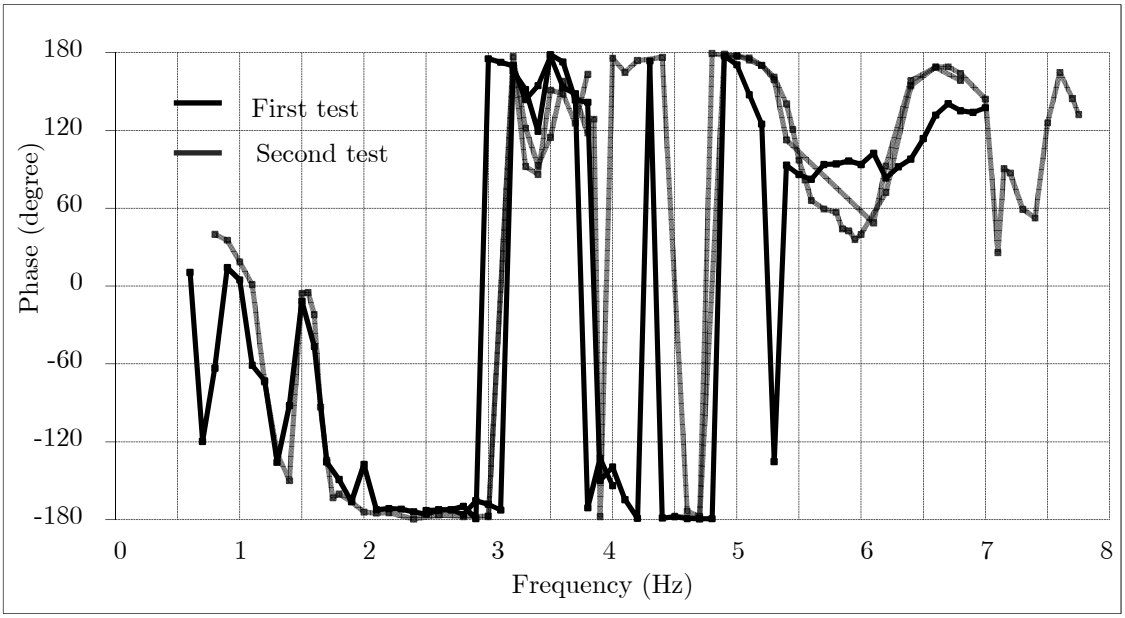

Figure 2.5.10 Comparisons between phase inertance diagraphs the first test (shaker in position 1)

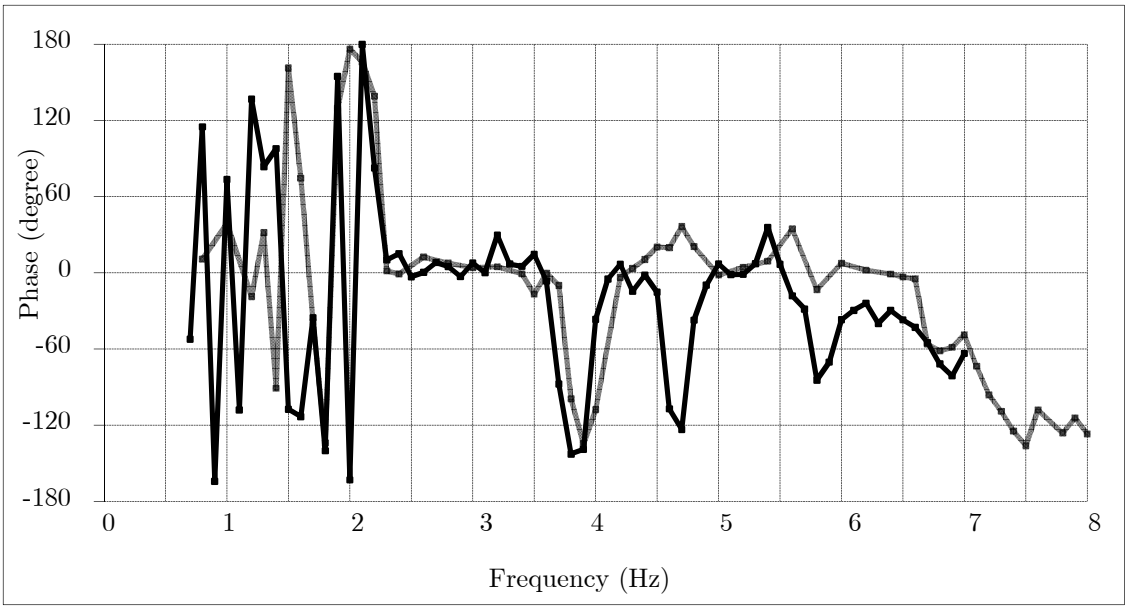

Figure 2.5.11 Comparisons between phase inertance diagraphs the second test (shaker in position 2)

Referring to the second test with N equal to 1024, if the sample is set to $\Delta t = 16/Nf_v$ and so the response time T* to $N\,\Delta t$, the related step of frequency of the corresponding FFT is equal to $\Delta f = 1/T^* = 1/N\Delta t = f_v/16$. Using this simple position it is observable that, in correspondence to the FFT 17th point,

the amplitude and the phase of the harmonic related to the exciting frequency fv are defined. Therefore, the inertance has been computed in module and in phase for each accelerometer and for both the vibrodyna positions and in correspondence to the related peaks the natural frequencies of the structure have been identified [Mazzotti et al., 2004]. The results of the two dynamic tests are summarized in table 2.

Table 2 Natural frequency for the two tests

Mode	Frequency test 2000 (Hz)	Frequency test 2005 (Hz)
1	1.3	1.2
2	1.4	1.4
3	1.7	1.7
4	2.2	2.2
5	3.7	3.8

Computation of modal damping and shapes

The computation of the structural damping with sufficient precision is certainly the most difficult aspect of the identification process. For the definition of the modal damping the half-power method has been used at the beginning; this method yields good results only if the modes of vibration are distinct, that happens if the structural system is little damped. The half-power method is applied in the neighbourhood of the peak of the FRF, where the frequencies correspond to a value of the FRF module equal to $\left|a/F\right|/\sqrt{2}$. The modal damping is defined by the relation (2.26), where ω_a and ω_b are the extremis of the considered interval (i.e. the frequencies immediately after and before the resonance).

$$\xi = \frac{\left(\omega_a - \omega_b\right)}{2\omega_r} \tag{2.26}$$

The extracted results are reported in table 3. To obtain the most reliable value of the damping, the curve-fitting method is applied afterwards. This procedure is based on the hypothesis that the behaviour of the system is dominated by a single mode in the neighbourhood of the resonance. If the inertance is represented in proximity of the peak in a plane Real-Imaginary part, a perfect and centred circle is obtained. In the real structure, the representation of the FRF in the Nyquist plane is a set of point that is distributed around a circle, that results shifted respect to the origin and scaled due to the influence of the other modes (see Figure 2.5.12 Figure 2.5.13).

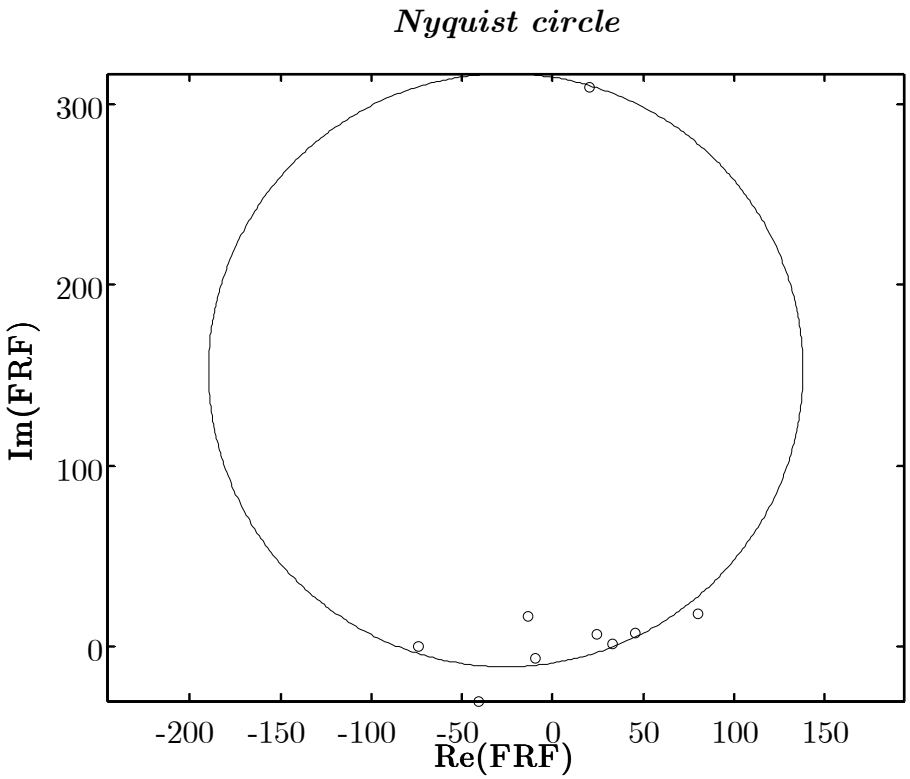

Figure 2.5.12 Nyquist-plot for A1(fv=2.2 Hz test one)

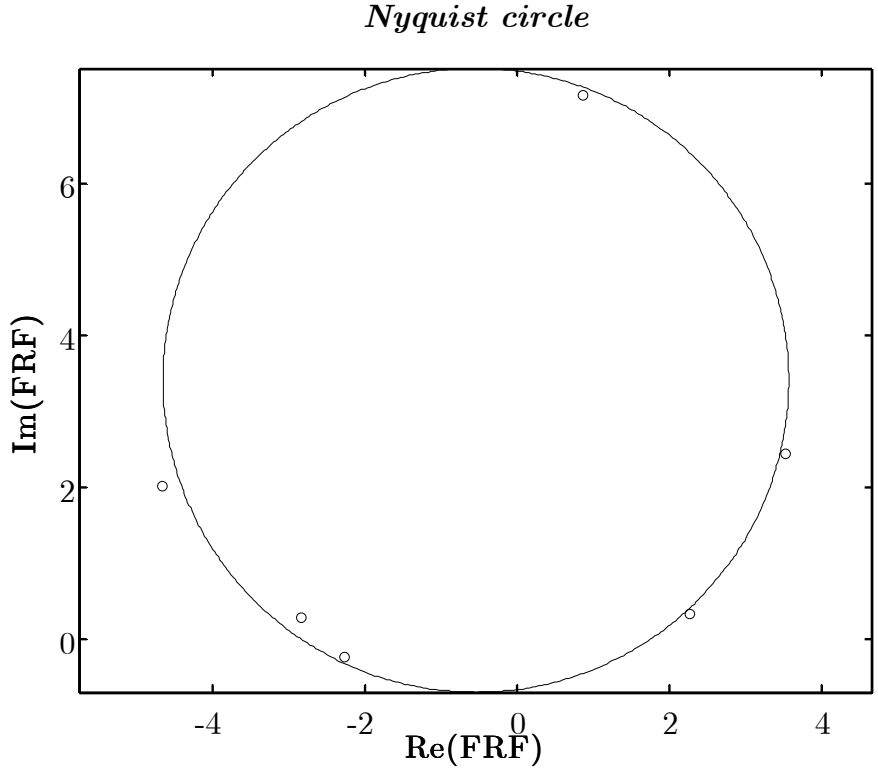

Figure 2.5.13 Nyquist-plot for A8 (fv=1.65 Hz test two)

Referring to the notation in Figure 2.3.2, the modal damping can be defined by the following relation:

$$\xi = \frac{{\omega_a}^2 - {\omega_b}^2}{2\omega_r \left(\omega_a \tan\left(\vartheta_a/2\right) + \omega_b \tan\left(\vartheta_b/2\right)\right)} \tag{2.27}$$

It is noticeable that for $\vartheta_a = \vartheta_b = \pi/2$ the circle-fit method coincides with the half-power method.

Regarding the real instance, the FRF representation in the Nyquist plane does not describe exactly a circle in the resonance peak proximity; instead, for every pulsation, that represents the value of both real and imaginary part of inertance, a series of points that tend to trace a circumference is obtained. The circumference that better describes these points is calculated through the minimum squares method. When the circle that better describes the points is found, it is possible to deduce the natural frequency and the damping factor of the structure, as shown in Figure 2.5.13. This methodology has been applied to the

footbridge dynamic tests but reasonable results have occurred only in two instances. This because, as is shown in the inertance diagram, the phases diagram is very discontinuous in correspondence to the peaks, with the exception of the 1.65 Hz and 3.3 Hz for the second test. In particular for the frequency 1.65 Hz the difference between the two method is of 10%; with the half-power method the modal damping is 0.0229, whereas with the circle-fit the damping is 0.0206 (similarly for fv=3.3 Hz the results are respectively 0.0187 versus 0.0174). For this reason the frequencies in the Nyquist plane that are just around the resonance peak are too much distanced each other, in other words the θ angle is greater than the π one (see Figure 2.5.12). This makes the tangent $\tan\left(\vartheta_b/2\right)$ lower than zero, so the damping factor becomes negative. In the only instance in which this methodology has been successfully applied, values of the damping factor that were near enough to those obtained before with the half-power methodology are obtained. In the next table the values concerning the tests are shown:

Table 3 Modal damping relating to the two test

Vibration mode	Damping test 2000	Damping test 2005
1	-	-
2	0.04135	0.0484
3	0.0315	0.0381
4	0.0175	0.0243
5	0.0177	0.0187

The modal shapes can be obtained soon observing, in correspondence to the peaks, the inertance module and phase. Below the modal shapes, concerning the initial three mode shapes, are shown; as it is noticeable, there are not real differences between them.

First mode

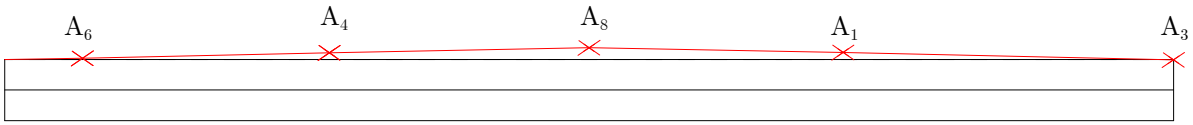

Figure 2.5.14 Transversal mode, pos 1 fv = 1.2 Hz; second test

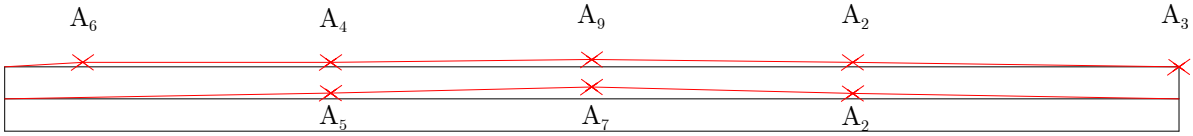

Figure 2.5.15 Transversal mode, pos 1 fv = 1.3 Hz; first test

Second mode

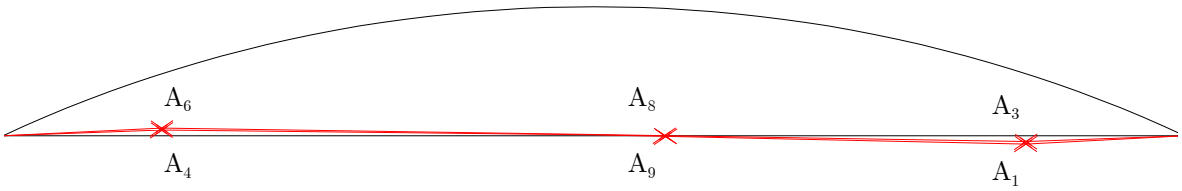

Figure 2.5.15 Vertical mode, pos 2 fv = 1.4 Hz; second test

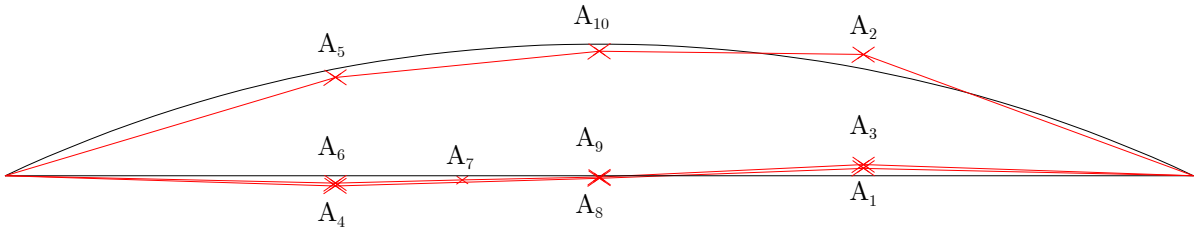

Figure 2.5.17 Vertical mode, pos 2 fv=1.4 Hz; first test

THIRD MODE

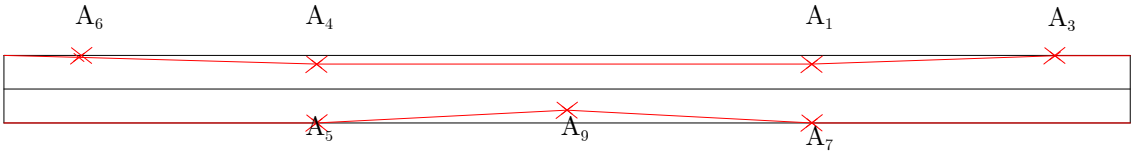

Figure 2.5.18 Torsional mode, pos 1 fv = 1.65 Hz; second test Figure 2.5.19

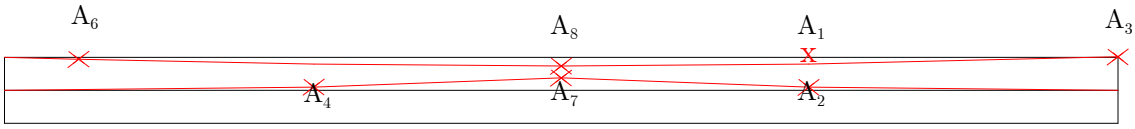

Figure 2.5.18 Torsional mode, pos 1 fv = 1.7 Hz; second test

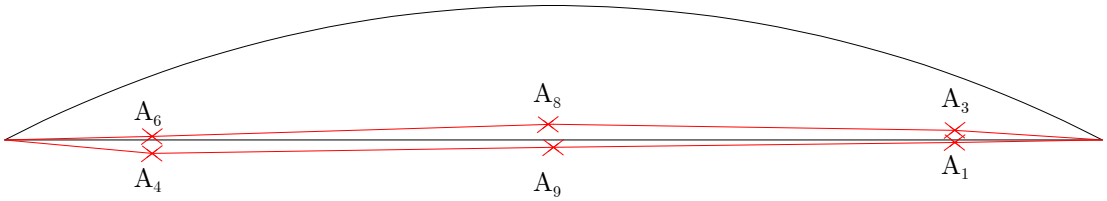

Figure 2.5.20 Torsional mode pos 2 fv = 1.65 Hz, second test

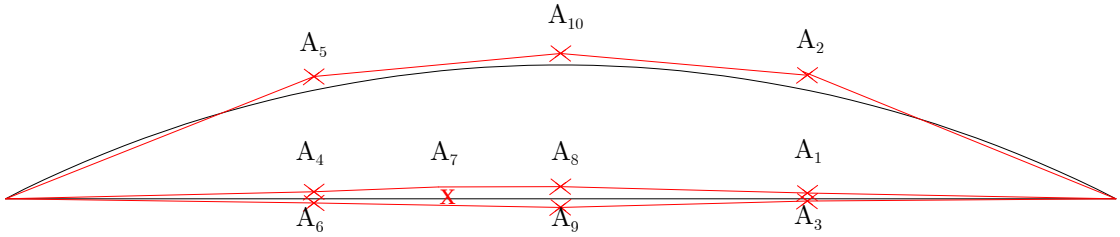

Figure 2.5.21 Torsional mode pos 2 fv = 1.7 Hz, first test

2.6 Computation of FRF through Lissajous Diagram

In the section 1.4 the construction of FRF through classical FFT was explained. In this chapter we define a different method in frequency domain, which, as the previous one, is able to define point by point the FRF for each signal acquired during a forced vibration test.

The proposed methodology is applied on the dynamic test carried put on the footbridge in Rimini to compare the FRFs obtained. Initially, as it was discussed in the chapter three, the amplitude ratio and the phase displacement (which corresponds to a single point of the FRF) at fixed frequency is obtained by the geometric characteristic of the ellipse, which better approaches the trend of the points by least square method. In this way the computed FRF is very far from that one obtained by classical FFT.

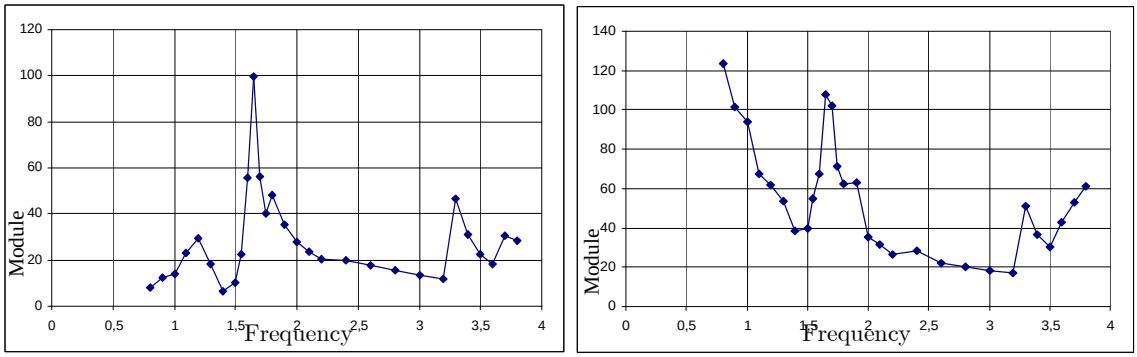

Figure 2.6.1 FRF module through FFT and ellipse method, respectlevy

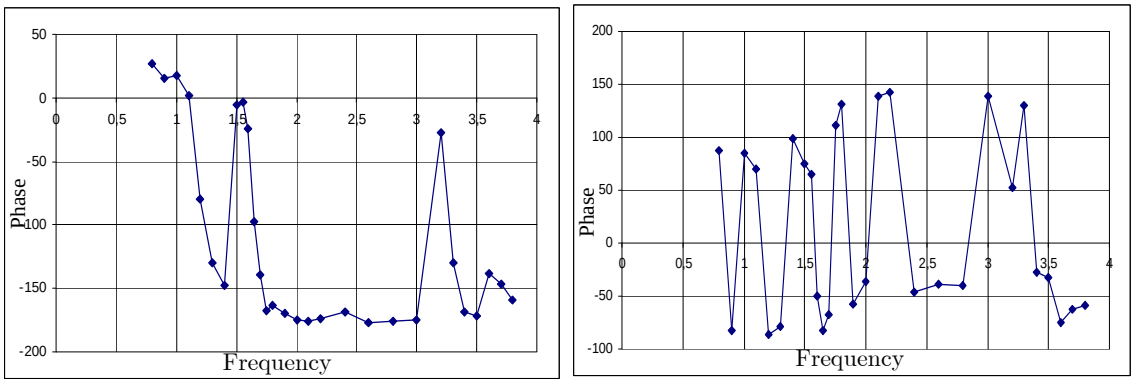

Figure 2.6.2 through FFT and ellipse method, respectlevy

The figures show an important difference of the FRF in module and in phase too.

These figures show in particular that the proposed method is not able to recognize all the natural frequencies of the system. A possible interpretation of this strong approximation is that with the simple least square approach we construct a single curve that resume a lot of different variable: possible interference during the recording of the signal, different value of frequency, presence of delay between the two compared signals etc. This entails the error during the computation of the FRF. To come through this limit, the idea is to define some constrains during the definition of the curve. First of all, looking at the general parametric equation of the ellipse, we decide that the ellipse that better approaches the point's trend is characterized by a particular expression of the x-value. We impose that this ellipse has the x-value coincident with the signal generated from the electromechanical shaker.

The second constrain concerns the output signal. In this case we have an acceleration that is really different from a sine function far of the resonance and for low level of excitation. This implies that the amplitude of the cosine signal with frequency different from the frequency of excitation cannot be neglected. This condition can be seen with a simple FFT of the output, which appears very irregular. The points, in plane input output, tend to describe a Lissajous Diagram completely different from a simple ellipse. To simplify the computation of the FRF the assumption is considering by the way an ellipse, characterized by y-value expressed from eq (2.19), where the frequency is equal to that one of the input force. In the figure below, the two ellipses described are represented in the same graph.

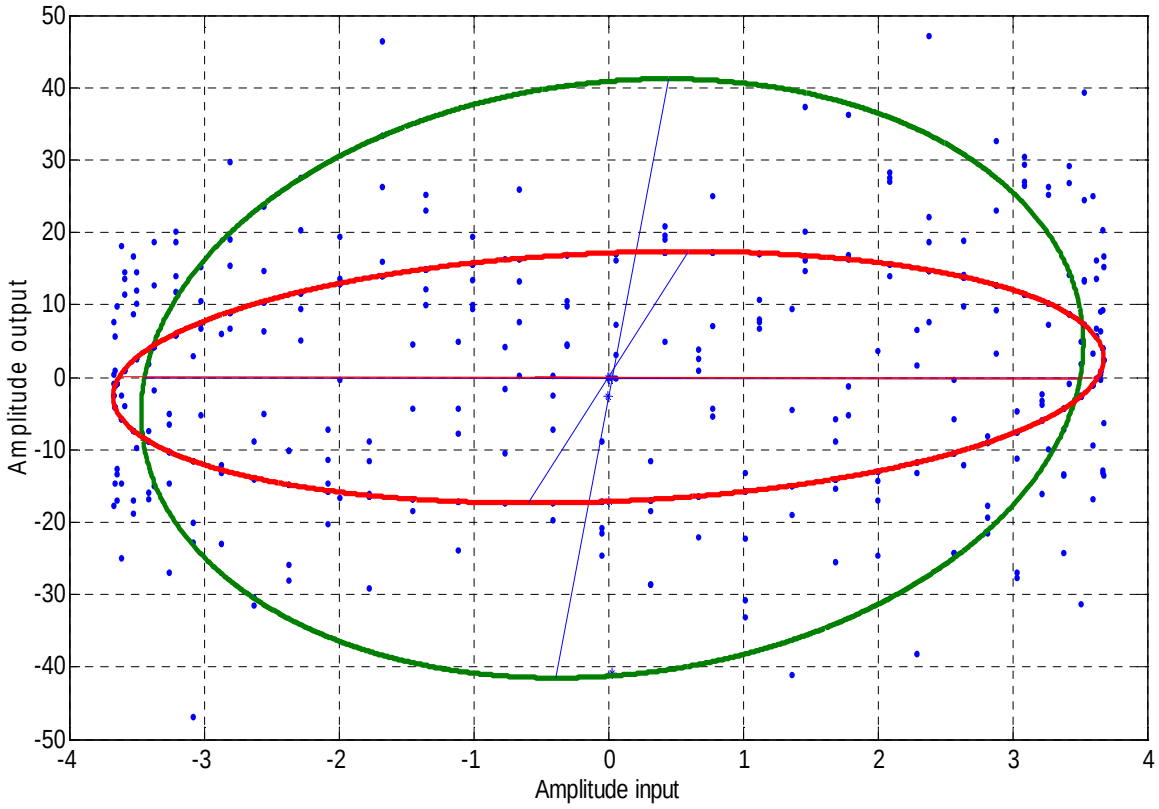

Figure 2.6.3 Ellipse computed trough MLS (in green), ellipse computed through sinefit (in red) for the signal acquired by accelerometer 3 at frequency fv = 2.4 Hz compared to the sinusoidal force (blu points)

The two ellipses are constructed both by least square method; the green one is obtained by any kind of constrain, the red one, instead, is defined by constrain previously illustrated. As it is clear from the figures, the two curves are very dissimilar, the ratio of the two axes, which defines a point in module of FRF, assumes values different. The inclination of the major axis is different too, so the phase of the FRF has dissimilar values according to the ellipse considered. Using for each signal acquired the red one, another FRF point by point is constructed. The figures below show that the FRF in this case is almost coincident with that one obtained by the classical application of the FFT. This happens in module and phase too.

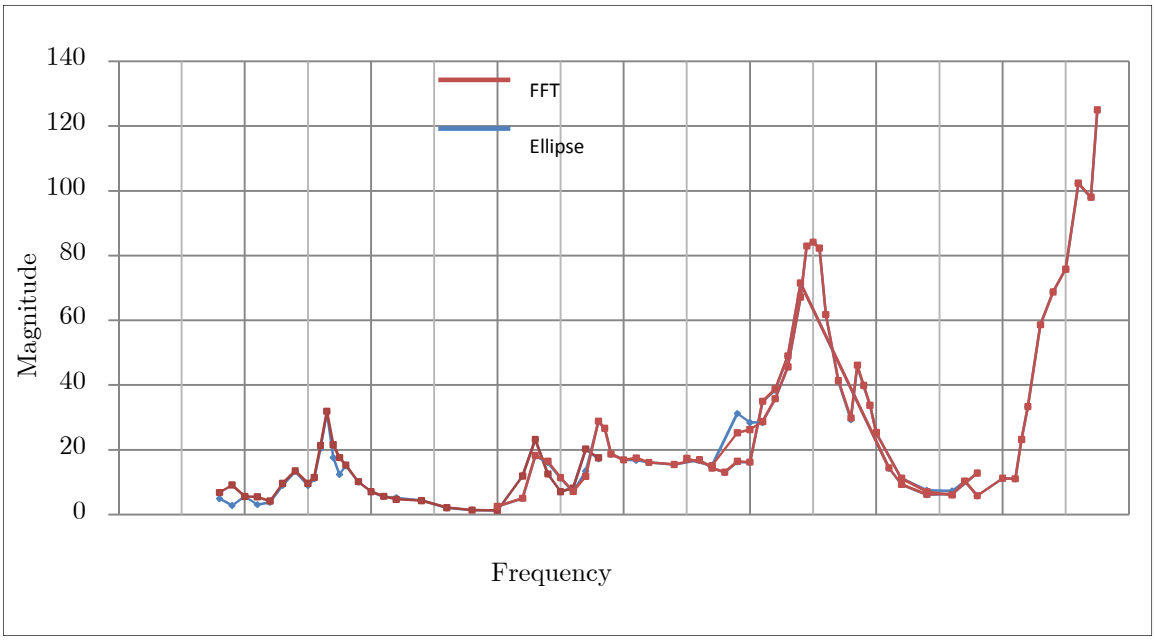

Figure 2.6.4 Module of FRF, accelerometer 1, shaker position 1

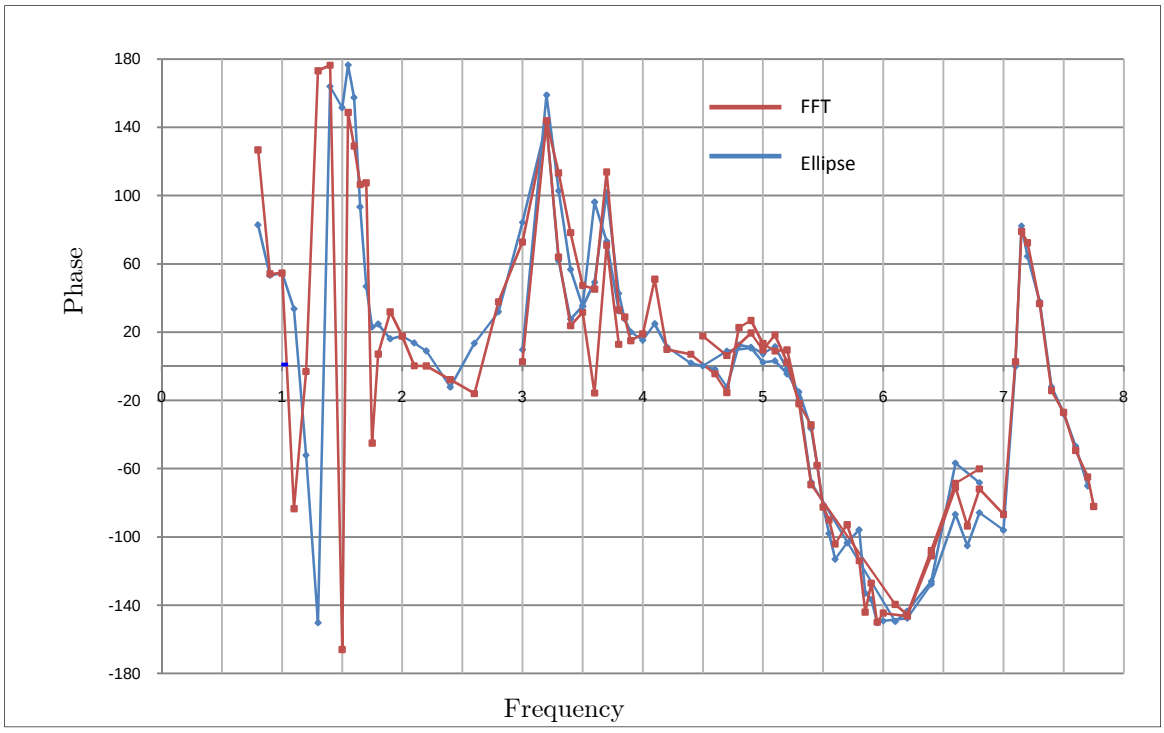

Figure 2.6.5 Phase of FRF, accelerometer 1, shaker position 1

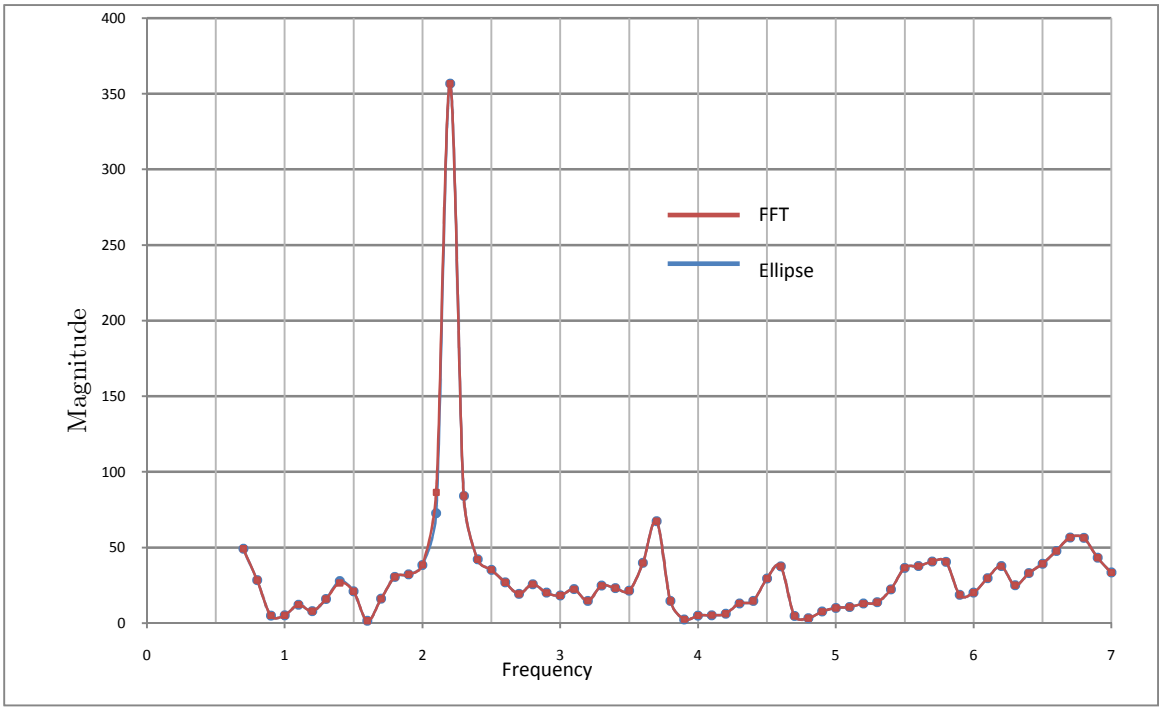

Figure 2.6.6 Module of FRF, accelerometer 3, shaker position 2

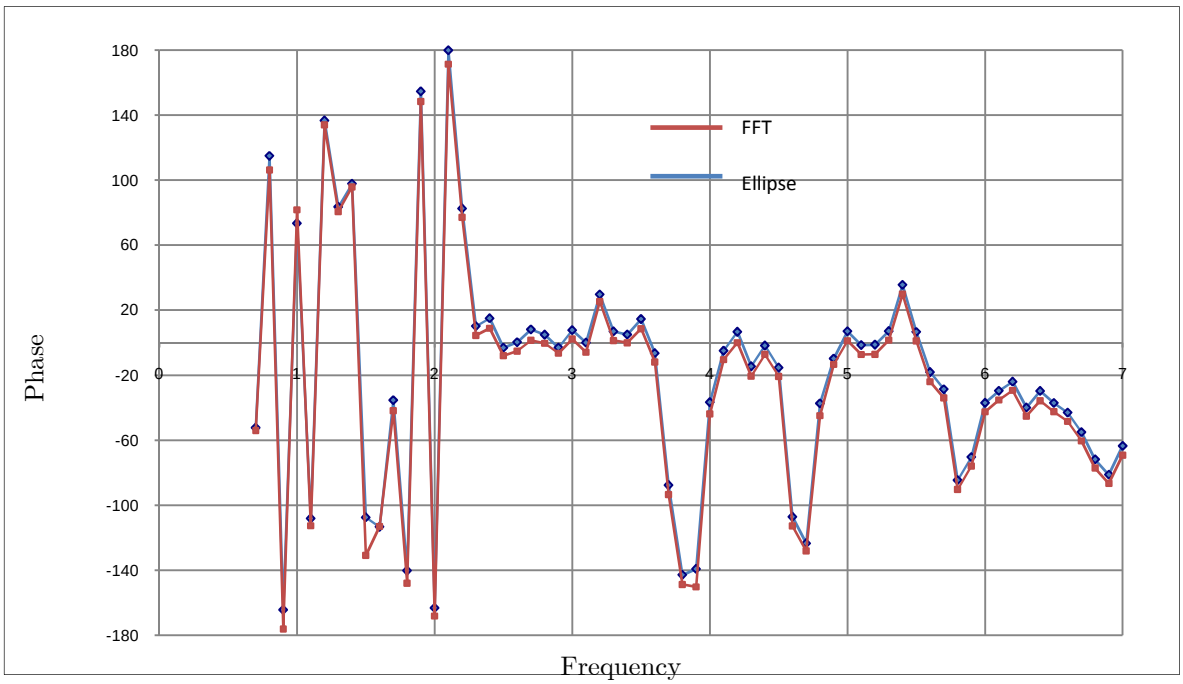

Figure 2.6.7 Phase of FRF, accelerometer 3, shaker position 2

The FRF is computed according to the test on the footbridge, described in the previous paragraph. The Inertance is defined when the electromechanical shaker excites transversally the structure, in module (

Figure *2.6.4*) and phase (Figure 2.6.5). The same is obtained when the vybrodina excites the structure by a vertical force, in module (Figure 2.6.6) and phase (Figure 2.6.7).

At this point it is possible to extract the modal parameters of the footbridge from the FRF. The results are the same already defined in the previous paragraph.

Some consideration on the method

The method works only if an important constrain about the frequency of the output signal is introduced. In this section an explanation of this circumstance is expressed. Looking at the parametric equation of the ellipse, the x equation is fixed and is equal to the sine function produced by the electromechanical shaker. In the y equation the frequency is fixed too, imposed equal to the frequency of the excitation, only the amplitude B and the phase ø can change. These characteristics are defined by the least square method. In the infinite ellipse with the y equation so defined, that one which approaches the points trend by least square is chosen. It is noticeable that the problem regards only the approximation in the representation of the response of the structure. In other words, the application of the procedures implies that the input signal is replace with the sine function that better approach it at fixed frequency, the sine-fit method is applied. In the following figures the sinefit application is represented when the frequency is not fixed and when is established. The signal acquired during the second test at frequency of the force equal to 2.3 Hz is considered.

The first graph shows the sine function that better approach the real trend of the response, with a general frequency, in general different from the excitation frequency. The RMS is evaluated and the frequency is equal to 2.34 Hz; amplitude and phase are computed. The same procedure is applied in the Figure 2.6.8 where the frequency is fixed and equal to 2.3 Hz. Note that the RMS in this case is greater than before. The two sinefit procedures compute different values of amplitude and phase, this justifies the important difference of the FRF, computed by the two procedures.

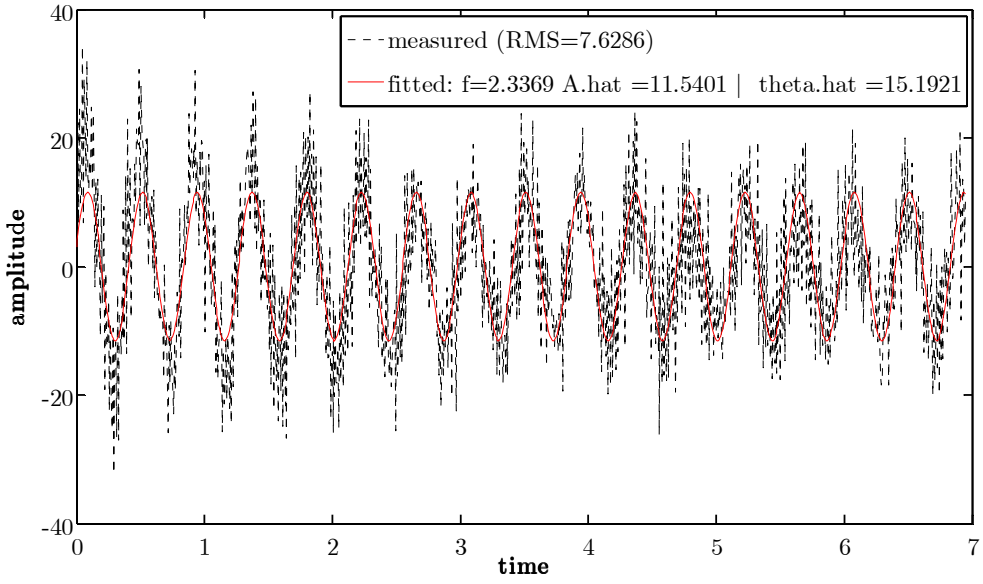

Figure 2.6.8 Sinefit of the signal with unknown frequency not equal to the exciting frequency, evaluation of RSM

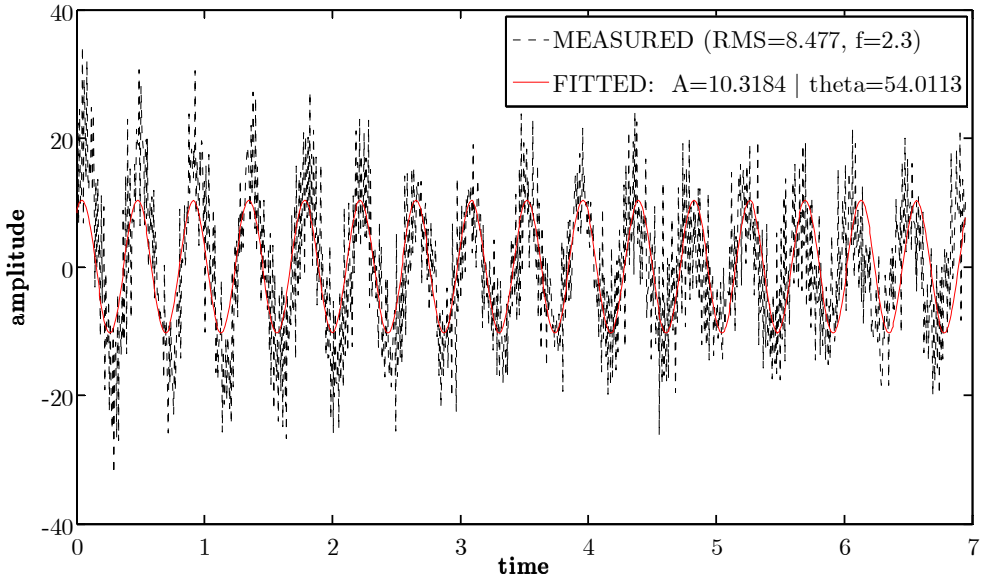

Figure 2.6.9 Sinefit of the signal with fixed frequency equal to the exciting frequency, evalutation of RSM

The amplitude of the signal is almost the same, but an important difference is obtained in the phase value. If we consider the first sinusoid, a diagram far from

an ellipse is obtained, because we are comparing two signals with different frequencies.

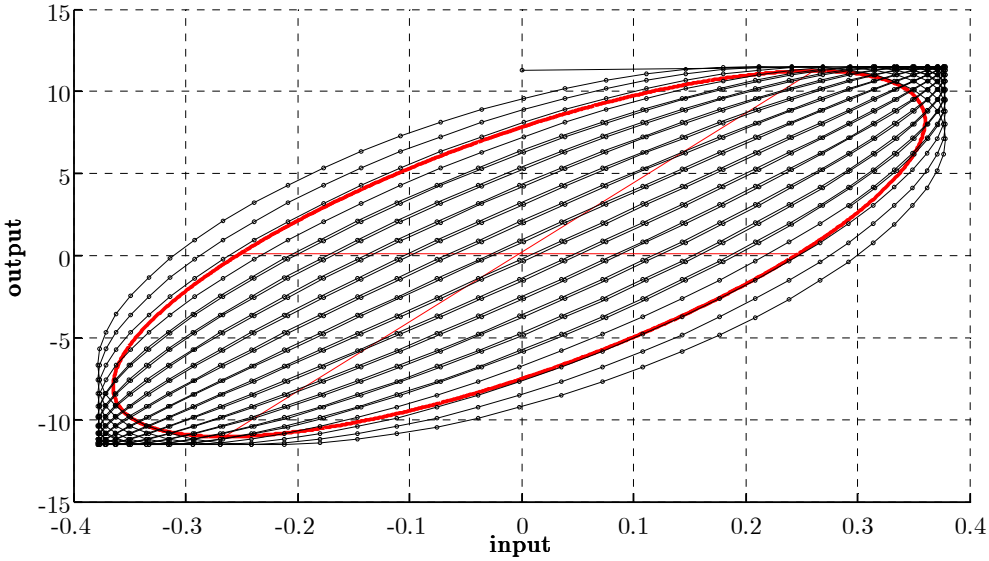

Figure 2.6.10 Lissajous Diagram when the output is approximated through a sine with frequency different from that one of the input

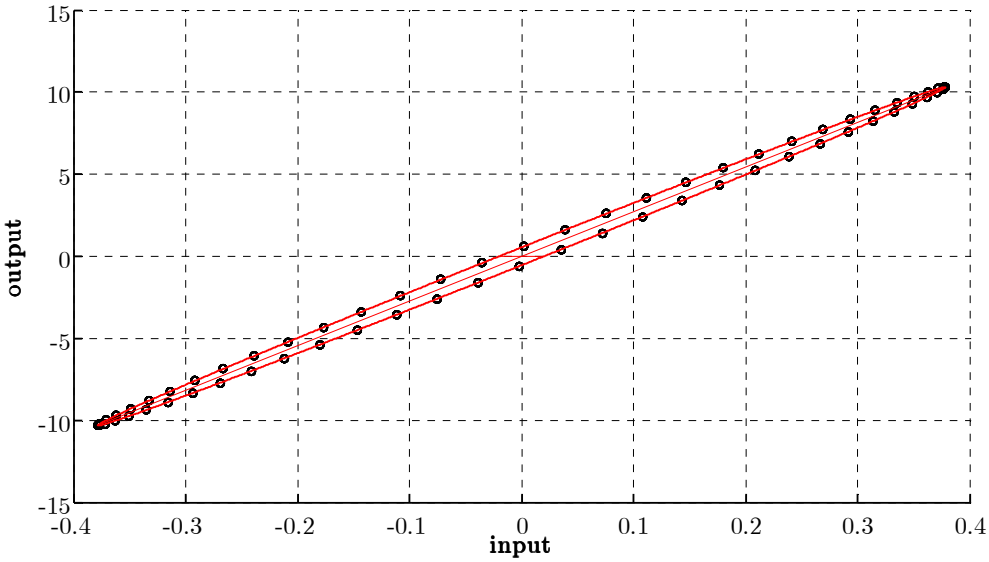

Figure 2.6.11 Lissajous Diagram becomes an ellipse when the output is approximated trough a sine with the same frequency of that one of the input

For this reason if the sine function 1 is considered to compute a point of FRF, a different value (in module and more in phase) respect to the other one related to FFT is obtained. The same procedure is applied when the sine two is analysed, in

this case the parametric equation of an ellipse are described, so the curve is represented below. In this case we obtain the same point of FRF for both the methodology.

In this case the shape and the orientation of the two ellipses, represented respectively in *Figure 2.6.10* and *Figure 2.6.11*, is not so different; in fact the considered signal is near to the resonance and in this case it is possible to consider the ellipse that better approach the point through minimum square method, without committing an important error. The situation is completely different if a signal far from the resonance is considered, as *Figure 2.6.12* shows.

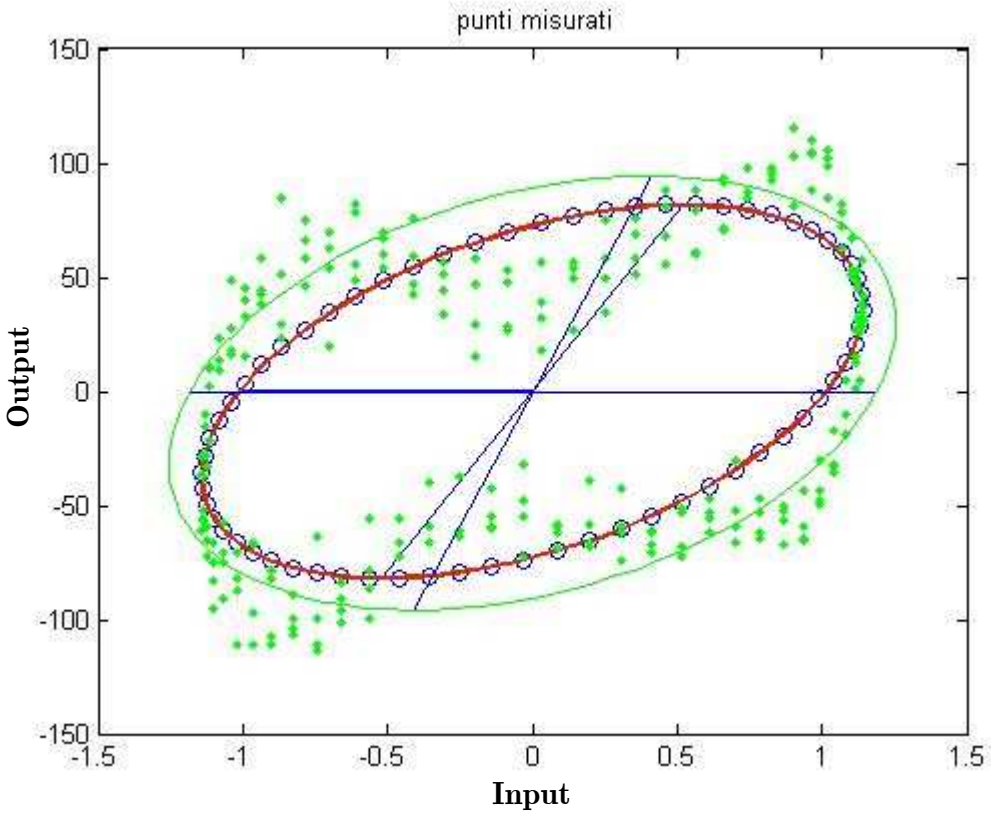

Figure 2.6.12 Ellipse in red represents the comparison input-output (blue points), when the output has the same frequency of the input; ellipse in green represents the comparison input-output (green points), when the output has different frequency of the input

In this case it is necessary to consider the red ellipse to define a point of the FRF; if the green one is used, we compare two signals with very different frequency and it is impossible to define a single point of the FRF in a frequency domain. Then

the constrained ellipse has to be considered when a coherent FRF graph has to be constructed point by point for each frequency.

Advantages of the proposed methodology

From what has been said, it is clear that the FRF can be constructed through FFT or the geometric characteristic of an ellipse and the same results can be reached. Another important aspect of the proposed methodology would be underline in this section. The ellipse construction can be in particular a good way to test, from the direct comparison between input-output signals, the goodness of the signal recorded during the dynamic test. In general an high dispersion of the points around the ellipse that better approaches them means that the response of the system is not coherent with the force, which excites the structure. This is very evident for the low frequency, where the sinusoidal force is so low that it not able to excites strongly the structure. Often in this case we have very bad recorded signal.

So this procedure is able to furnish a clear visual effect of the signal acquired qualitatively. As we are going to see in the next pages, it is possible to define an index which computes quantitatively the goodness of a signal respect to the applied force. To understand and apply this characteristic of the method we start from some consideration on the FRF obtained for the test of 2000 on the footbridge with vibrodyne, which excites the structure vertically. As it is noticeable in Figure 2.5.8, there are two peaks very proximal, corresponding to 1.1 Hz and 1.3 Hz. It is impossible to say which of the two is the real natural frequency of the system. A reason of this situation is that with so low frequency the force is not able to excite the footbridge and the signal is full of noise. It is necessary defining a parameter able to indicate the more reasonable natural frequency of the system. A prove of the fact that only one peak corresponds to a natural frequency of the system is gave by the FFT of the signal acquired during a free vibration test on the same structure, carried out in 2000 too, under the same condition of the forced test analyzed. The FFT of the signal acquired after a shock test is illustrated in the figures below.

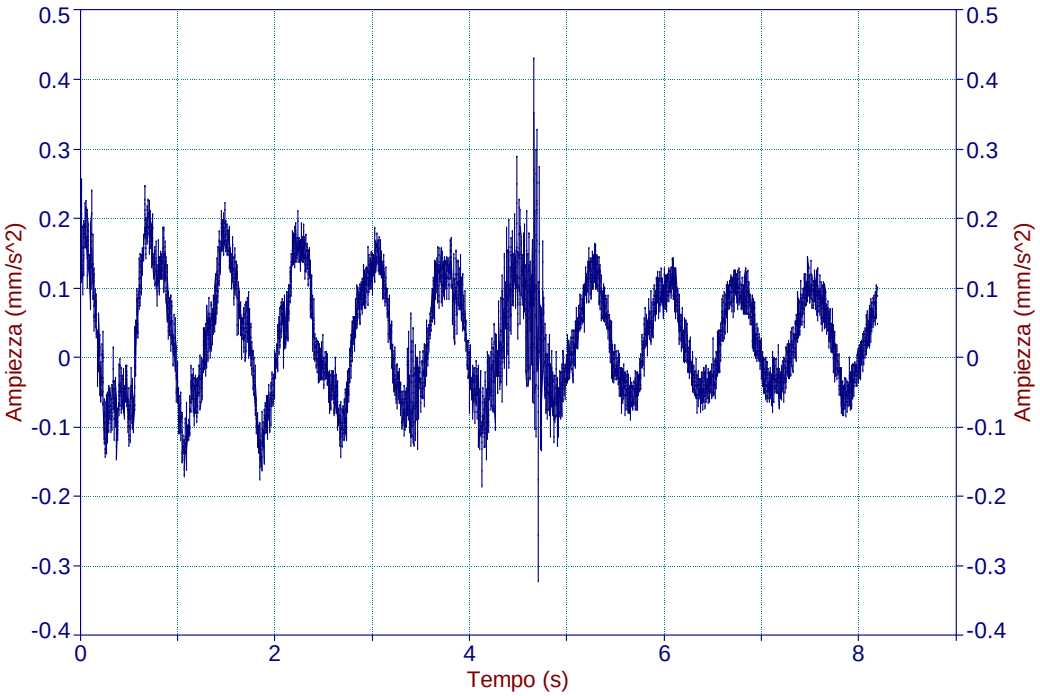

Figure 2.6.13 Trend of free vibration of the laminated footbridge after an impact test

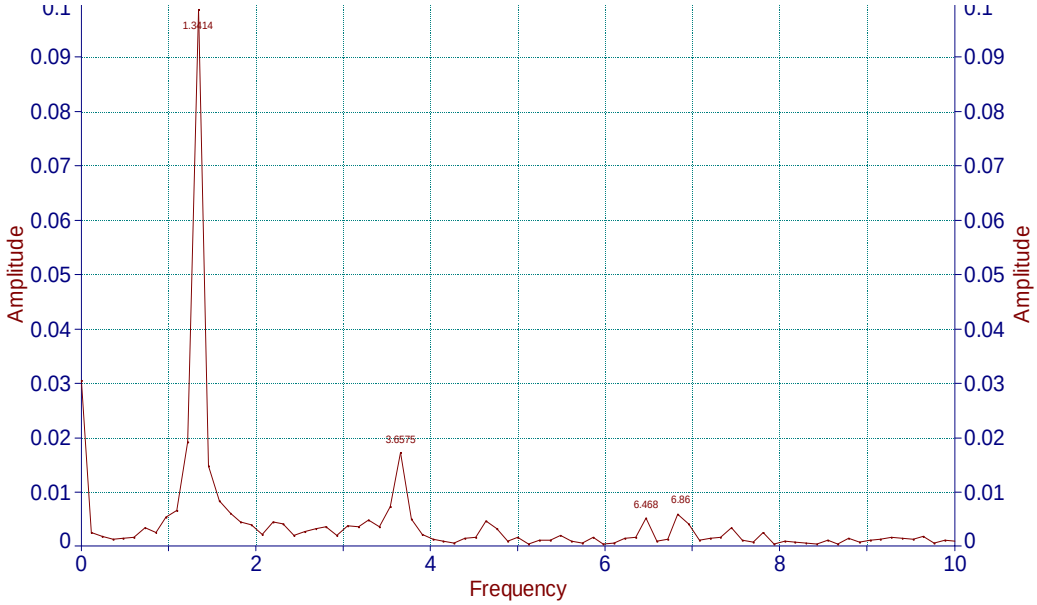

Figure 2.6.14 FFT of the recorded signal

The FFT confirms that there is only one peak and the natural frequency is equal to 1.3 Hz, so the frequency 1.1 Hz detects only noise. The goal is to define which

is the natural frequency without considering another kind of test, using only the data collected during the forced vibration test. To understand which frequency between them could be the real natural frequency of the system, the correlation between the structure reply registered in correspondence of each accelerometer and the perfectly sinusoidal force applied by the vibrodyna can be observed for both the tests.

The assumption is that, for the real resonance frequency, the structure reply will be almost sinusoidal and will be greater than the applied force. This assumption is better observed for the 1.3 Hz frequency.

However, this correlation can be computed for each accelerometer using the r^2 correlation index, that is not influenced at all by the amplitude of the compared sinusoids, while it is affected by the sinusoids phase displacement and by the pattern of the structure reply; in fact, the r^2 index varies more as the structure reply becomes less sinusoidal (from the graphic below it is observable that, in correspondence to each value of the sinusoid amplitude, different values of the amplitude of the recorded acceleration are obtained; the distance of these points from the red ellipse increases as the structure reply becomes less sinusoidal). In particular, the computation of r^2 defines the distance between the points, relating to the real case, and the ellipse that better approaches their distribution (the best fit is obtained through the minimum squares method).

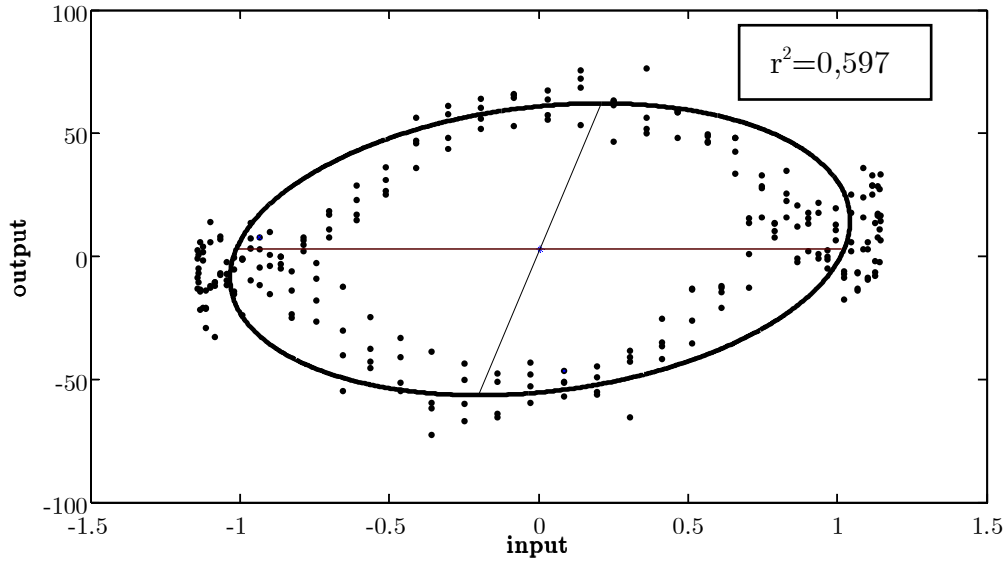

2.6.15 Direct comparison between the force and the structure responce for the A2 with fv = 1.1 Hz, computation of index r2

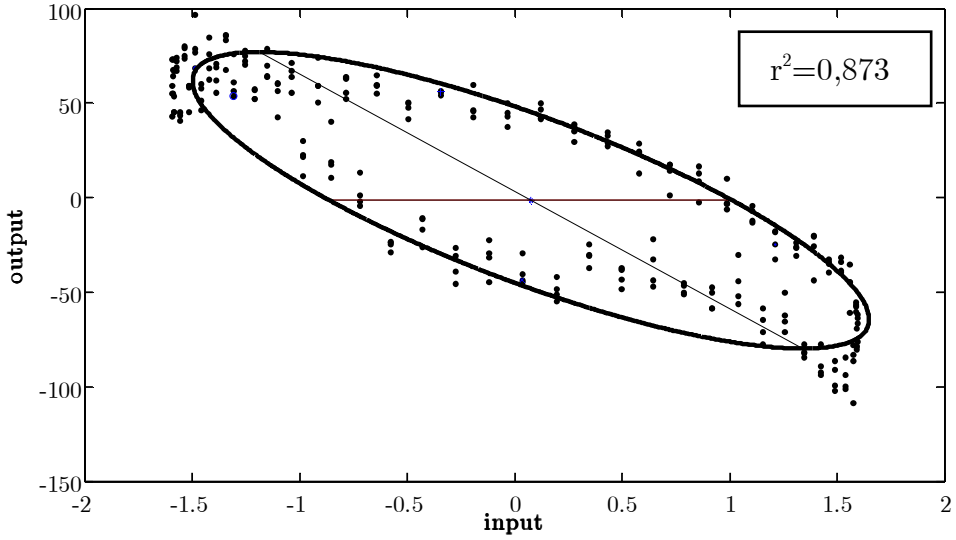

2.6.16 Direct comparison between the force and the structure responce for the A2 with fv = 1.3 Hz, computation of index r2

The computation of this index for both the frequencies has shown that the second one (1.3 Hz) has a greater correlation between the applied force and the structure reply, and so it has been considered as the real natural frequency of the structure. Thus is confirmed by the computation of the FFT of the free vibrations.

Conclusive remarks

The modal parameters of a laminated timber footbridge are obtained by the application of two methods, both in frequency domain and for forced vibration test. The proposed method allows on the one hand the construction point by point of the FRF, by which the modal parameters can be extracted through PP method or circle-fit; on the other hand it is a way to define the correlation between the signal that excites the structure and the response acquired as its acceleration. This aspect has allowed, in the specific analyzed case, to establish the more reasonable first natural frequency of the system, because of the presence of two very proximal peaks in the FRF.

We would like finally to emphasize the visual immediacy that the methodology described offers.

2.7 Numerical simulation

Once the structure modal parameters were found, obtained by the experimental results of the two vibration tests, a finite elements model of the structure was realized using the Sap2000 software. In the model the Young module value of the laminated timber has been set to minimize the differences between the experimental natural frequencies and those obtained with Sap2000. In the model definition a linear behaviour of the structure is assumed, besides the twin arcs, the lower beams that maintain the floor and the two higher beams that joint the twin arcs have been treated as beam elements, while the remaining elements of the structure have been treated as truss ones. Because the action induced by the vibrodyna is negligible compared to an earthquake, the ties of the friction forces have not been reached and so the footbridge has been treated as it was constrained by four hinges. Besides, to minimize the differences between the modal parameters obtained by the model and the experimental ones, the model have considered the loads present during the test like loads distributed on the structure placed below the trampling level, as shown in table 1.

Table 4 Lower eigenfrequencies of both model and frame

Mode shape	Frequency first test (Hz)	Frequency FEM model	Dominant displaced shape	Different percentages
1	1.2 (1.3)	1.23	Horizontal	+ 3%
2	1.4	1.47	Vertical	+ 5%
3	1.7	1.92	Torsional	+ 11%

The laminated timber and steel elastic modules have been set respectively to 18 GPa and 210 GPa. The value of laminated timber Young module has been chosen to minimize the differences between the modal parameters obtained in the experimental tests and those obtained by the model.

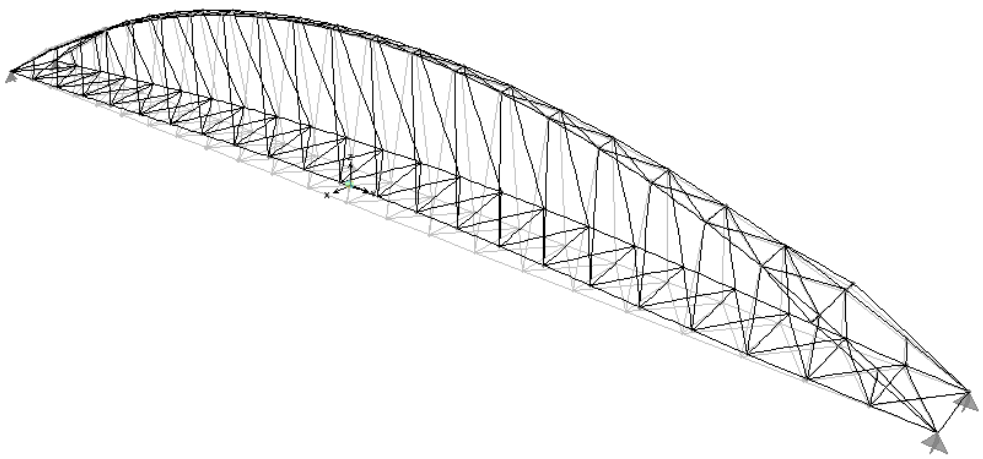

Figure 2.7.1 Horizontal mode fv = 1.23 Hz

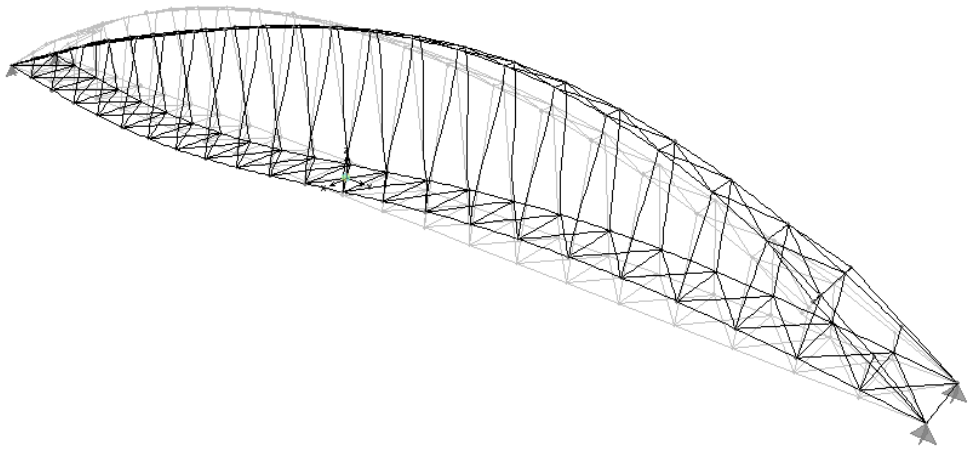

Figure 2.7.2 Vertical mode fv = 1.47 Hz

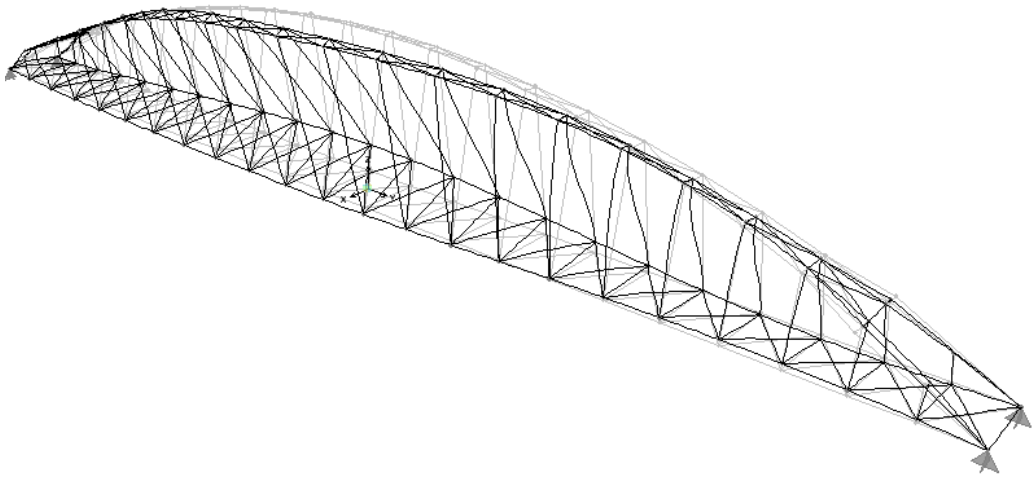

Figure 2.7.3 Torsional mode fv = 1.92 Hz

The results obtained by the finite elements model are compared with the experimental ones in the table 4.

It is observable that the results of both the tests are almost the same. The choice of a greater Young module value for the laminated timber (it is usually assumed to be equal to 11 GPa along the wood grain) can be justified because the vibrodyna brings weak forces to the structure and so causes a low strain in the wood elements. This implies that the strains tend to vibrate around the origin of

the material stress-strain law. In the figures 2.7.1, 2.7.2 and 2.7.4 the initial three mode shapes of the structure are shown, assuming that the structure has been modelled as described in the previous paragraph.

It worth noting that the first modes are characterised by low frequencies and movements in both vertical and horizontal directions and torsional rotations. These eigenmodes are also characterised by a small quantity of energy absorption, that means a small human pacing or a swing wind flow gives rise to perceptible movements.

2.8 Comparisons between modal parameters extracted by the two dynamic tests

The two dynamic tests have been applied to the studied footbridge in two different moments of its life-time: the first test has been done at the footbridge creation, especially to verify the validity of the theoretical design assumptions about its dynamic behaviour. Instead, the second test has been realized five years after the footbridge launch, to verify the structure solidity and, in detail, to valuate which is the laminated timber behaviour in the course of time under particular weather conditions. Regarding the comparison between the damping factors obtained in the first and in the second test, a modest increase of this factor can be noticed in the second instance. This can be considered an effect of a possible damage of the structure in the time. Instead, the frequencies analysis shows almost the same results in both the tests. However, there are some doubts regarding the correctness of the first natural frequency found in the first dynamic test; this because in the inertance function two very proximal peaks are obtained (they are equal to 1.1 Hz and 1.3 Hz). To understand which frequency between them was the real natural frequency of the system, the correlation between the structure reply registered in correspondence of each accelerometer and the perfectly sinusoidal force applied by the vibrodyna can be observed for both the tests using the r2 correlation index.

The computation of this index for both the frequencies has shown that the second one (1.3 Hz) has a greater correlation between the applied force and the structure reply, and so it has been considered as the real natural frequency of the structure. Therefore, the first natural frequency related to the first test reduces of 0.1 Hz, the second one remains the same while the reduction of the third one is negligible. If the higher modes are exanimate, it is noticeable that the fourth natural frequency remains the same while a little raise (almost 0.1 Hz) is observable for the sixth natural frequency.

Considering the initial three natural frequencies, it is finally noticeable a little raise of the structure own period, which seems to suggest that the footbridge rigidity has slightly decreased.

In situ dynamic tests have been conducted in order to estimate the dynamic behaviour of a timber footbridge. The lowest frequencies have been evaluated to be in the range between 1 and 2 Hz including both flessional and torsional mode shapes. It was thus argued that the footbridge is sensitive to low frequency loads, such as human pacing, mainly due to the material choice compared to the bridge shape and dimensions. This can entail low comfort level for the users, because the footbridge can resonate during pedestrian crossing.

A light decrease of the first natural frequency of the footbridge was obtained in the first test compared to the second. This entails a light decrease of the rigidity of the structure, which is attributed to a possible damage of the footbridge, as the modal damping variation confirms.

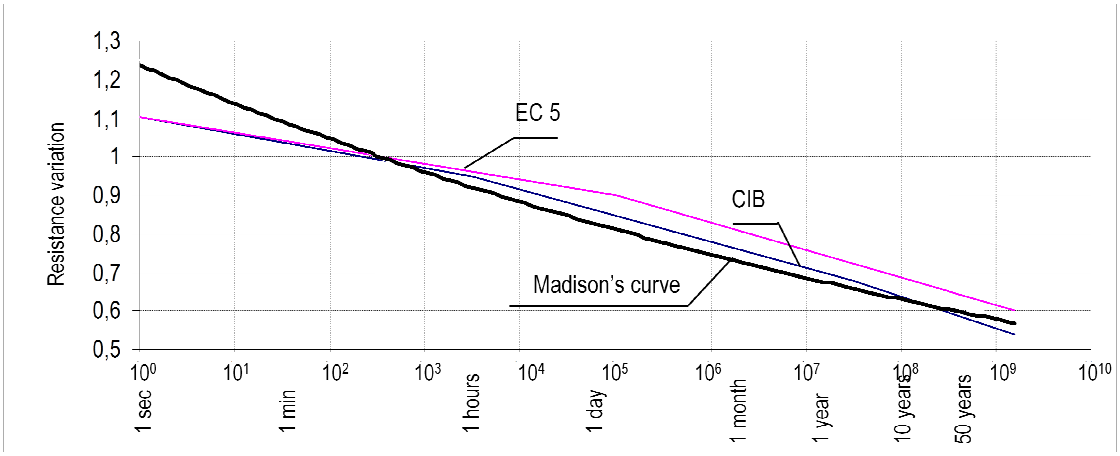

Figure 2.8.1 Effect of live load duration

A possible interpretation of this variation can be the effect of the duration loads to the resistance (see Figure 2.8.1). The long lived loads (see table 1) entail the reduction of the laminated timber resistance [Giordano, 1993]. Referring to the curve of the Eurocode 5 (EC 5) it is noticeable that the load duration involves a decrease of the mechanical characteristics of the wood, as obtained by the analysis of the modal parameters of the structure.

CHAPTER THREE

Modal parameters extraction through Continuous Wavelet Transforms

3.1. Introduction

Wavelets are mathematical functions that cut up data into different frequency components, and then study each component with a resolution matched to its scale. They have advantages over traditional Fourier methods in analyzing physical situations where the signal contains discontinuities and sharp spikes. Wavelets were developed independently in the fields of mathematics, quantum physics, electrical engineering, and seismic geology. Interchanges between these fields during the last ten years have led to many new wavelet applications such as image compression, turbulence, human vision, radar, and earthquake prediction. For many decades, scientists have wanted more appropriate functions than the sines and cosines which comprise the bases of Fourier analysis, to approximate choppy signals (Lardies & Gouttebroze, 2002). By their definition, these functions are non-local (and stretch out to infinity). They therefore do a very poor job in approximating sharp spikes. But with wavelet analysis, we can use approximating functions that are contained neatly in finite domains. Wavelets are well-suited for approximating data with sharp discontinuities. The wavelet analysis procedure is to adopt a wavelet prototype function, called an analyzing wavelet or mother wavelet [Meyer, 1992; Daubechies, 1990 and 1993]. Temporal analysis is performed with a contracted, high-frequency version of the prototype wavelet, while frequency analysis is performed with a dilated, low-frequency version of the same wavelet. Other applied fields that are making use of wavelets include astronomy, acoustics, nuclear engineering, sub-band coding, signal and image processing, neurophysiology, music, magnetic resonance imaging, speech discrimination, optics, fractals, turbulence, earthquake-prediction, radar, human vision, and pure mathematics applications such as solving partial differential equations.

Mathematically, wavelet transforms are inner products of the signal x(t) and a family of wavelets. Let $\Psi(t)$ be the analyzing wavelet called also the mother

wavelet of the analysis or the wavelet 'prototype'. The corresponding family of wavelets consists of a series of son wavelets, which are generated by dilatation and translation from the mother wavelet $\Psi(t)$ shown as follows:

$$\Psi_{\tau,s} = \frac{1}{\sqrt{|s|}} \overline{\psi}\left(\frac{t-\tau}{s}\right) \tag{3.1}$$

where s is the dilatation or scale parameter defining the support width of the son wavelet and t the translation parameter localising the son wavelet function in the time domain. The idea of the wavelet transform is to decompose a signal x(t) into wavelet coefficients $W_{\psi(a,b)}$ using the basis of son wavelets $\psi_{a,b(t)}$. The mother waves need to have particular properties [Tang et al, 2001; Rioul and Vetterli, 1991]. Under the hypothesis that x(t) satisfy the condition:

$$\int_{-\infty}^{\infty} \left|x(t)\right|^2 dt < \infty \tag{3.2}$$

which implies that x(t) decays to zero as $t \to \pm\infty$, the wavelet transform of x(t) is expressed by the following inner product in the Hilbert space:

$$W_{\psi}(a,b) = \left\langle x(t), \psi_{a,b}(t) \right\rangle = \int_{-\infty}^{\infty} x(t)\, \psi^{*}_{a,b}(t) dt \tag{3.3}$$

where the asterisk stand for complex conjugate. This shows that the wavelet transform is a linear scalar product normalized by the factor $1/\sqrt{a}$ and this scalar product is a measure of the fluctuation of the signal x(t) around the point b at the scale a. The scaling operation is nothing more than performing stretching and compressing operations on the son wavelet, which in turn can be used to obtain the different frequency information of the signal to be analyzed. The compressed version is used to satisfy the high-frequency needs, and the dilated version is used to meet low-frequency requirements. Then, the translated version is used to obtain the time information of the signal to be analyzed. In this way, a family of scaled and translated wavelets is created and serves as the base, the base for representing the signal to be analyzed. In other words, the wavelet transform $W_{\psi(a,b)}$ can be considered as functions of translation b with each fixed scale a. It gives the information of x(t) at different levels of resolution and also

measures the similarity between the signal x(t) and each son wavelet $\psi_{a,b(t)}$. Note that the wavelet transform represents also the convolution between the signal x(t) and the wavelet function. This implies that a wavelet can be used for feature discovery if the wavelet used is similar to the feature components (eventually eigenfrequencies and damping coefficients) hidden in the analyzed signal. For the function $\psi(t)$ to qualify as an analyzing wavelet, it must satisfy the admissibility condition

$$0 < c_{\psi} = \int_{-\infty}^{\infty} \frac{\left|\psi(\omega)\right|}{\left|\omega\right|} d\omega < \infty \tag{3.4}$$

where $\psi(\omega)$ is the Fourier transform of $\psi(t)$. Then the wavelet transform can be inverted and the signal x(t) recovered:

$$x(t) = \frac{1}{c_{\psi}} = \int_{\infty}^{\infty} \int_{\infty}^{\infty} W_{\psi}(a,b) \psi_{a,b} \frac{da\, db}{a^2} \tag{3.5}$$

Note that since $|\psi(\omega)|$ tends to 0 when ω tends to $\pm\infty$, the Fourier transform of the wavelet can be considered as a band-pass filter.

For practical purposes, the possibility of time-frequency localisation arises if the wavelet g(t) is a window function, which means that $\psi(t)$ decays to zero as $t \rightarrow \pm\infty$:

$$\int_{-\infty}^{\infty} \left|\psi(t)\right| dt < \infty \tag{3.6}$$

and the wavelet transform analyses a signal x(t) only at windows defined by the wavelet function $\psi(t)$. If one assumes a fast decay of $\psi(t)$: the values of $\psi(t)$ are negligible outside a given time domain interval, the transform becomes local in time domain, in this interval.

The frequency localization can be explained when the wavelet transform is expressed in terms of the Fourier transform. Note $X(\omega)$ the Fourier transform of the signal x(t) and $a\psi^*(a\omega)\ e^{j\omega b}$ the Fourier transform of the son wavelet $\psi^*(t-b)/a$. Using the Parseval's theorem, we obtain

$$W_{\psi}(a,b) = \frac{\sqrt{a}}{2\pi} \int_{-\infty}^{\infty} X(\omega)\psi^{*}(a\omega)e^{j\omega b}d\omega \tag{3.7}$$

and the frequency localization depends on the scale parameter a. Note that this operation is equivalent to a particular filter band analysis in which the relative frequency bandwidth $\Delta\omega/\omega$ are constant and related to the parameters a,b and to the frequency properties of the wavelet. The local resolution of the wavelet transform in time and frequency is determined by the duration and bandwidth of analysing functions given by $\Delta t = a\ \Delta t_{\psi}$ and $\Delta f = \Delta f_{\psi}/a$, where Δt_{ψ} and Δf_{ψ} are the duration and bandwidth of the wavelet function. The resolution of the analysis is therefore good for high dilatation in the frequency domain and for low dilatation in time domain.

Before the calculation, the relevant parameters must be discretised for being computed by a computer. Instead of continuous dilatation and translation, the wavelet may be dilated and translated discretely by selecting $a=a_0^m$ and $b=nb_0a_0^m$ where a_0 and b_0 are fixed values with $a_0>1, b_0>0, m,n \subseteq Z$ and Z is the set of positive integers. We obtain then a discretised son wavelet and a corresponding discrete wavelet transform which provides a decomposition of a signal into sub-bands with a bandwidth that increases linearly with frequency. In the case of dyadic discretisation, the most popular method, we have $a_0=2$ and $b_0=1$ and each spectral band is approximately one octave wide. In this form, the wavelet transform can be viewed as a special kind of spectral analyzer.

The Wavelet transform is able to furnish information both in frequency and time domain. In general, for a generic signal x(t), the Wavelet transform is defined by the following integral:

$$CWT_x^{\psi}(a,b) = \frac{1}{\sqrt{|a|}} \int_{-\infty}^{+\infty} x(t) * \overline{\psi}\left(\frac{t-b}{a}\right) dt \tag{3.8}$$

where the function $\Psi_{a,b} = \frac{1}{\sqrt{|a|}} \overline{\psi}\left(\frac{t-b}{a}\right)$ is a scaled (a) and translate (t) version of the mother function.

To perform a wavelet transform of a generic signal, it's possible to follow this step [Matlab Toolbox, 2007]:

(i) Step: choice of the wavelet mother

In this case the Morlet function is considered, expressed by the following equation and rapresent in the following figure:

$$\psi(t) = e^{i\omega_0 t} e^{-t^2/2} \tag{3.9}$$

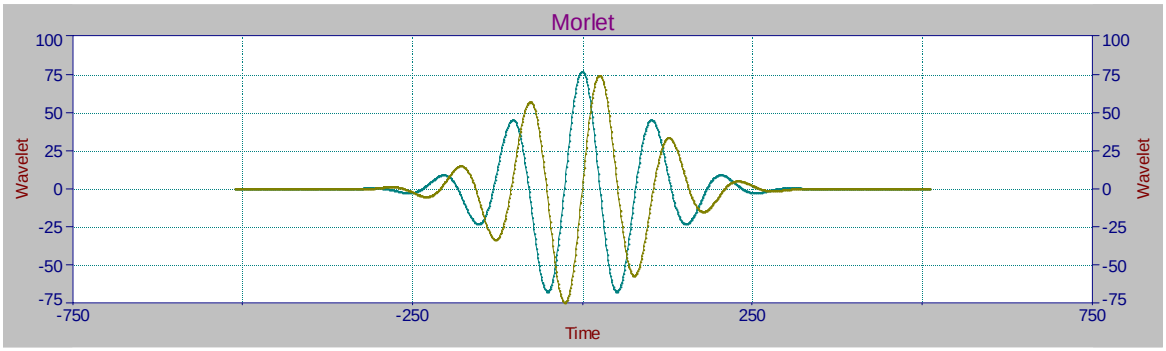

Figure 3.1.1 Morlet, mother wave, real and imaginary part

(ii) Step: definition of a scalar factor.

A frequency of the Morlet is defined and the wave is compared with part of the signal in the time domain at time zero

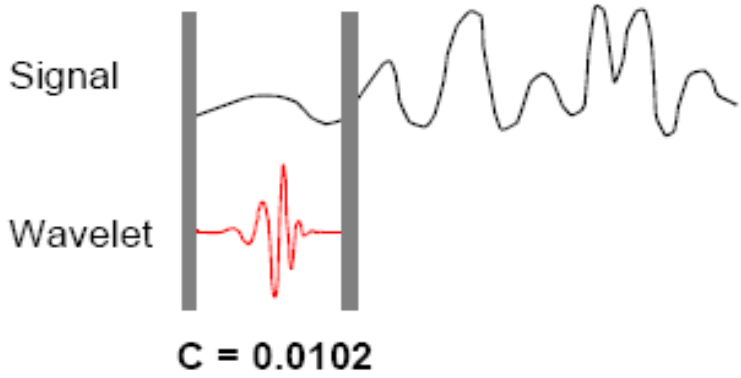

Figure 3.1.2 First step: wave is setted with a fixed scale and it is compared with the signal in the first time step

(iii) Step: translation of the wave

The same wave, with the same scalar factor, is translate in the time and for each time is compared with the signal

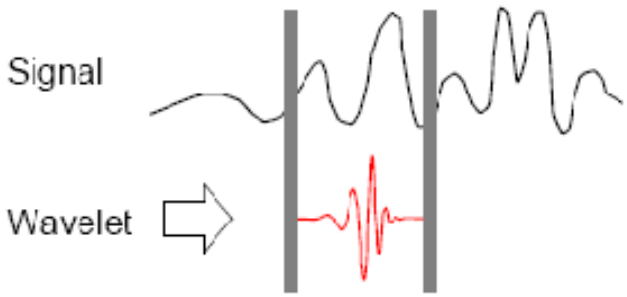

Figure 3.1.3 The wave with fixed scale a is only translate in time domain

(iv) Step: variation of the scalar factor

The frequency of the Morlet is changed and the pervious steps are repeated

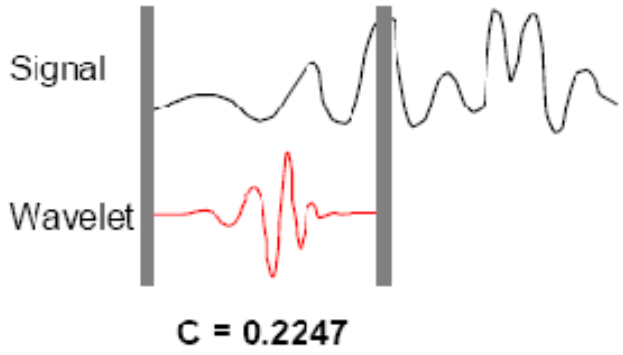

Figure 3.1.4 A second value of scale is define for the mother wave and the step 1-2 are reiterated

Wavelet transformations have been frequently applied to determine the dynamic characteristics of a time invariant linear system in the last decade. [Schoenwald 1993] identified the parameters in the equation of motion for a system with a single degree of freedom by applying a continuous wavelet transform to the equation of motion. Ruzzene et al. (1997) applied a discrete wavelet transform

and the Hilbert transform technique to determine the natural frequencies and damping of a structure system from its free vibration responses. [Robertson et al. (1998a and 1998b)] developed a procedure for extracting impulse response data from the dynamic responses of a structure and used an eigensystem realization algorithm to identify the dynamic characteristics of the structure. Gouttebroze and Lardies (2001) developed a wavelet identification approach in the time–frequency domain for elucidating the natural frequencies and damping of a structure from free vibration responses. Their approach cannot directly determine the mode shapes. Lardies and Gouttebroze (2002) further applied their wavelet identification technique (Gouttebroze and Lardies, 2001) to process the measured ambient vibrations of a TV tower, by first extracting a free vibration signal from the measured ambient vibration responses, using the conventional random decrement technique. [Alvin et al. 2003] presented an overview of the use of the wavelet transformation technique for extracting impulse response functions; they also reviewed robust ways of identifying both proportional and nonproportional damping parameters.

Then, the computation of the CWT is done at the beginning for an ideal case, where the signal is defined by the expression

$$x\left(t\right) = A e^{-\xi 2\pi f_v t} \, \mathrm{s}\, en\left(2\pi\sqrt{1-\xi^2} f_v t\right) \tag{1.10}$$

to extract the natural frequency of the signal and its modal damping using only one Wavelet transform. The trend of the CWT is described in the Figure 3.1.5. If the diagram of the CWT is sectioned at a value of the time constant, the natural frequencies of the signal could be obtained in correspondence of the peaks of the CWT.

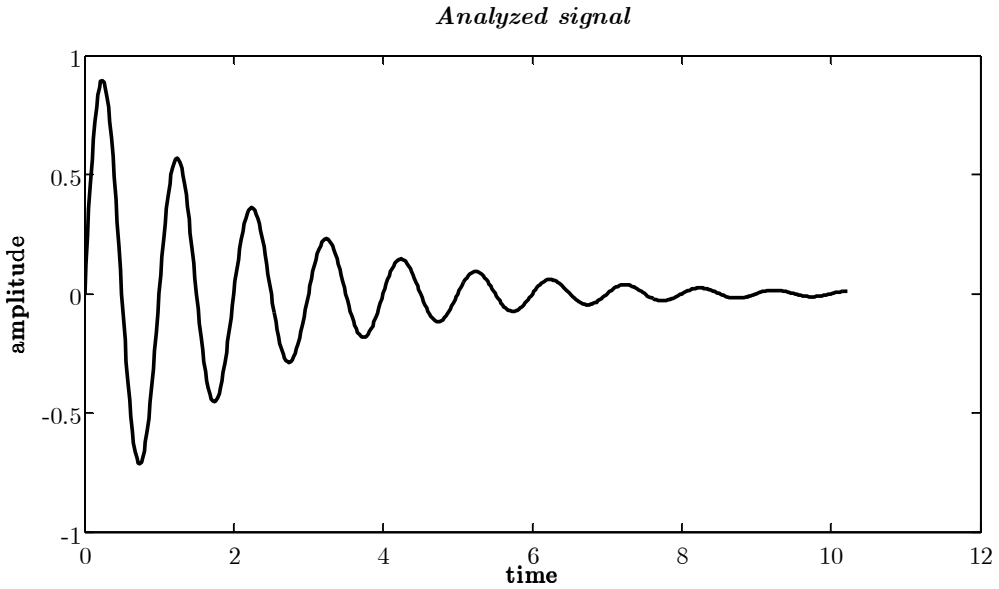

Figure 3.1.6 simulated signal with natural frequency 2 Hz and modal damping 7.2 %

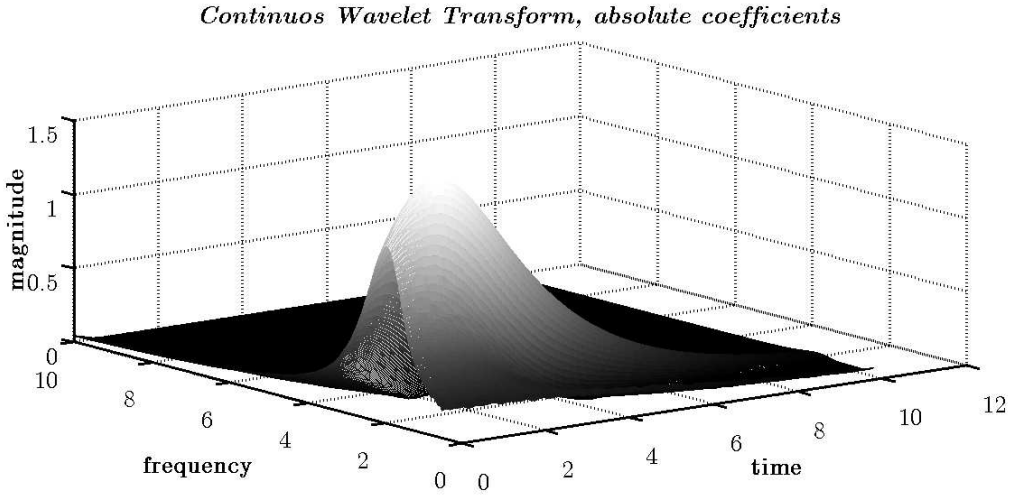

Figure 3.1.7 Its Continuous Wavelet Transform

When the natural frequency of the simulated signal is known, the same diagram is sectioned at constant frequency equal to its resonance frequency. It is possible define how the amplitude of the signal damps during the time. The exponential function, that better represented this trend obtained through the minimum square method, permits to define the damping factor of the system.

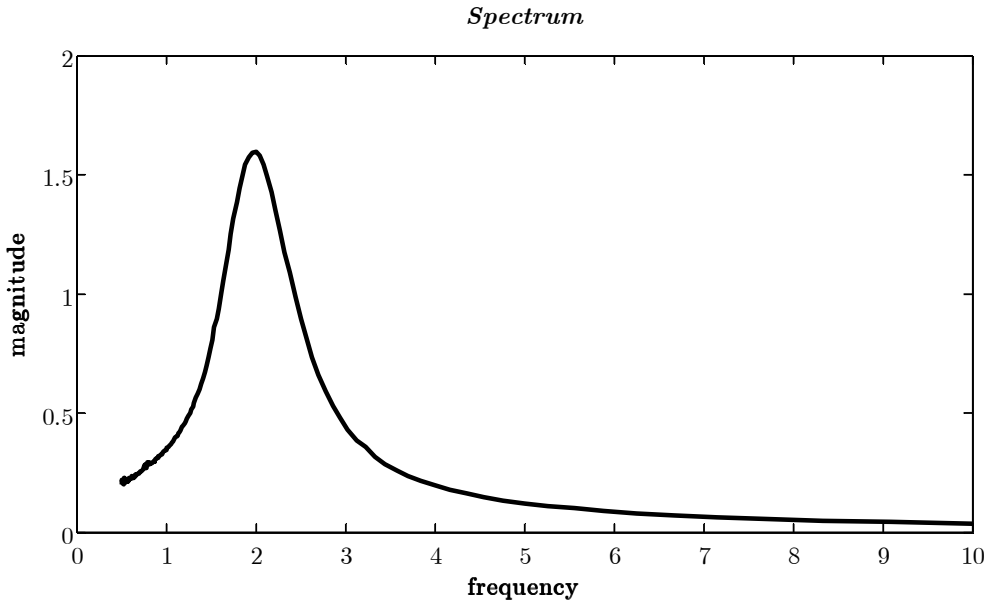

Figure 3.1.8 Spectrum of simulated signal, CWT in frequency domain

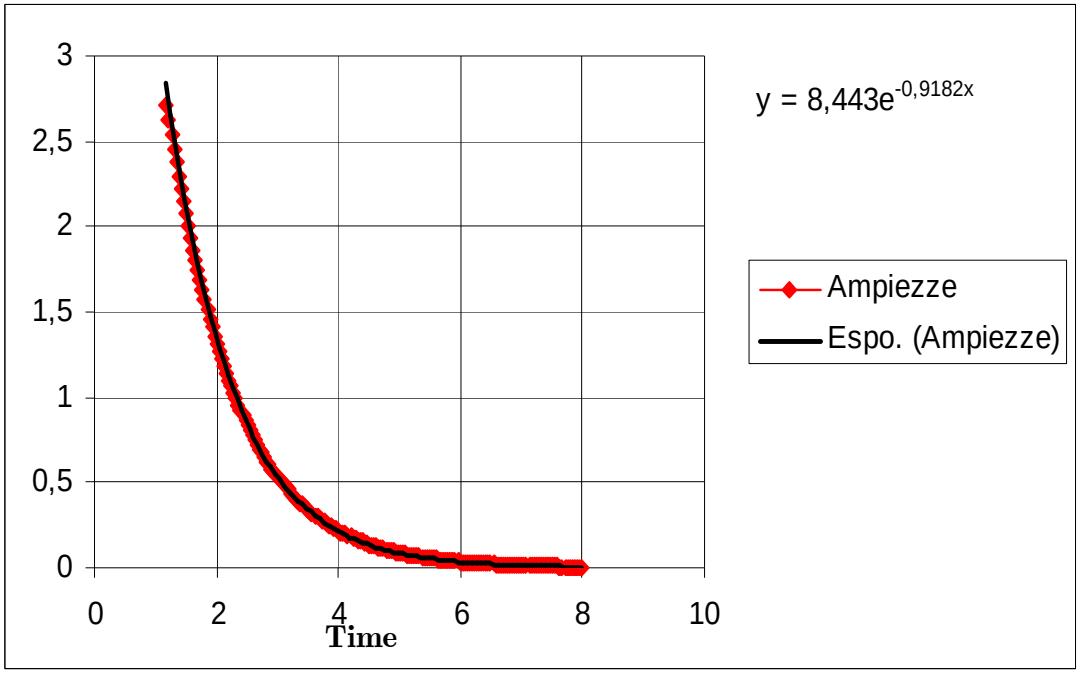

Figure 3.1.9 Wavelet trend in time domain at fixed frequency.

The same mythology is applied in the real case; in the following figures the trend of the CWT is shown for the signal acquired by a sensor during a free vibration test. In Figure 3.1.7 the 3-D Wavelet transform is represented, in Figure 3.1.8 it is sectioned at constant time and in Figure 3.1.9 it is sectioned at constant frequency, equal to the natural frequency of the system.

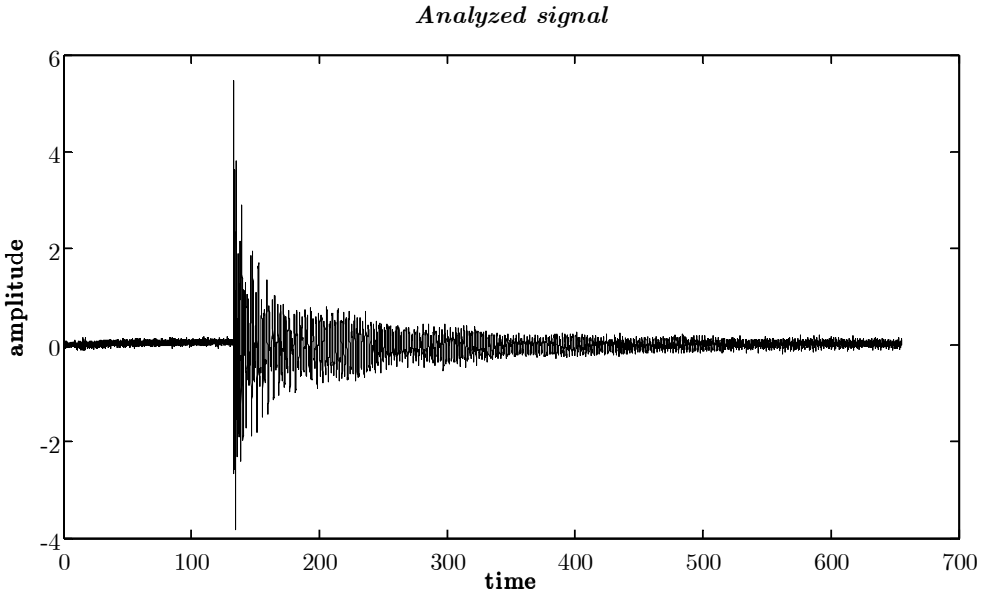

Figure 3.1.10 signal acquired during a free vibration test.

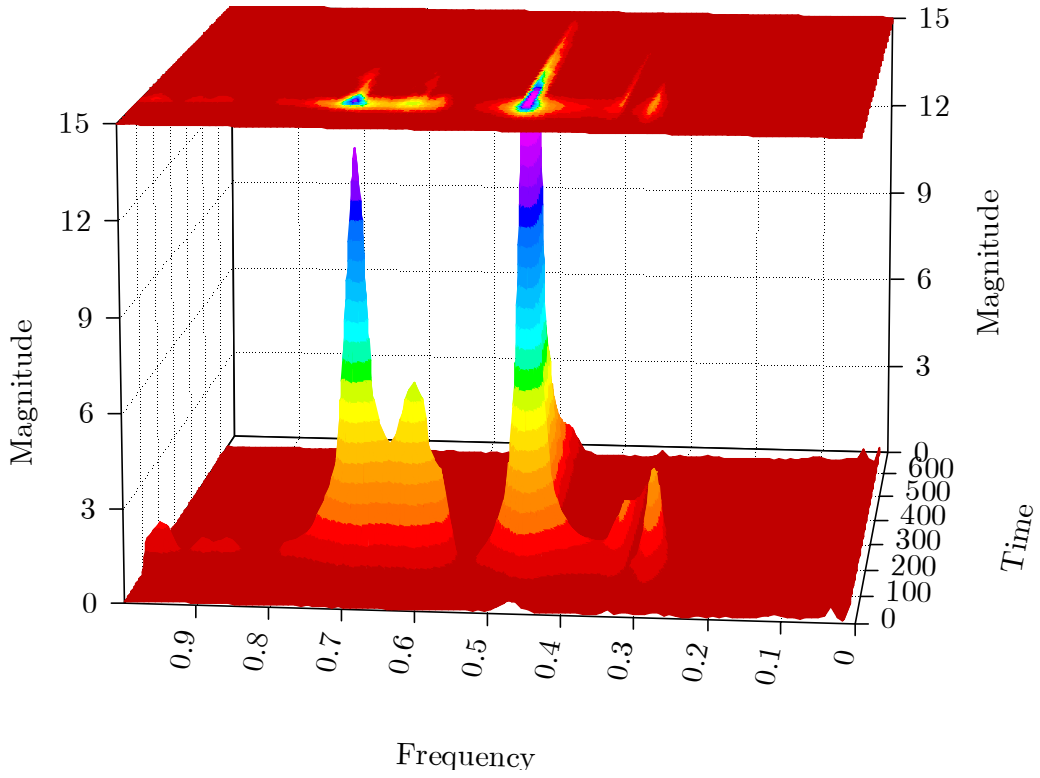

Figure 3.1.11 CWT, front view

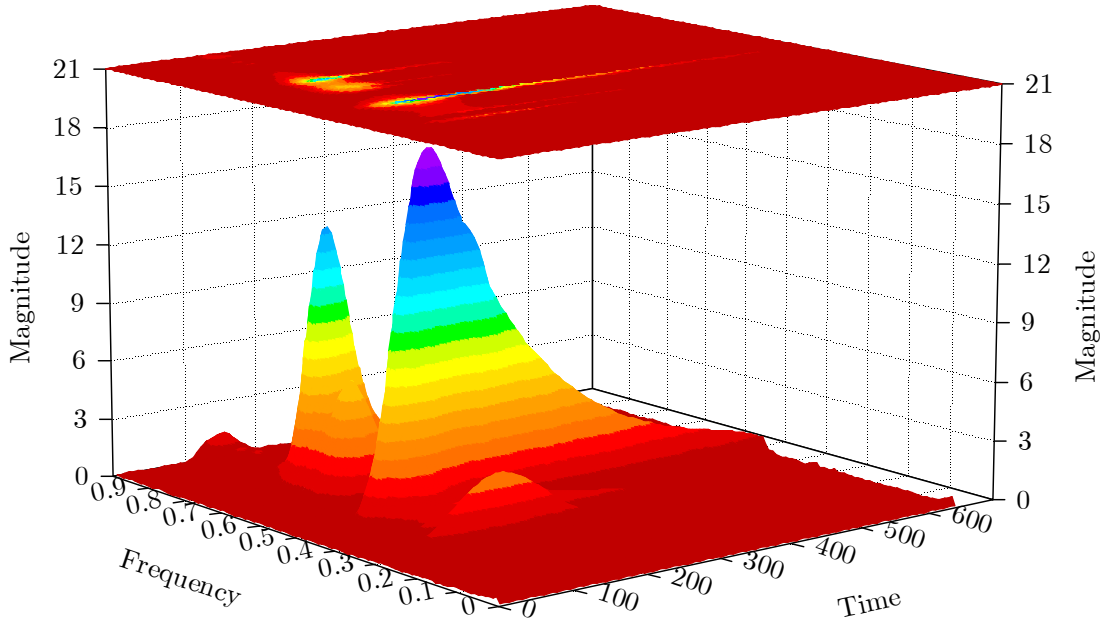

Figure 3.1.12 CWT time-frequency domain representation, lateral view

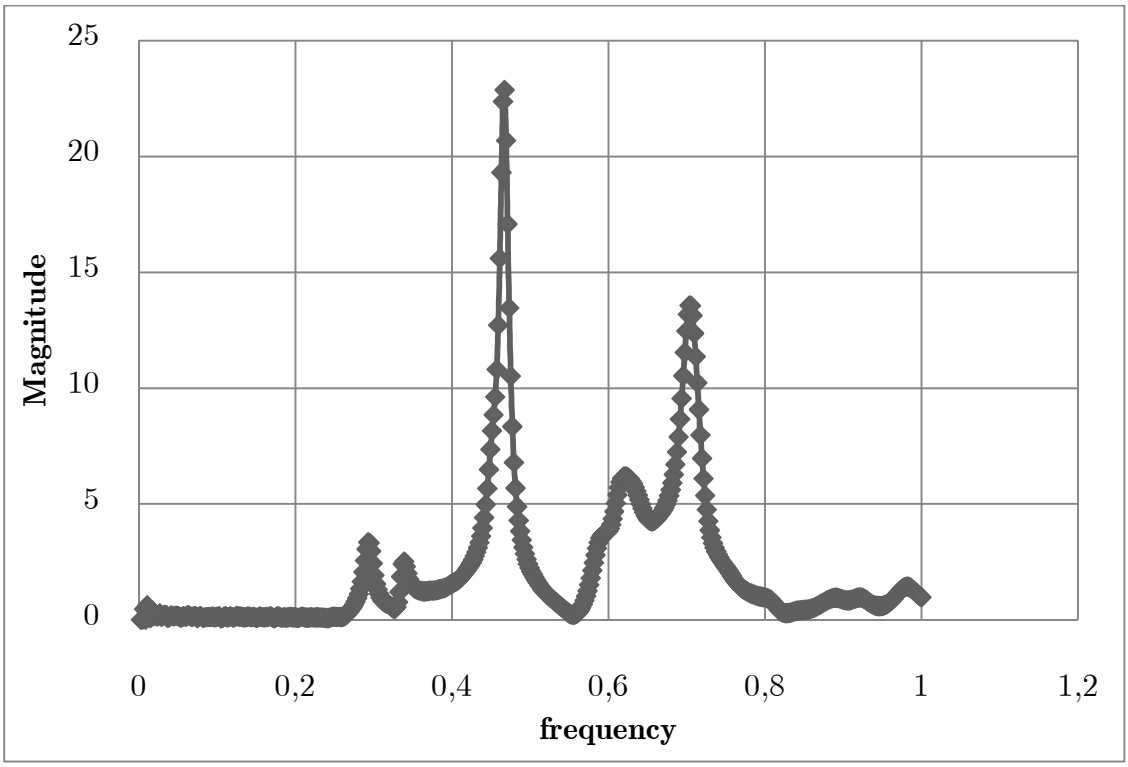

Figure 3.1.13 CWT, representation in frequency domain

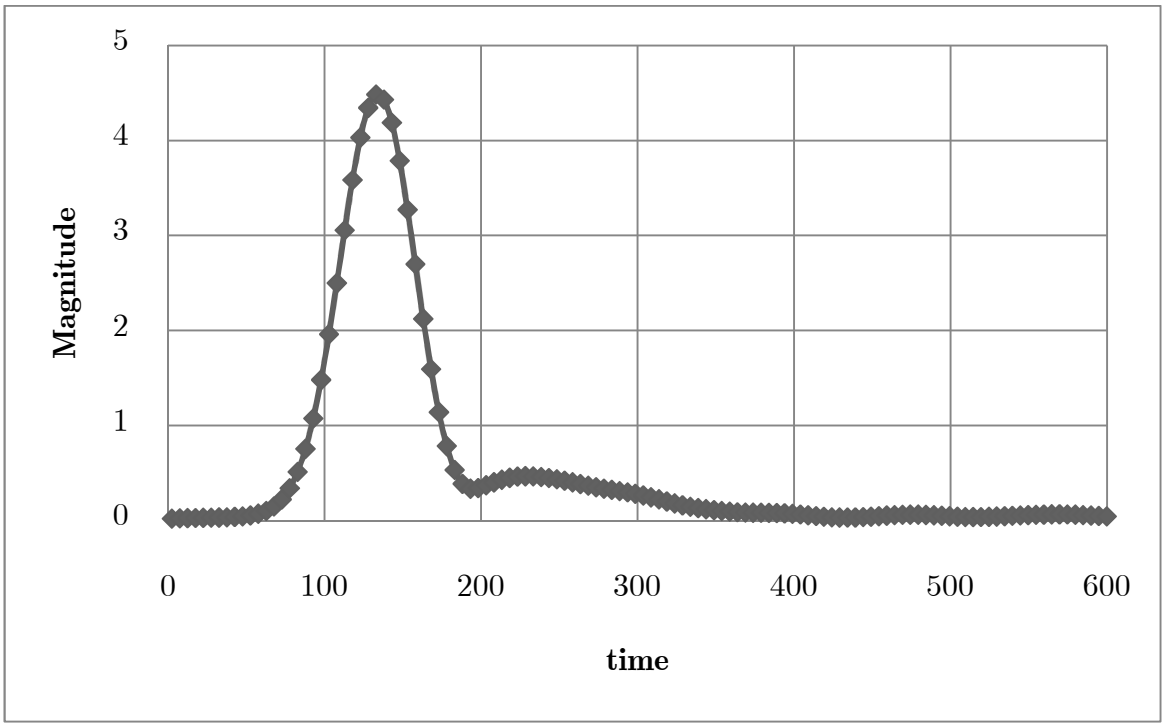

Figure 3.1.14 *CWT in time domain at fv = 0.647 Hz*

3.2. Extraction of the modal parameters from the free vibration test via WT

The first case analysed via WT is a vibration test carried out on the footbridge described in the chapter two. To verify the validity of the modal parameters obtained by the analysis of the acquired signals, the free vibrations of the system was considered afterward. The footbridge was subjected to a shock test only in first instance (2000 test) and the response of the structure was recorded through the same accelerometers previously described. An example of the recorded signal is reported in the Figure 3.2.1, where accelerometer 2 is considered. In particular, the acquired signal of the free vibrations are described through 16384 sampled points and with a sampling step equal to 1000 points for second, this entail that the frequency step of the FFT of the same signal is equal to 1000/16384 = 0.06 Hz. At the beginning the FFT is computed for each signal acquired and the

natural frequencies of the system are defined. The interpretation of the first natural frequency of the footbridge is very difficult because two very proximal peaks of the FRF (they are equal to 1.1 Hz and 1.3 Hz) are obtained.

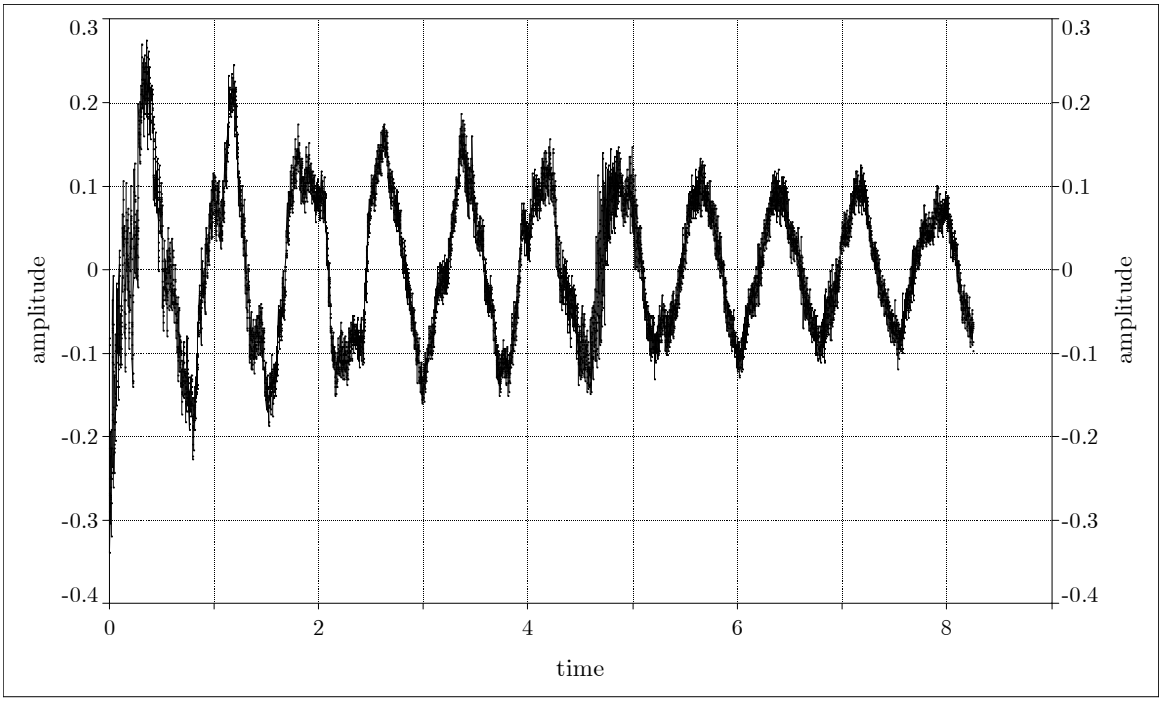

Figure 3.2.1 Time trend of the signal acquired by accelerometer A2

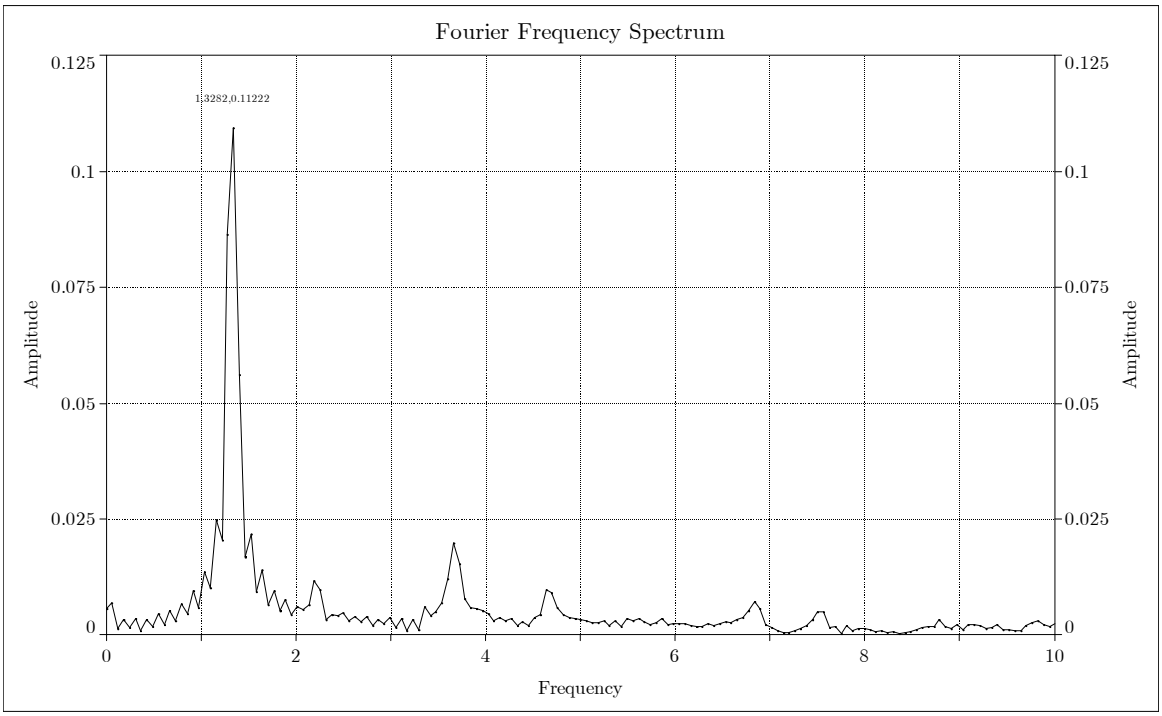

Figure 3.2.2 Signal acquired during the shock test and its Fourier Transform

The computation of the FFT gives good information about the frequencies of the analyzed signal but is not able to give any information about its behavior during the time. Then the use of the FFT, when the signal is not stationary, does not describe completely the behavior of the system. For this reason, note the natural frequencies of the system trough the classical FFT, for each recorded signal the Wavelet transform, that is able to furnish information both in frequency and time domain, is computed. Then, the methodology previously described is applied in the real case; in the following figure the trend of the CWT is defined for the signal acquired by the accelerometers 1.

The section of the diagram at constant time allows the individuation of the natural frequencies of the footbridge. For each value of the resonance frequency the CWT is sectioned and the variation of the amplitude of the signal in the time is obtained. By the exponent of the exponential function that better describes the trend of the variation of the amplitude of the signal, it is possible define the damping factor for each vibration mode of the footbridge.

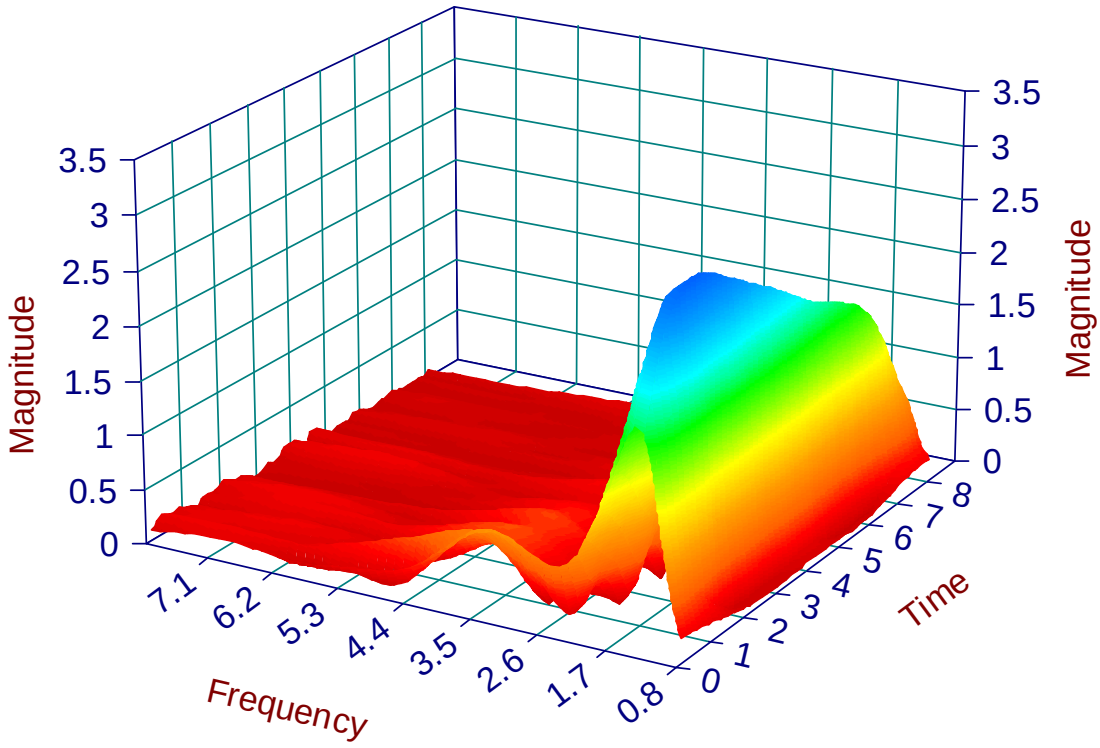

Figure 3.2.3 Example of Wavelet Transform of the signal acquired by A1

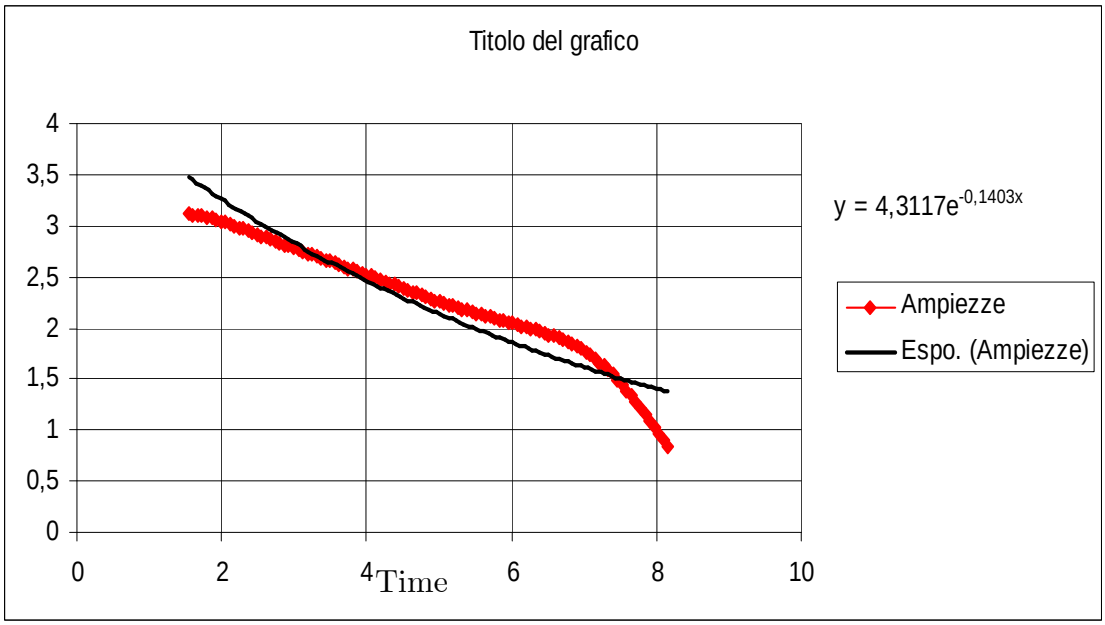

Figure 3.2.4 Time trend of CWT, evaluation of modal damping

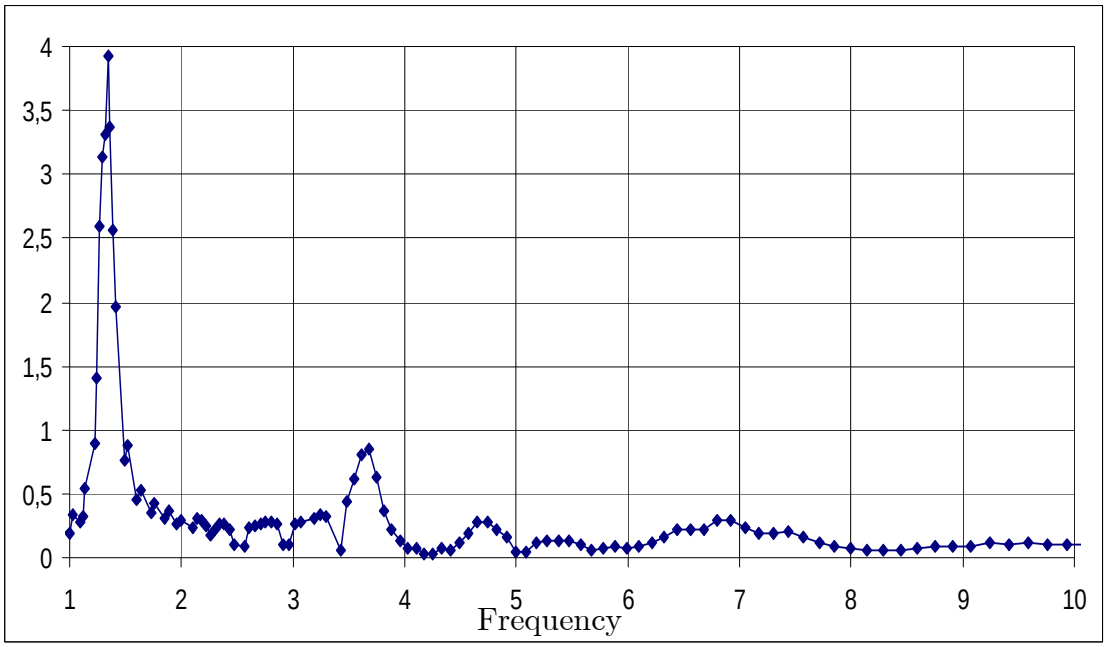

Figure 3.2.5 Frequency domain representation of CWT, evaluation natural frequencies

The obtained results are summarized in the following table and compare with the value previously obtained through the forced vibration test (see chapter two).

The frequencies are in good agreement between the two methods, instead the modal dampings are very different.

Table 1 Modal parameters, extracted by the FFT and CWT

Frequency (FRF)	Frequency (Wavelet)	Damping (Half power)	Damping (Wavelet)
1.3	1.34	-	0.0165
1.4	1.52	0.04135	0.0125
1.7	1.75	0.0315	0.0087
2.2	2.18	0.0175	0.0085
3.7	3.69	0.0177	0.0106

The frequencies of the system are almost the same, whereas the modal dampings are very different. This because the half-power method can be applied successfully only if the vibration modes are distinct. This hypothesis entail that the each mode cannot be influenced considerable from the another modes. From the results obtained by the Half-power method, the FRF, corresponding to the SDFOS characterized by the natural frequency and the modal damping identified from the inertance, was described. The diagram shows that the contribution of the modes, which are immediately before and after the considered mode, cannot be neglect.

3.3. Free vibration test on Vasco de Gama Bridge.

3.3.1. Bridge description

The Vasco da Gama Bridge is a cable-stayed bridge flanked by viaducts and roads that spans the Tagus River near Lisbon. It was designed and built by the consortium LUSOPONTE. SA.. It is the longest bridge in Europe (including viaducts) with the total length of 17300m, involving three interchanges, a 5km long section on land and a continuous 12300m long bridge. Its purpose is to

alleviate the congestion on Lisbon's other bridge (25 de Abril Bridge), and to join previously unconnected motorways radiating from Lisbon. The bridge was opened to traffic on March 29, 1998, 18 months after construction first began, just in time for Expo 98, the World's Fair that celebrated the 500th anniversary of the discovery by Vasco da Gama of the sea route from Europe to India [Caetano, 2000].

Figure 3.3.1 Cable-stayed component of Vasco da Gama Bridge

This bridge includes a cable-stayed component over the main navigational channel with a main span of 420m and three lateral spans on each side (62m+70.6m+72m), resulting in a total length of 829.2m (Figure 3.3.1). The bridge deck is 31m wide and is formed by two lateral prestressed concrete girders, 2.6m high, connected by a cast in situ slab 0.25m thick and by transversal steel I-girders every 4.42m. The bridge is continuous along the total length and is fully suspended at 52.5m above the river by two vertical planes of 48 stays connected to each tower. The two H-shaped towers are 147m high and a massive zone exists at their base as a protection against ship impact. With regard to the stay cables, that consist of bundles of parallel self-protected strands covered by an HDPE sheath, specific protection against vibration was adopted, namely by inclusion of a double helical rib in the cable cover for prevention of rain wind vibration, and by use of innovative damper devices placed inside the steel guide pipe of the cables at the deck anchorages. Given the actively seismic location of the bridge

site, specific measures were taken in the design of the bridge, namely the adoption of a full suspension deck from flexible towers in order to minimize the seismic forces. Additionally, a set of hysteretic steel dampers connecting the pylons and the deck were introduced, in order to limit the displacements. Under service loads, the transverse dampers work within the elastic range, acting as elastic supports, while the longitudinal dampers allow low speed displacements. In case of earthquake, Innovative elastoplastic dampers were placed between the deck and the towers to reduce horizontal seismic movements.

3.3.2. Experimental setup

The free vibration test was carried out on the Vasco da Gama bridge due two main reasons : 1) to check the previously developed model and 2) to define the damping factors associated to the vibration modes of the structure.

Figure 3.3.2 Eccentrically suspended barge, its cutting and release

A barge weighting 60t was attached at one point of the deck close to the section 1/3 spam North. The barge became suspended with the low tide (Figure 3.3.4 Sensors localization on the structure) and was subsequently released by cut of the suspension Dewing bar at the deck level. A vibratory phenomenan was then generated, which was recorded during 16 minutes by 6 triaxial accelerographs, located at the sections 1/3 and 1/2 span (upstream and downstream).

The time series are formed by 32768 points, sampled at 50Hz, what corresponds to a total acquisition time of 655s. An example of the acquired signal is represented in the following figure, in particular the signal recorded in correspondence of the 1/3 span South downstream is considered.

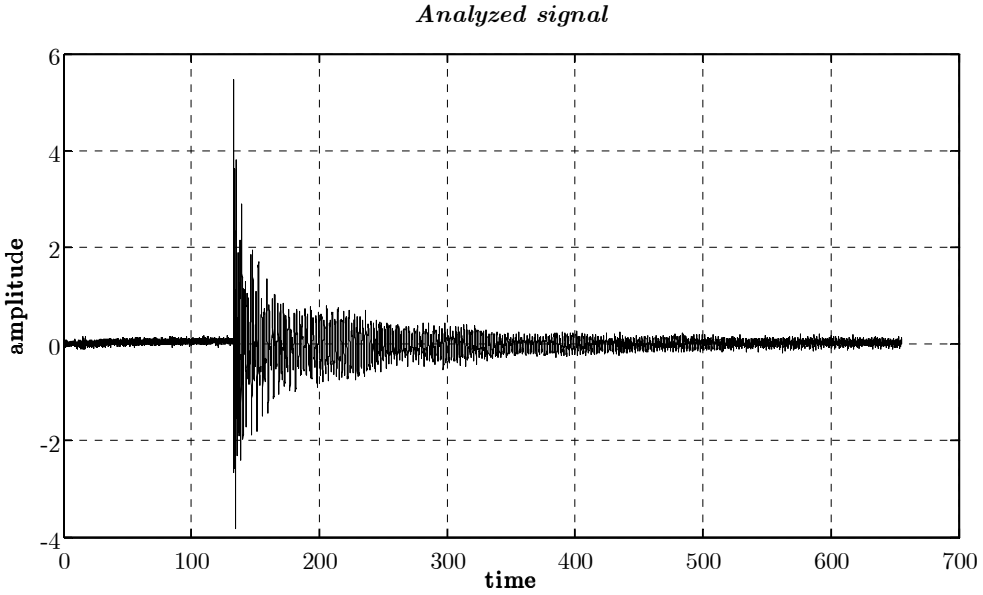

Figure 3.3.3 Signal acquired by the accelerographs located in position M10, z-direction

The free vibration response associated with the cutoff of a 60 ton mass from 1/3rd span Upstream was measured, using three different measurement systems:

- triaxial accelerographs Geosys, GSR-16, which were mounted at the edges of the bridge deck, at the following locations: 1/3 span north, upstream and downstream; ½ span, upstream and downstream, and 1/3rd span South, upstream and downstream. The nodes involved in the measurements are marked in the Figure below. The 5 accelerographs were synchronized by the PC clock and should be considered all synchronized;

- uniaxial FBA11 accelerometers, connected to a Kinemetrics recorder, mounted at station located on 1/3rd span South, upstream. Although the acquisition parameters were identical, the three records measured using this system are not perfectly synchronized with the other records, as it was not possible to use the same trigger. Moreover, the data is presented in different format, and one of the records (along the transversal direction was not good);

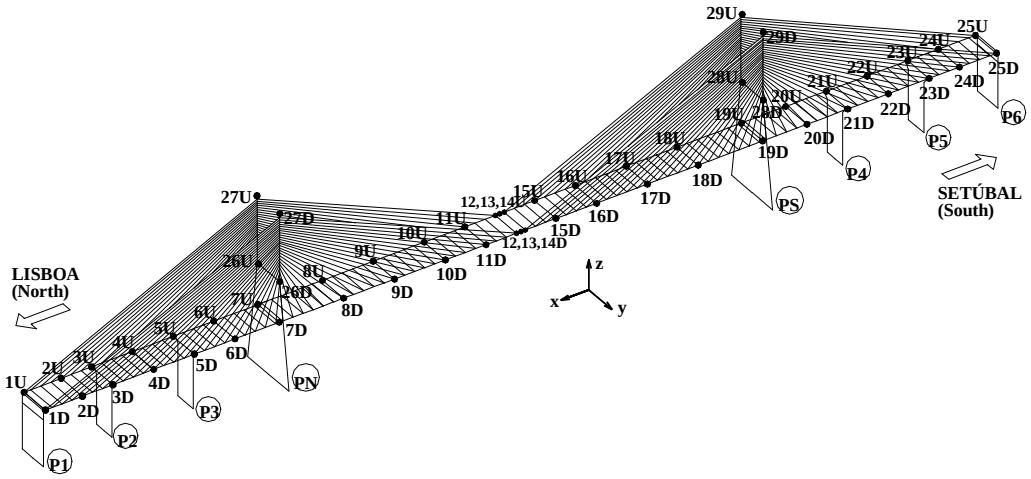

Figure 3.3.4 Sensors localization on the structure

This data represents the core data and was sampled at 50Hz. The records associated with the measurements are named according to the table indicated below. The Figure 3.3.4 Sensors localization on the structure the location of all the sensors used to recorded the structure response. The free vibration test involved only the central part of the cable-stayed bridge; the other sensors, represented in the Figure 3.3.4 Sensors localization on the structureThe data were analyzed by many researchers; Prof. Elsa Caetano studied it in her PhD thesis, Rune Brinker extracted the structural modal parameter through FDD, Guido de rock used instead a method in time domain and updated a FE model starting from these data. In this thesis only the free vibrations are considered and analyse through WT. This data represents the core data and was sampled at 50Hz. The records associated with the measurements are named according to the table indicated below.

Table 2 Accelerometers location for the free vibration test

Station	File	Node
1/3 span North, upstream	M10.asc	10U
1/3 span North, downstream	J10.asc	10D
1/2 span, upstream	M13.asc	13U
1/2 span, downstream	J13.asc	13D
** 1/3 span South, upstream	M16x.asc M16z.asc	16U
1/3 span South, downstream	J16.asc	16D

3.3.3. Results

The modal parameters of the structure were extracted in 1998 through the classical Peak-picking method. In the PhD thesis "Dynamics cable-stayed bridges: experimental assessment of cable-structure interaction", natural frequencies, modal dampings and mode shapes are available. The same signals, acquired during this test, are analyzed by the wavelet transform and the results are compared. An example of the Wavelet transform is represented in the following figures. The signals acquired at section j10 and j 16 are considered; the CWT are computed both in y e z direction, to define the transversal and vertical modes shape of the bridge. In both the case the CWTs are very clean and it is easy to define the natural frequencies in correspondence of their peaks. The time trend of the CWTs is very clean too, and the modal damping can be easily define through

the exponential function that better approachs the CWT time decay for each natural frequency.

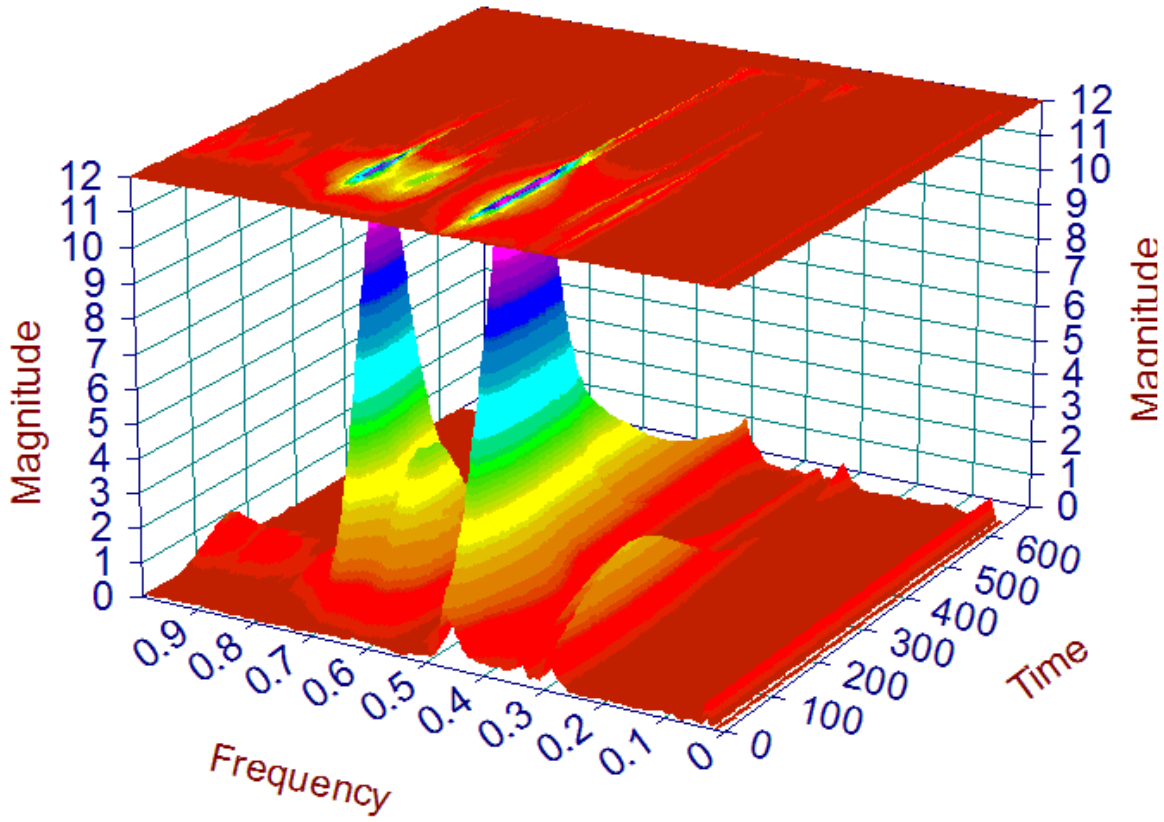

Figure 3.3.5 D Wavelet Transform of J10 y-direction

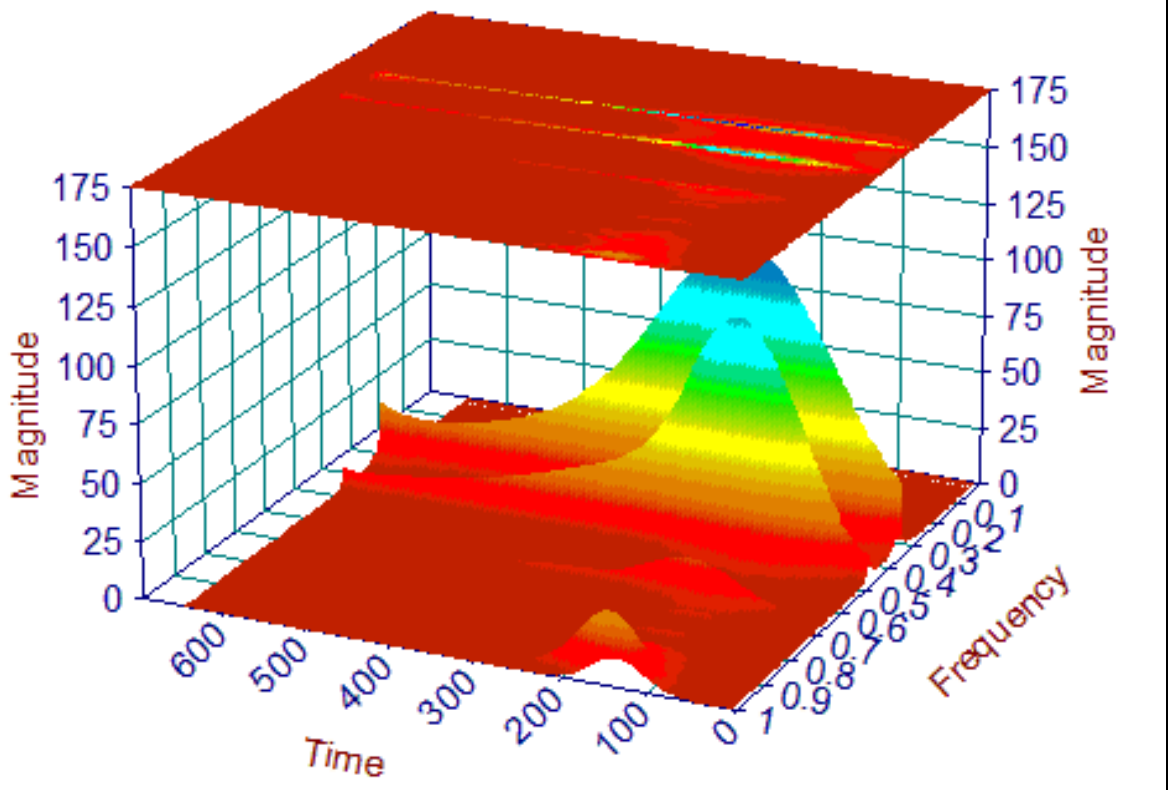

Figure 3.3.6 Wavelet Transform of J16 z-direction (b)

The natural frequencies of the structure are defined by the peaks in the frequency domain of the WT. In the free vibration test of the Vasco da Gama bridge the natural frequencies of the system are summarized in the following table; in particular the natural frequencies are compared to the frequencies, execrated from the same test but by classical FFT. Prof. Elsa Caetano, in her PhD Thesis, defined for each recorded acceleration the FRF and she extracted the natural frequencies through the Peak-Peaking method, explained in chapter two. The results show a good agreement; it is noticeable that the CWT is able to indentify some additional frequencies. In particular these frequencies were computed through the analysis of the ambient test carried out on the bridge at the same time. The modal parameters were extracted by the FDD and the results are available in the paper Cunha et al., 2004.

Table 3 Natural frequencies trough WT and PP, comparisons

NATURAL FREQUENCIES			
FFT	WT		
0,296	0,296	1 transversal	
0,338	0,338	1 vertical	
0,456	0,456	2 vertical	
0,467	0,467	1 torsional	
0,591	0,591	2 torsional	
	0,616	3 torsional	
0,647	0,647	3 vertical	
0,653	0,651	4 torsional	
0,707	0,708	4 vertical	
0,814	0,817	5 transversal	
	0,889	torsional	
	0,92	torsional	
0,982	0,98	5 vertical	

As Figure 3.3.3 shows, the signal acquired is very clean, only its detrend is necessary; for this reason too a good agreement of the results are obtained, both in free and ambient tests, for each methods applied. The modal damping for each frequency of the system was extracted by the WT and the results are compared with damping defined by FFT.

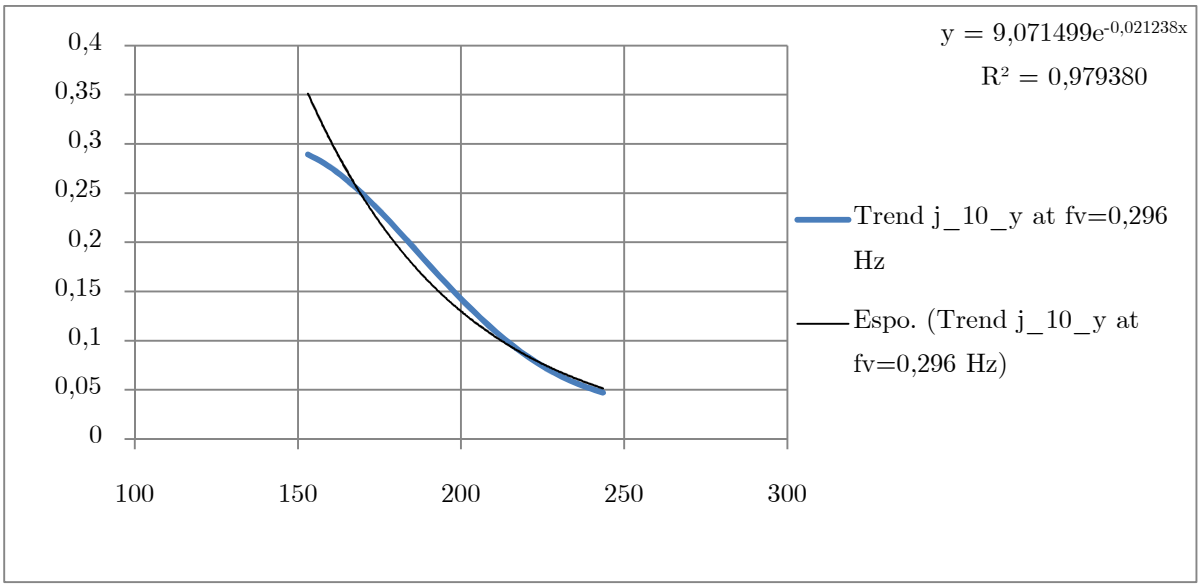

Figure 3.3.7 Trend of the WT in the time domain for a defined value of the natural frequency

The results are in good agreement except for the frequency 0,707 Hz (4^{th} vertical vibration mode). In particular, to extract modal damping, the same WT represented in figure 2.5, is sectioned at constant frequency (equal to a natural frequency). The trend of the WT in the time domain defines the modal damping at a fixed natural frequency, how described above. An example is represent in the following figure

The modal dampings for each mode are summarized and compared with the other one obtain trough the logarithmic decrement. It's noticeable that the modal dampings are completely different in correspondence to the frequency 0.591 Hz. A possible interpretation of this important variation is the presence of very close torsional mode around that frequency.

Table 4 Modal dampings trough WT and logarithmic decrement, comparisons

FREQUENCY	DAMPING FACTOR		VARIATION
WT	COMPLEX EXPONENTIAL	WT	
0,296	1,23	(0,78)1,35	9,756098
0,338	0,21	0,23	9,52381
0,456	0,23	0,23	0
0,467	0,24	0,24	0
0,591	0,34	0,71	108,8235
0,616			
0,647	0,37	0,48	29,72973
0,651			
0,708	0,78	0,65	-16,6667
0,817	0,48	0,52	8,333333
0,889			
0,92			
0,98	0,74	0,62	-16,2162

When the free time responses recorded from several points of the structure are available, phase and amplitude relationships between the different degrees of freedom of the system can be obtained through the wavelet transform analysis. The ith mode shape of the structure can be estimated by evaluating the wavelet transform of the time signals from all measured points, at the corresponding i-th frequency, that is for a = a_i. Let W_j (a_i; b) be the wavelet transform of the signal obtained from the accelerometer positioned at point j and let W_r (ai; b) be the wavelet transform of the signal obtained from the accelerometer of reference, positioned at point r. The quantity

$$\chi_{ij} = W_{\psi}^{j}(a_i, b) \Big/ W_{\psi}^{r}(a_i, b) \tag{3.11}$$

represents the jth component of the ith complex mode shape of the structure, referred to point r. Through eq. (3.11) and the comparison between the wavelet phase of the two signal, it is possible to define modes shape of the structure for

each natural frequency. The mode shape, obtained by the WT are compared to the mode shapes obtained by classical FFT method.

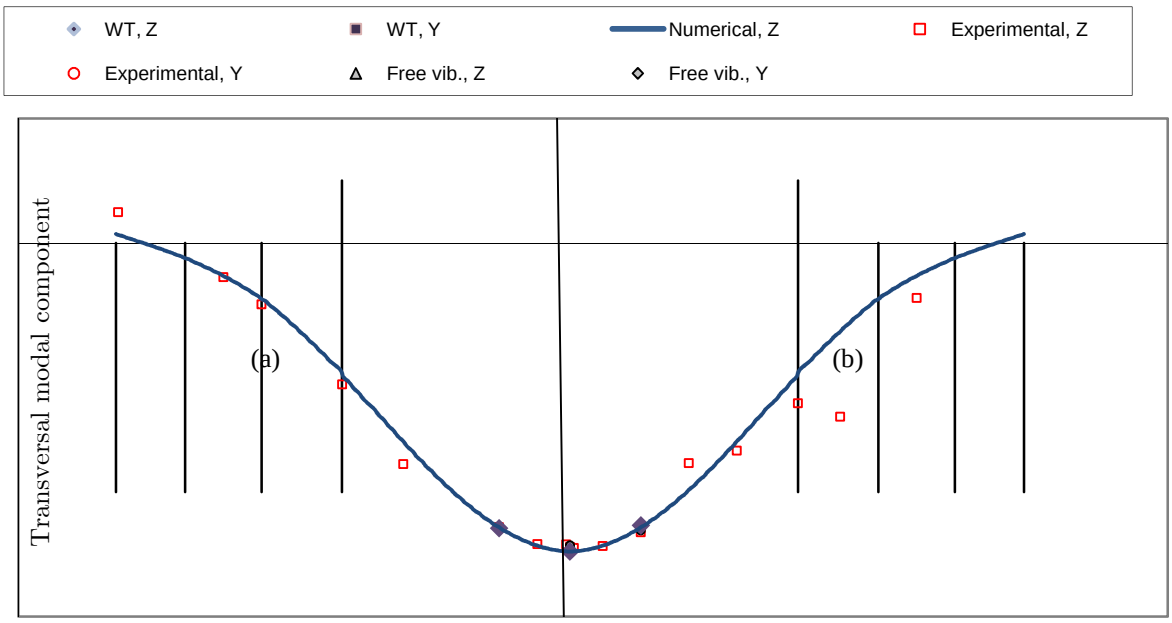

Figure 3.3.8 Comparisons between identified mode shapes using PP and WT: Mode 1 transversal fv= 0.296 Hz

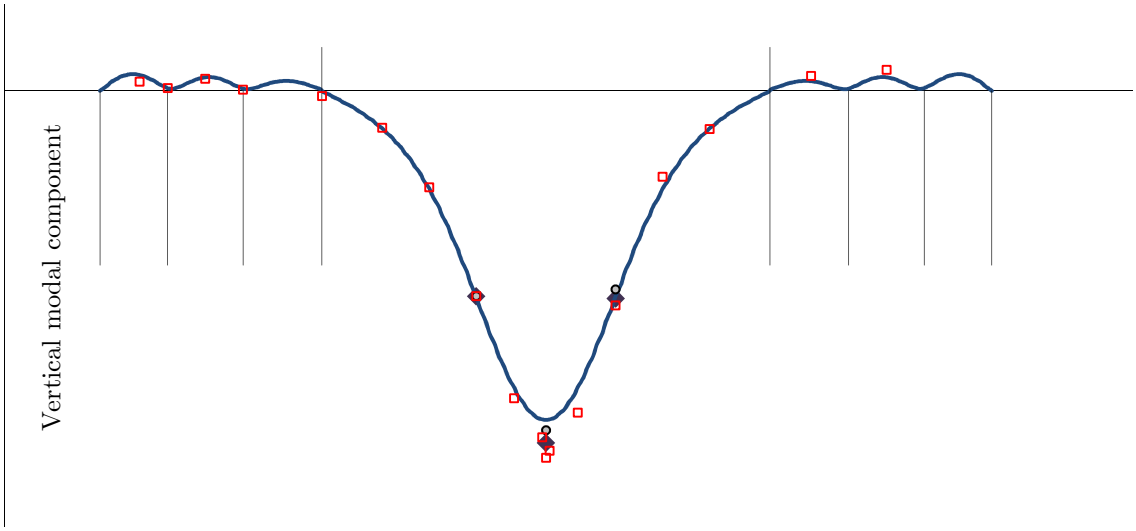

Figure 3.3.9 Mode 1 vertical fv = 0.338 Hz

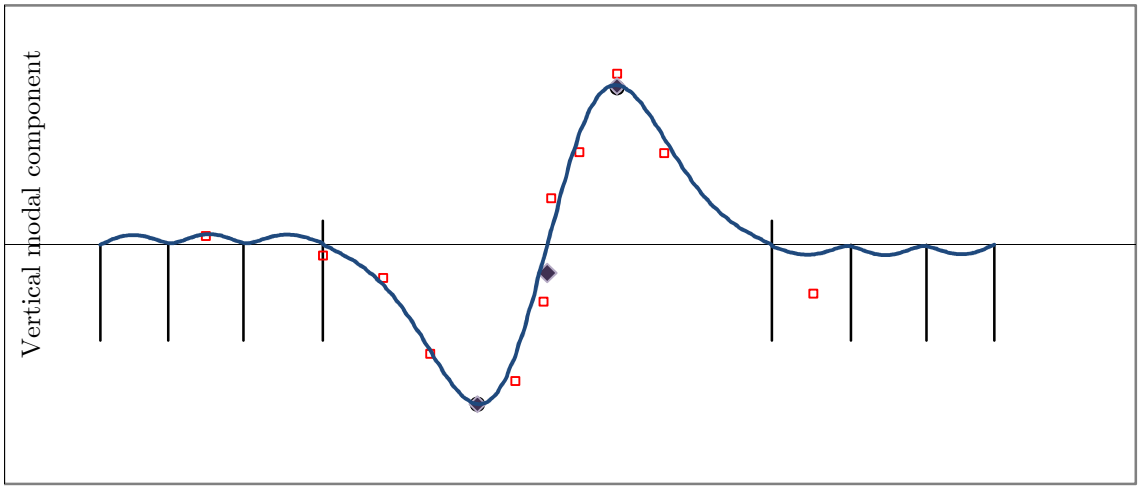

Figure 3.3.10) Mode 2 vertical fv= 0.456 Hz

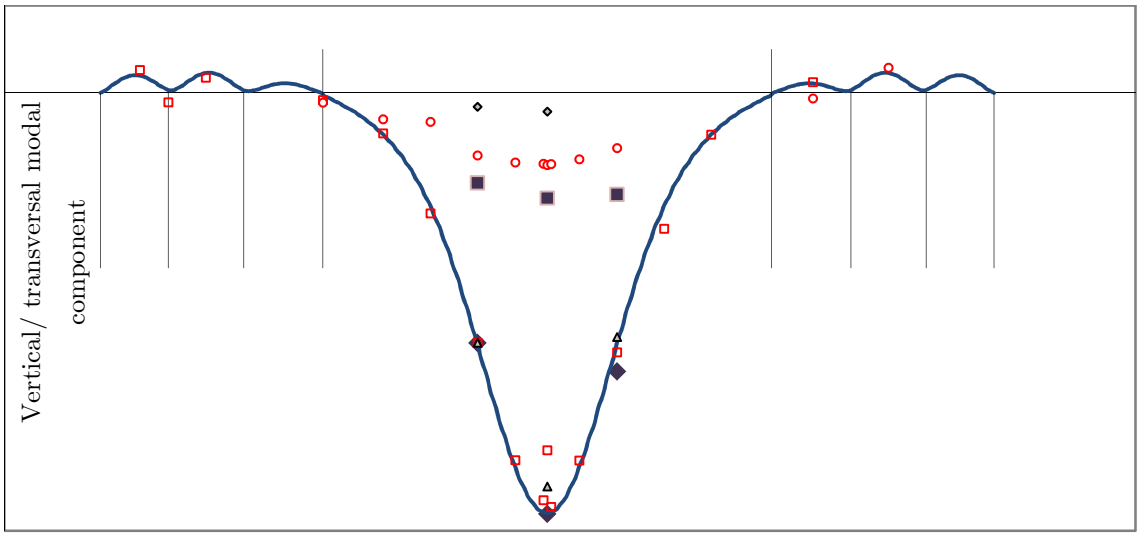

Figure 3.3.11 Mode 1 torsional + transversal fv = 0,467 Hz

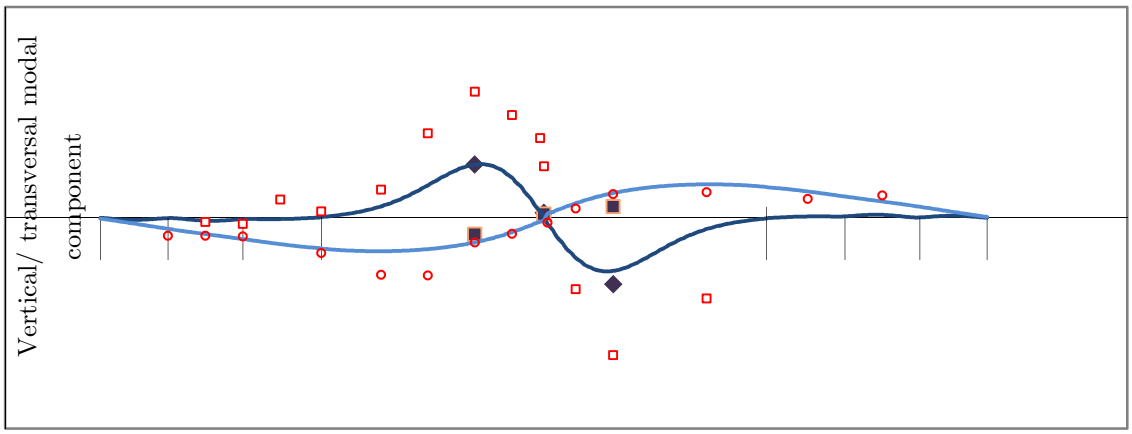

Figure 3.3.12 Mode 2 torsional + transversal fv = 0.591 Hz

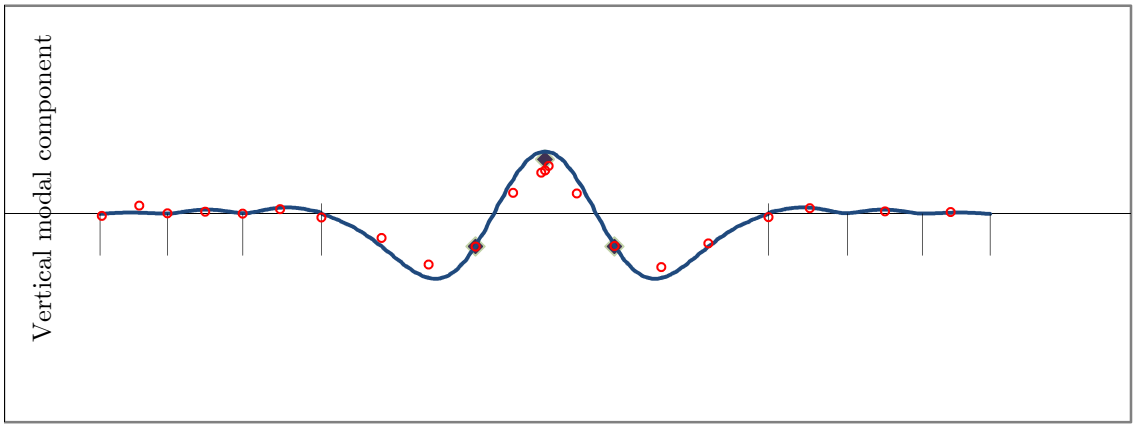

Figure 3.3.13 Mode 3 vertical fv = 0.647 Hz

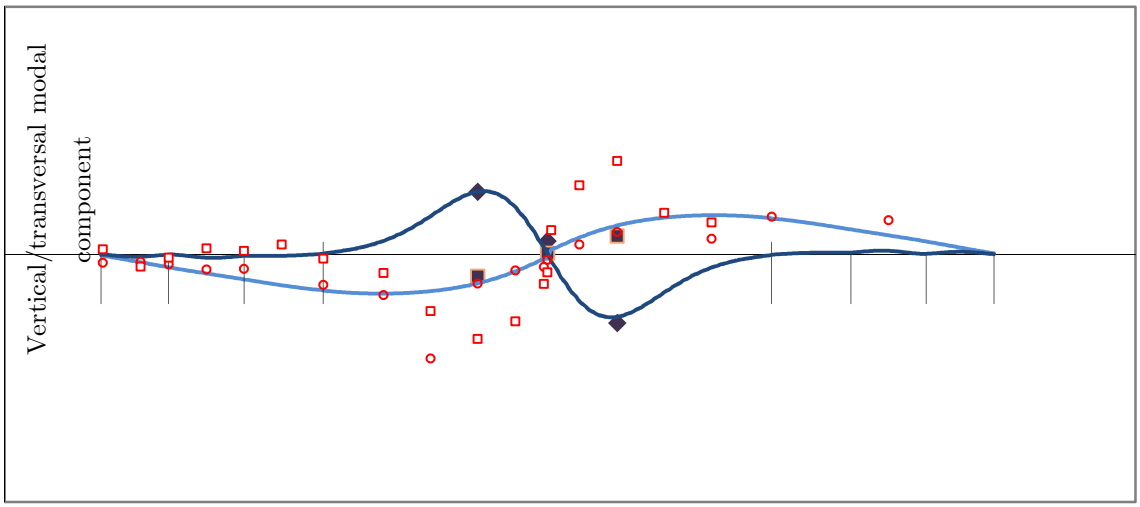

Figure 3.3.14 Mode 3 torsional + transversal fv= 0,651 Hz

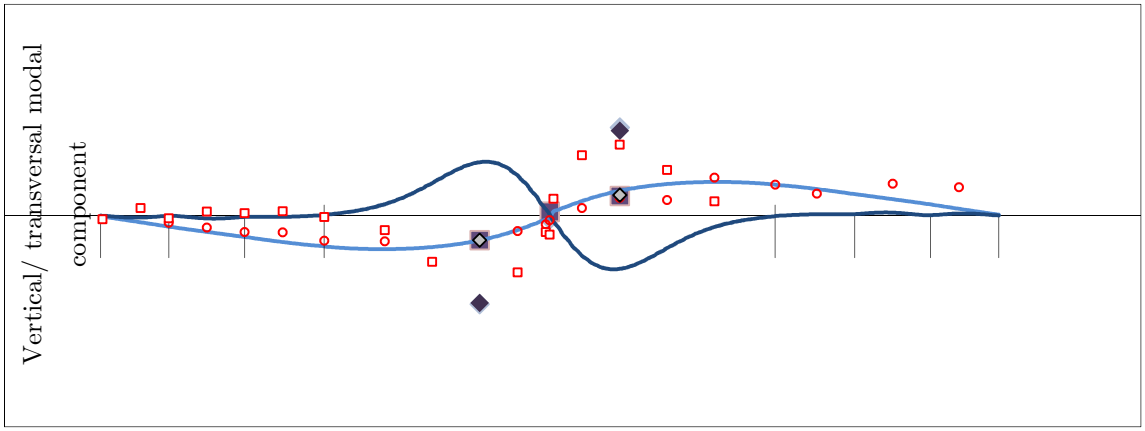

Figure 3.3.15 Mode 3 torsional + transversal fv = 0.707 Hz

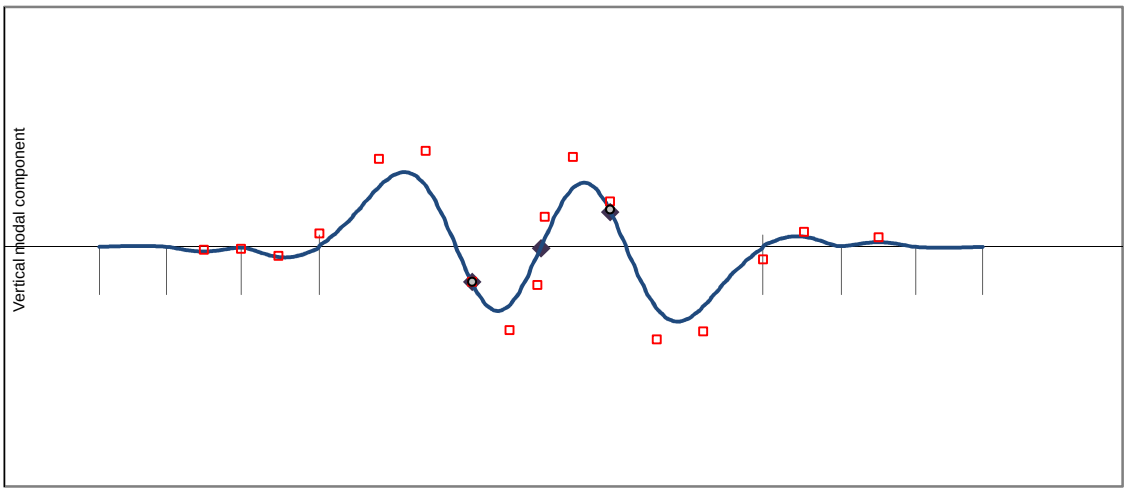

Figure 3.3.16 Mode 4 vertical fv= 0.816 Hz

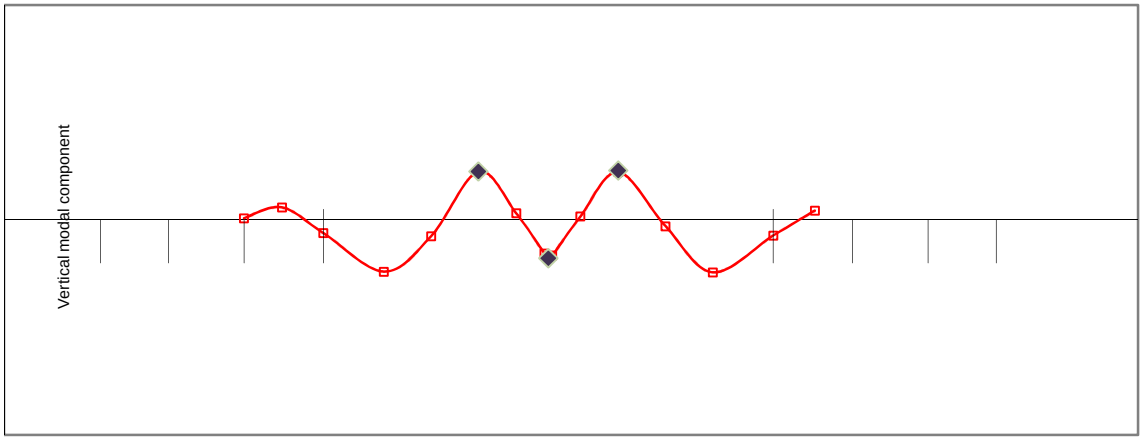

Figure 3.3.17 Mode 5vertical fv = 0.92 Hz

3.4. Ambient vibration test on Pinhao bridge

3.4.1. Bridge description

The Pinhão Bridge (Figure 3.4.1), constructed in 1906, is a metallic roadway bridge over the Douro River, in Portugal, formed by three truss simply supported spans of about 69.2m (Figure 3.4.3). The main beams have the shape of a semi-parabolic arch with a height varying from 2.67m to 8.86m at the middle of the span. The deck has a total width of 6.00m, arranged in two traffic lanes of 4.60m and two sidewalks of 0.70m wide on each side of the deck. The pavement is a concrete slab, supported by a steel grid that transfers the loads to the main steel beams (Figure 3.4.2) [Magalhães et al. 2006].

Figure 3.4.1 View of Pinhão Bridge

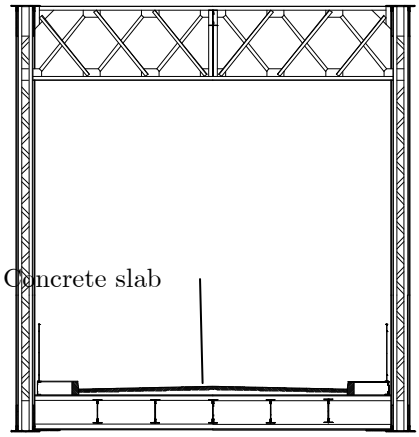

Figure 3.4.2 Cross-section

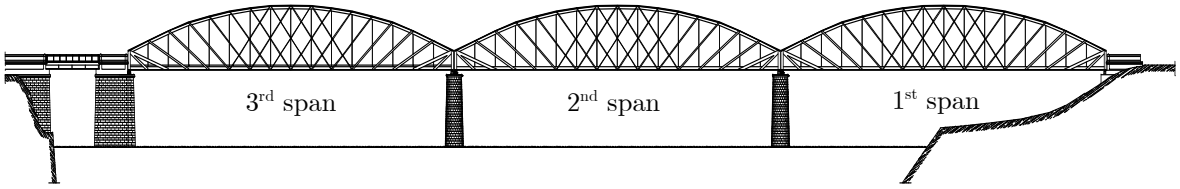

Figure 3.4.3 Lateral view of the Bridge

3.4.2. Experimental setup

An ambient vibration test is based on the measurement of time histories of the response at different points of the structure, motivated by the actions that excite the bridge during its normal use, which are, essentially, the traffic and the wind. To accomplish that, accelerometers are normally used, whose required sensitivity is very high, considering the typical low levels of vibration.

The signals are acquired by four tri-axial 18-bit strong motion recorder. These devices, based on very sensitive internal force balance accelerometers (linear behaviour from DC to 100 Hz), analogue to digital converters with 18 bit (to guarantee a good resolution), batteries that enable autonomy for one day of tests, memories materialized by removable Compact Flash cards that permit a fast download of the acquired data and external GPS sensors to deliver a very accurate time, so that they can work independently and synchronously. With this equipment, the use of cables is avoided and the labour associated with the preparation of the dynamic test is drastically minimized. In order to obtain a good characterization of the mode shapes, in each span the accelerations at 7 cross sections were measured (Figure 3.4.6). As torsion modes were expected, at each section two points were instrumented (see Figure 3.4.5). The three spans of the bridge are structurally independent, so they were also tested independently. They have exactly the same characteristics, so if the bridge was new, the same modal parameters would be expected for each of the spans. In this report only the data, acquired on the second span are analised.

In the developed test setups two recorders served as references, permanently located at section 3 (see Figure 3.4.6) on both sides of the deck. The other two recorders scanned the bridge deck in 6 consecutive setups for each span, measuring the acceleration along the 3 orthogonal directions. For each setup, time series of 13 minutes were collected with a sampling frequency of 100 Hz, value that is imposed by the filters of the acquisition equipment.

Figure 3.4.4 Strong motion recorder

Figure 3.4.5 Position of the measuring devices

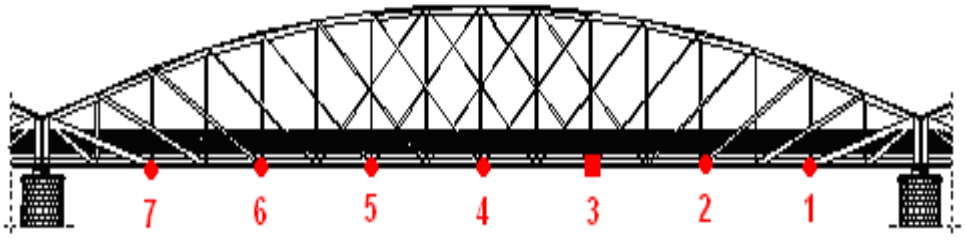

Figure 3.4.6 Measured sections

The test was developed without inducing significant restrictions in the bridge use, so it was possible to quantify the level of the vibrations motivated by the traffic.

In, the accelerations measured in the downstream point of section 5 are presented. In the graphic, the passage of a heavy truck can easily be identified, which motivated a considerably high vertical acceleration – 1.5 m/s2. The graphic also shows that the level of the lateral accelerations is approximately 1/10 of the vertical accelerations, fact that contributed for the lower quality of the identified lateral mode shapes.

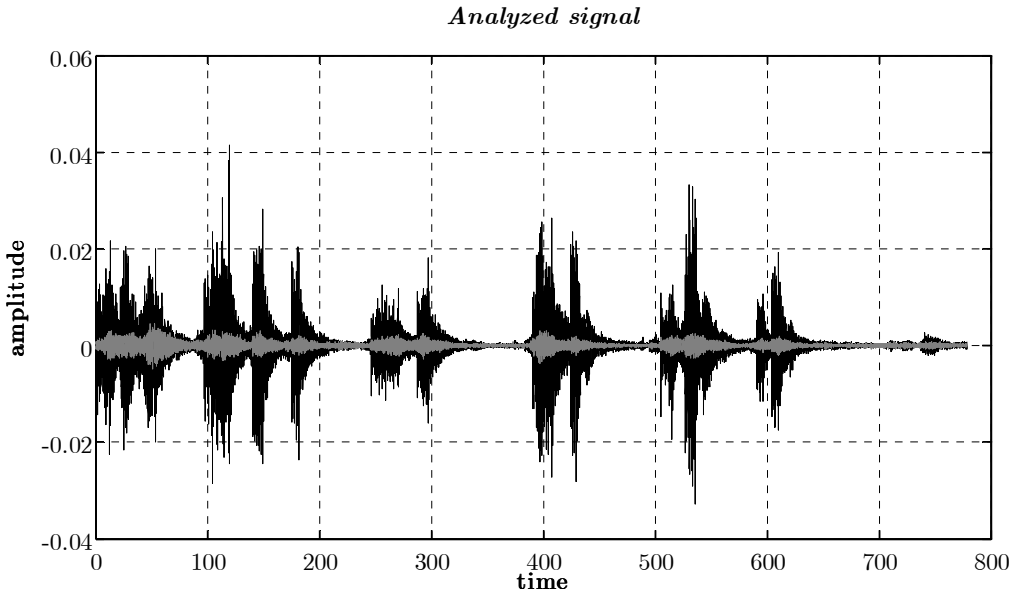

Figure 3.4.7 Acceleration time series measured at section 1

3.4.3. Results

The modal parameters of the structure were extracted in 2000 through the classical Peak-picking method. In the paper "Experimental validation of the Finite Element modelling of Pinhão Bridge" natural frequencies and mode shapes are available. The same signals, acquired during this test, are analyzed by the wavelet transform and the results are compared. An example of the Wavelet transform is represented in the following figures (Figure 3.4.8 and Figure 3.4.9)

From this graphs it is possible to see that the WT in time domain presents different trends; each trend is referred to the various part of the signal, that correspond at different excitation of the structure (see figure 3.7). If the wavelet transforms of the signals acquired during the test on Vasco da Gama bridge (free vibration) are compared with the other one recorded during the test on Pinhao

Bridge (ambient vibration) it is possible to note the difference of the WT in the time domain.

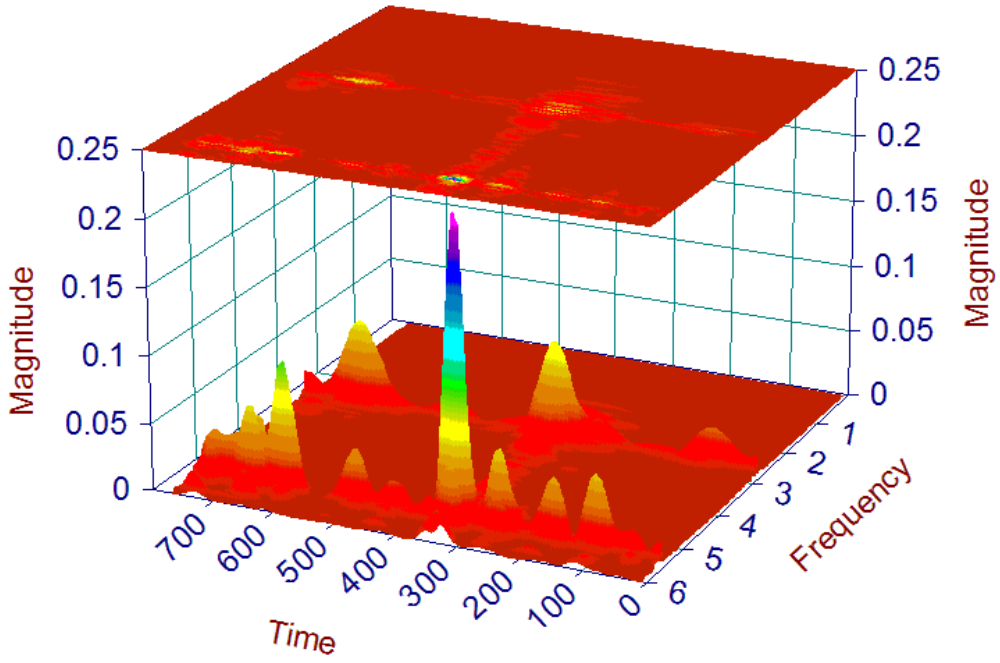

Figure 3.4.8 3-D Wavelet Transform of the signal acquired at section 2 (vertical direction)

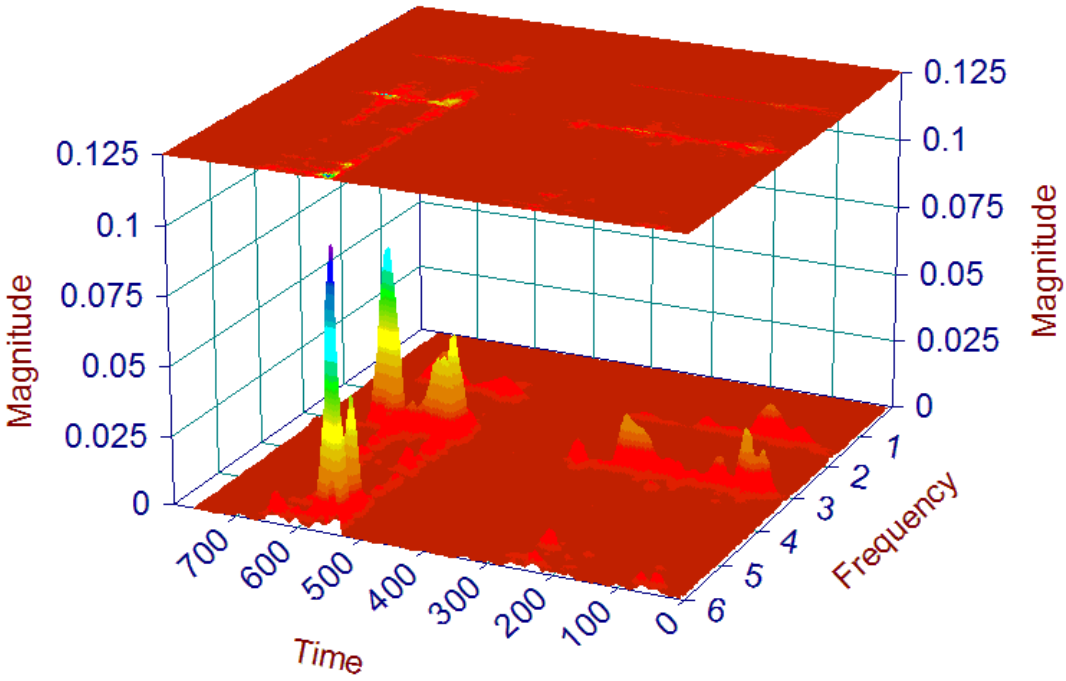

Figure 3.4.9 3-D CWT of the signal acquired at section 2 (vertical direction)

In particular, in the first one (Figure 3.3.5 and Figure 3.3.6) in the time domain the WT presents only one peak, then the modal damping has an unique value, meanwhile in the second one the WT presents many peaks and different trend at each peak. It's possible, for this reason, to obtain several value of the modal damping for the same natural frequency.

The dampings are computed for each peach of the WT and its trend varies with the amplitude of the peak, as it shows in Figure 3.4.10 Figure 3.4.11. It is noticeable that the value of the modal damping depends on the amplitude of the excitation. In this case each modal damping is computed in correspondence of the maximum value of the amplitude of the recorded signal. The natural frequencies and modal dampings of the system are summarized in table 5 and compared with results obtained through the classical PP method and EFDD. The results present a good agreement.

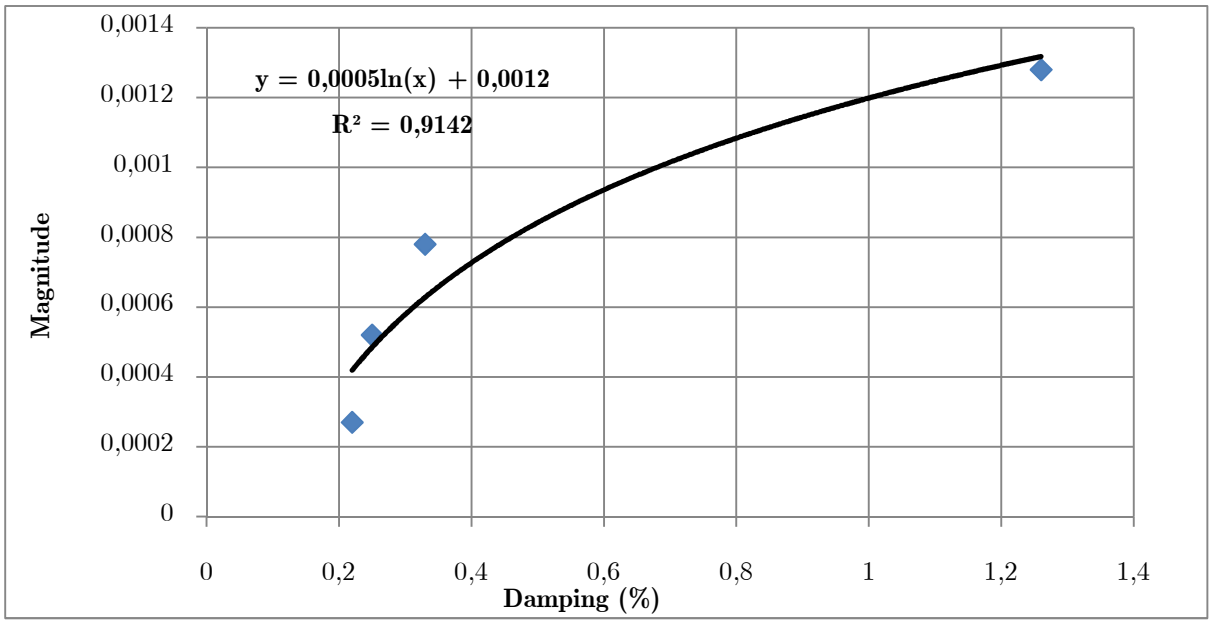

Figure 3.4.10 Damping versus magnitude at frequency 1.719 Hz transversal mode; each point represents the damping associated to a track of the signal considered

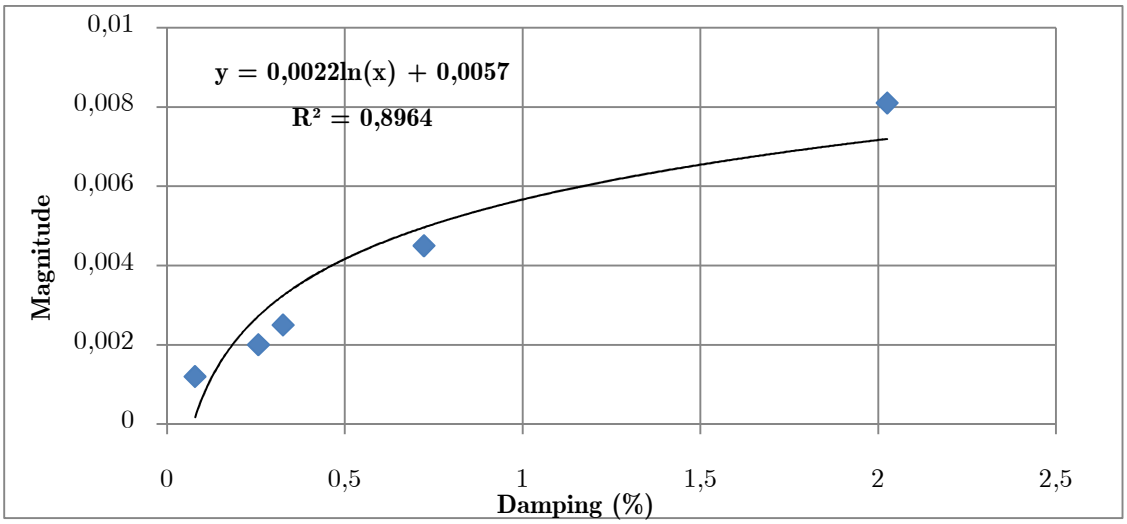

Figure 3.4.11 Damping versus magnitude at frequency 2.782 Hz vertical mode; each point represents the damping associated to a track of the signal considered

Table 5 Natural frequencies trough WT and PP, comparisons

Mode type		Frequency WT	Frequency PP	Damping WT	Damping EFDD
Vertical Bending	1st	2.782	2.771	1.56	1.15
	2nd	5.483	5.493	0.39	0.32
	3rd	8.209	8.228	0.14	0.2
	4th	10.623	10.608	0.34	0.33
	5th	12.676	12.671	0.14	0.2
	6th	14.07	13.965	0.2	0.5
	7th	15.593	15.649	0.39	0.33
Transversal Bending	1st	1.719	1.721	1.03	1.21
	2nd	3.201	3.210	0.93	0.9
	3rd	4.222	4.224	0.53	0.41
Torsional	1st	5.935	5.957	0.35	0.33

When the ambient time responses recorded from several points of the structure are available, phase and amplitude relationships between the different degrees of freedom of the system can be obtained through the wavelet transform analysis. Through eq. (3.11) an absolute value of the mode shape can be found, considering the ratio between the magnitude of the CWT of the signal acquired at generic section and the magnitude of the CWT of the signal acquired at the section of control (section 3). The sign of the point of the mode shape is define trhough the comparisons between the phase CWT of the signal at generic section and at section 3. It is in this case, where we have different track with different time trend, to compare the phase at the same instant. When the CWT is plotted in the frequency domain, the maximum module for each time instant are considered. Of course these maximum values can happen in different time, characterized by a specific value of phase displacement. To obtain a coherent comparison between the phase od the signal acquired in a generic section and that one recorded in the section control, it is necessary to check that the same instants are considered. The mode shape, obtained by the WT are compared to the mode shape obtained by PP method (in blue the mode shapes obtained by PP are shown and in azure the mode shapes obtained by WT are represented).

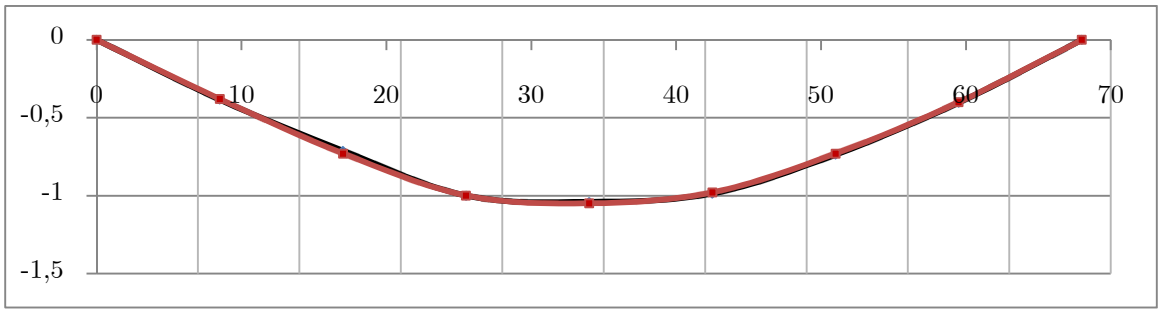

Figure 3.4.12 Mode 1 vertical fv = 2.782 Hz

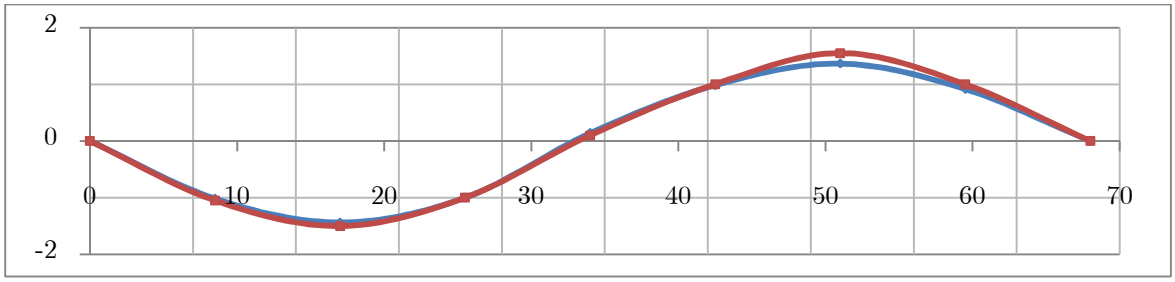

Figure 3.4.13 Mode 2 vertical fv = 5.483 Hz

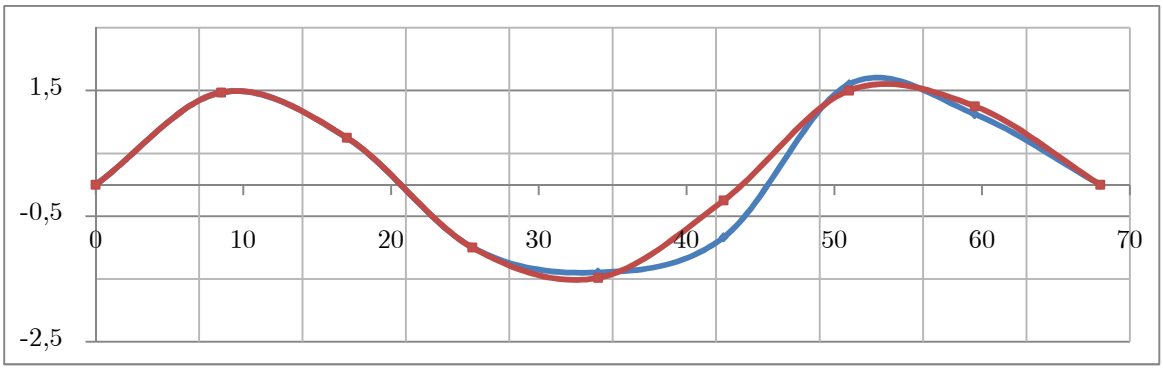

Figure 3.4.14 Mode 3 vertical fv = 8.209 Hz

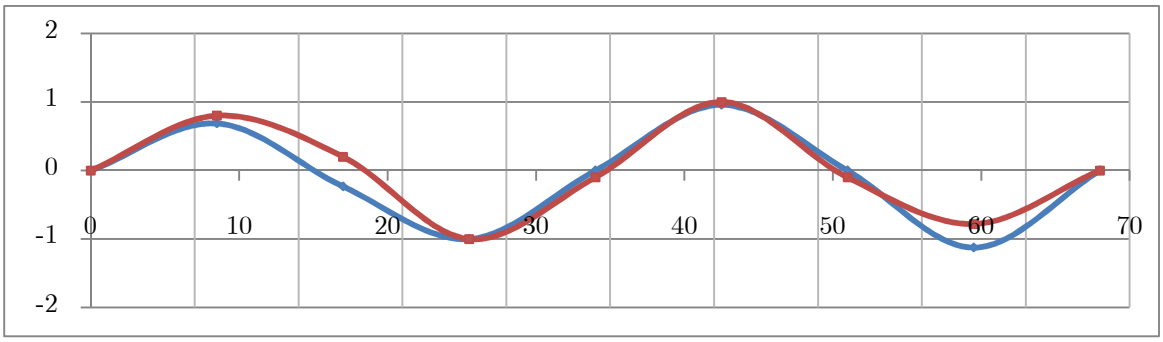

Figure 3.4.15 Mode 4 vertical fv = 10.623 Hz

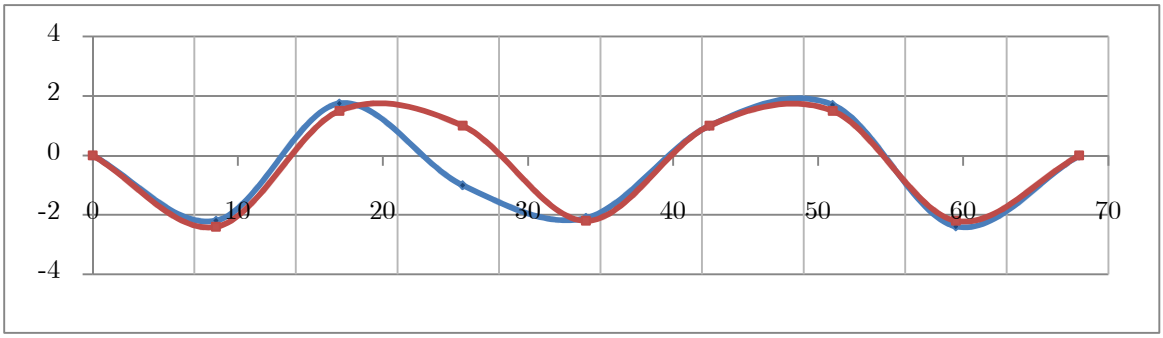

Figure 3.4.16 Mode 5 vertical fv = 12.676 Hz

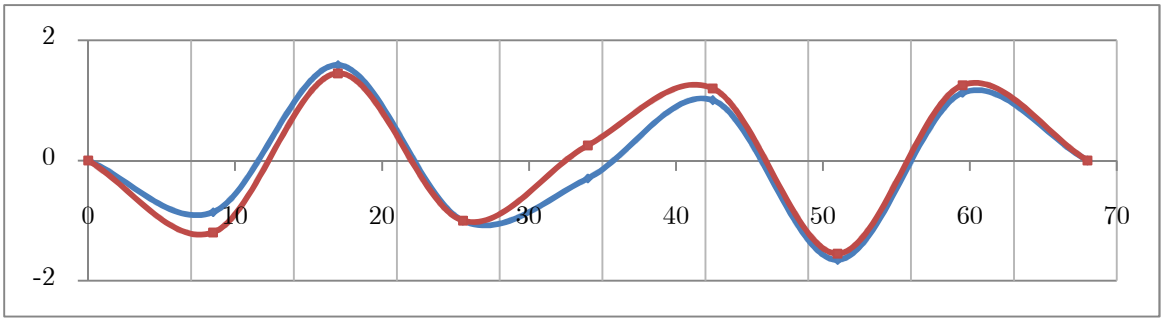

Figure 3.4.17 Mode 6 vertical fv = 14.07 Hz

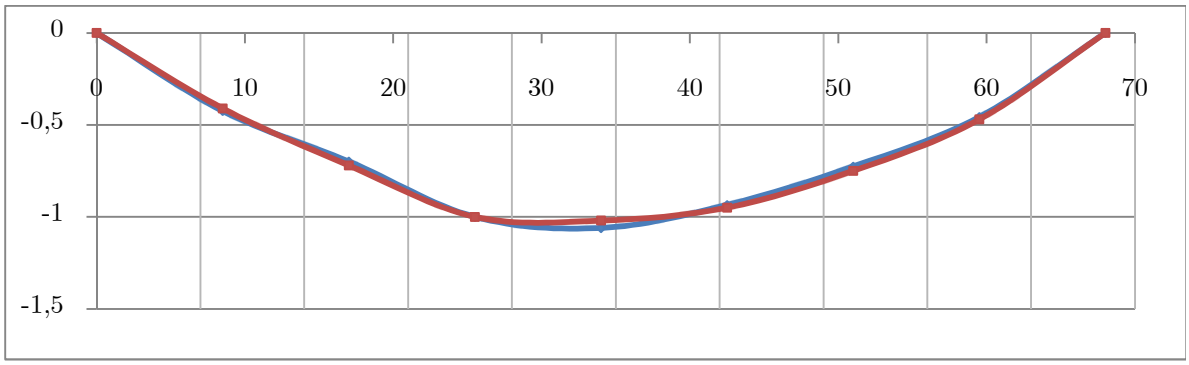

Figure 3.4.18 Mode 1 lateral, fv = 1.719 Hz

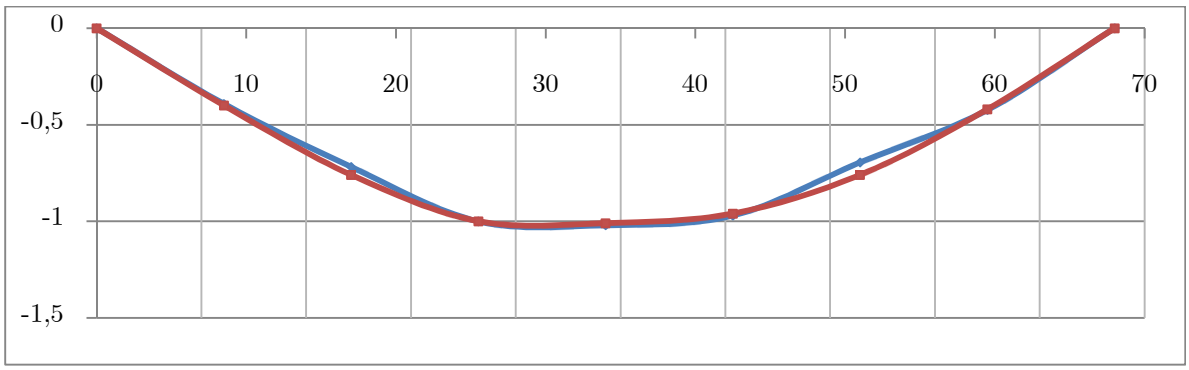

Figure 3.4.19 Mode 2 lateral fv = 3.201 Hz

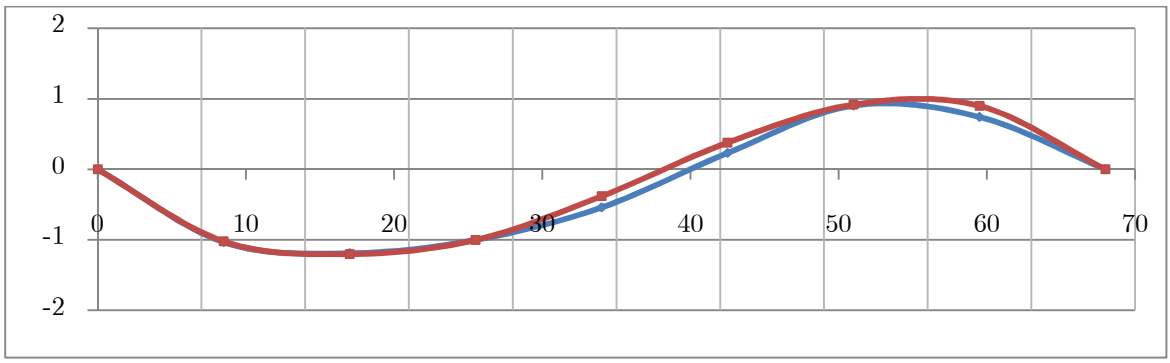

Figure 3.4.20 Mode 3 lateral fv = 4.222 Hz

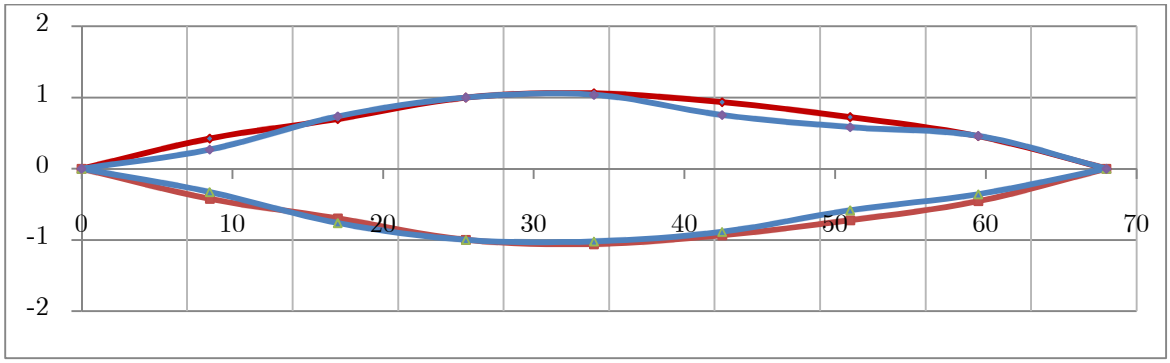

Figure 3.4.21 Mode 1 torsional fv = 5.957Hz

Conclusive remarks

This chapter shows how the Continuous Wavelet Transform can be used to define the modal parameters of a generic system, subject to dynamic test. CWT is applied with good results initially to a free vibration test; in this case it is very easy to define all modal parameters through only one transform for each signal acquired. The same procedure is applied on the signal acquired from an ambient test. In this case the natural frequencies of the system are immediately defined from the CWT, some difficult are, instead, present in the computation of the damping values. It is in this case necessary to consider only a part of the signal recorded and then the modal corresponding damping. The same thing is necessary to define the sign of the points, which define the mode shape.

CWT is a good procedure to identify a dynamic system, it is easy to implement, computationally efficient and it is the only method, which is able to work in the time and frequency domain by only one transform. For this reason it can summarize the signal behaviour in both domains, then completely.

CHAPTER FOUR

FILTERING AND SIGNAL RECONTRUCTION THROUGH DISCRETE WAVELET TRANFORMS

4.1. Introduction

The discrete wavelet transform was applied to denoise the signals acquired during an ambient test carried out on a very stiff bridge in masonry. The use of the some wavelets and translation invariant denoising were found to be very efficient for this purpose. An important improvement was obtained, as compared with Savitzky-Golay and Fourier, which are the most commonly used techniques for denoising in the instrumentation software packages [Savitzky-Golay, 1964]. A better removal of the noise and, especially, a better preservation of the shapes of very sharp peaks were achieved. Removal of the baseline variations was also investigated. Smoothing or filtering techniques, such as mean filtering, exponential smoothing, Savitzky-Golay, or Fourier are commonly used in many fields, because they are simple and easy to implement. Fourier, for instance, is a very efficient technique for the processing of analytical signals in which all real features have approximately the same width and shape (the signal is then called stationary); however, it is not efficient for the processing of signals containing features with varying shapes and widths (unstationary signals, as in the studied case) because of the global character of the sine and cosine basis functions. Some improvement can be achieved using the windowed Fourier transform, but the simultaneous processing of local and global changes in the signal is still not possible. To achieve proper denoising, a compromise has to be found between an accurate representation of temporally localized changes, such as peaks, and an efficient removal of noise, which is spread over the whole signal.

4.2. From CWT to DWT

Wavelets are a family of basis functions, well-localized in both the time and frequency domains. They have a compact support, which means that they differ from zero only in a limited time domain. This property makes the wavelet very

appropriate to represent the different features of a signal, especially sharp signals and discontinuities.

The foundations of DWT go back to 1976 when techniques to decompose discrete time signals were devised. Similar work was done in speech signal coding which was named as sub-band coding. In 1983, a technique similar to sub-band coding was developed which was named pyramidal coding. Later many improvements were made to these coding schemes which resulted in efficient multi-resolution analysis schemes [Hubbard, 1998; Walczak & Massart, 1997; Riuol & Verletti, 1991; Daubechies et al., 1993].

In CWT, the signals are analyzed using a set of basis functions which relate to each other by simple scaling and translation. In the case of DWT, a time-scale representation of the digital signal is obtained using digital filtering techniques. The signal to be analyzed is passed through filters with different cutoff frequencies at different scales. The WT decomposes the signal into a set of basis functions called a wavelet basis. Each member of the basis is obtained by dilation and translation of a single prototype, called the mother wavelet, as we already said previously. Thus is expressed by the following relation:

$$\Psi\left(t\right) = \frac{1}{\sqrt{a}}\,\Psi\left(\frac{t\text{ - }b}{a}\right) \tag{4.1}$$

where a is a scaling variable, and b is a translation variable.

In practical signal processing a discrete version of wavelet transform is often employed by discretizing the dilation parameter a and the translation parameter b. In general, the procedure becomes much more efficient if dyadic values of a and b are used, i.e.,

$$a = 2^{j},\ b = k2^{j};\ \ j,k \in Z \tag{4.2}$$

where Z is a set of positive integers. Constraints on $\Psi\left(t\right)$, a and b ensure an orthogonal decomposition of the signal in order to avoid redundancy and to

achieve a perfect reconstruction of the signal; the corresponding discretized wavelets $\left\{\Psi_{(j,k)}\right\}$ is

$$\Psi_{(j,k)} = 2^{-j/2}\,\Psi\left(2^{-j}t - k\right) \tag{4.3}$$

constitute an orthonormal basis for $L^2(R)$. Using the orthonormal basis, the wavelet expansion of a function f(t) and the coefficients of the wavelet expansion are defined as

$$f\left(t\right) = \sum_{j}\sum_{k} d_{j,k}\Psi_{j,k}\left(t\right) \tag{4.4}$$

and

$$d_{j,k} = \int_{-\infty}^{+\infty} f\left(t\right)\overline{\Psi}_{j,k}\left(t\right)dt \tag{4.5}$$

This is the form of the DWT. The wavelet coefficients $d_{j,k}$ are considered as a time-frequency map of the original generic function of time f(t). In discrete wavelet analysis the signal can be represented by its approximations and details. The detail at level j is defined as

$$D_j = \sum_{k\in Z} \alpha_{j,k}\Psi_{j,k}\left(t\right) \tag{4.6}$$

And the approximation at level J is defined as

$$A_J = \sum_{j>J} D_j \tag{4.7}$$

It becomes obvious that

$$A_{J-1} = A_J + D_j \tag{4.8}$$

and

$$f\left(t\right) = A_J + \sum_{j\le J} D_j \tag{4.9}$$

To define the DWT it is necessary to solve eq. (4.5). One of the first widely applied parent wavelets was developed by Daubechies. Development of this parent wavelet begins with the solution of a dilation equation to determine a

scaling function $\phi(t)$, dependent on certain restrictions. The scaling function is used to define the parent wavelet function, $\psi(t)$. The relation between the discrete scaling function and the wavelet function $\psi(t)$ is

$$\left|\hat{\phi}(\omega)\right|^2 = \sum_{j=-\infty}^{\infty} \left|\hat{\psi}(2^j \omega)\right| \tag{4.10}$$

The discrete scaling function corresponding to DWT is

$$\phi_{j,k}(t) = 2^{-j/2} \phi\left(2^{-j} t - k\right) \tag{4.11}$$

This is used to discretize the signal; the sample value are defined as the scaling coefficients $c_{j,k}$

$$c_{j,k} = \int_{-\infty}^{+\infty} f(t) \overline{\phi}_{j,k}(t)\, dt \tag{4.12}$$

We obtain the wavelet decomposition algorithm

$$\begin{aligned} c_{j+1}(k) &= \sum_{l \in Z} h(l)\, c_j(2k - l) \\ d_{j+1}(k) &= \sum_{l \in Z} g(l)\, c_j(2k - l) \end{aligned} \tag{4.13}$$

where the terms g and h are high-pass and low-pass filters derived from the wavelet function $\psi(t)$ and the scaling function $\phi(t)$. The coefficients $d_{j+1}(k)$ and $c_{j+1}(k)$ represent a decomposition of the (j-1)th scaling coefficient into high-frequency and low-frequency terms. Thus, the algorithm decomposes the original signal f(t) into different frequency bands in the time domain

In particular a DWT algorithm was developed by Mallet, which computes the solution of Eq. (4.5) without solving for either $\left\{\Psi_{(j,k)}\right\}$, or directly. The algorithm uses a series of high and low pass filters to progressively find the wavelet coefficients, , from the highest level to the mean value level. In the first iteration, the upper half of the frequency content is filtered from the original signal. The high pass signal is used to generate the wavelet coefficients that describe the high detail portion of the signal. The low pass filtered data is sent to the next

iteration. In the next iteration the upper one half of the remaining frequency content of the signal is high pass filtered once again, this time to generate the next wavelet coefficients. The iterations continue until all wavelet coefficients are determined. This is referred to as Mallet's tree algorithm or Mallet's pyramid algorithm.

As it is clear through eq. (4.5) the DWT can be represented in a vector matrix form

$$\mathbf{w} = \mathbf{W}f \tag{4.14}$$

where f is the signal of interest, **w** is the vector of the wavelet transform coefficients, and **W** is an orthogonal matrix consisting of the wavelet basis functions. Each basis vector is characterized by a set of coefficients d_0, d_1, d_2, etc. The coefficients are organized in the matrix W into a low pass and a high pass filter. The first acts as a smoothing filter, and the latter brings out details of the signal. The wavelet coefficients obtained by convolving each basis function with the signal reflect a measure of the similarity of the signal with the basis function at a certain scale and position in time. The matrix W can be defined by the Mallet algorithm. The only restriction in applying this algorithm is that the length of the signal must be a power of 2. The full length vector describing the noisy signal is passed through the low-pass and the high-pass filters. Outputs are split in two into approximation and detail (or wavelet) coefficients. Approximation coefficients represent a smooth version of the signal at half resolution, and detail coefficients contain details of the signal at that level of decomposition. Approximation coefficients are then used as new input of the matrix W to obtain a new vector of approximation coefficients and new details of the signal. With increasing level of decomposition, less information is contained in the approximation coefficients. The information lost between approximation coefficients of two successive levels of decomposition is encoded in the detail coefficients. Detail coefficients of the first levels of decomposition contain information about the high frequency components of the signal, that is, noise, spikes, etc. In the last levels of decomposition, they mainly contain the low-

frequency components of the signal.

The process can continue until one approximation coefficient remains. At the end, the WT contains the mean of the signal and all of the encoded details at the different levels of decomposition. Reconstruction of the signal is done by the inverse wavelet transform, whose transform matrix is the transpose of the WT matrix, $\mathbf{W}^{\mathrm{T}}$.

The Wavelet Series is just a sampled version of CWT and its computation may consume significant amount of time and resources, depending on the resolution required. The Discrete Wavelet Transform (DWT), which is based on sub-band coding is found to yield a fast computation of Wavelet Transform. It is easy to implement and reduces the computation time and resources required.

4.3. Comparisons between CWT and DWT

This section presents results of wavelet analysis for some simulated signals; the Daubechies wavelet DB4 was used in both and continuous transforms. The Morlet wave cannot be used in this section because it is not able to give good results in the case of discrete transforms because it is not orthogonal. The DB4 has the shape illustrates in the following figure

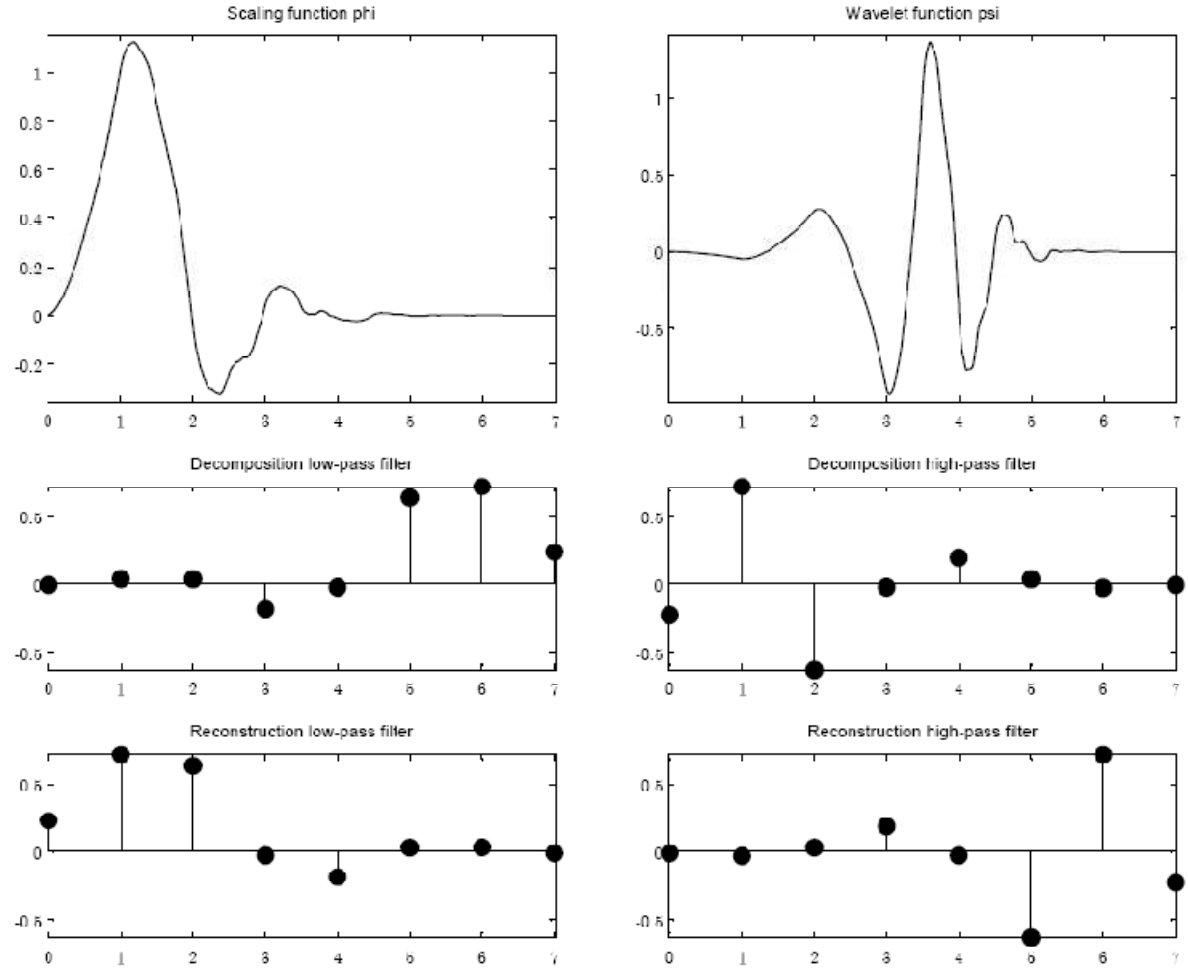

Figure 4.3.1 Trend of the DB4 wave and its decomposition and reconstruction

The first simulated signal analyzed is expressed by the following relation

$$y(t) = 10\sin\left(2\pi 8t\right) + 10\sin\left(2\pi 2t\right) \tag{4.15}$$

And it is represented in the Figure 4.3.2 ***Simulated signal without any decay in time domain***

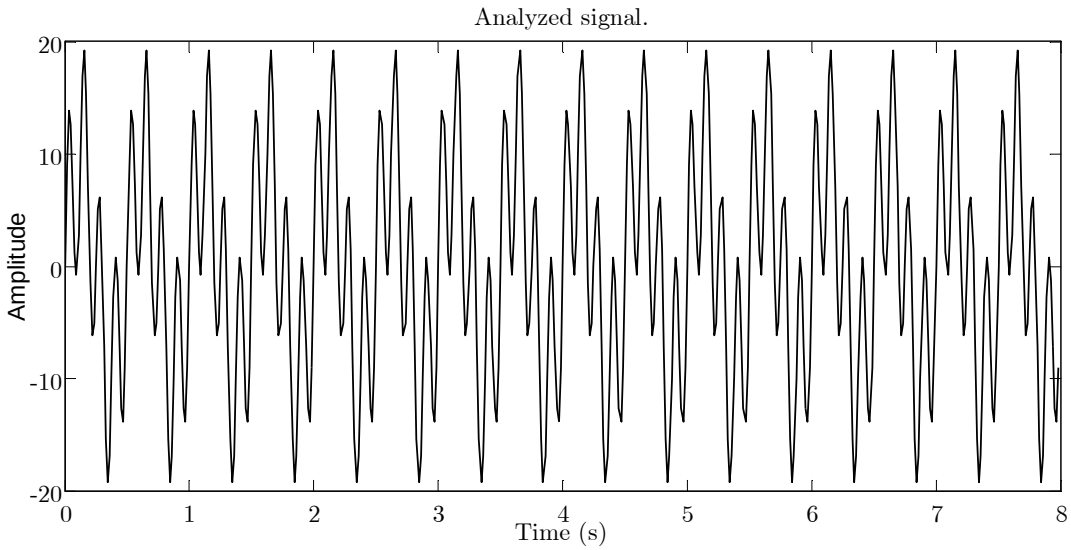

Figure 4.3.2 Simulated signal without any decay in time domain

At beginning we considered a signal without decay to investigate on the behavior of DWT only in frequency domain, compare with CWT. In the figure below the signal decomposition through the eqs. previously described is represented. As ***Figure 4.3.3*** shows the DWT decomposes the signal in a sum of time function, by the same way used through the classical application of FFT. There is an important difference: the FFT decomposes the signal in a sum of sinusoidal signal or in other words in a sum of stationary time function. Instead the DWT is able to define the original signal as a sum of time function that can have different amplitudes in the time domain. For this reason the DWT is a powerful instrument to define the behavior of a non-stationary signal and it can overcome the principal limit of the application of FFT.

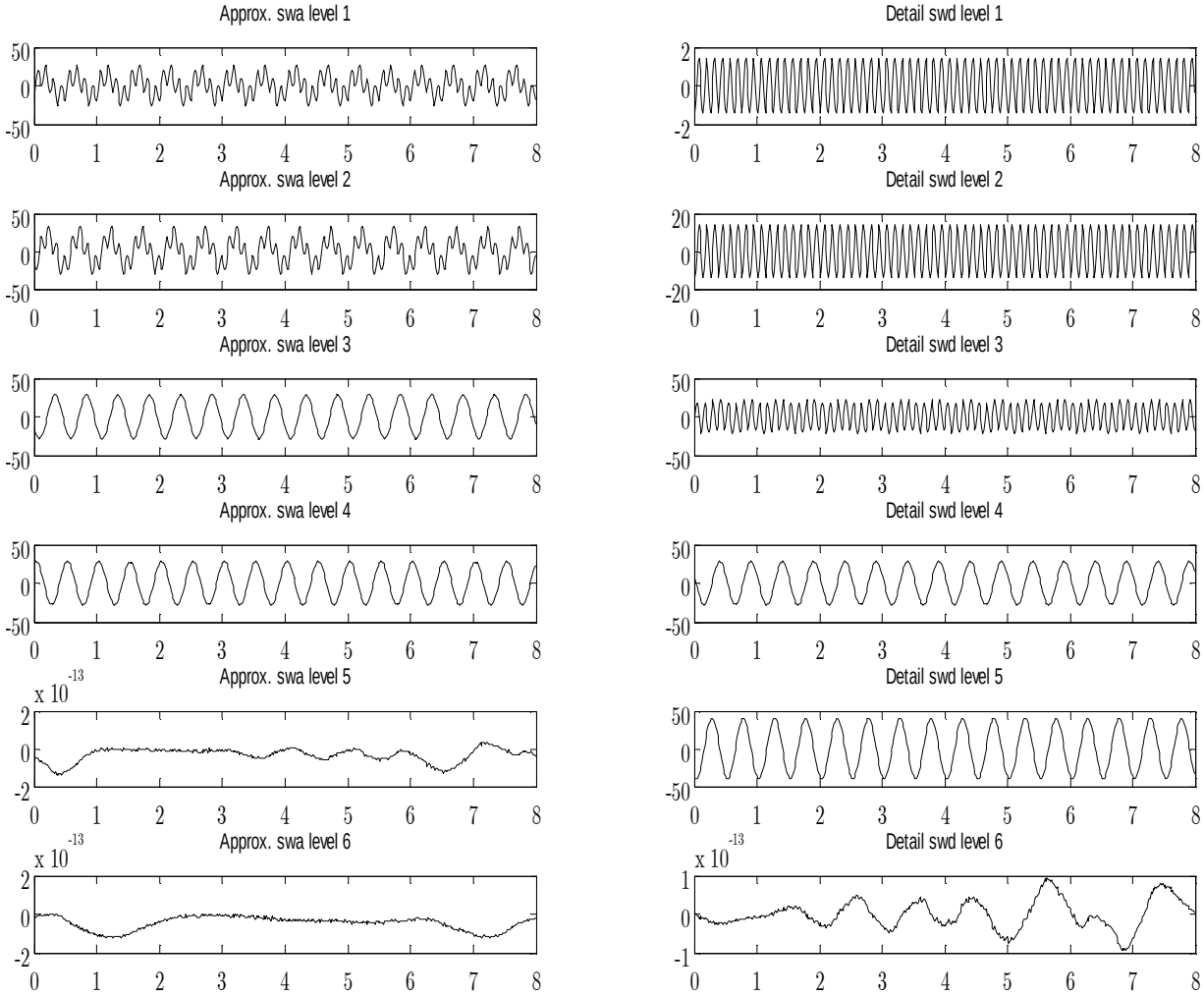

Figure 4.3.3 DWT decomposition until level 6

Through this decomposition the matrix **W** can be computed and the DWT is represented in Figure 4.3.4, the DWT is compared with the corresponded CWT. The figures show clearly that the DWT introduces an important approximation in the representation of the simulated signal.

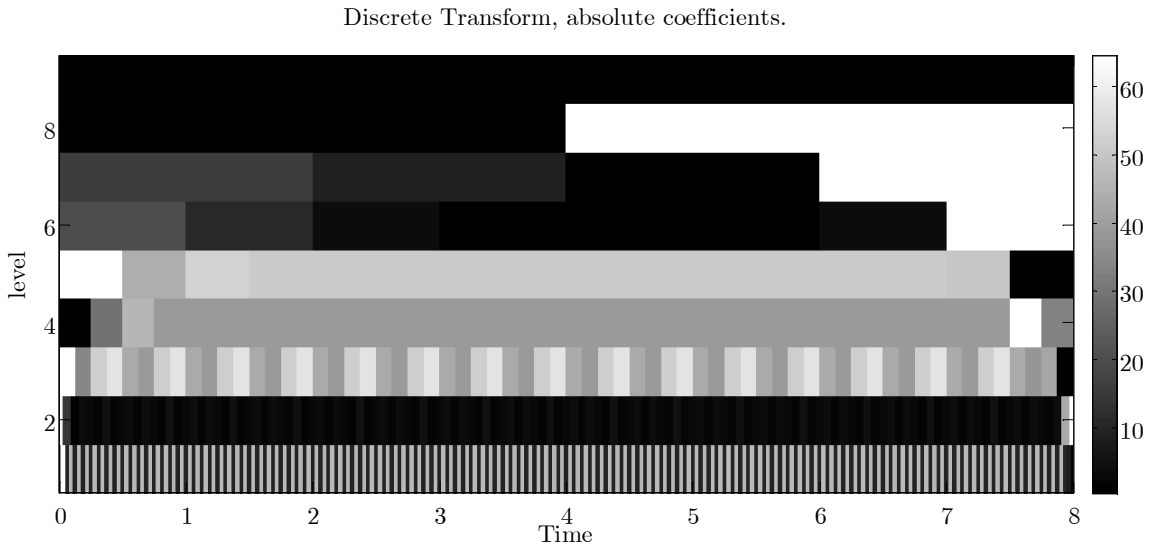

Figure 4.3.4 DWT of the signal, plane view

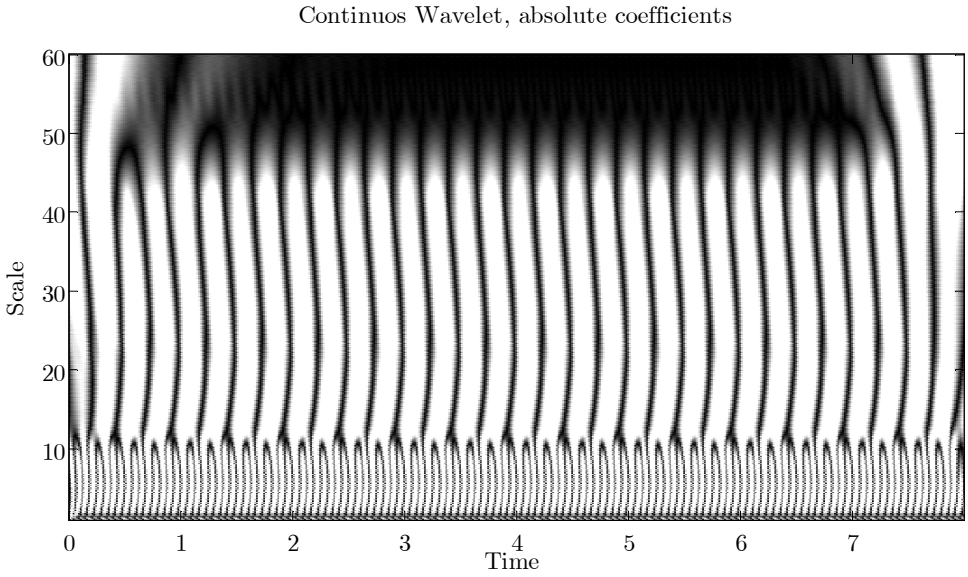

Figure 4.3.5 CWT of the signal, plane view

In this figure the CWT is represented in a plane scale-time. To define the frequency from the scale, the expression of the mother wave needs to be analysed. In general the realtion between scale and frequency is:

$$f = \frac{F_c}{a\Delta t} \tag{4.16}$$

Where a is the scale, Δt the sampling period and Fc is the center frequency of the mother wavelet considered. In this case a DB4 is considered, and in this case the centered frequency is equal to $F_c = 0.7143Hz$.

So, note the scale where the magnitude of the CWT or DWT, it is possible to define the natural frequencies of the system easily. In the figures below, a 3D plot in both the case is represented.

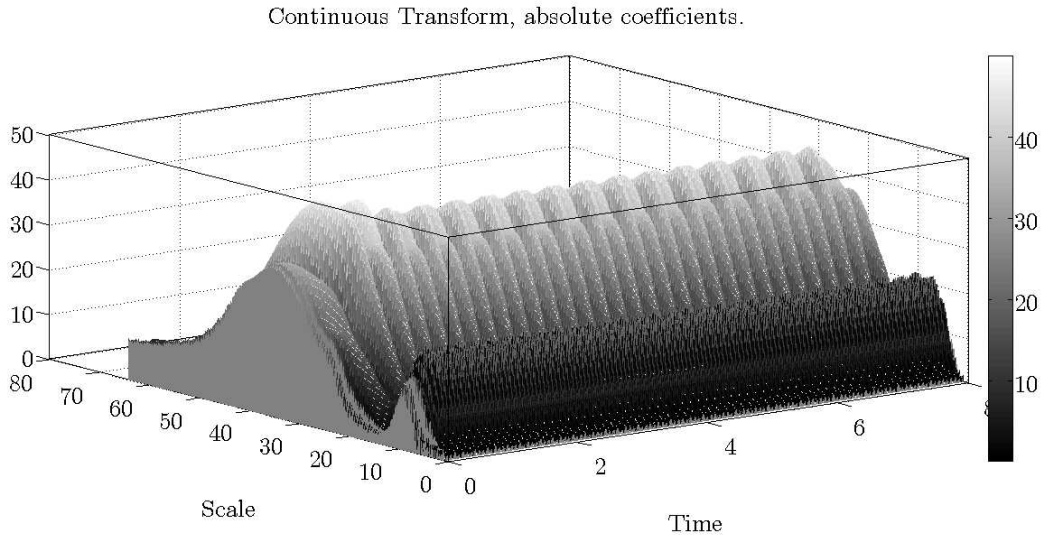

Figure 4.3.6 CWT, 3D representation

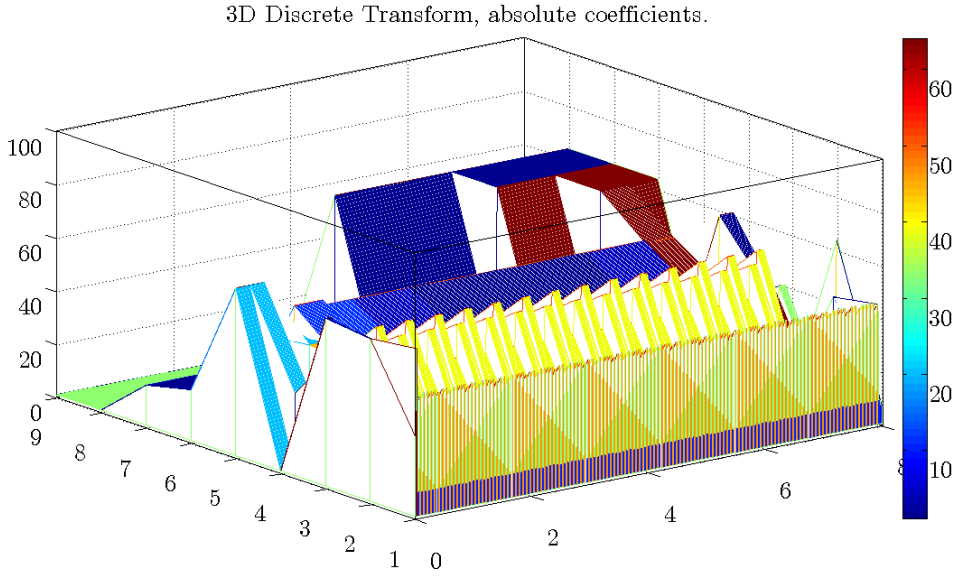

Figure 4.3.7 DWT, 3D representation

It is clear, observing Figure 4.3.6 and Figure 4.3.7, that the DWT introduces a very important approximation respect to the corresponding CWT. We want to underline that in this case we have used the DB4 wave; it defines with less accuracy the modal parameters obtained by the complex Morlet wave. The choice

was necessary to obtain a comparison between DWT and CWT. The situation becomes less clear when we simulated a signal with frequencies nearer

$$y(t) = 25\sin\left(2\pi 7.8t\right) + 10\sin\left(2\pi 10t\right) \tag{4.17}$$

Its trend is represented in the figure below

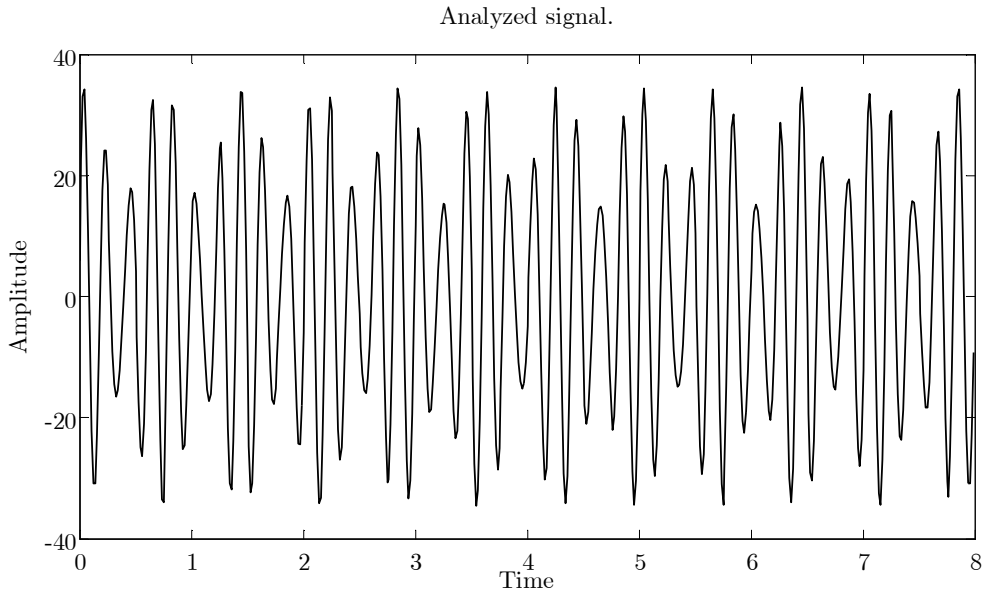

Figure 4.3.8 Trend of simulated signal

The DWT and CWT, represented in the plane scale-time, are reported below.

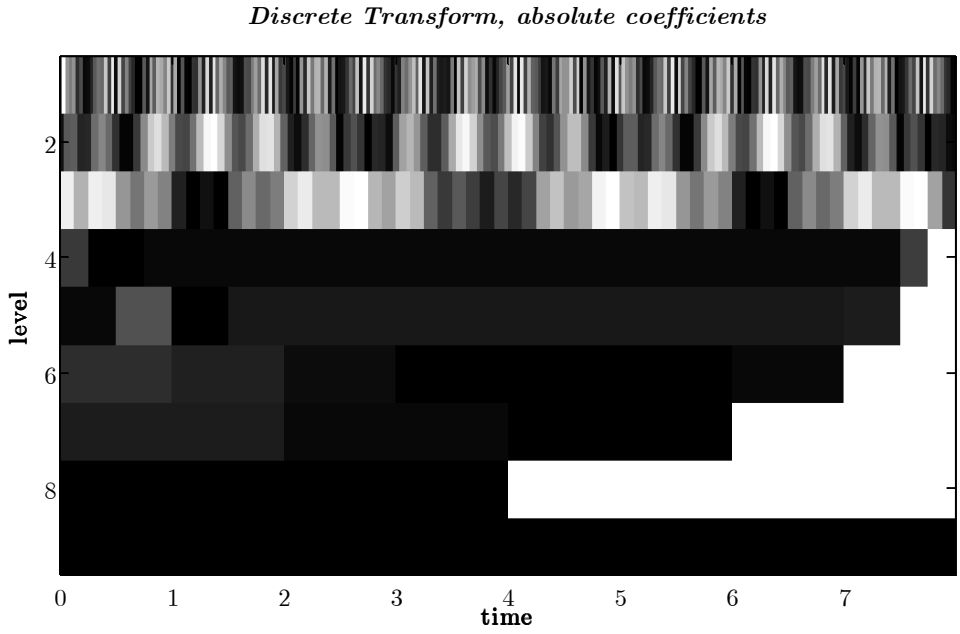

Figure 4.3.9 2D representation of the DWT

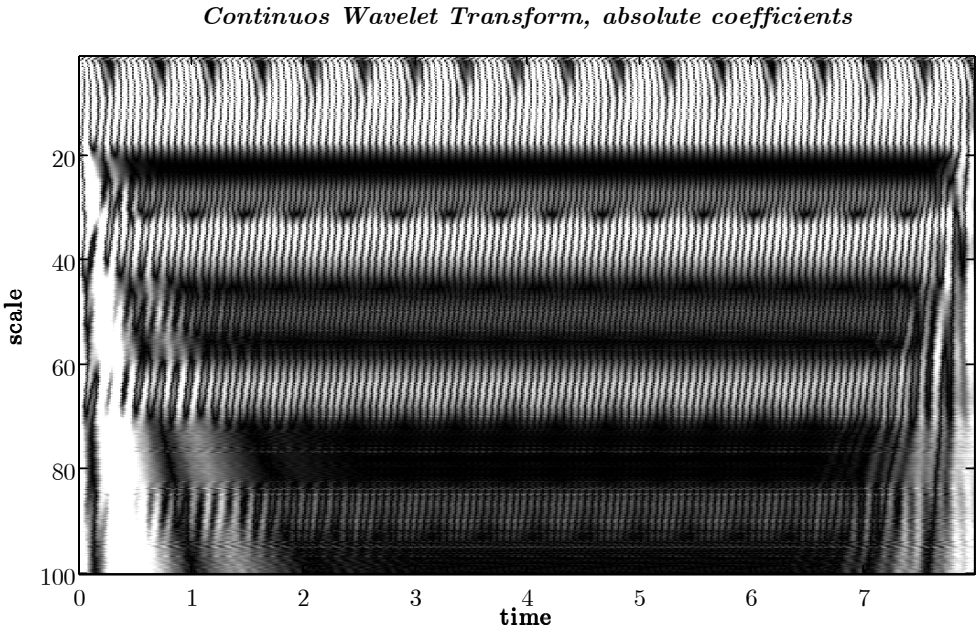

Figure 4.3.10 2D representation of CWT

It is more evident through the 3D graphs; for the DWT, in correspondence of the level three it is difficult to separate the two frequency. In the CWT graph, instead, the two frequencies are separated, because it is possible to define a variation of the scale with a lower interval, so a better frequency resolution can be achieved.

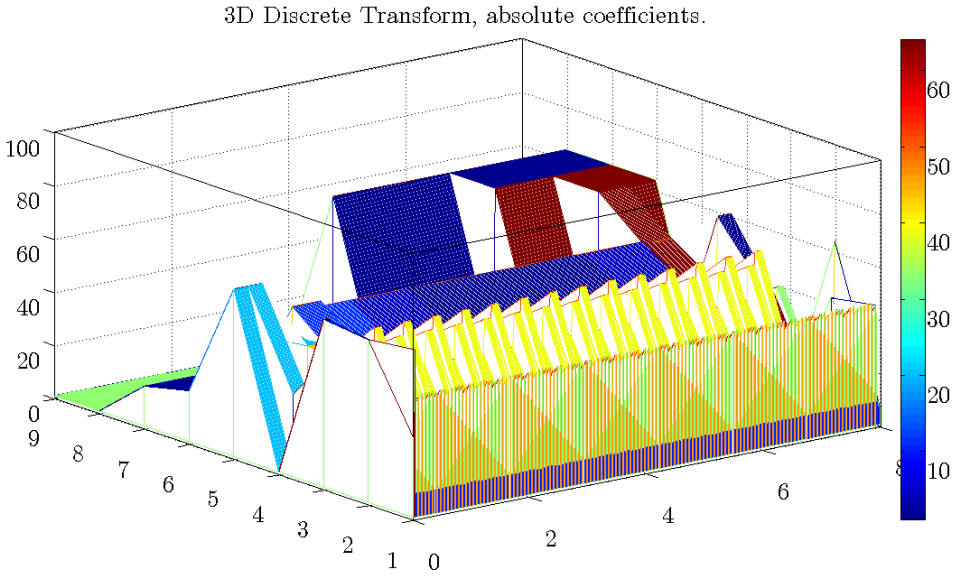

Figure 4.3.11 3D DWT of a simulated signal with proximal natural frequencies

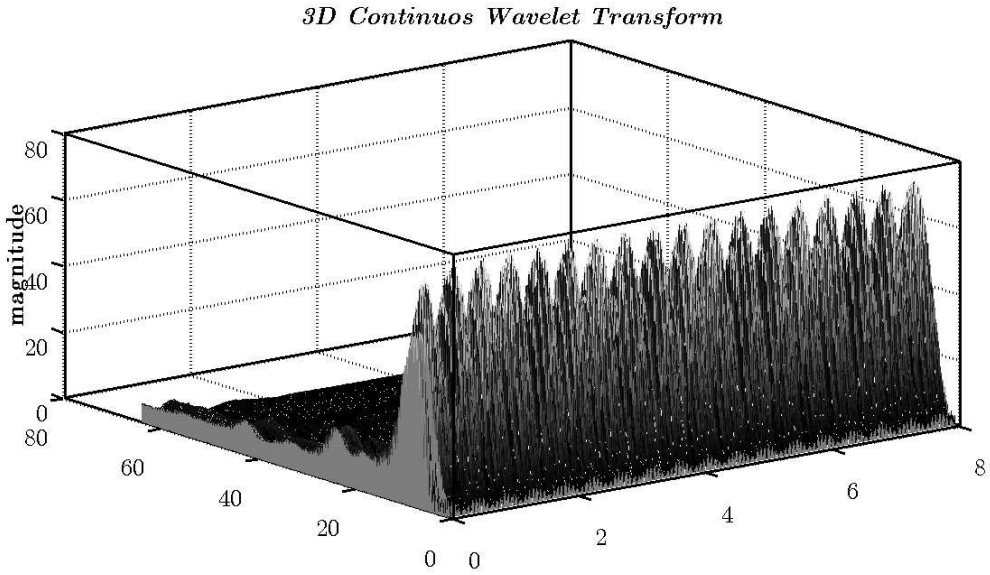

Figure 4.3.12 3D CWT of a simulated signal with proximal

The difference between the two transforms is more evident when we consider a signal with a generic decay in the time. The simulated signal has the following expression and it is represented in Figure 4.3.13.

$$y(t) = 25\sin\left(\left(2\pi 6t\right)e^{-2\pi 0.05*6t} + \pi/13\right) + 10\sin\left(2\pi 10t\right)e^{-2\pi 0.05*10t} \qquad (4.18)$$

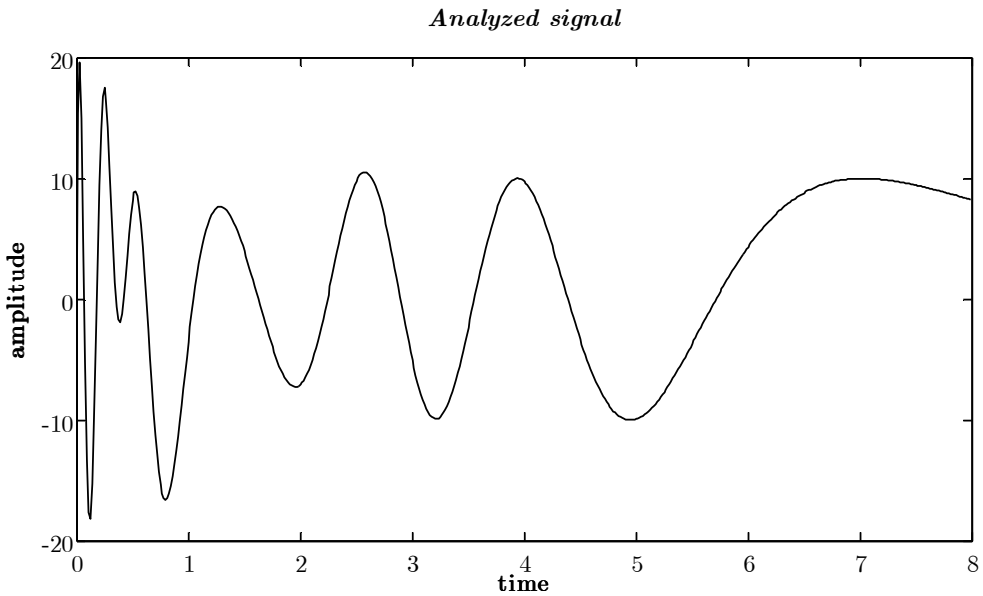

Figure 4.3.13 Simulated non-stationary signal

In this case the transform is used to define the modal damping, a very difficult value to define during the modal identification. For this reason we need of a

graph that remarks the time behavior of the signal in very accurate way. This does not happen with the DWT, as it is possible to see in the following figures:

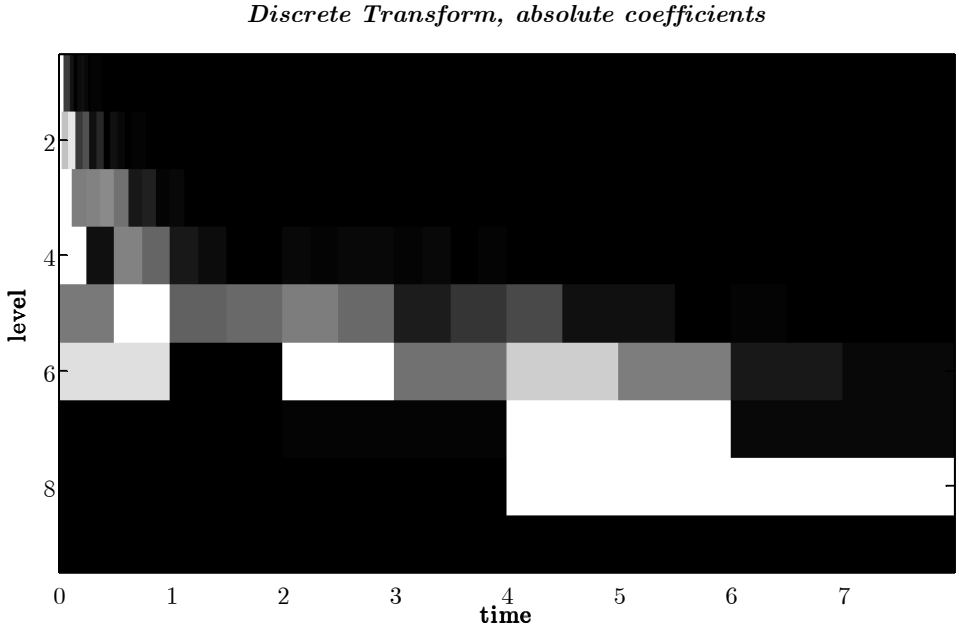

Figure 4.3.14 2D DWT of signal

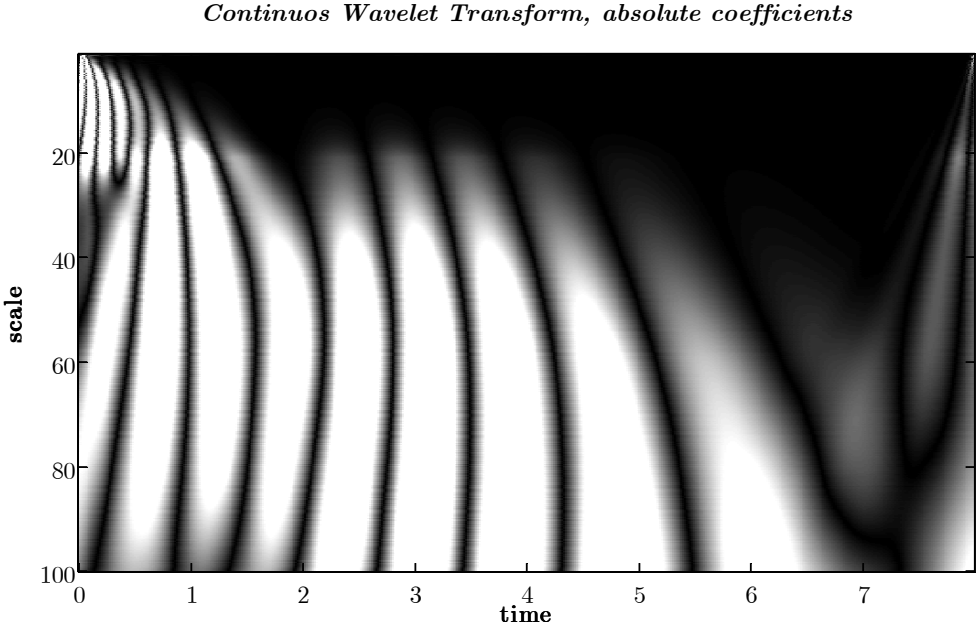

Figure 4.3.15 2D CWT of signal

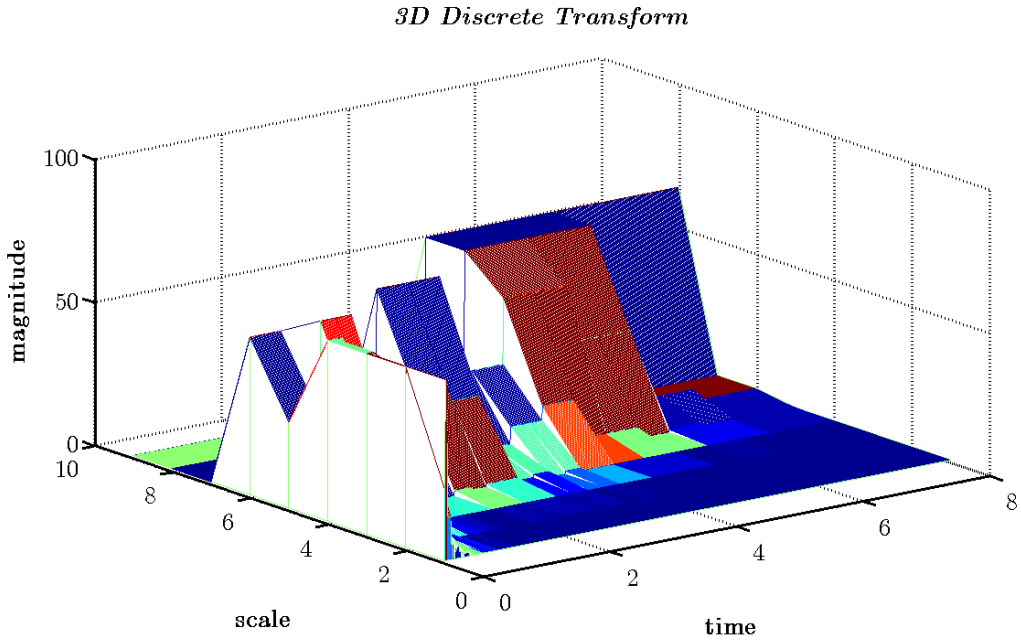

Figure 4.3.16 3D DWT of signal

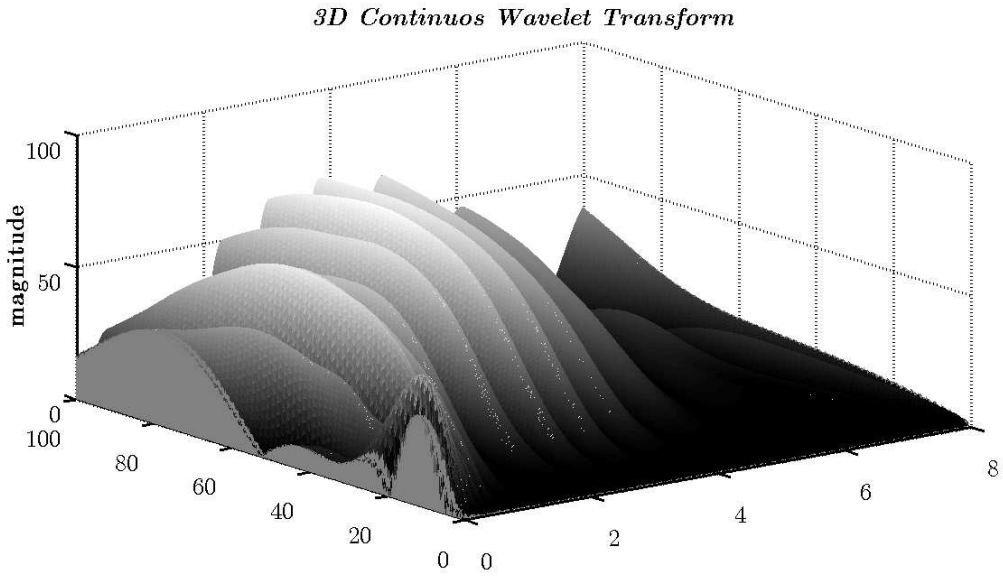

Figure 4.3.17 3D CWT of signal

At least we try to apply the two algorithms to define the DWT and the CWT in the case of a real signal, acquired during a dynamic test.

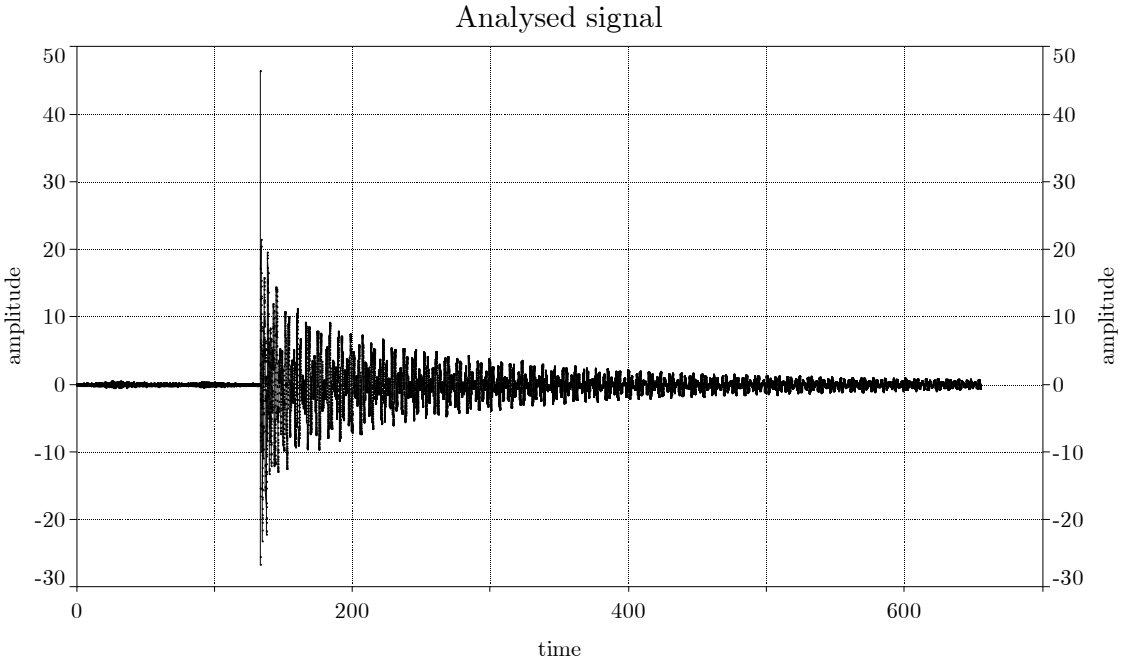

Figure 4.3.18 Response of the Vasco da Gama bridge after a release test

Discrete Transform, absolute coefficients

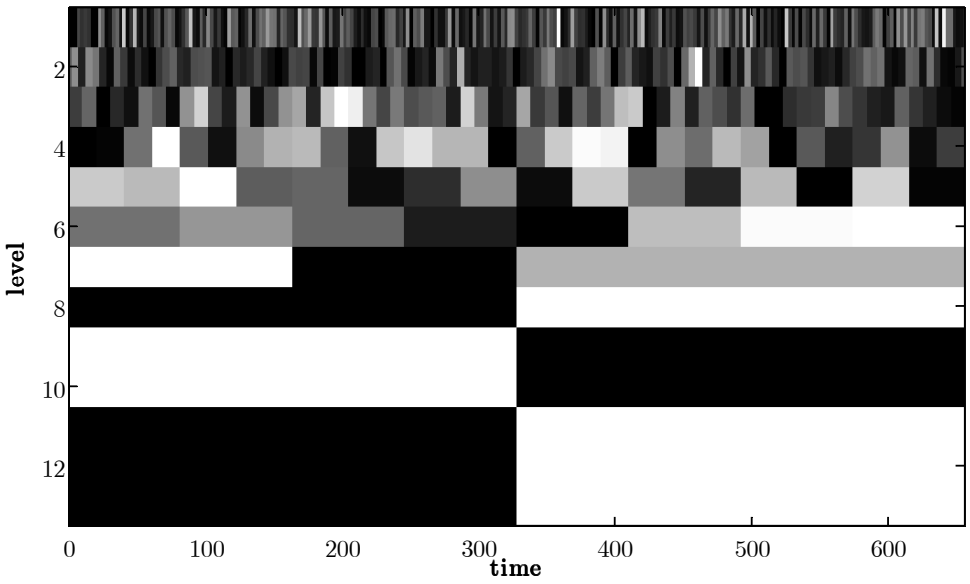

Figure 4.3.19 2D DWT, plane representation

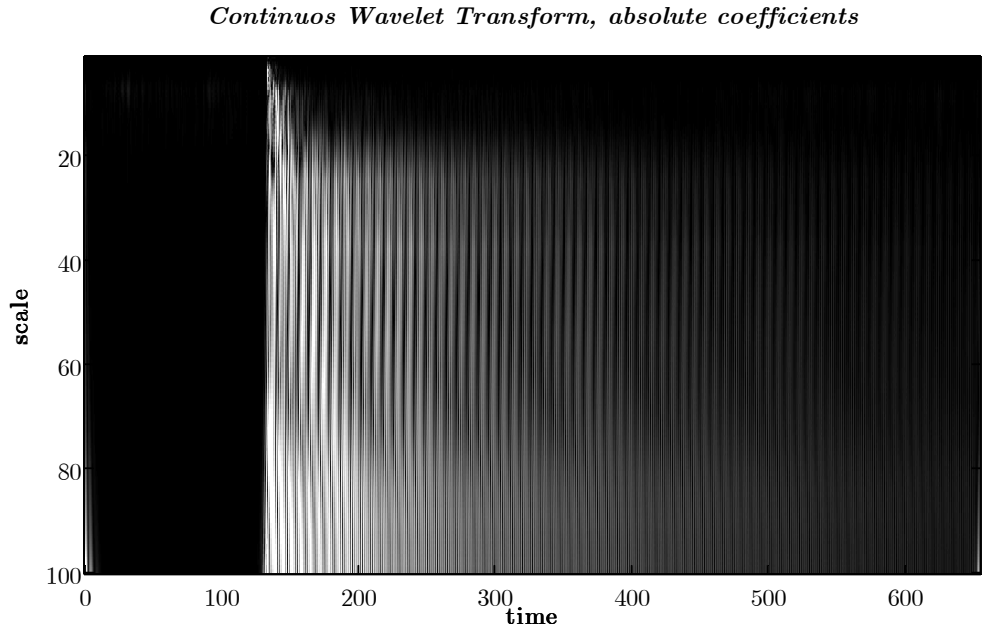

Figure 4.3.20 2D CWT, plane representation

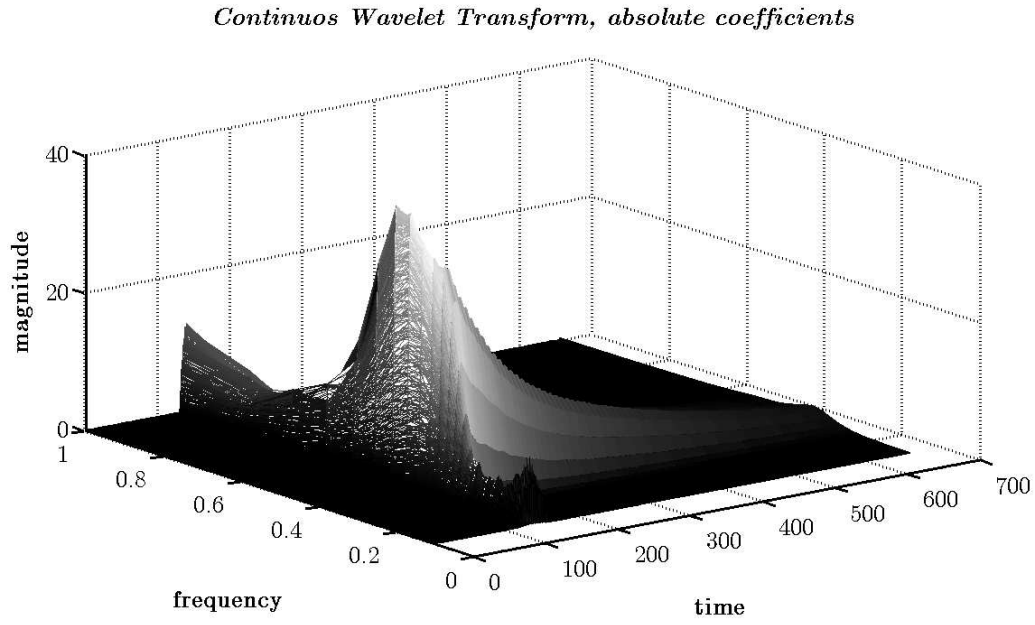

Figure 4.3.21 3D CWT of a real signal, acquired during an free vibration test

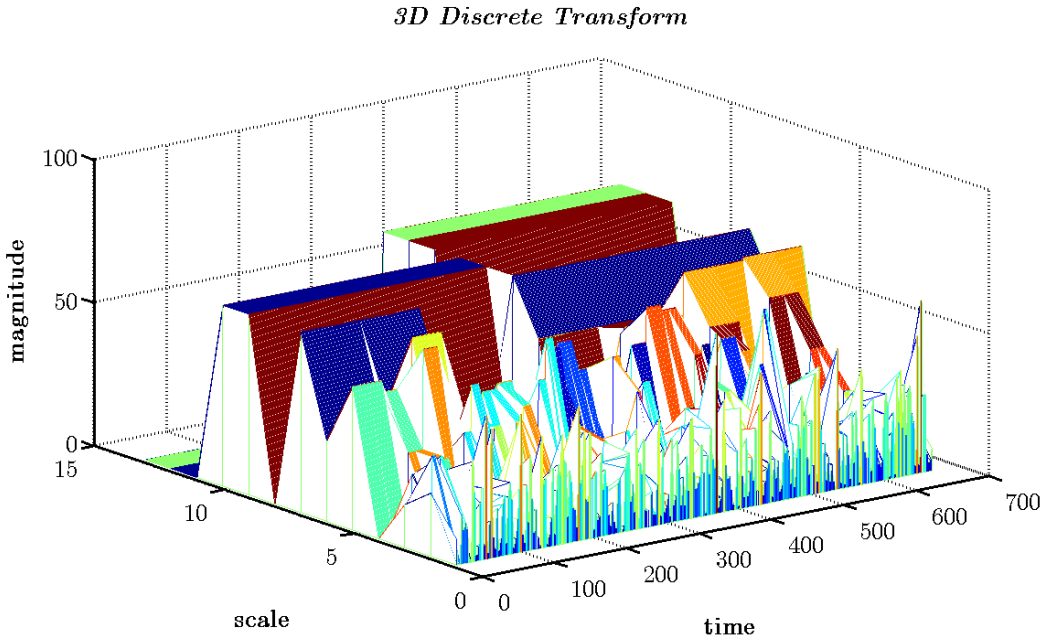

Figure 4.3.22 3D DWT of a real signal, acquired during an free vibration test

The graphs previously described show that the DWT introduce an important approximation of the signal analyzed on one hand and it is able to reduce the computation time on the other hand. The signals acquired during a dynamic test have usually a number of sampled points equal to 2^16. In this case the computation time using DWT it is not so different of that one using CWT. The difference it is important when a signal acquired during a monitoring of a generic structure is analyzed, where the signal length is very long. For this reason we decided to not use DWT to define the modal parameters of a generic structure when it is subject to a dynamic test, because in this case we want to obtain more precise reconstruction of the signal behavior both in time and frequency domain. The algorithm is instead used to filter the signal, during an ambient test carried out on a very stiff masonry bridge. The following paragraph describes how a generic signal can be filtered through DWT.

4.4. Filtering signal through DWT

Discrete wavelet transform (DWT) denoising contains three steps: forward transformation of the signal to the wavelet domain, as it was explained in the

previous section, reduction of the wavelet coefficients, and inverse transformation to the native domain. Three aspects that should be considered for DWT denoising include selecting the wavelet type, selecting the threshold, and applying the threshold to the wavelet coefficients. Although there exists an infinite variety of wavelet transformations, orthonormal wavelet transforms are typically used, which include Haar, daublets, coiflets, and symmlets. Four threshold selection methods have usually considered: universal, minimax, Stein's unbiased estimate of risk (SURE), and minimum description length (MDL) criteria [Johnstone, & Silverman]. The application of the threshold to the wavelet coefficients includes global (hard, soft, garrote, and firm), level-dependent, data-dependent, translation invariant (TI), and wavelet package transform (WPT) thresholding methods. Many researchers tried to compare the results obtained through classical filtering methods with the DWT filtering and the comparisons have shown that most DWTs are very powerful methods for denoising and that the MDL and the TI methods are practical. The MDL criterion is the only method that can select a threshold for wavelet coefficients and select an optimal transform type. The TI method is insensitive to the wavelet filter so that for a variety of wavelet filters equivalent results were obtained.

4.4.1. The mother wave

Experimental measurements usually contain noise that interferes with the interpretation of the data. High noise levels may be due to the instrumental instability, temperature fluctuation, etc., especially, when the measured signal is close to the detection limit. Denoising often is a preprocessing step before other analyses. In the last years the DWT is used to denoise experimental data as an alternative method to the Fourier transform (FT) and Saitzky-Golay (SG). The commonly used wavelets are Haar, daublets, coiflets, and symmlets. Some wavelets are shown in Figure 4.4.1

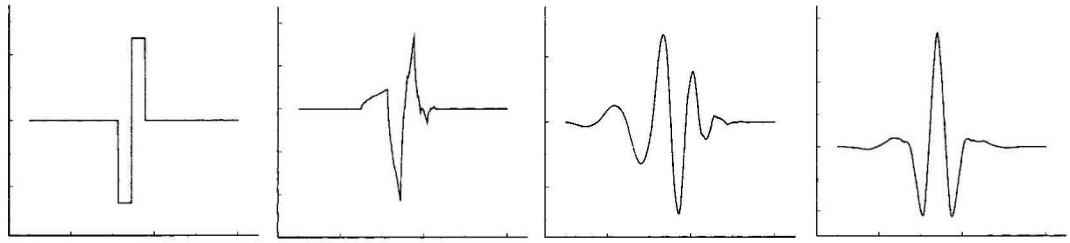

Haar Daublet 4 Daublet 12 Coiflet 3

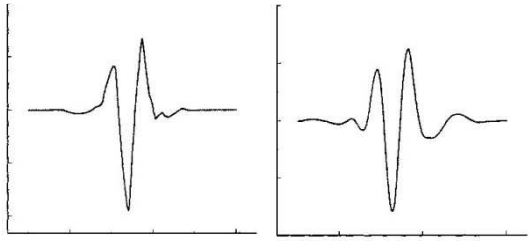

Symmlet4 Symmlet 9

Figure 4.4.1 Mother wavelet used with DWT

WT decomposes the original domain data into a series of wavelets that have different scales and intensities. Mathematically, the computational procedures for these transforms are the same. The signal is multiplied by a transform matrix constructed from these filters. The results are permuted so that the detail and the smooth parts are separated, which is the first level transform. This procedure is repeated recursively on the smooth parts until the last level is reached at log2N steps. The wavelet computation is implemented by a sequence of special finite-length filtering steps. The Haar transform is a special case of Daubechies 2. Coiflets usually consist of five filters, hence referred to as coiflet 1 to coiflet 5 with corresponding filter lengths that are multiples of six coefficients. Thus the coiflet 1 has six coefficients and coiflet 5 has 30 coefficients. The symmlet family has seven members that range from symmlet 4 to symmlet 10 with filter lengths that are multiples of two. In general the choice of the mother wavelet depends on the analyzed signal; in the following section this problem is studied in the case of a simulated signal.

4.4.2. The thresholding of signal

There are four common threshold selection methods: universal, minimax, Stein's unbiased estimate of risk (SURE), and minimum description length (MDL). The universal threshold is defined by

$$t = \sigma\sqrt{2\ln\left(N\right)} \tag{4.19}$$

Where N is the length of the data array and σ is the standard deviation of noise. For most real data, σ is unknown, but can be estimated as s. The first detail part of the wavelet coefficients Xi can be used to estimate the noise by

$$s \approx \frac{median\left(\left|x_i\right|\right)}{0.6745} \tag{4.20}$$

The minimax criterion gives a table of the threshold values for given data sizes that is based on calculations of the minimax risk bound for the wavelet estimate. Minimax thresholds were first introduced for soft thresholding (see below for the thresholding methods). These threshold values are smaller in magnitude than the universal threshold values. Recently, minimax thresholds for hard, firm, and non-negative garrote thresholding have been derived. Minimax thresholds optimize the risks for the worst cases, and therefore they are relatively conservative. This method estimates the noise level in the data using eq (4.20) and is biased toward retaining signal at the cost of retaining noise.

SURE is used to obtain an unbiased estimate of the variance between the filtered and unfiltered data [Donoho, 1993]. SURE is defined as

$$SURE\left(t,d\right) = N - 2M_{\left(i:\left|d_i\right|\le t\right)} + \sum_{i=1}^{N}\left(\left|d_i\right| \wedge t\right)^2 \tag{4.21}$$

for which t is the candidate threshold, di is the wavelet coefficient, N is the data size, and M is the number of the data points less than t.. The t that yields the minimum SURE value is selected as the threshold value. The last term in the SURE function determines the residual energy after thresholding ($\left|d_i\right| \wedge t$ is the

minimum value between $|d_i|$ and t). This criterion was originally developed for leveldependent soft thresholding. The SURE criterion can be applied to other thresholding methods. A modification of SURE threshold for global thresholding, called SPINSURE, was proposed by combining the SURE and cycle-spinning technique (see below).

The MDL criterion is defined by [Saito. 1994]

$$MDL\left(k^*, m^*\right) = \min\left(\frac{3}{2}k\log N + \frac{N}{2}\log\left(\sum\left(d_m^2 - d_{mk}^2\right)\right)\right) \tag{4.22}$$

for which k is the number of largest coefficients that are retained, m designates the filter type,d_m for wavelet coefficients from transform type m, d_{mk} for the k largest coefficients in amplitude, and k* and m* are the optimized values. The corresponding wavelet coefficient at k* is assigned as the threshold. The 3/2k log (N) term is a penalty function, which is proportional to the number of retained wavelet coefficients. The second log term characterizes the residual energy, which is the error between the reconstructed signal and the original noisy signal. Note this unique method not only picks a threshold but also a filter type. Neither the SURE nor the MDL criteria require an estimate of the noise level s.

Thresholding methods refer to the ways of applying a threshold to the wavelet coefficients, i.e., how to modify the wavelet coefficients. Traditional thresholding methods all transformed coefficients whose magnitudes are below the threshold. There are other means to modify the coefficients. Because DWTs are multilevel transforms and the transformed coefficients come from different levels as shown in Figure 4.5.5, different thresholds may be applied to each different level. In DWT-based denoising family, cycle-spining and wavelet packet transform are two special cases. Noise is assumed to have a Gaussian distribution due to the central limit theorem. Global thresholding assumes that Gaussian noise has the same frequency distribution and amplitude for all orthogonal bases that span the same data space. There are several ways to apply these thresholds to the wavelet coefficients: hard, soft, non-negative garrote, and firm [Gao, 1997]. They are defined as:

Hard

$$d_i^* = \begin{cases} 0 & if \left|d_i\right| < t \\ d_i & if \left|d_i\right| > t \end{cases} \tag{4.23}$$

Soft

$$d_i^* = \begin{cases} 0 & if \left|d_i\right| < t \\ sign\left(d_i\right)\left(d_i - t\right) & if \left|d_i\right| > t \end{cases} \tag{4.24}$$

Garrote

$$d_i^* = \begin{cases} 0 & if \left|d_i\right| < t \\ d_i - t^2 \Big/ d_i & if \left|d_i\right| > t \end{cases} \tag{4.25}$$

Firm

$$d_i^* = \begin{cases} 0 & if \left|d_i\right| < t_1 \\ sign\left(d_i\right) t_2 \left(\left|d_i\right| - t_1\right) \Big/ \left(t_2 - t_1\right) & if\ t_1 < \left|d_i\right| < t_2 \\ d_i & if \left|d_i\right| > t_2 \end{cases} \tag{4.26}$$

for which d_i and d_i^* stand for the wavelet coefficients before and after thresholding, respectively.

For the first three methods, the wavelet coefficients are partitioned into two parts by the threshold t. Hard thresholding is a classic way to remove noise and is the only thresholding method whose function is discontinuous (i.e., removes coefficients with low magnitude). Soft thresholding shrinks all large coefficients by the value of the threshold as well as removes all small coefficients. Soft thresholding is analogous to apodization in the Fourier transform methods. Hard thresholding introduces discontinuities into the denoised data but has smaller RMS errors than soft thresholding. Soft thresholding tends to generate denoised

data that is continuous at the expense of larger RMS errors. Soft thresholding tends to over-smooth abrupt changes and broaden sharp peaks and may give a visually better estimator. Non-negative garrote thresholding shrinks the large coefficients by a nonlinear continuous function and removes small coefficients. Firm thresholding has two thresholds; the wavelet coefficients are partitioned into three treatments: (l) retain the large coefficients, (2) remove the small coefficients, and (3) linearly shrink the middle coefficients. Both garrote and firm thresholding methods attempt to moderate the limitations of the hard and soft thresholding methods.

Level-dependent thresholding uses different thresholds for each transform level. SURE is usually applied to select thresholds for the coefficients in different levels. Universal soft threshold can also be applied if different levels have different noise values, as calculated by eq 2. SURE does not work well when the wavelet representations are sparse (i.e., contain mostly zero values). SURE has been combined with the universal method to yield a hybrid method that circumvents this problem. The hybrid method uses a sample variance at each level to determine if the representation at that level is sparse. If the level is not sparse, the SURE threshold is used, otherwise a universal threshold is used.

Data-dependent threshold (DDT) is determined by a statistical test within each level. The change-point (CP) approach is a datadependent level-by-level recursive scheme, based on the standard likelihood ratio test. First, all coefficients in a level are assumed to represent noise. Then a test statistic is computed and compared with the critical value. If the test is significant, the largest absolute value is considered non-noise and is removed from the noise coefficients. Using the retaining coefficients, the procedure continually repeats until the test is insignificant. After determining the threshold, which is the maximum of the coefficients tested to be noise, a soft thresholding is performed. Therefore, this method tries to extract a subset of coefficients that behave like pure noise. By adjusting the level a of the hypothesis tests, one can control the smoothness of the resulting estimator. Common thresholding methods use the magnitudes of the

wavelet coefficients only. Because a sharp peak in the signal results in several nonzero wavelet coefficients that are adjacent to each other, it is possible to use CP approaches to take advantage of this positional information.

Cycle-Spin Thresholding. DWT is similar to FT denoising in that denoising may introduce artifacts to the regenerated data, especially around some discontinuities such as sharp peaks or abrupt changes in the data. The cyclespin thresholding denoising method is intended to reduce the artifacts. The data are first cycle-spun (i.e., translated) by h points, transformed and thresholded, transformed back, and spun back by h points to their original position. Spinning refers to translating the data with the points shifted past the zero index added onto the other side of the data object (i.e., rotated). The reason for this transformation is that the artifacts caused by DWT are connected intimately with the actual location of the discontinuity in the data. A given signal can be realigned to minimize artifacts, but there is no guarantee that this will always be the case. For example, when a signal contains several discontinuities, they may interfere with each other: the best shift for one discontinuity may also be the worst shift for another discontinuity. Therefore, the idea of averaging all shifts, which is called translation invariant (TI) denoising, usually can give a much better result than ordinary cycle-spin denoising. Moreover, there is no guarantee that the TI averaging result is better

There are several approaches for defining a threshold criterion. A global threshold may be applied to all the wavelet coefficients. A threshold may be defined for each level of the wavelet transform. A data-dependent threshold criterion can also be used, which is a special case of the level-dependent threshold. There are many other threshold criteria and methods that may be applied to wavelet denoising. than the results of best shift and the uncycled methods. The cycle-spin approach provides a natural way to generate multiple estimators for the same object. However, it is more computationally intensive compared to ordinary DWT de-noismg.

Wavelet Packet Transform. Wavelet packet transform (WPT) is another powerful denoising tool. WPT is a generalized form of DWT, in which both smooth and detail parts are subject to further transforms. A full transformed matrix containing J (= log N) transform levels is used to search for a best basis. The best basis can be chosen using different criteria. Shannon entropy is a very common one, which is defined as

$$S = -\sum p_i \log\left(p_i\right) \quad (4.27)$$

for which $p_i = \left|d_j\right|^2 \Big/ \left\|d\right\|^2$, and P log P = 0 for P = 0. By comparing the possible combinations of all the wavelet coefficients at the different levels, a best basis can be obtained that is the combination of coefficients x with minimum entropy. The other criteria include (A) minimum $\sum \log\left|d_j\right|$, (B) minimum number larger than t, and (C) minimum SURE.

Practically, all of these DWT methods leave intact the last two or three levels, i.e., the four or eight points in wavelet domain spectrum, because they represent the most important information. In the last years many researchers studied this kind of filtering; they compared the results obtained with the classical threshold methods described previously with that one obtained by the WTP. This method is very powerful and very good results are obtained, but the limit of WPT is that the results depend strongly on the filter selected or in other word the mother wave. In the next paragraph we show this limit using a simulated sinusoidal signal with an additional Gaussian white noise.

4.4.3. WPT and the mother wavelet

The choice of the mother wavelet depends on the signal that is analyzed. To understand which is the best wavelet it is possible to define reconstruction square error RSE, calculated starting from the denoised signal, D_s and the ideal, x(t)

$$RSE = \sum_{t=1}^{N} \left(D_s\left(t\right) - x\left(t\right) \right)^2 \Big/ N \tag{4.28}$$

In practice this kind of estimation is easy when the ideal signal is know. To understand it we start from a simulated sinusoidal signal with an additional Gaussian white noise as it is represented below. In this case we try to filter the signal through the DB4, used previously, the Coif3 and Sym5.

At the beginning the signal is filtered through DB4, already represented in Figure 4.3.1, the threshold is SURE, soft and level independent. This kind of filtering does not modify the characteristic of the sinusoidal signal, as it is evident in the figure of the residuals. In this graph it is clear that only the noise is eliminated from the original signal.

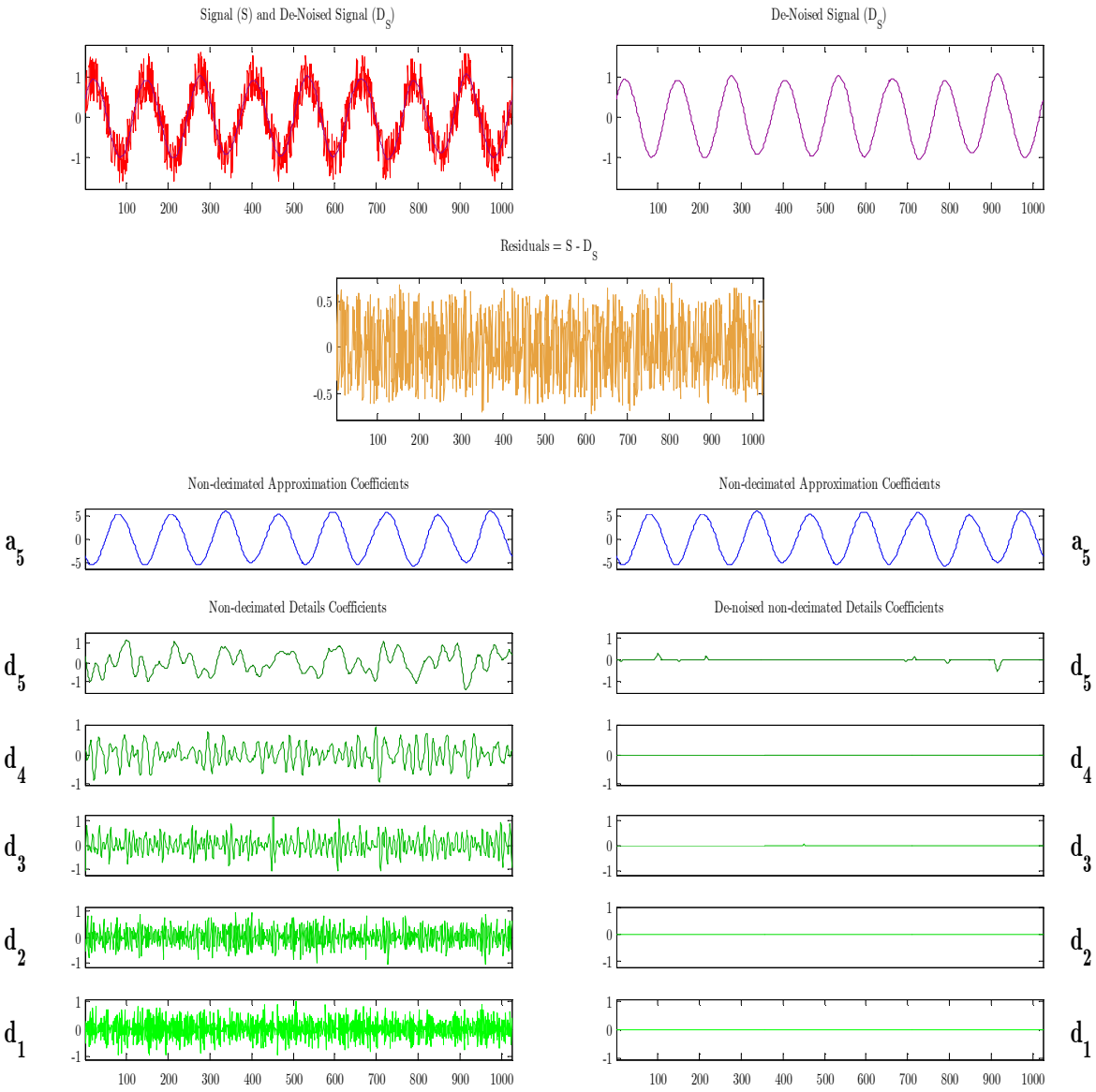

Figure 4.4.2 Signal denoising through WPT

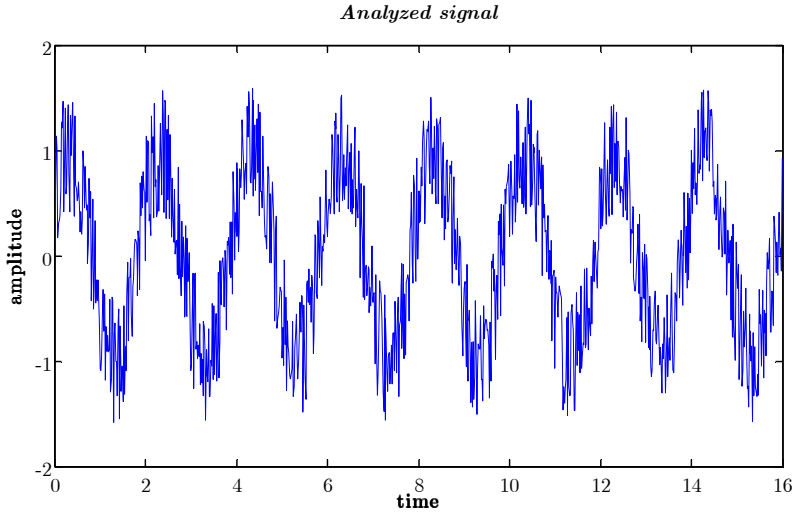

Figure 4.4.3 Simulated sinusoidal signal with an additional Gaussian noise

In this case it is possible to define how much the denoise signal D_s is near to the ideal x(t), computing the RSE, defined in equation (4.28).

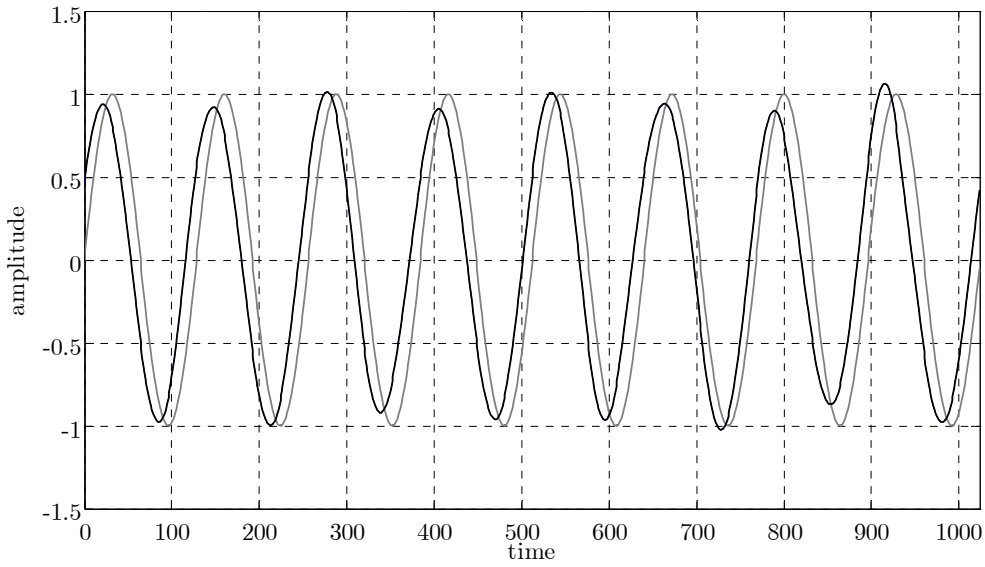

Figure 4.4.4 Comparison of the original signal (black) and reconstructed signal through DWT (grey)

The same procedure is applied choosing DMEY, COIF3 and SYM5, the RMS error are summarize in the table below:

Table 1 Values of RSM for different mother wavelet

Mother Wavelet	**RSM**
DB4	0,8043
DMEY	0,8749
COIF3	0,8294
SYM5	0,8368

The table shows on one hand that good results are obtained for each mother wavelet, one the other hand it demonstrates that even in a ideal case there are some difference depending on the mother selected.

The problem is that in the real case the ideal signal is unknown and the computation of RSE is not possible. In this case it is necessary define a process of optimization, defining a cost function able to define the best mother wavelet. In this section we do not want to study this problem, and we decide to look at the plot of the residuals, it can be a good indicator of the denoising obtained. It is necessary that the residuals plot does not contain any contents frequency of the signal analyzed.

4.5. Application in a real case: the ambient vibration test on the Sao Lazaro Bridge

In order to check the modal parameters extracted by a finite element model on the Sao Lazaro bridge, a free vibration test and an ambient vibration test were carried out in 2009. The structure is an asymmetric arch stone bridge, rehabilitated some years ago. Its span is almost 23 meters.

Figure 4.5.1 General view of the bridge

An ambient vibration test is based on the measurement of time histories of the response at different points of the structure. Due to the stiffness of the structure and the low level of excitation, accelerometers are normally used, whose required sensitivity is very high, considering the typical low levels of vibration.

The signals are acquired by four tri-axial 18-bit strong motion recorder. These devices, based on very sensitive internal force balance accelerometers (linear behaviour from DC to 100 Hz), analogue to digital converters with 18 bit (to guarantee a good resolution), batteries that enable autonomy for one day of tests, memories materialized by removable Compact Flash cards that permit a fast download of the acquired data and external GPS sensors to deliver a very accurate time, so that they can work independently and synchronously. With this equipment, the use of cables is avoided and the labour associated with the preparation of the dynamic test is drastically minimized. In order to obtain a good characterization of the mode shapes, on the total span the accelerations at 10 sections were measured (Figure 4.5.2). As torsion modes were expected, at each section two points were instrumented.

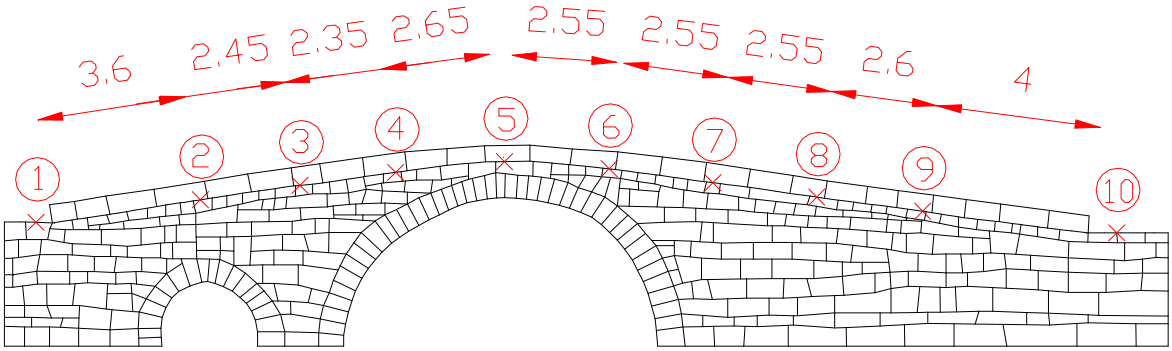

Figure 4.5.2 Location of sensors during the signal acquisition

In the developed test setups one recorder served as references, permanently located at section 5 on both sides of the deck. For each setup, time series of 8 minutes were collected with a sampling frequency of 100 Hz, value that is imposed by the filters of the acquisition equipment. The bridge is very stiff and due to the signal acquired was noisy and it was very difficult to define the natural frequencies of the system. An example of the signal acquired is represented in the figure below. The signal was acquired at point 9, very close to the end of the bridge; in this case a high level of noise is expected.

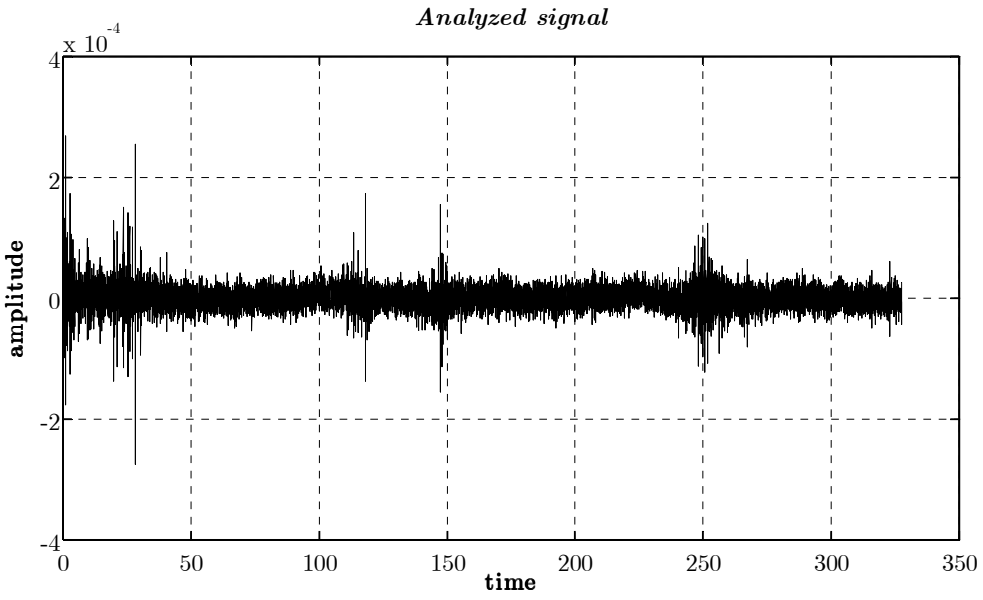

Figure 4.5.3 signal acquired during the ambient vibration test at point 1

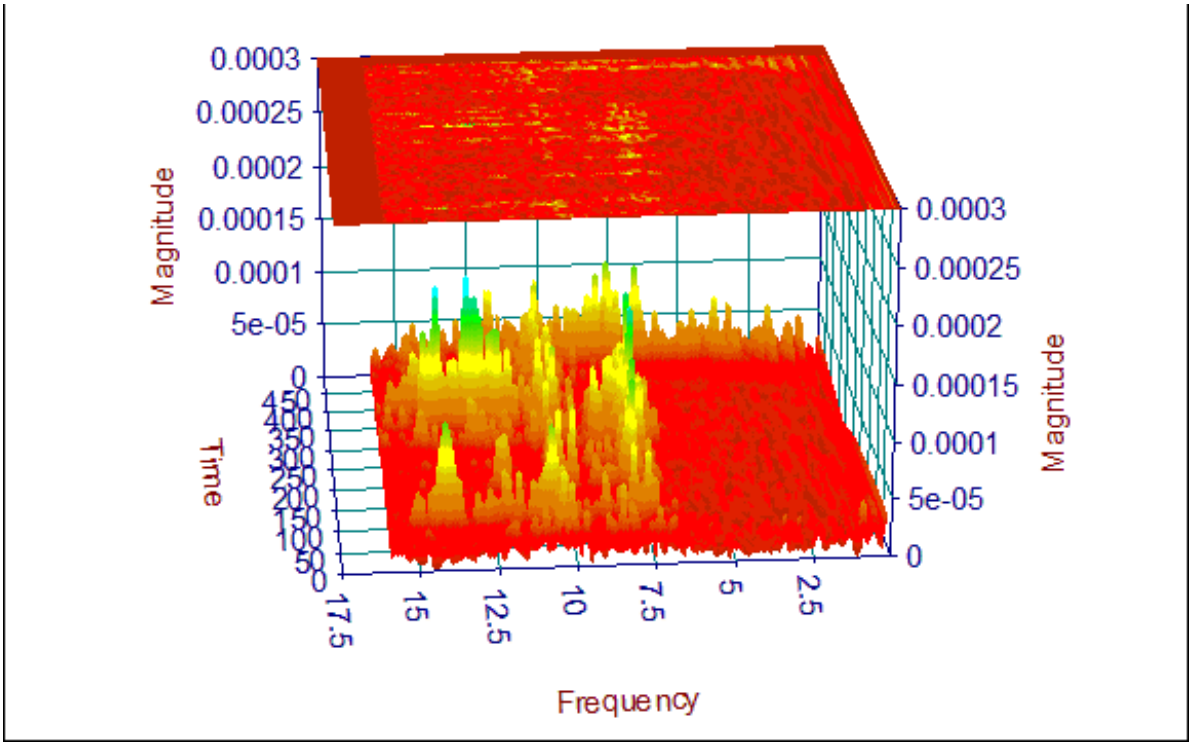

Figure 4.5.4 Its 3-D Wavelet Transform

As the previous figures show, it is very difficult to define the modal parameters of the structure, due to the presence of a lot of noise, combined to a low level of amplitude of the signal acquired. A denoising is in this case necessary, and it is obtained through the application of the DWT. In particular the mother DWT used was DB4, the threshold SURE-soft.

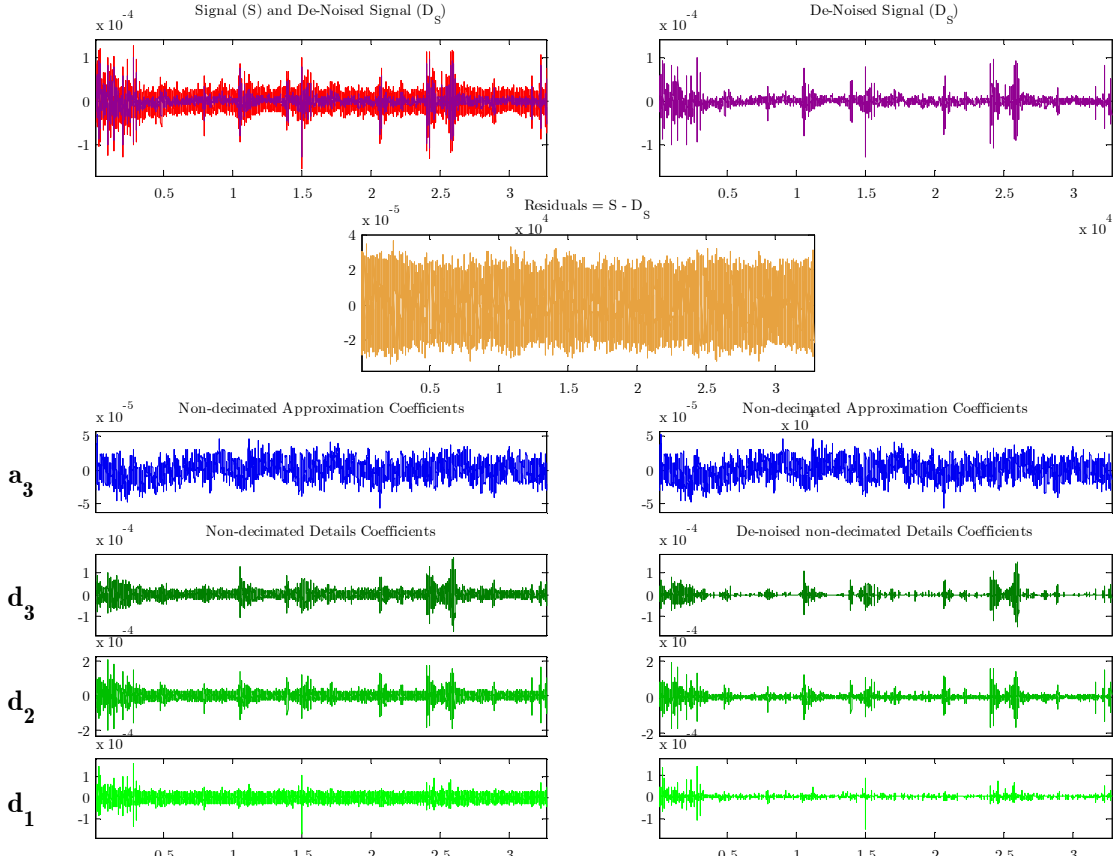

Figure 4.5.5 Signal denoising through WT, SURE threshoulding

In this case looking at the plot of residuals the procedures eliminate only the noise component, the frequency contents are not modified.

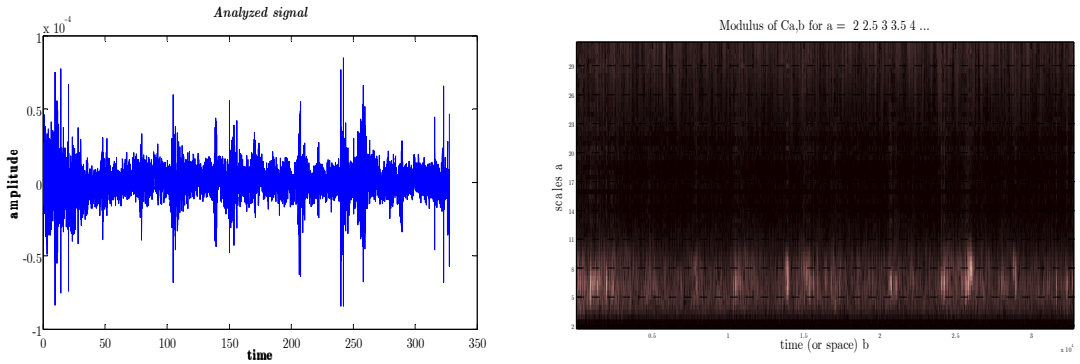

Figure 4.5.6 Signal after deinoising process and its 2 D CWT

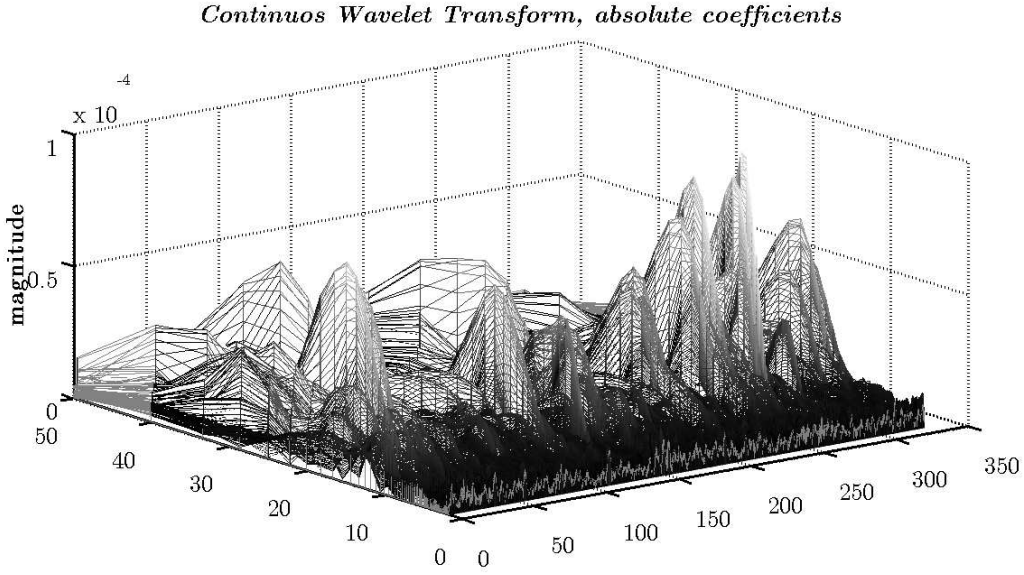

Figure 4.5.7 3D CWT of the signal with noise

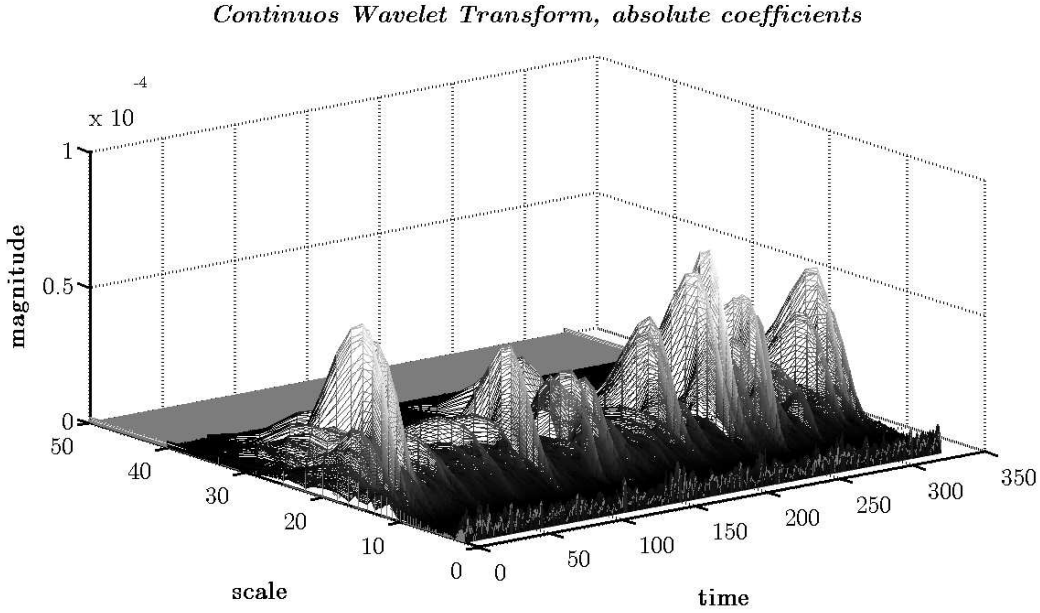

Figure 4.5.8 3D CWT of the signal after WT filtering

Using the decomposition of the signal obtained through the DWT, another kind of filtering can be applied. Performing an FFT of each signal decomposition, the frequency content can be defined, then a threshold level dependent can be applied to filter the signal, as Figure 4.5.9 shows

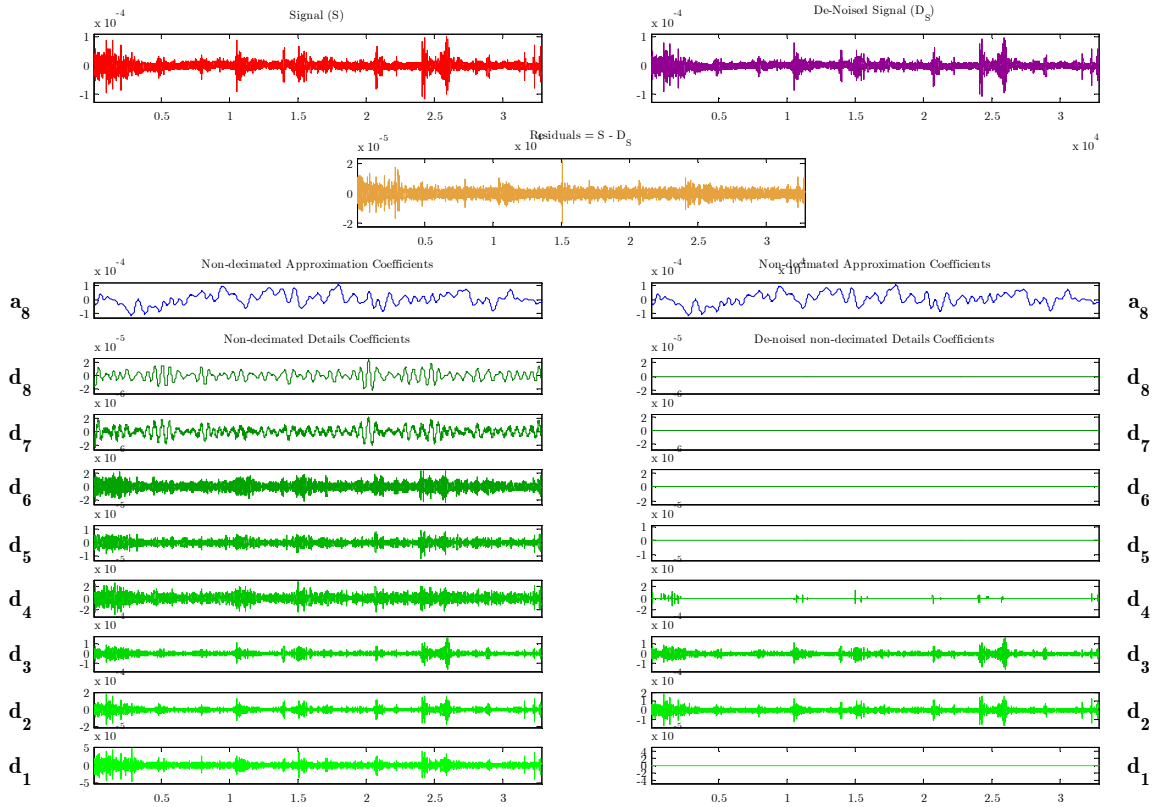

Figure 4.5.9 Signal denoising through WT, level dependent thresholding

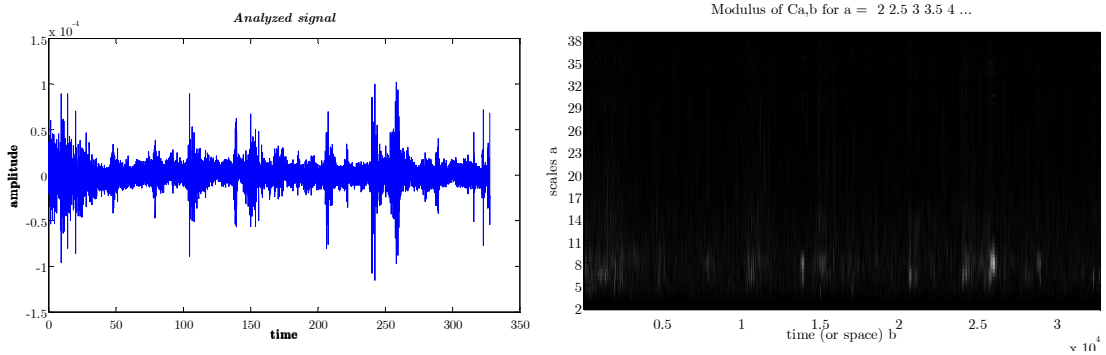

Figure 4.5.10 Signal after denoising through WT reconstruction

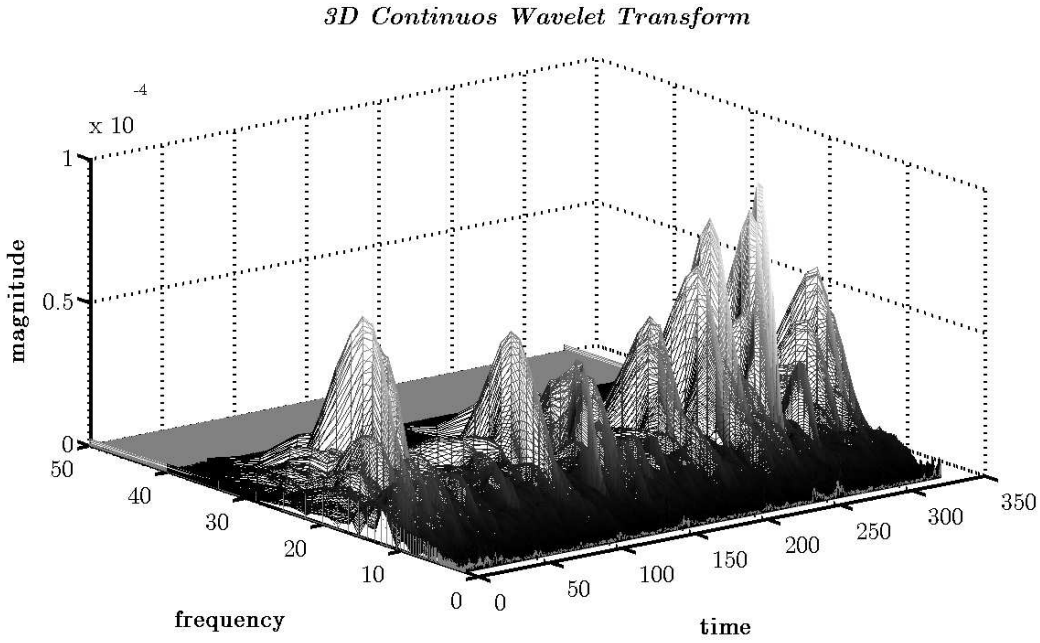

Figure 4.5.11 3D CWT after denoising

As the figures show, almost the same results are obtained. This king of filtering is used to filter each signal acquired during the ambient test. The figures below describe the filtering process for the longitudinal component of signal acquired at point 6.

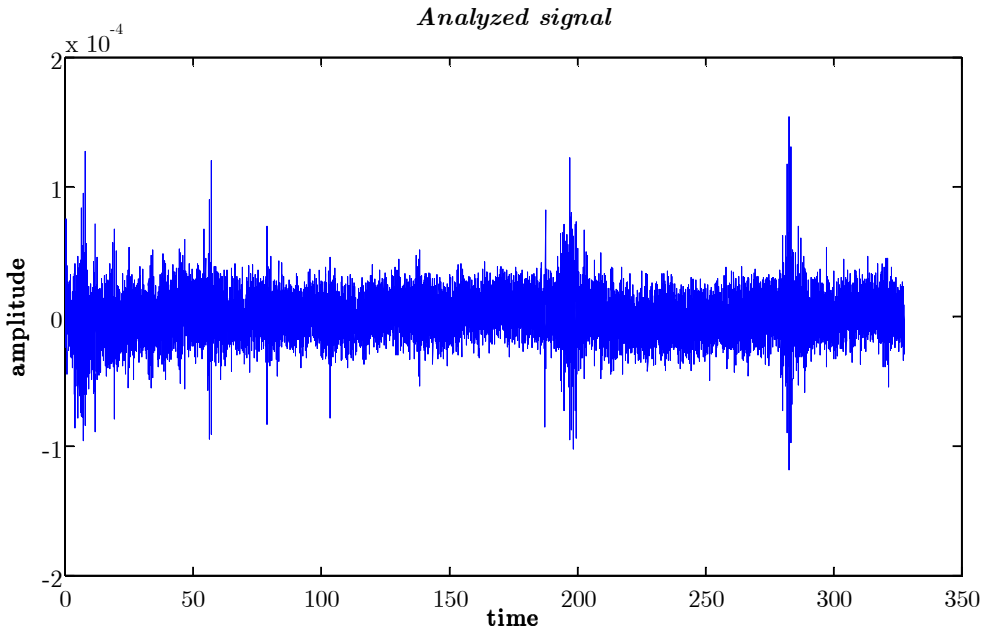

Figure 4.5.12 Time trend of the longitudinal component of the signal acquired at section 6

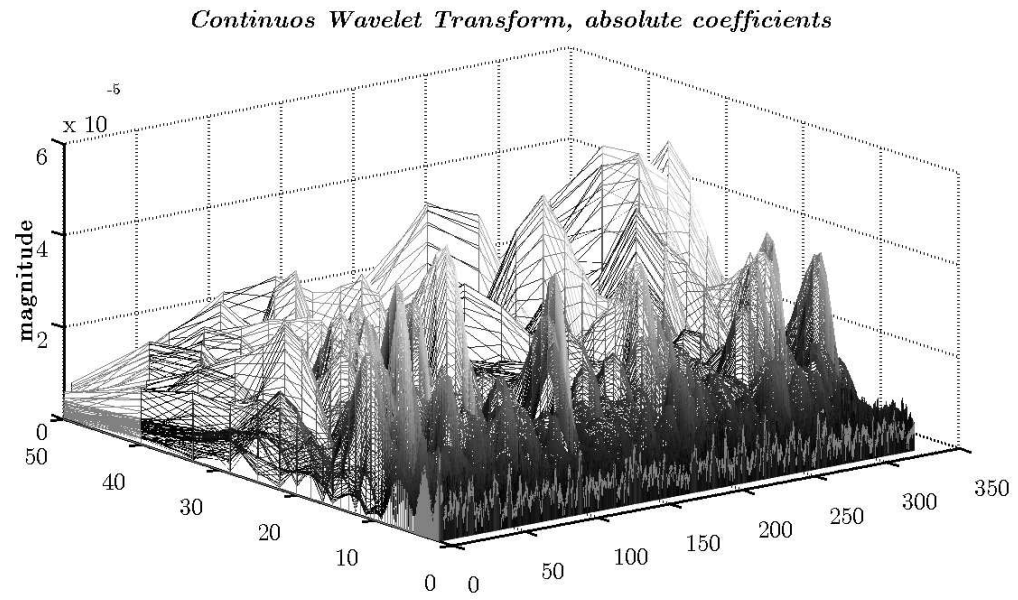

Figure 4.5.13 CWT pre-denoising

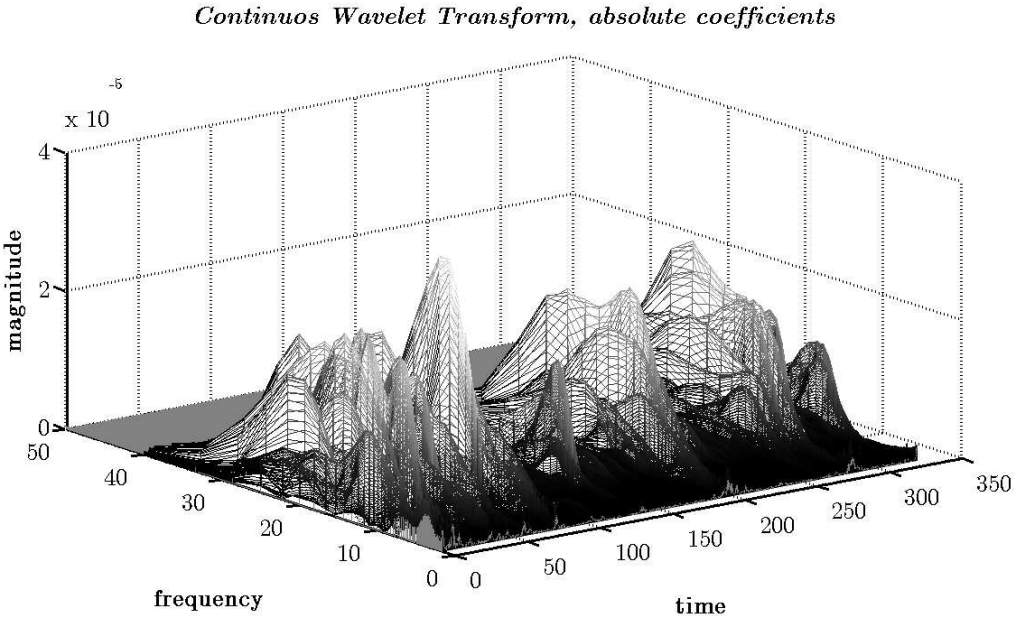

Figure 4.5.14 CWT after denoising process

Finally we would like to underline that the noise is not so important in the transversal component of the signal acquired, as you can see through the following CWT

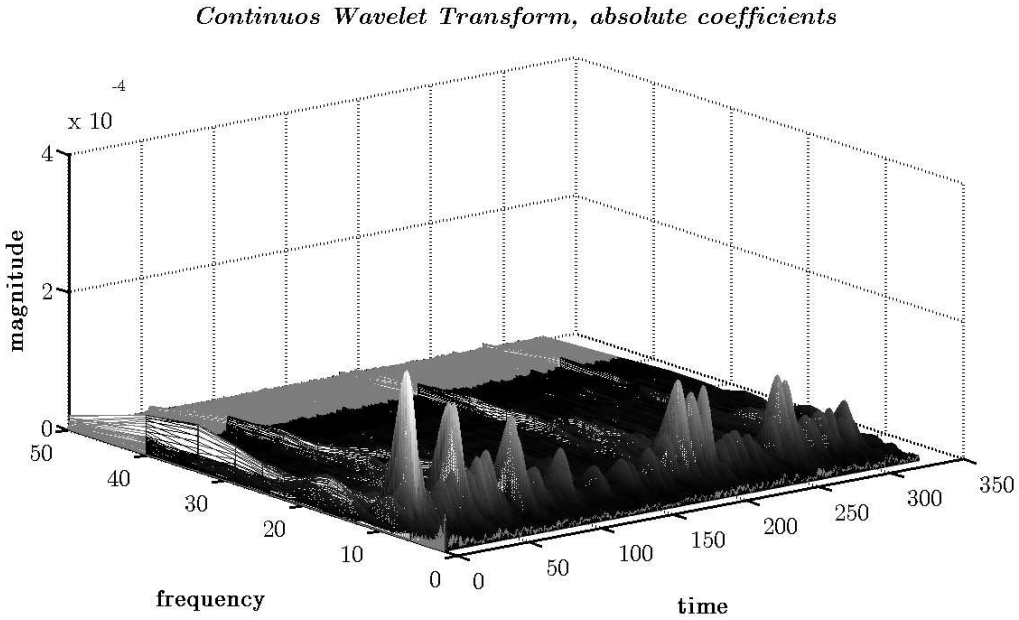

Figure 4.5.15 CWT of the transversal component without filtering

Then, the signal acquired in x-direction are filtered by the method previously described, that one acquired in y-direction does not need to be filtered. The natural frequencies are extracted computing for each signal the CWT: in the following table, the results are summarized.

Table 2 Natural frequencies and type mode of the structure

MODO	Frequency	Type of mode
1	7.83 Hz	Transversal
2	10.632	Transversal + longitudinal
3	12.588	Transversal + longitudinal
4	14.394	Transversal
5	15.752	Torsional

On the same bridge another dynamic test was performed; in particular the signal was acquired after some jumps of 4 people in the middle of the structure (first part of the signal) and after their running (second part of signal). In this case all

the sensors were positioned at point 5. An example of the signal acquired is represented in figure below

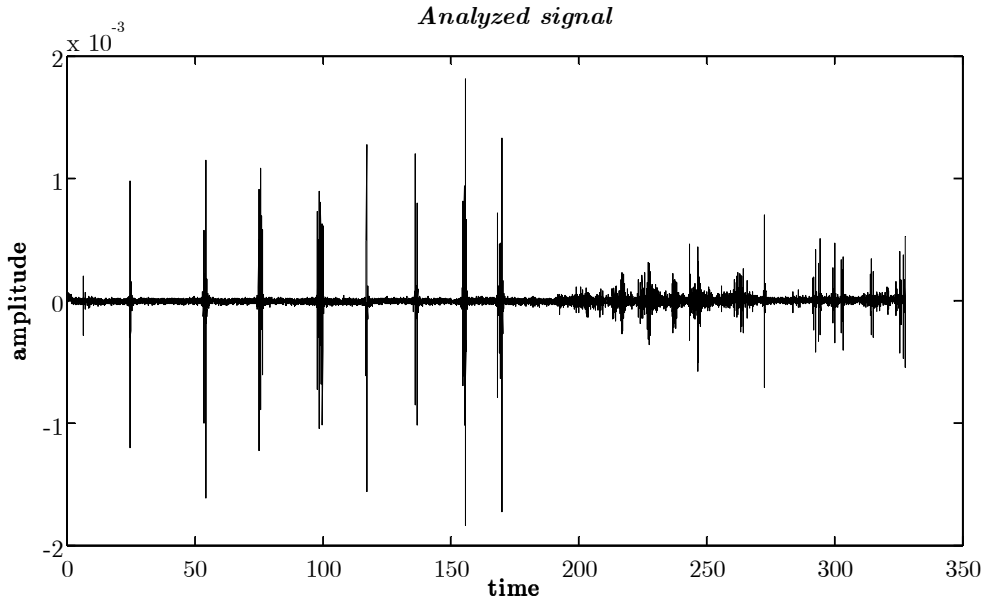

Figure 4.5.16 ***Example of the signal acquired during the free vibration test***

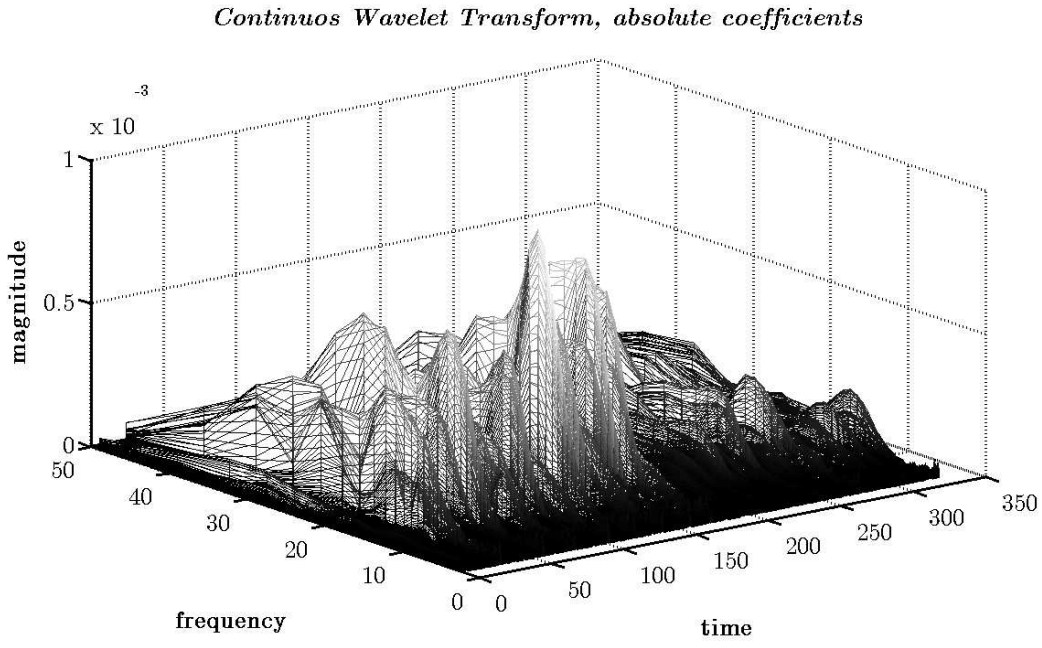

Figure 4.5.17 CWT of the transversal component, without any filtering

In this case the noise is not predominant, as the CWT of the transversal component of the signal shows. From the CWT the natural frequencies of the

system are extracted, an example of the spectrum is described in the following figures in x, y and z direction for the signal acquire from sensor 4 at section 5.

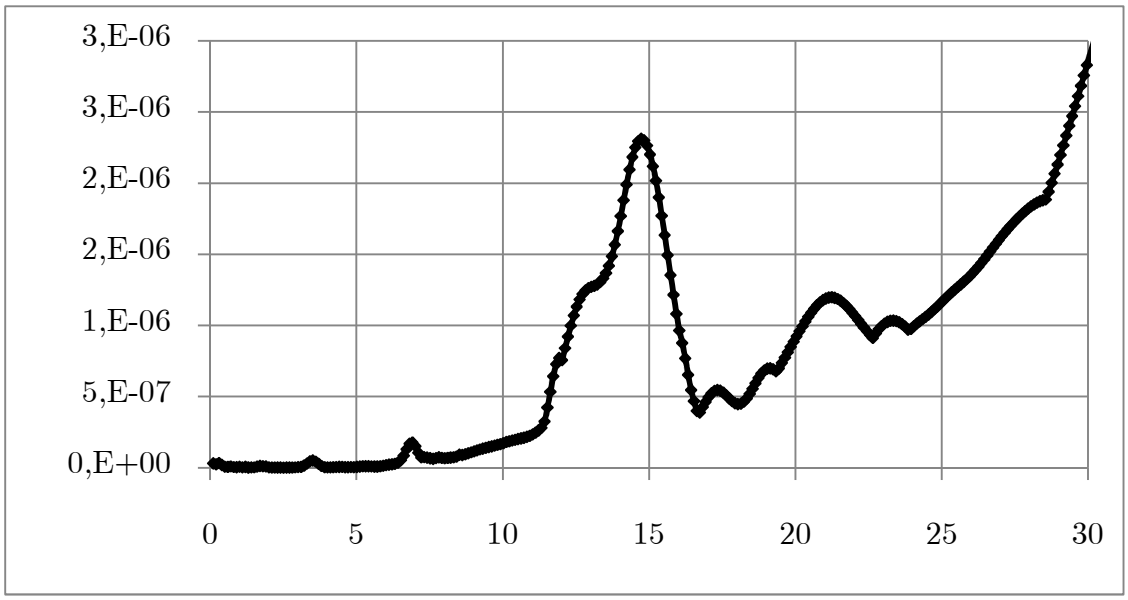

Figure 4.5.18: Spectrum of x-component, extracted from the relative CWT

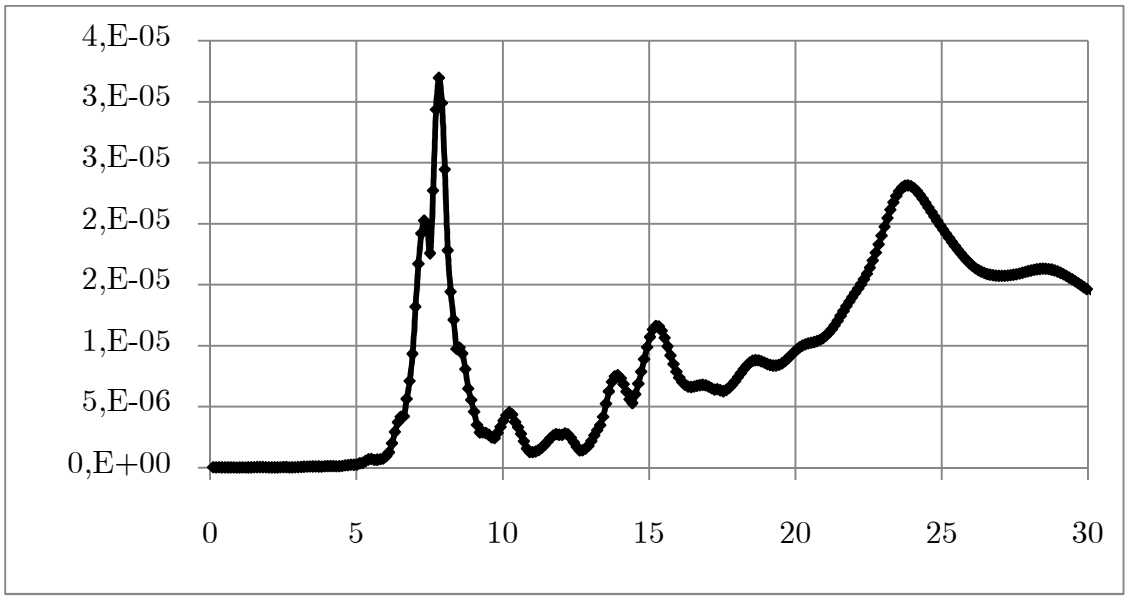

Figure 4.5.19 Spectrum of y-component, extracted from the relative CWT

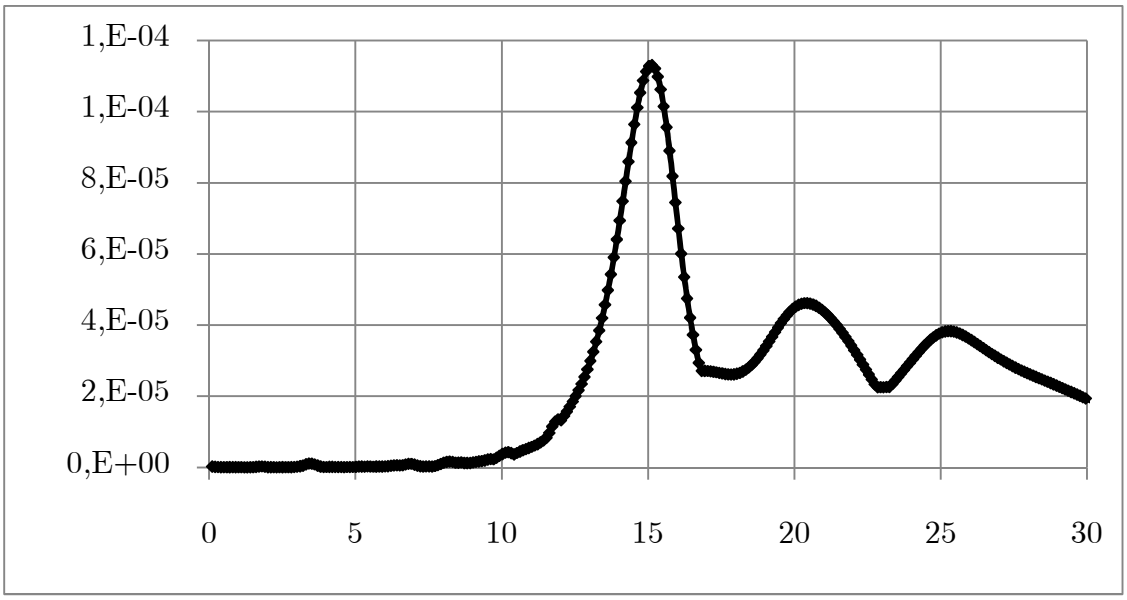

Figure 4.5.20 Spectrum of z-component, extracted from the relative CWT

The signal does not need of filtering (only detrend) and the results are summarized in the following table and they are compared with the frequencies obtained by ambient test.

Table 3 Natural frequencies of system from the free vibration test and the ambient test

MODO	**Frequency Ambient Test**	**Type of mode**	**Frequency Free test**	**Type of mode**
1	7.83 Hz	Transversal	7.84 Hz	Transversal
2	10.632 Hz	Transversal + longitudinal	10.471 Hz	Transversal + longitudinal
3	12.588 Hz	Transversal + longitudinal	12.809 Hz	Longitudinal
4	14.394 Hz	Transversal	14.465 Hz	Transversal + longitudinal
5	15.752 Hz	Longitudinal and vertical	15.372 Hz	Longitudinal and vertical

The table shows that similar results are obtained from the ambient and free vibration test. Of course due to the stiffness of the structure also the free vibration test was not able to excite strongly the bridge. In this kind of structure a better test can be a forced dynamic test. An ambient test can be used also, but the signal needs of an important post processing. Instead a forced test excites the structure and the noise it is not fundamental in the signal acquired. Some uncertainties can be overcame, besides the input is known and it is possible to define the quality of the signal acquired through its comparison with the recorded output, as it was described in chapter two.

CHAPTER FIVE

The Humber Bridge: experimental and numerical survey

5.1. Introduction

The Strornsund Bridge, in Sweden was considered the first cable-stayed bridge of the modern era. In effect, a systematic structural analysis was, for the first time, performed in connection with the bridge construction, which permitted a permanent control of the cable forces, assuring the efficiency of all cables in the final structure (Caetano, 2000; Gimsing, 1983).

In the short period of about 45 years, the design and construction of cable-stayed bridges showed a very deep evolution. In effect, the technological progress of the last decades, conjugated with the development of numerical methods of analysis, have permitted both to take advantage of improved material properties and to analyse more complex highly indeterminate structures. For technical, economical and also aesthetic reasons, cable-stayed bridges, that became very popular in Germany in the post-war reconstruction, have gained an increasing importance, establishing themselves as a new category amongst classical structural systems, and their use quickly spread all over the world, in a multitude of innovative solutions.

With the completion of the Normandy Bridge in France, in 1994, a multiple suspension bridge with a total length of 2141m and a record main span of 856m, it was even possible to prove that cable-stayed bridges, whose range of applications had been traditionally considered the 150m to 500m spans, can also be successfully applied, and with economic advantage, in the domain of the very long spans. The Tatara Bridge, which was completed in Japan in 1999, and has a main span of 890m, enhanced this aspect. In fact, since no element in the bridge has reached a feasibility threshold yet, and since the ratio cost/span has not shown a steep increase with the increase of span, it is still possible to expect an increase in the span range (Taylor, 1991). The former proposals for cable-stayed bridges with main span larger than 1000m are indeed older than 20 years.

Leonhardt and Zellner (1980) mentioned the limit of 100m and 500m for highway

traffic and for railroad, respectively, in prestressed concrete cable-stayed bridges. As for steel cable-stayed bridges, they referred two proposals presented for the Messina Straits Crossing, with main spans of about 1300m and 1500m (6 lanes highway and 2 tracks railroad) which, according to the designers, presented no structural difficulties and even were superior to a classical suspension bridge, not only in terms of the required amount of steel, but also with respect to deformations and dynamic behavior.

Still worth of reference is the proposal dated from 1989 for a 1204m main span cablestayed bridge, presented in the bid for the construction of the East Bridge, across the Great Belt. At that time, the largest existent cable-stayed bridge was the Annacis Bridge, in Canada, a composite bridge with 465m main span. The cable-stayed bridge option was considered too risky for construction, and a suspension bridge with a main span of 1624m was chosen instead (Gimsing, 1991).

The most significant restriction to an increase of the span length of a cable-stayed bridge is associated with the development of high compression forces introduced in the deck by the stay cables. According to Mathivat (1994), this fact limits the main span length to about 1500m. Above this length, it is normally assumed that the classical suspension type, with cables anchored to the ground, is the best solution.

But even in those large spans can the inclined stay cable suspension play an important role. In effect, the addition of inclined stay cables into a suspension bridge in the vicinity of the pylons provides a higher global stiffness for the bridge and, consequently, a better wind stability, and allows for a better control of static deformations, particularly important in the case of railroad bridges. This hybrid system was used in an empirical form by Roebling , in the railroad bridge across the Niagara River (1855), in the Ohio Bridge (1867) and in the Brooklyn Bridge (1883). And it was several times proposed for the construction of recent bridges, as is the case of a 1500m bridge across the Great Belt, presented in 1977

in an international bid. But no modern applications are known.

Another hybrid approach, presented by Lin and Chow (1991), consists in a double cantilever suspension system, where the main cable is suspended from the tips of inclined struts, which are themselves back stayed to the pylons. This structural system was one of the considered feasible schemes for a 5km main span bridge to integrate a 14km Crossing at the Gibraltar Strait. A more recent proposal by Menn (1998) employs the same concept of conjugating the inclined stayed system with classical suspension cables, achieving simultaneously the purposes of increasing the lateral stiffness of the bridge, and minimizing the construction time.

Most of the studies already performed for very long spans are based on the use of conventional materials, steel and concrete, whose properties were significantly improved during the last decades. But also during the last years investigation on the application of new high-strength lightweight materials has progressed a lot. Several small span girder bridges have already been constructed using the so-called Advanced Composite Materials (ACM), in the form of carbon fibers and plastics . These materials have an enormous potential for long span cable-stayed bridges applications, since the self-weight of the deck can represent a high percentage of the bearing capacity in a very long span.

The design of long span bridges is governed by their dynamic behaviour to wind and, for certain locations, to earthquake excitations. In spite of the tremendous progress achieved during the last decades in the areas of Dynamic Modelling, Seismic Analysis, Wind Stability, Structural Monitoring and Control of Vibrations, the vulnerability of these extremely complex systems to several types of dynamic actions has not been completely assessed yet.

The large flexibility of cable-stayed bridges, which is naturally augmented with the large span lengths achieved in recent years, is responsible for an accentuated geometric nonlinear behaviour, in addition to the nonlinearity associated with the

cable sag, and with other nonlinearities related with the properties of the materials. These characteristics, combined with the various and complex types of actuating loads, are responsible for very demanding requirements of analysis and explain why only recently, during the last two decades, dynamic analysis has been incorporated on a regular basis in the design of cable-stayed bridges.

The third and last level of approach in the numerical modelling of a cable-stayed bridge consists in the use of the finite element method. One of the former applications to cable-stayed bridge response analysis is due to Kajita & Cheung (1973), who discretized the bridge deck into a number of small shell elements supported at the cable anchorages by equivalent springs, and performed a three-dimensional linear dynamic analysis, arriving at a set of torsional and bending vibration modes. More recent applications involve both linear and nonlinear static and dynamic analyses, using a variety of finite elements, and different possibilities for modelling joints and particular devices, such as cable dampers (Kanok-Nukulchai, 1992; 1993).

The progress in computer technology made the finite element method one of the most powerful tools for structural analysis, not only by offering a wide range of possibilities in terms of selection of finite element types and formulations, but also, by the possibility of running very large applications in PCs and workstations. In effect, most design companies have presently access to very sophisticated finite element software packages, allowing the performance of large displacement nonlinear material and geometric static and dynamic analyses, by idealization of the bridge as an association of several types of finite elements, like beam, shell and truss elements. The assessment of cable tensions and the control of displacements throughout the construction phase is also possible, by simple activation/de-activation of specific groups of finite elements in successive stages of the analysis. Moreover, the comparison between natural frequencies and modal shapes evaluated on the basis of these algorithms, and the corresponding measured values on the prototype, has proven that extremely good correlations can be obtained, what evidences the enormous sophistication that can be

achieved in structural analysis.

An interesting aspect to emphasize is that, despite the various alternatives offered for the modelling of the stay cables, the most common numerical idealizations of cable-stayed bridges don't include an appropriate mass distribution for the stay cables, i.e., the dynamic behaviour of the stay cables is not included in the global dynamic analysis of the bridge, the problem of cable vibration being treated separately. The dynamic interaction between the cables and the structure, here designated as cable-structure interaction, has been investigated by several researchers, such as Kovacs (1982), Maeda et al. (1983), Causevic and Sreckovic (1987), Abdel-Ghaffar and Khalifa (1991), Fujino (1993) and Tuladhar et al. (1995). Although different approaches have been followed, most authors stressed the importance of the performance of a global dynamic analysis, where the stay cables' dynamics is included in the global numerical model of the bridge. For this purpose, the distributed mass of the stay cables is required to be conveniently modelled, either by employing specific cable elements, like the two-node curved element (Gambhir & Batchelor, 1977), the elastic catenary element (Jayaraman & Knudson, 1981), or the four-node isoparametric truss element (Ali, 1991), or by discretizing the stays into series of truss elements.

In this chapter a numerical model of a suspended bridge is proposed. In particular the Humber Bridge was subjected to an ambient test, carried out by the laboratory ViBest of the University of Porto. The model tries to update the natural frequencies of the bridge, obtained through the processing of data acquired during the test.

More of all, the FEM model is able to find some local modes, which cannot be indentified during the dynamic test.

5.2. The Humber Bridge Prototype

The Humber Bridge, with a main span of 1410 m, had the longest bridge span in

the world, 112 m more than the previous longest, Verrazano Narrows Bridge in New York. In particular it held the world record as the longest single span suspension bridge for 17 years. Now the Bridge is the fifth-largest single-span suspension bridge in the world. A long-span bridge was necessary because the Humber estuary has a mobile bed and 1410 m covers the likely movements of the navigation channel; piers supporting short spans would have interfered with the natural regime of the river.

Figure 5.2.1 General view

The north tower is sited just above the high water line and the south tower is in the estuary about 500 m from the shore line. Because of topological and geological conditions there is a marked inequality in the lengths of the two side spans: that on the north side is 280 m long and that on the south side 830 m. However the bridge is so long that the asymmetry is not readily apparent.

The bridge has been built to aid industrial and social development along both

banks of the estuary. The structure carries dual two-lane roadways (which gives it a practicable capacity of about 40000 vehicles a day) with a combined footpath and cycle track along each side of the bridge. The underside of the road deck is a minimum 30 m above high water to give clearance for shipping using the river.

Design of the Humber Bridge and all the associated works was undertaken by Freeman Fox & Partners who had been retained as consulting engineers for the project since 1928, and had proposed designs in 1930, 1935, 1955 and 1966.

The bridge has been designed to carry the highway loading intensity specified in British Standard 5400 which deals with steel, concrete and composite bridges. The load intensity varies with the length of load considered with a minimum lane load of 8.7 kNm^{-1}; for short loaded lengths, the load intensity increases to 32.1 kN m – 1. In addition the bridge has been designed to carry a special vehicle with an all-up weight of 176 kN (180 tons). Consideration has been given to many patterns and combinations of loading, e.g. alternate spans being fully loaded with traffic on one side and empty on the other, so that the most onerous combinations of loading are catered for throughout the different elements (deck, suspenders, cables, towers, anchorages) of the bridge.

Wind loading and its effects are of major importance for a bridge of this size of span and the design caters for wind speeds of approximately 47 m/s on the deck structure and, for the towers, a speed that increases with height to 66 m/s at the top. Of even greater significance than the highest wind loadings are-pace Tacoma Narrows Bridge oscillations due to dynamic instability. The deck girder for Humber has a streamlined cross section of the type previously used successfully by the designers, Freeman Fox & Partners, for the Severn Bridge (main span 988 rn, completed in 1966) and the Bosporus Bridge (1074 m, 1973). Wind tunnel tests were carried out at the National Maritime Institute at Teddington on models of the proposed Humber deck to establish its aerodynamic stability and to determine lift and drag coefficients. Similarly, tests were also made on a model of a tower to determine drag coefficients for various angles of wind incidence and

the possibility of tower oscillation during erection (i.e. when the tower is free standing without any restraining effect by the cables of the completed structure).

The forces involved in a structure are very large. For example, the deck structure, before the application of live load, weighs some 21000 t and the maximum pull in each main cable is 194000 t. From these and other primary loads and the geometry of the structure stresses can be calculated for any point in the structure. However, an additional complication of any suspension bridge is that it does not respond linearly to applied loads. Furthermore, good judgment is required to assess what loads will, or will not, occur simultaneously - for example it is improbable that maximum traffic loads will be experienced at the same time as very high wind speeds - and the worst likely combination has to be catered for.

Fluctuating stresses

Bridges were at that time designed to have a normal life of 120 years and appropriate regard has to be paid to components subjected to fluctuating stresses so that proper allowance is made for fatigue. It is in matters such as this that sound engineering experience and appreciation of structural and materials behaviour are of great value in tempering the results of stress investigations.

Long-span bridges are very flexible structures subject to very large movements arising both from strain due to external load and from temperature effects. To accommodate these movements between - 20C and + 60 T the three spans at Humber are supported at each end by A-frame rockers (two-legged hinged struts) mounted on the bottom cross-beam of the towers and on the anchorage blocks that permit longitudinal movement and small changes in gradient of the deck but constrain lateral movement. At the towers continuity of road surface above the rockers is provided by a joint of the “rolling leaf” type which works after the fashion of a roll-top desk. At the Barton Tower the joint can cope with a movement of 2.8 m, partly due to temperature but mainly due to longitudinal movement of the cables under uneven traffic loading. At the anchorages road

continuity is provided by rubber joints.

Main towers and deck

The main towers of the Humber Bridge are of reinforced concrete, a complete break from tradition at that time. Previously, all the major suspension bridges (spans over 700 m) had been built with steel towers. The towers, however, are essentially compression members and concrete is an inherently good material in compression. The towers are slightly tapered and hollow and one leg in each tower contains a service lift for maintenance purposes.

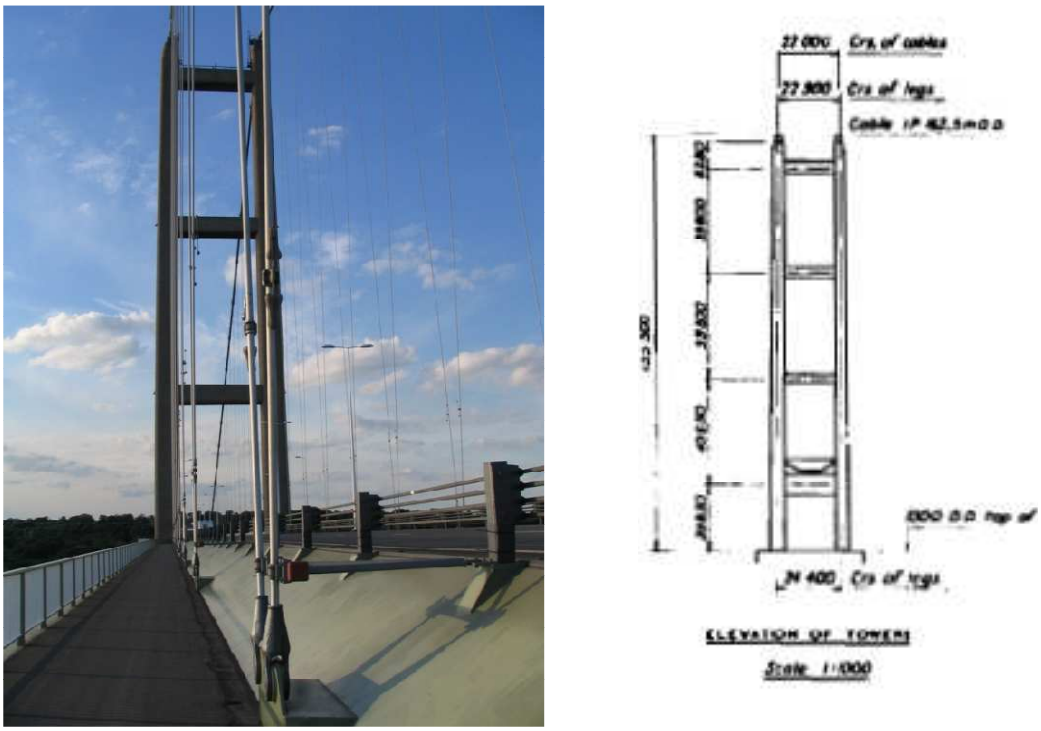

Figure 5.2.2 The main tower of the bridge

The concrete is heavily reinforced. At the Forth Bridge the steel towers oscillated in the wind when free standing (i.e. before the cables and deck were in position) and on subsequent bridges with steel towers measures were taken to prevent this. At Humber, although provision was made to damp down any oscillation, no such movement was experienced. Prior to erection of the cables, the tops of the towers

had to be pulled backwards by some 900 mm to ensure that they would be vertical when the deck structure was in place.

The stiffening girder at Humber is a streamlined hollow box. The upper flange of which is covered with mastic asphalt and provides the roadway surface. This shape is preferred because it greatly reduces the wind forces on the structure, at the same time enabling the required strength and stability to be achieved with less steel than with a truss girder. The box section also bestows a number of other advantages. The smaller weight of the deck (0.032 m) reduces the forces in (and therefore the size of) the cables and, consequently, the size of the anchorages. The towers benefit in a twofold manner, since both the dead load and the wind load from the suspended structure are reduced.

Figure 5.2.3 View of the inside of the deck.

Figure 5.2.4 The box-girder shape of the deck of Humber Bridge

The box section is shallower than the corresponding truss which improves the appearance of the structure. It is also vastly easier to paint the large flat surfaces of the boxes than the many components of a truss, with its large number of joints to clean and protect. In other words the box dramatically reduces points where corrosion is likely to start.

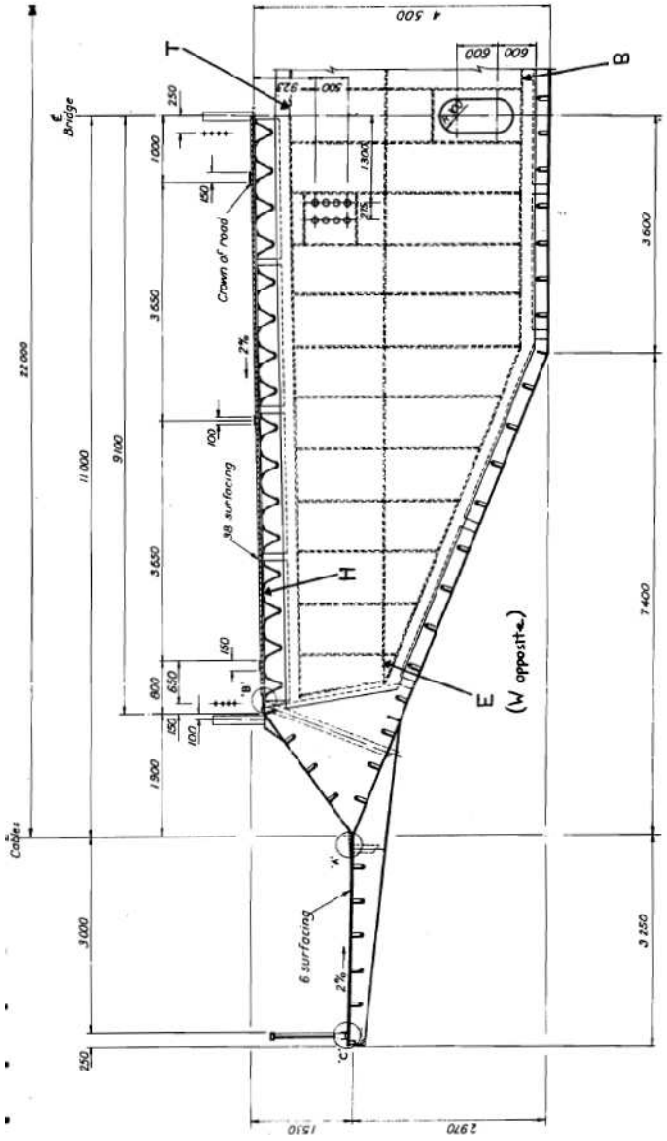

Figure 5.2.5 Typical section of the box-girder

On Humber, as at Severn and Bosporus, any incipient oscillation of the deck due to aerodynamics excitation is further checked by the 'triangulated' suspension system. Although the inclined hangers or suspenders apply some constraint on longitudinal movement of the deck, the resulting strain energy generated in each suspender by any movement is dissipated by the hysteresis characteristics of the spirally wound wire ropes to dampen out oscillation.

Foundations and anchorages

The design and construction of the foundations of the Humber Towers and of the

anchorages were dictated by the geology of the site which differs greatly between the north and south side of the estuary. On the north side a deep bed of chalk comes to the surface and resolving foundation problems there was relatively straightforward. On the south side, however, the chalk has been eroded by glacial action; leaving a 30 m deep bed of boulder clay, gravel saturated alluvium overlying a thick bed of over-consolidated Kimmeridge clay. The foundations for both the tower and anchorage had to be taken down into the clay but laboratory tests had shown that the clay, when in contact with water, turned into a slurry, It was therefore necessary to design and construct the foundations so that the clay was exposed for only a short period, with only relatively small areas excavated at anyone time.

For the foundation of the south tower the contractor first built an artificial sand island inside a steel cofferdam: severe scouring of the river bed followed and 12000 t of chalk had to be dumped in the river to provide protection. Two circular concrete caissons, each 24 m in diameter, were sunk through the sand island and into the river bed by excavating the ground below them, but the rate of sinking was much slower than expected. Further delay was experienced when the west caisson struck a pocket of underground water and the resulting inflow of water flushed away the lubricating skin of Bentonite on the outside of the caissons, greatly increasing the friction and thus the load required to sink them. Attempts to restore the Bentonite were unsuccessful and 3000 t of temporary steel ingots -'kentledge'- and 4000 t of permanent concrete had to be added to each caisson before they could be sunk sufficiently (8 m) into the Kimmeridge clay. The bottom of the caissons were 'plugged' with a concrete slab and the tops capped and bridged to form the concrete pier that provides the base for the tower.

Figure 5.2.6 Barton anchorage nearing completion.

The south anchorage consists of a large concrete structure. 20 m high, 65 m long and 36 m wide, built above a massive cellular box founded in the Kimmeridge clay 35 m below ground level. The box was built within a framework of diaphragm walls that divided the site into five longitudinal strips. These strips were excavated no more than two at a time, thereby limiting the extent of open excavation, the walls being supported by permanent concrete struts between them. The bottom of each trench was sealed with a concrete slab and the cellular box structure built within the protection of the diaphragm walls and back-filled with sand and water to restore ground loading. Because of the massive size of the anchorage structure itself, concrete had to be placed at rates up to 1000 m ' per day. To reduce the heat of hydration and lessen the risk of cracking, up to 60% of the Portland cement was replaced by blast furnace slag. The anchorage, including

the substructure, has a total mass approaching 300000t and to maintain a uniform pressure on the clay and prevent any tilting of the anchorage as the pull on the cables increased, parts of the upper block of the anchorage, including the architectural facings and the deck, were built step-by-step as the erection of the bridge proceeded.

The stiffening girder, or deck, at Humber is built of welded stiffened steel plate panels that were fabricated off site. The panels were then assembled and welded in a disused railway yard about a mile from the bridge into 124 boxes, generally 18.1 m long, that formed a section of the deck 22 m wide and 4.5 m deep, with 3 m wide panels cantilevering from each side to carry the walkways. So that the boxes would closely fit together ready for welding when erected into the bridge, they were assembled in threes using a completed box from the preceding batch of three as a template for the next two and so on. For erection into the structure the boxes (each weighing about 140 t) were taken up river by pontoon and lifted into place by travelling gantries running on the main cables.

The first boxes were erected adjacent to the two anchorages and at the middle of the main span. Erection then continued on four fronts, working towards the towers. Initially the concentration of load at the centre of the main span caused the boxes to adopt a sagging profile that was self-correcting as erection progressed. When the boxes were correctly aligned, they were spliced together by welding. The deck was then given a mastic asphalt wearing surface.

A large number of calculations were required to analyse loads, deflections and stresses at the different stages of erection of the bridge, when components would be lacking the support that would be forthcoming when the structure was complete. These calculations were primarily concerned with the suspended structure. For example, the most severe conditions on the tower due to wind loading occurs when all the deck is suspended from the cables but not yet connected at its ends to the towers.

Prevention of corrosion is essential for all large steel structures in exposed sites. Following established practice for bridgework and prior to assembly of the boxes, each panel was blast cleaned and given a preliminary protective coat of primer followed by three coats of epoxy-ester paint. After erection all external surfaces of the steel were given two further coats of chlorinated rubber paint. Similarly the main cables, each of which are made up of 14948 parallel wires of drawn steel 5 mm in diameter and heavily galvanised, have to be fully protected against corrosion. The wires were laid into place by 'aerial spinning', involving assembly of the cables four wires at a time. The cables were then compacted by a travelling ring of jacks and the cable bands, to which the suspenders are attached, put into place. With the deck in position the cables were almost fully loaded and compaction complete. The cables then received a thick coat of red lead paint and were bound with soft iron wire which formed a casing that was finally painted along with the rest of the exposed steel.

The following table summarizes the structural geometrical characteristics of the main elements that constitute the bridge.

Table 1 Humber Bridge: geometrical characteristics

Main span	1410 m
Hessle side span	280 m
Barton side span	530 m
Total length between anchorages	2220 m
Clearance over high water	30 m
Carriageways	Dual two-lane carriageways plus separate footpaths
Deck width excluding footpaths	22 m
Total deck width including footpaths	28.5 m
Depth of deck	4.5 m
Tower height above piers	155.5 m
Main cables	Two cables, each of 14,948 wires of 5mm diameter and 1540MN/m^2 uts plus an extra 800 similar wires in each cable on the Hessle side.
Diameter of main cables	0.68 m
Total length of wire	71000 Km
Total cable pull of each anchorage	40000 tonnes
Load in each cable	19400 tonnes
Weight of steel in deck structure in main cables	16500 tonnes
Total weight of concrete	480000 tonnes
Mass of Hessle anchorage	300000 tonnes
Mass of Barton anchorage	190000 tonnes
Depth of foundations:	
Hessle anchorage	21 m
Barton anchorage	35 m
Hessle tower	8 m
Barton tower	36 m

5.3. Experimental survey on the Humber bridge

From the 14th to the 18th of July of 2008 an ambient vibration test was preformed on the Humber Bridge under the leadership of Prof. James Brownjohn from the University of Sheffield, with the collaboration of the Laboratory of Vibration and Structural Monitoring (ViBest - www.fe.up.pt/vibest) of the Faculty of Engineering of the University of Porto and the Profs. Ivan Au and Paul Lam from the City University of Hong Kong.

The team from the Faculty of Engineering of the University of Porto (FEUP) provided 6 of the 10 used recorders, contributed to the test planning, helped on the configuration and calibration of the measuring equipment and was deeply involved on the field test and on the in situ validation of the acquired database. The test was conducted using 10 triaxial Geosig seismographs, model GSR-24. During the test of the main span, two pairs of seismographs were permanently located at two reference sections (marked with the red circles in Figure 5.3.1), while the other 6 worked as moving sensors, three in each side of the bridge, covering the remaining measurement points in different test setups. Each measured section was instrumented at both side walk [Magalhães et al, 2008].

The side spans are not monolithically connected to the main span. Therefore, the existence of local modes is expected. As a consequence, for the setups that include sections of the side spans, additional reference sections were adopted, reducing the number of moving sensors from 6 to 4.

The choice of the reference points stems from inspection of the set of experimental and calculated mode shapes of the bridge presented in the report of the ambient vibration test performed in 1985 [Browjonh et al, 1986], trying to guarantee that the reference points are not close to nodal points of the majority of the most significant modes of vibration.

During the last day of tests, measurements were performed also at several points

of the towers. However, the analysis of the tower modal ordinates is reserved to the data analysis with more powerful methods that will certainly allow to obtain 3D representations of the global mode shapes.

The measurements were performed using a sampling frequency of 100Hz and for each layout of the sensors, 4 time segments of 895 seconds were recorded, which correspond to a total acquisition time of almost one hour.

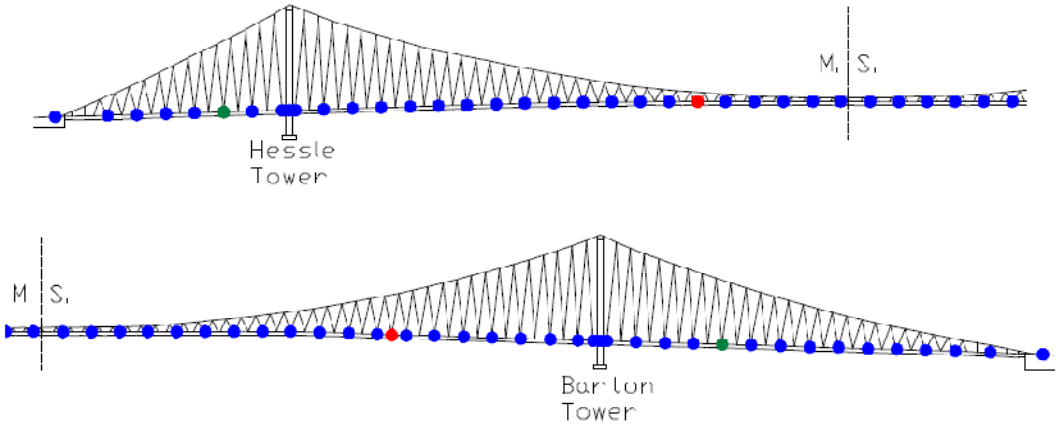

Figure 5.3.2 sensors location during the ambient test

The modal parameters of the bridge were computed by the University of Porto; in particular the signal was preprocessed and an application of the classical Peak-Picking method, identifies more than 30 natural frequencies in the frequency range 0-1 Hz. The estimates of the corresponding modal shapes were obtained on the basis of the transfer functions relating the ambient response at each measurement point with the corresponding response at one of the reference points. All the modes shapes were estimated using each reference section and then the best estimate was chosen.

The experimental results, obtained by the team of ViBest, are used to improve the FEM model of the bridge, described in the following sections.

5.4. The FE model: the first example (1985)

The first finite element model of the Humber Bridge was realized in 1981, when the bridge was ended (in 1985), by Prof Brownjonh, of the University of Bristol. The model was defined in order to obtain modal parameters similar to that one defined by an ambient vibration test, carried out on the bridge when it was opened. The main objective of the test was to check the accuracy of the mathematical model developed for asynchronous excitation analyses. There are several features of the model which can be checked:

i) The mechanism of the main cables and hangers with particular regard to geometric stiffness properties.

ii) The connections between towers/anchorages and main/side spans.

iii) The simulation of the box-girder deck.

iv) The linear elastic behaviour of all elements.

This section sets out to examine all these features by comparing the measured modal frequencies and shapes with those predicted by the model.

The mathematical model is described fully in [Browjonh et al, 1986]. A brief description and sets of eigenmodes for two-dimensional vertical and horizontal plane representations and for a full three-dimensional version are given below.

Each hanger is represented by a single beam element, as are the sections of deck and main cable between hangers. The three-dimensional mesh is similar, but with the deck being represented by 4-noded thin plate/shell elements.

Comparison of mode shapes had been done for lateral and vertical modes using the two-dimensional representations, and for the torsional modes using the full three-dimensional representation. In the comparisons, sets of modes have been identified where direct correspondence between predicted and measured mode

shapes and frequencies is possible. Some measured modes and some predicted modes in the lateral plane do not bear comparison. Comparison of measured and predicted modes is not as straightforward as for vertical modes for a number of reasons. Firstly, some of the measured modes are ambiguous, consisting of two or three close modes with similar mode shapes. Secondly, some of the predicted modes indicate appreciable cable motion. No measurements were made of cable motion, and depending on the degree of excitation and damping of the cables, the deck motion accompanying these modes, if they occur, could be insignificant by comparison with deck-only modes or vice-versa. Thirdly, there is no well-defined sequence of symmetry or constantly increasing numbers of nodes and antinodes.

5.5. Actual FE model

Starting from the John Brownjonh's model defined in 1986, the goal of this chapter is an improving of the original model in order to obtain the natural frequencies, extracted through the ambient vibration test carried out on the Humber Bridge in 2008 by the University of Porto, previously described. The University of Porto works in collaboration with the University of Bristol to improve the Bridge model, realized in 1985. The Prof. Brownjonh made available the original 2d and 3d model, developed in eighteen. At the beginning the 2d Model, edited in Sap IV, was imported in Sap 2000. This model was very easy and all the characteristics used in its definition were very clear in the test file used in Sap IV. The imported model works well and the natural frequency are very near to that one of the original model. The same procedure was applied for the 3D model. Of course this one is more complicated and the test file, used in Sap IV it is sometimes difficult to understand, in particular in the definition of the shell, which models the bridge deck. In this case the imported model did not work, and very different frequencies were obtained, mainly for lateral modes. For this reason, we prefer to create the 3d model, directly in Sap2000, starting from the 2d model of Prof. Brownjonh. The first 3d model is very easy and it is

characterized by this kind of elements: frame for all the towers; shell for the deck and cable for all the cables present. The attach of the deck with the tower is modeled by 2 rigid link that permit only longitudinal movement and rotation around lateral and vertical axes. Another model was implemented, where the deck is model as a frame element and the cable are connected through horizontal rigid link. The first one works better and in the following figure its results are illustrated.

The modes predicted by the three-dimensional model can also be compared with the experimental modes, and some correspondence is found for the first three or four modes. The three-dimensional model has more degrees of freedom and should therefore be more flexible. Despite this the predicted frequencies are generally higher, and there is also a certain amount of coupling between main and side spans.

The results seem good, there are some differences with the high modes; for example the new model is not able to see some horizontal modes, obtained in the experimental evalutation, like the 16° mode. The model presents other modes where only the cables are involved, so the deck is almost fix and they cannot see with the experimental test (the sensors were putted only on the deck).

The figures below shows a graphical comparisons between the experimental mode shape, obtained by ViBest and reprented in blu and imported from [Magalhães et al, 2008]; the mode shape obtained by the first model, implemented by Prof. Brownjohn, represented in black and imported from [Browjonh et al, 1986]; the mode shape of the model implemented in Sap2000, represented in green. The respective frequency are also reported.

MODE1 HORIZONTAL

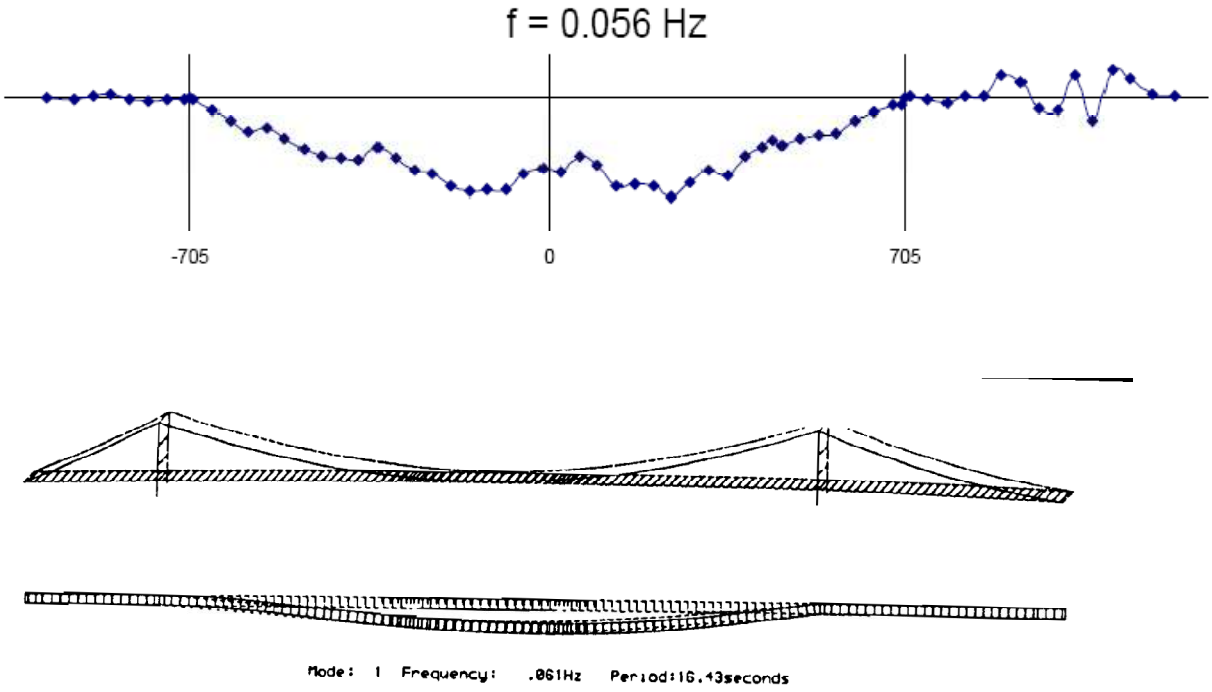

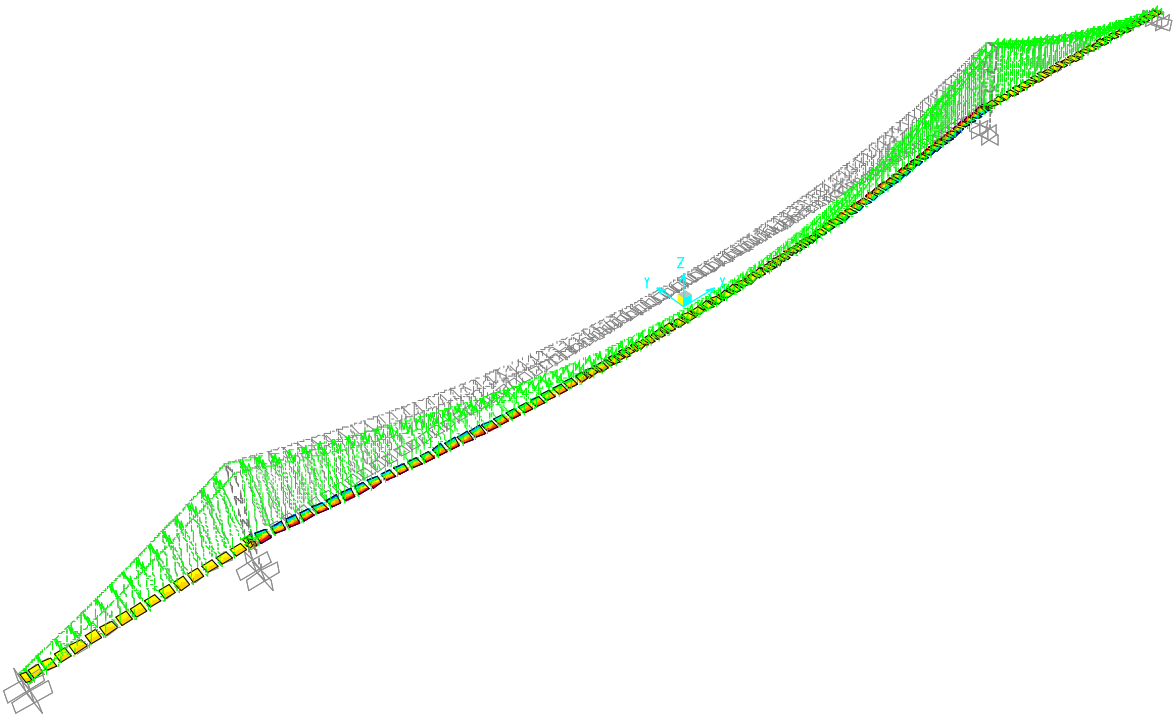

F= 0,06199 Hz

MODE2 VERTICAL

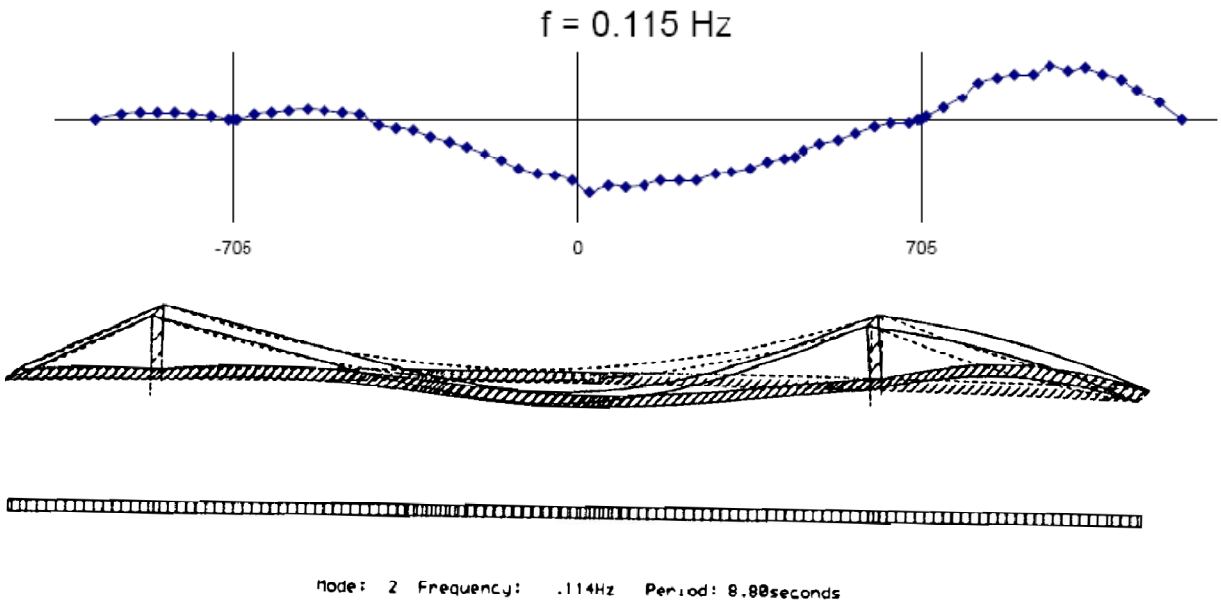

Mode: 2 Frequency: .114Hz Period: 8.88seconds

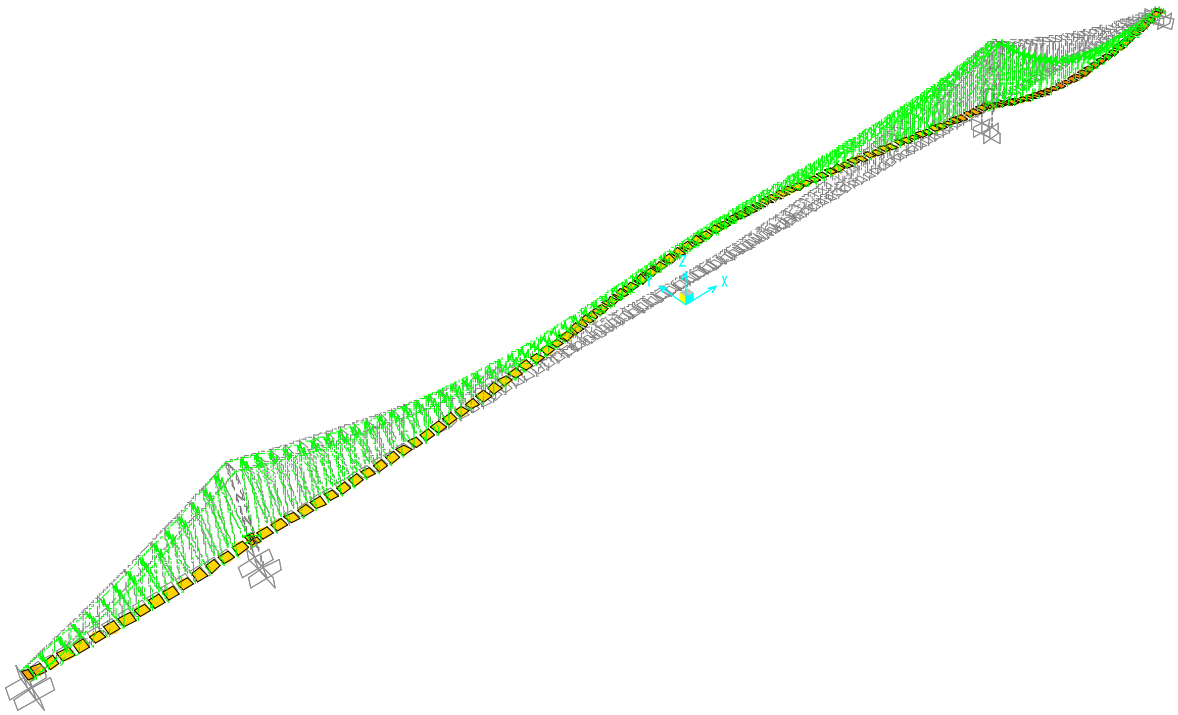

F= 0,11485 Hz

MODE3 HORIZONTAL

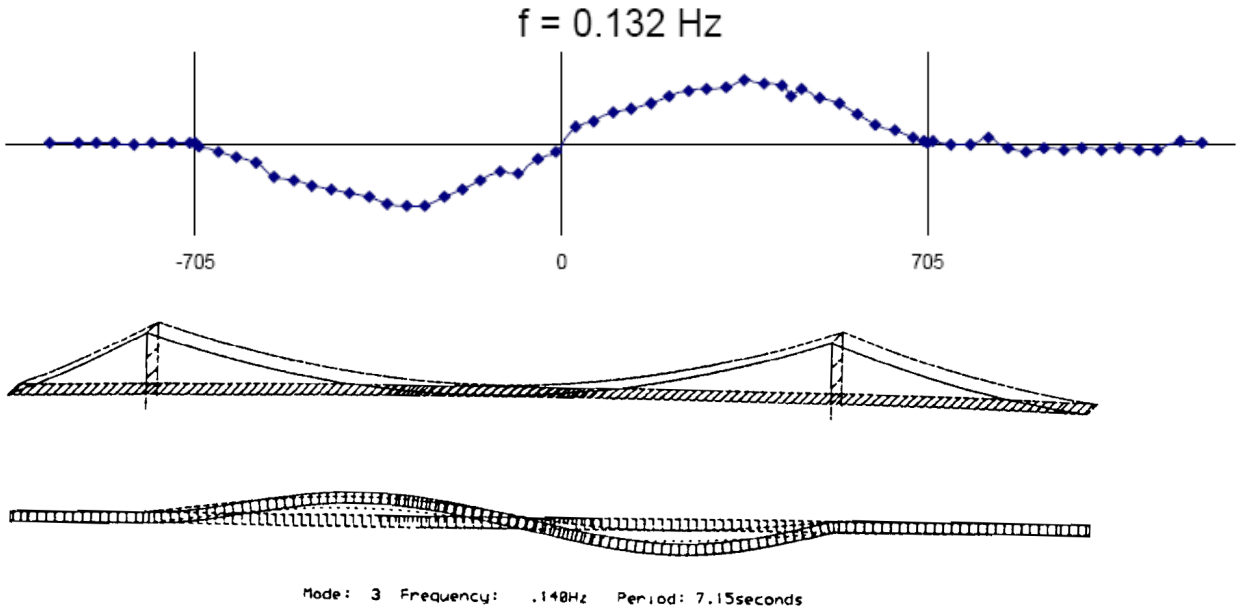

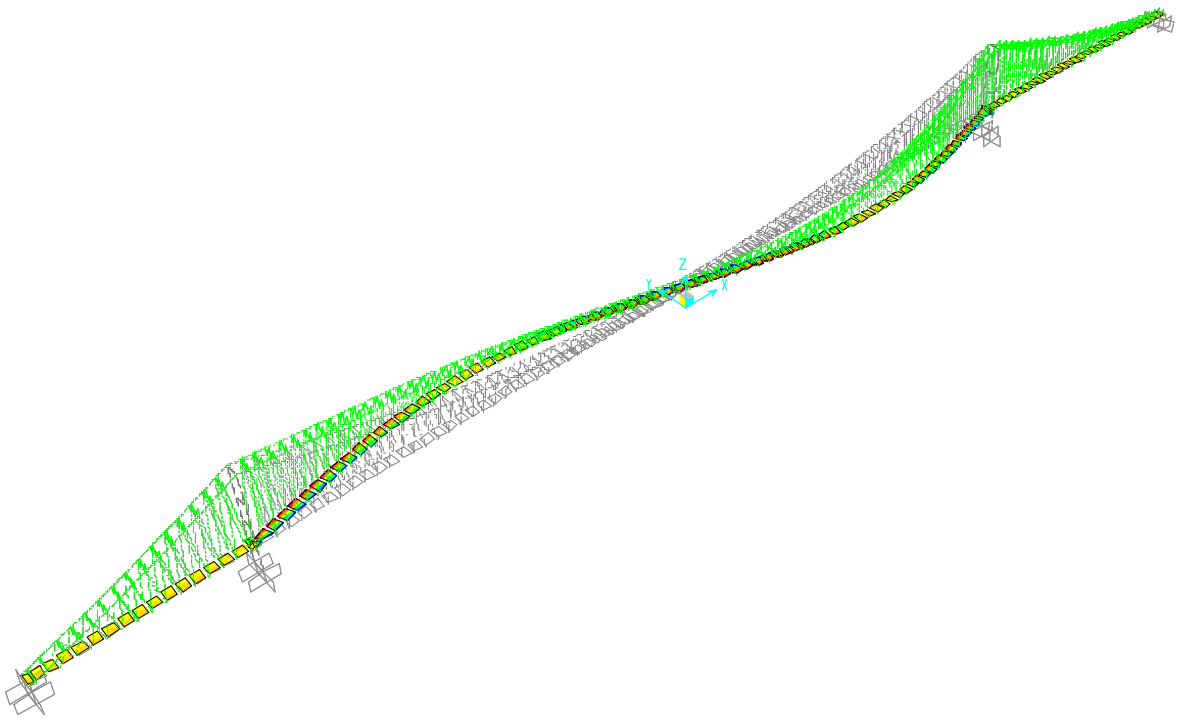

F = 0,14 Hz

MODE4 VERTICAL

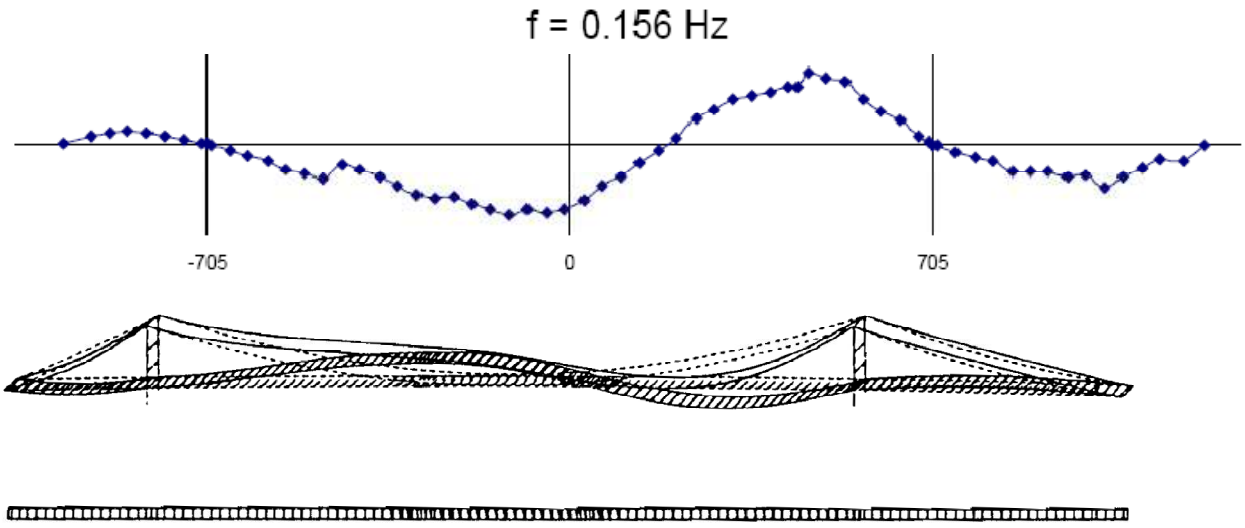

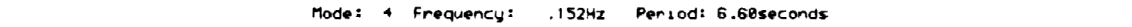

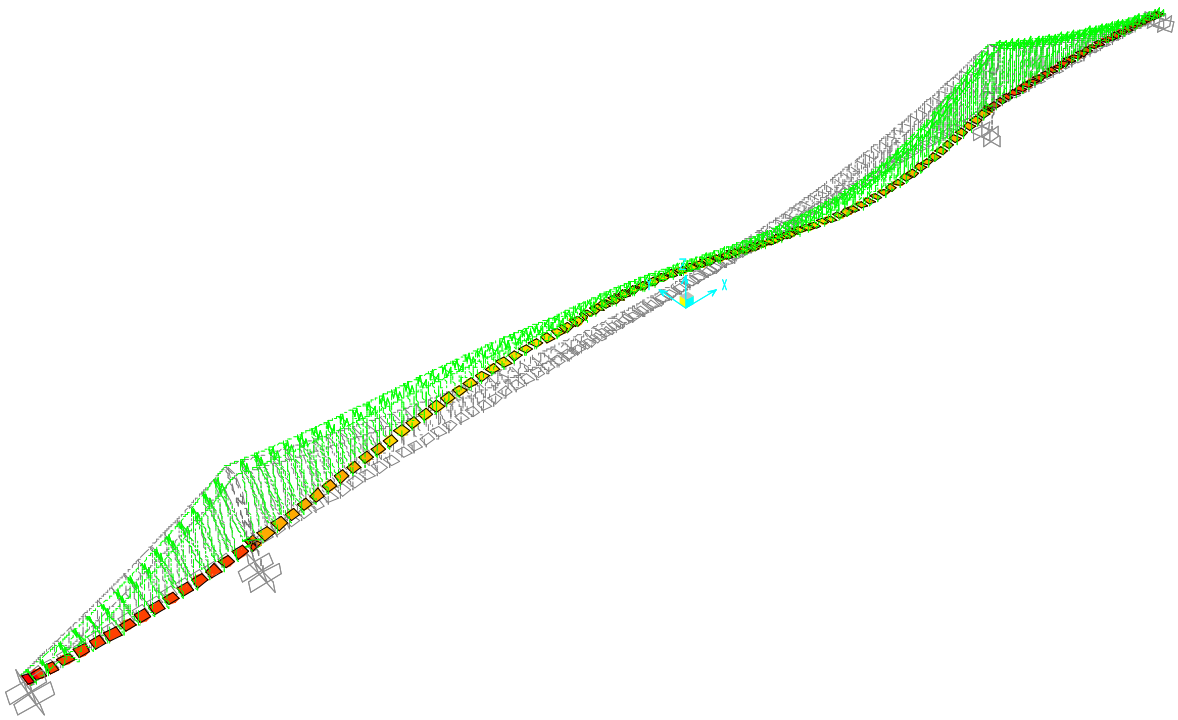

F= 0,15047 Hz

MODE5 VERTICAL

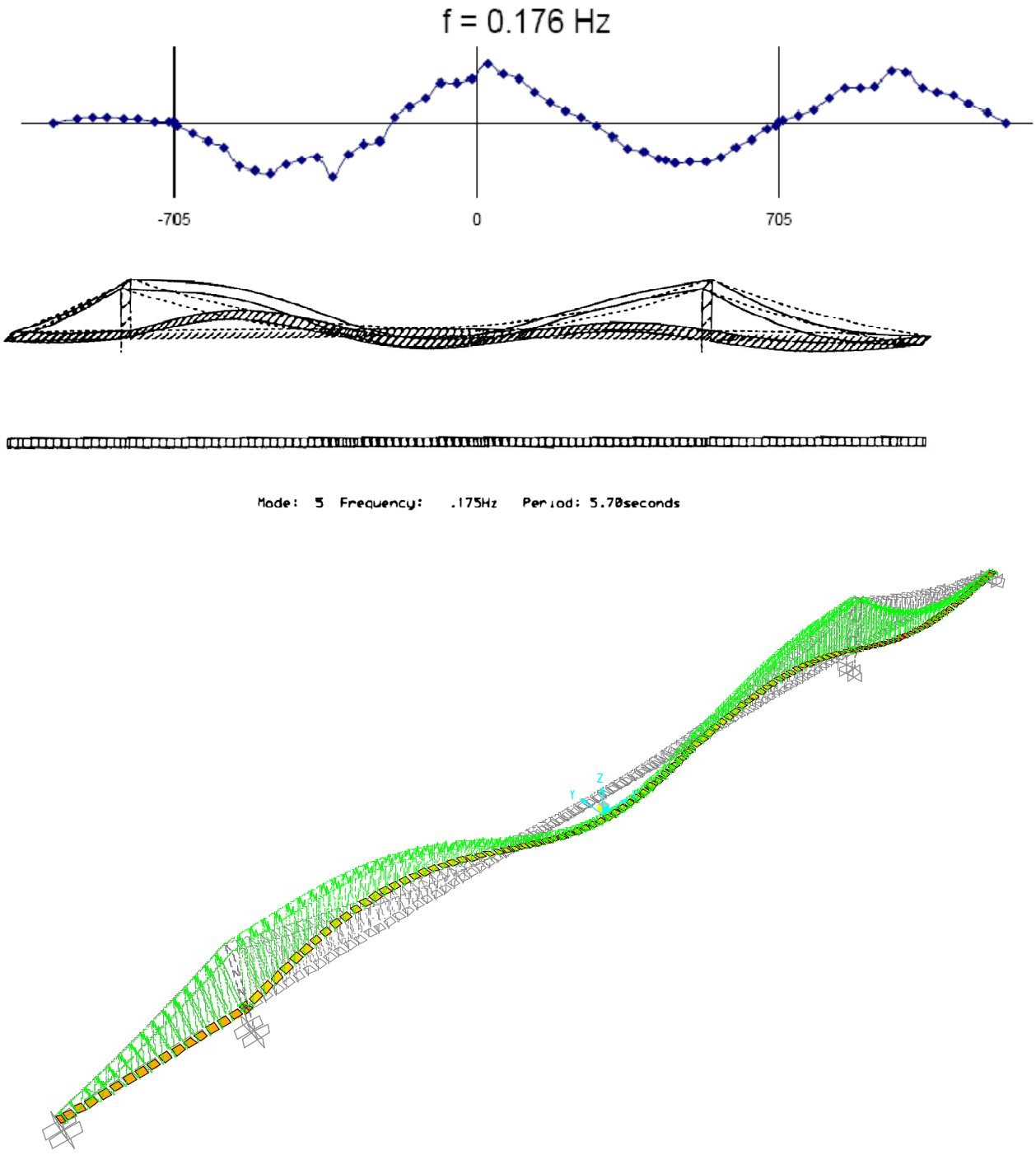

F = 0,17476 Hz

MODE6 VERTICAL

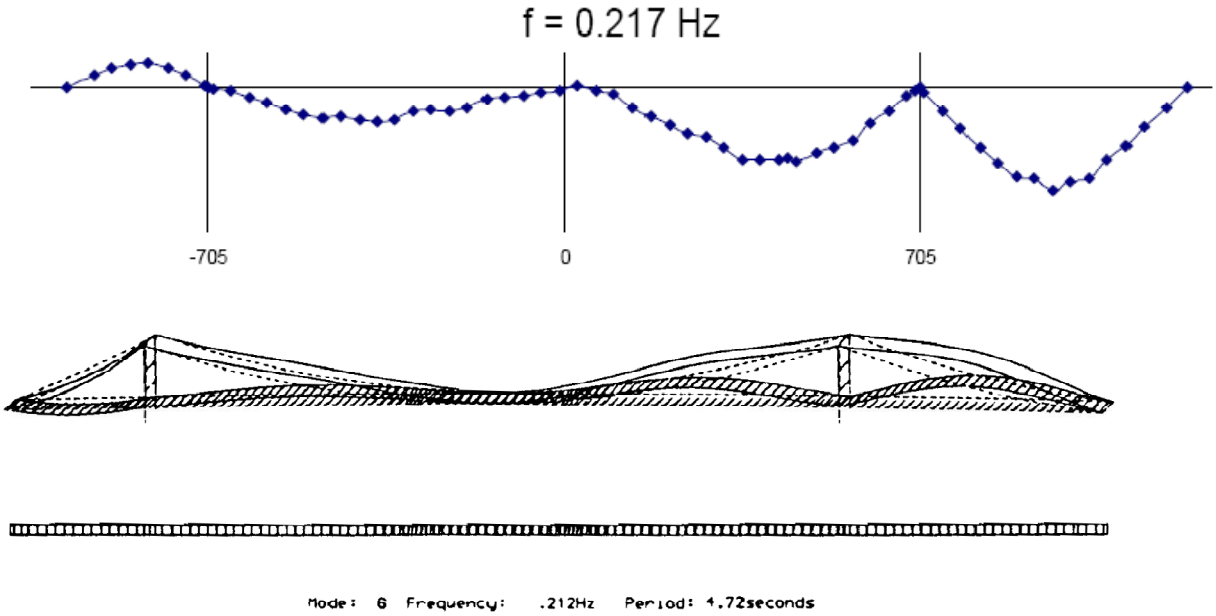

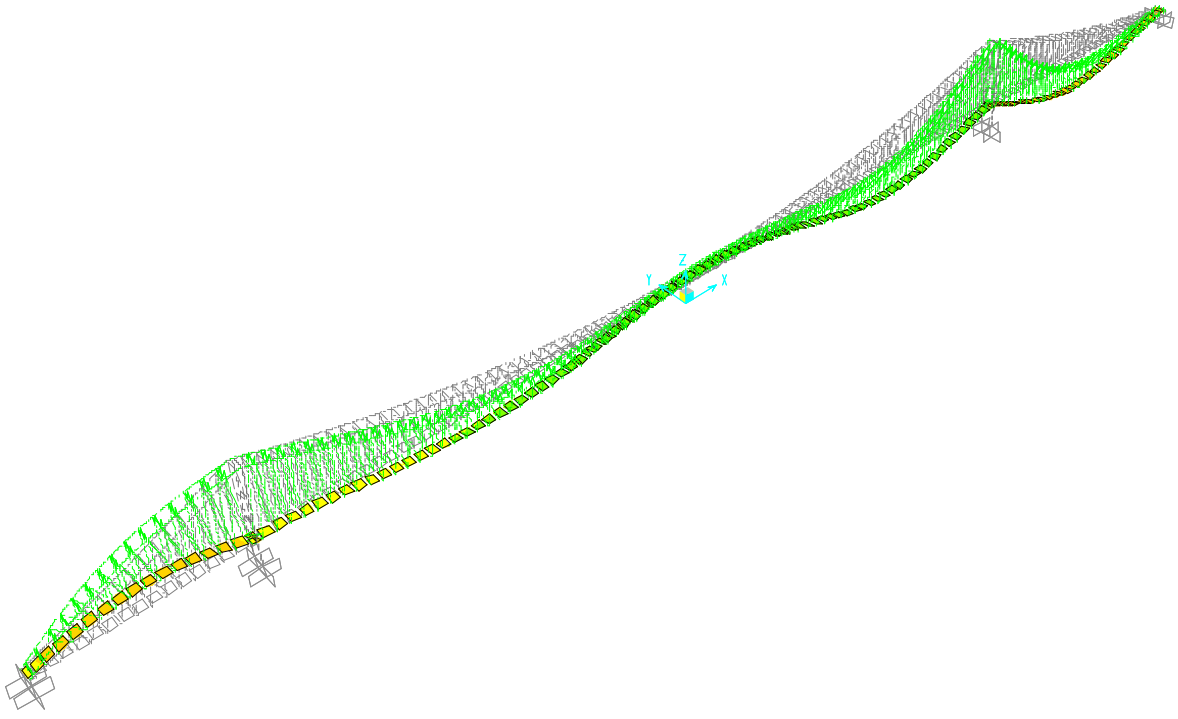

F = 0,21525 Hz

MODE7 VERTICAL

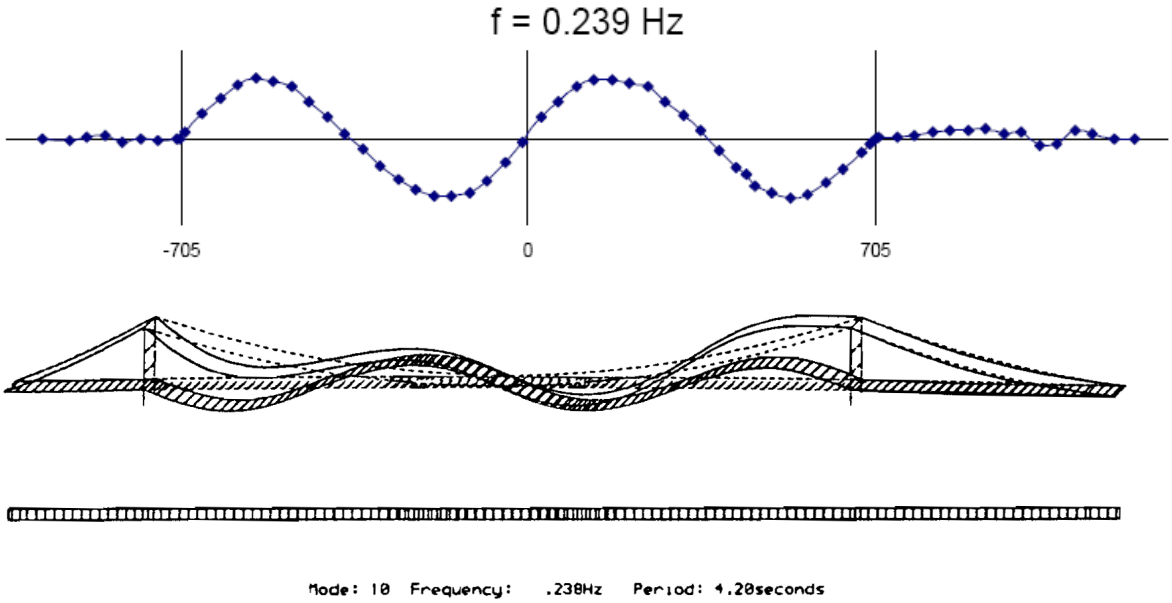

Mode: 10 Frequency: .238Hz Period: 4.20seconds

F = 0,23235 Hz

MODE 8 HORIZONTAL

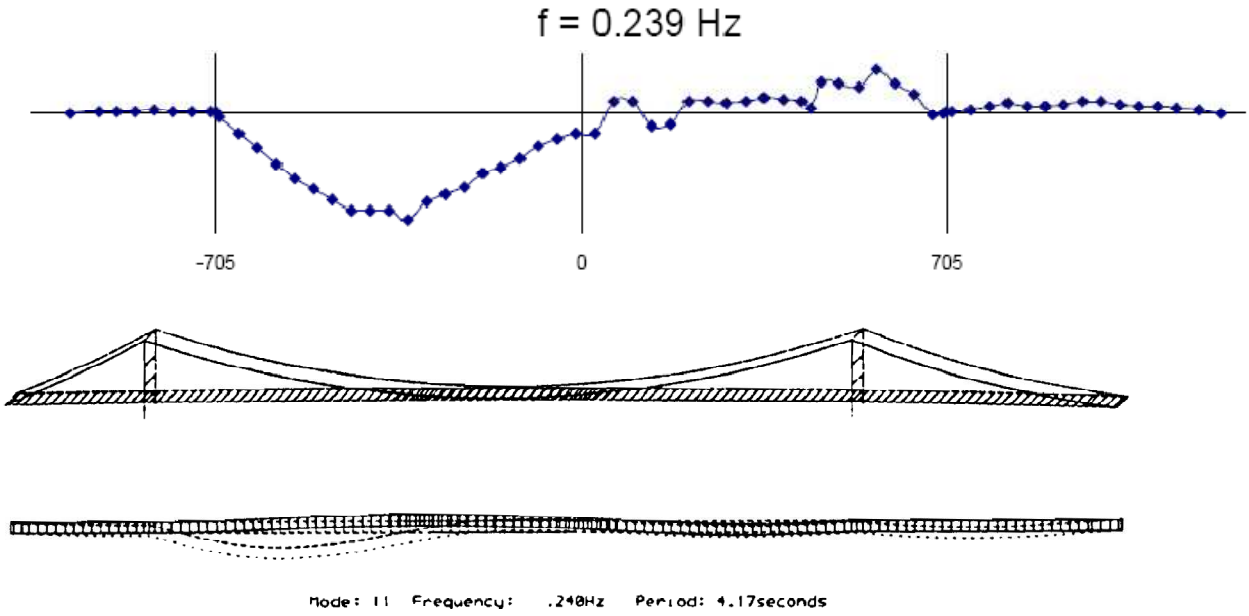

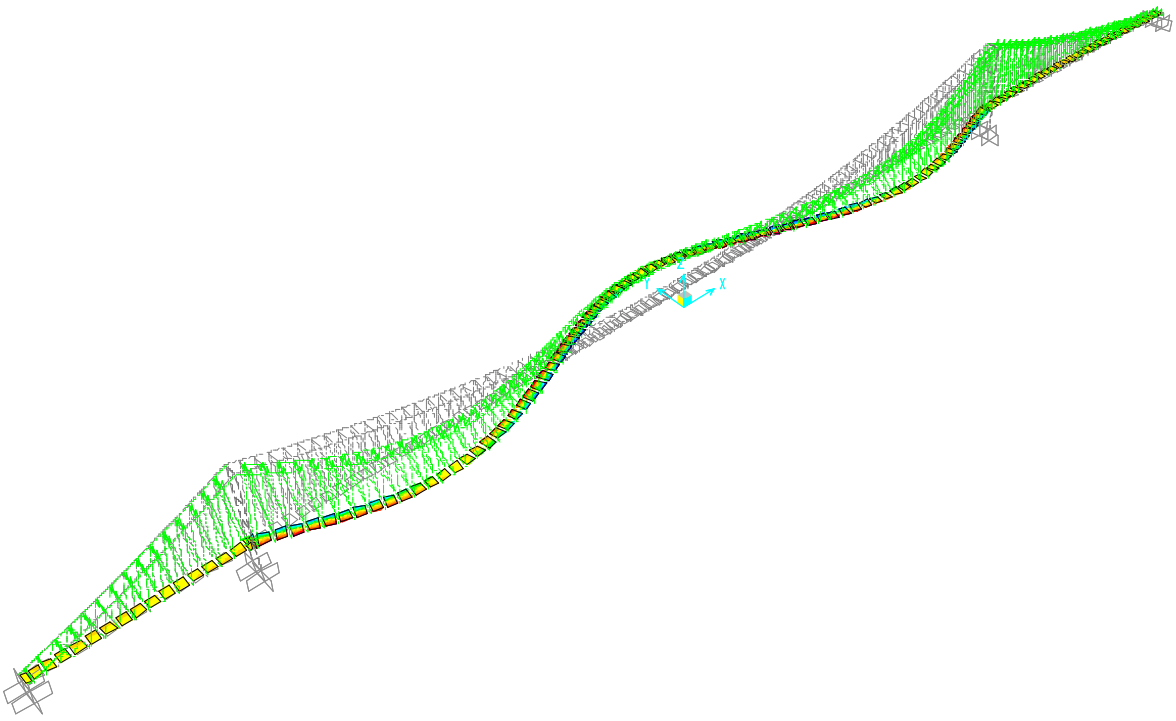

F = 0,23711 Hz

MODE9 HORIZONTAL

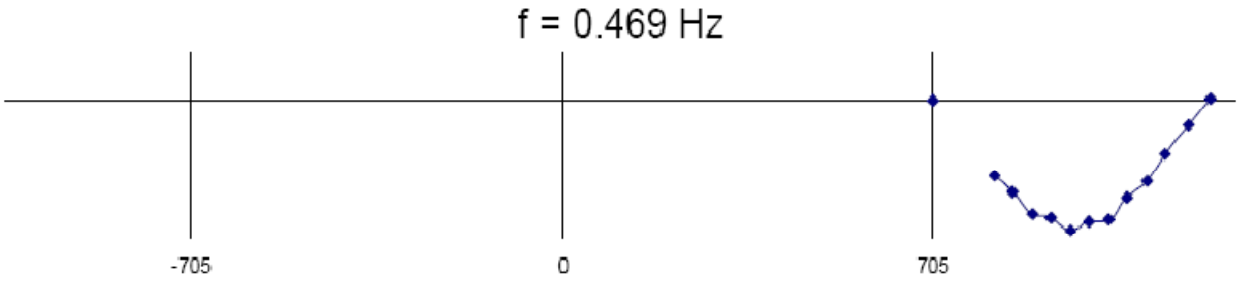

There is an error and the real frequency is 0,269 Hz.

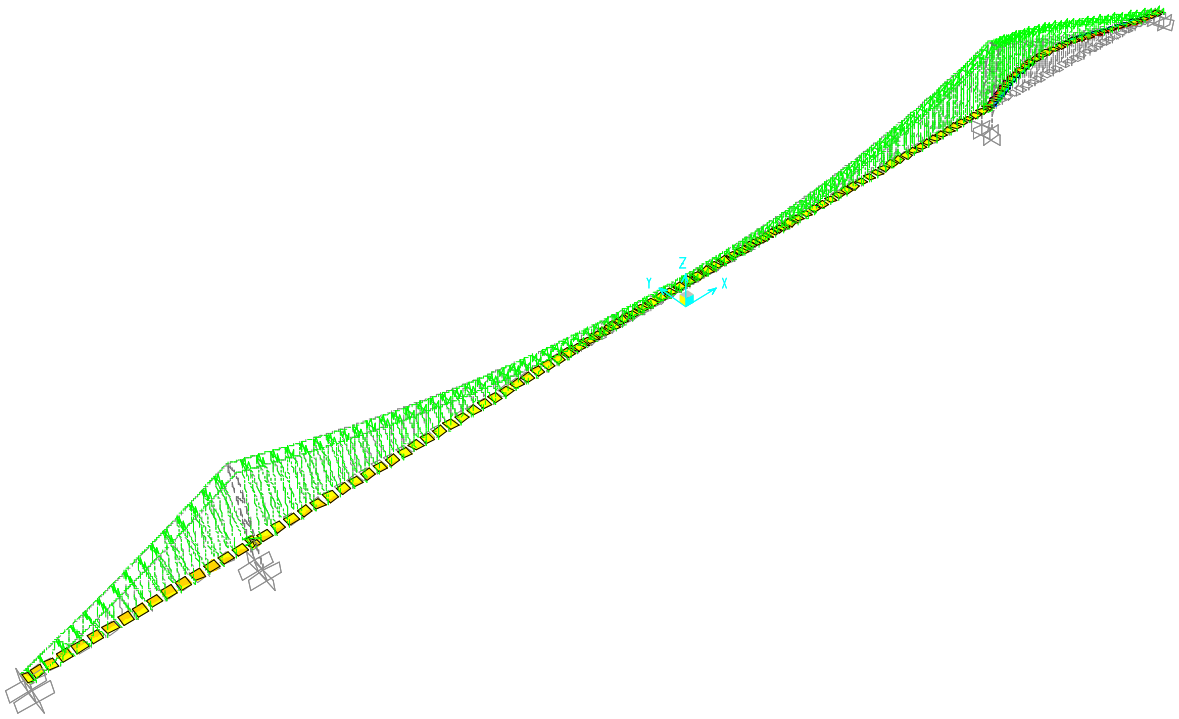

F = 0,25586 Hz (model not present)

MODE 10 VERTICAL

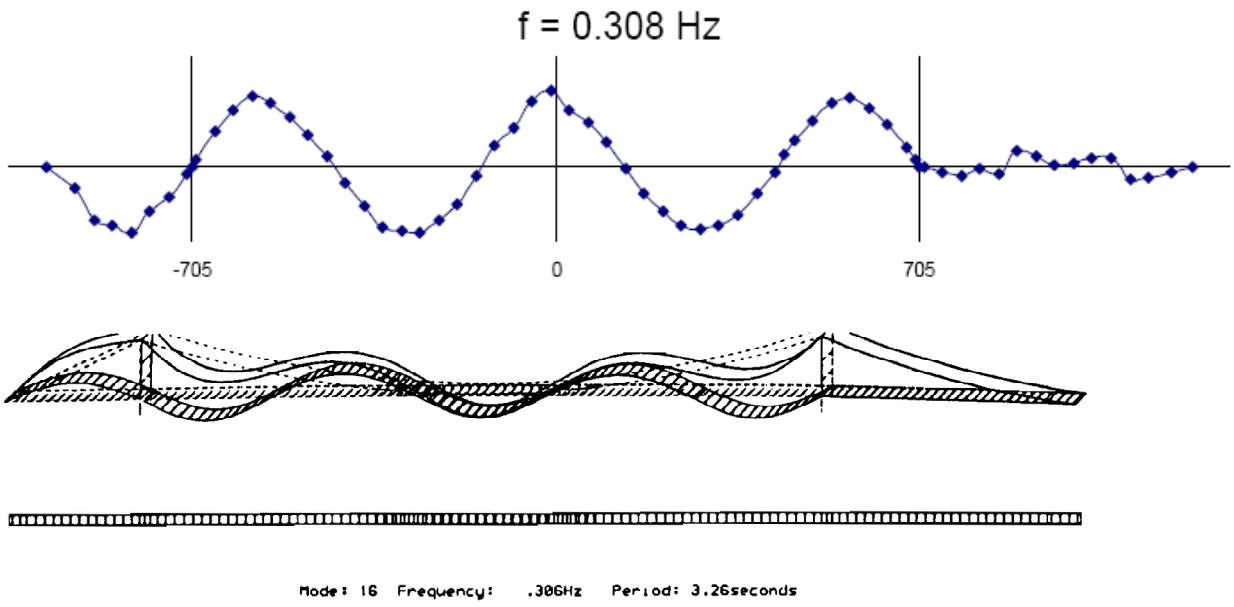

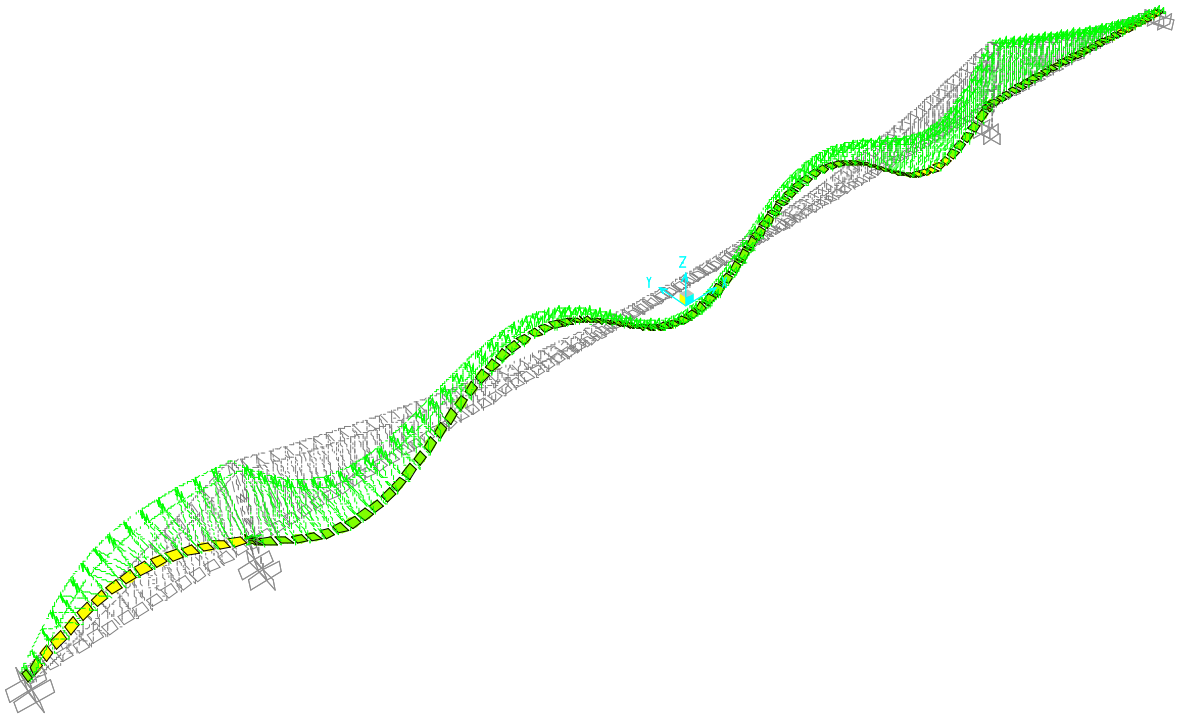

F = 0,29894 Hz

MODE 11 HORIZONTAL

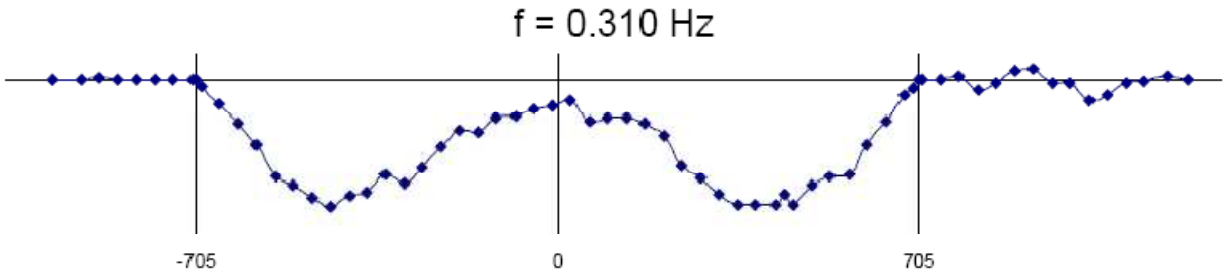

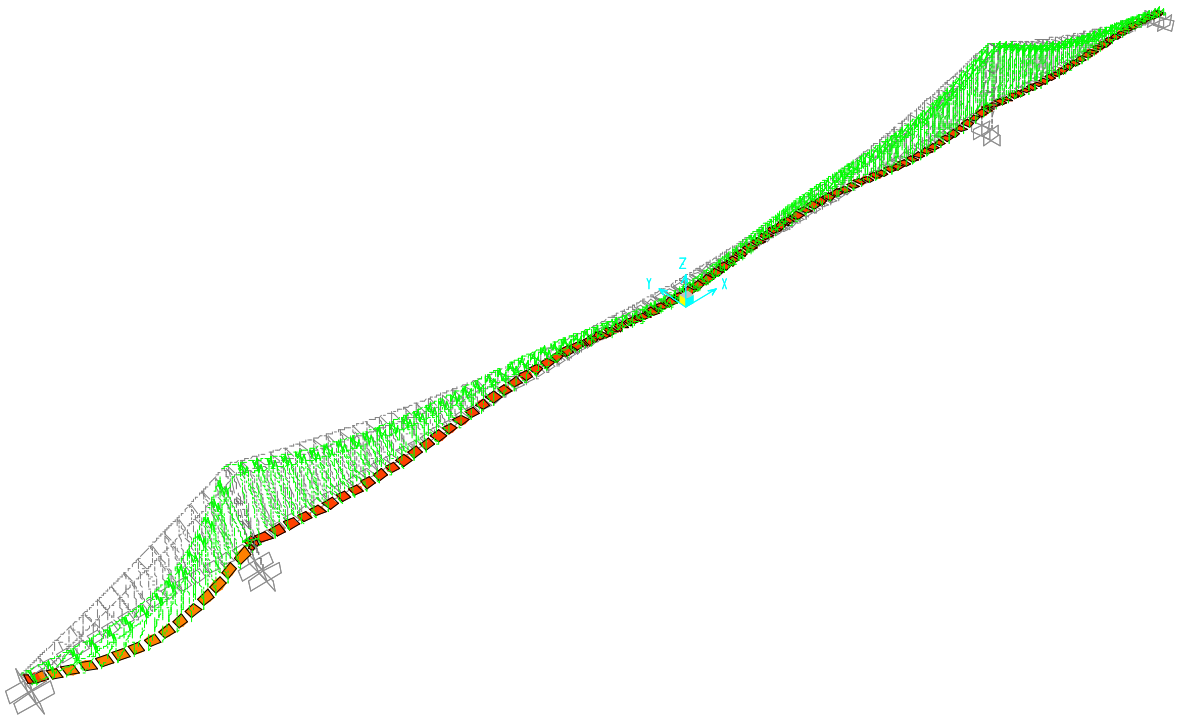

F = 0,30261 Hz (model 0,329 Hz)

MODE 12 VERTICAL

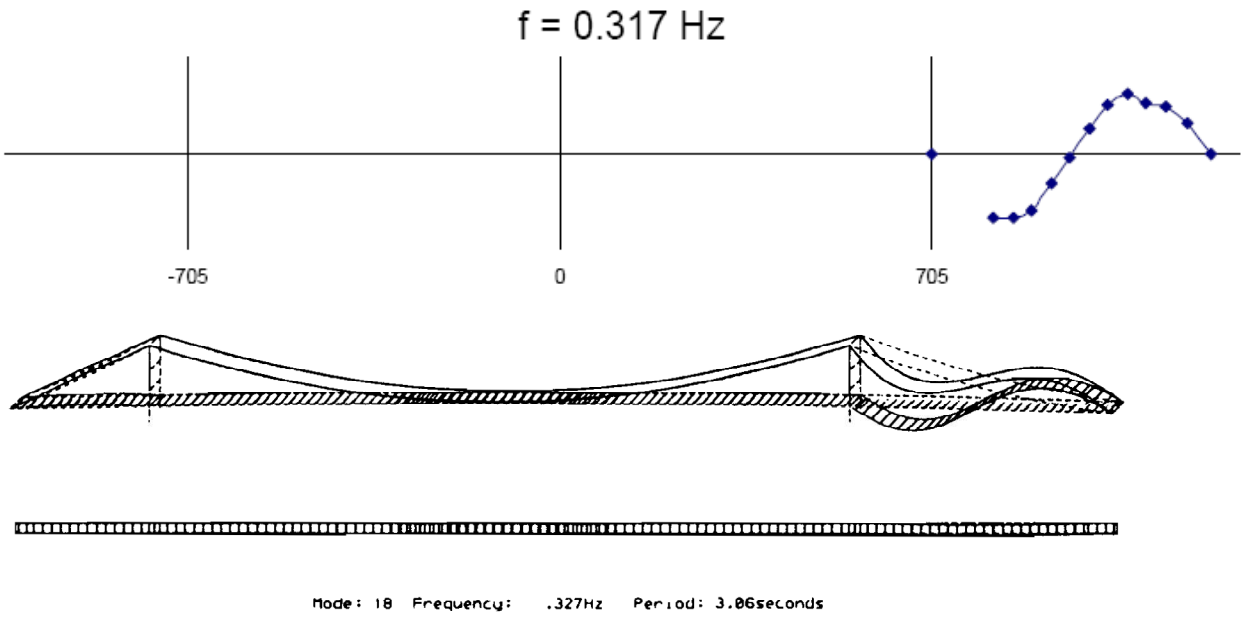

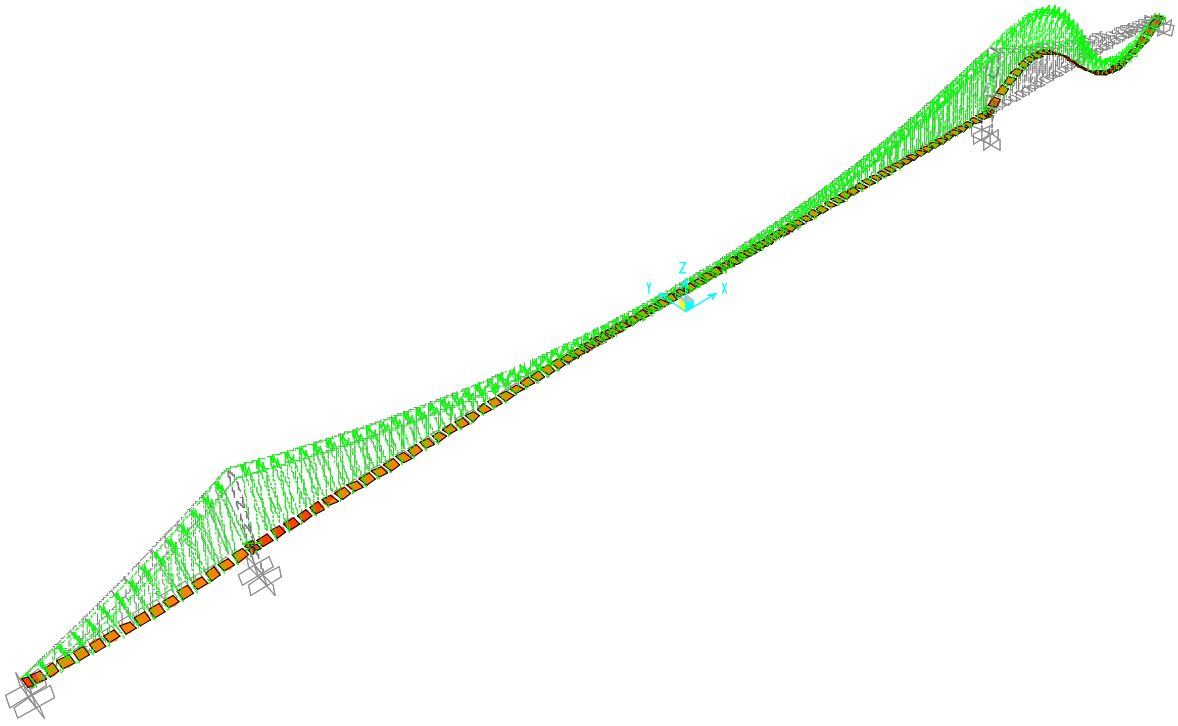

F = 0,3428 Hz

MODE 13 VERTICAL

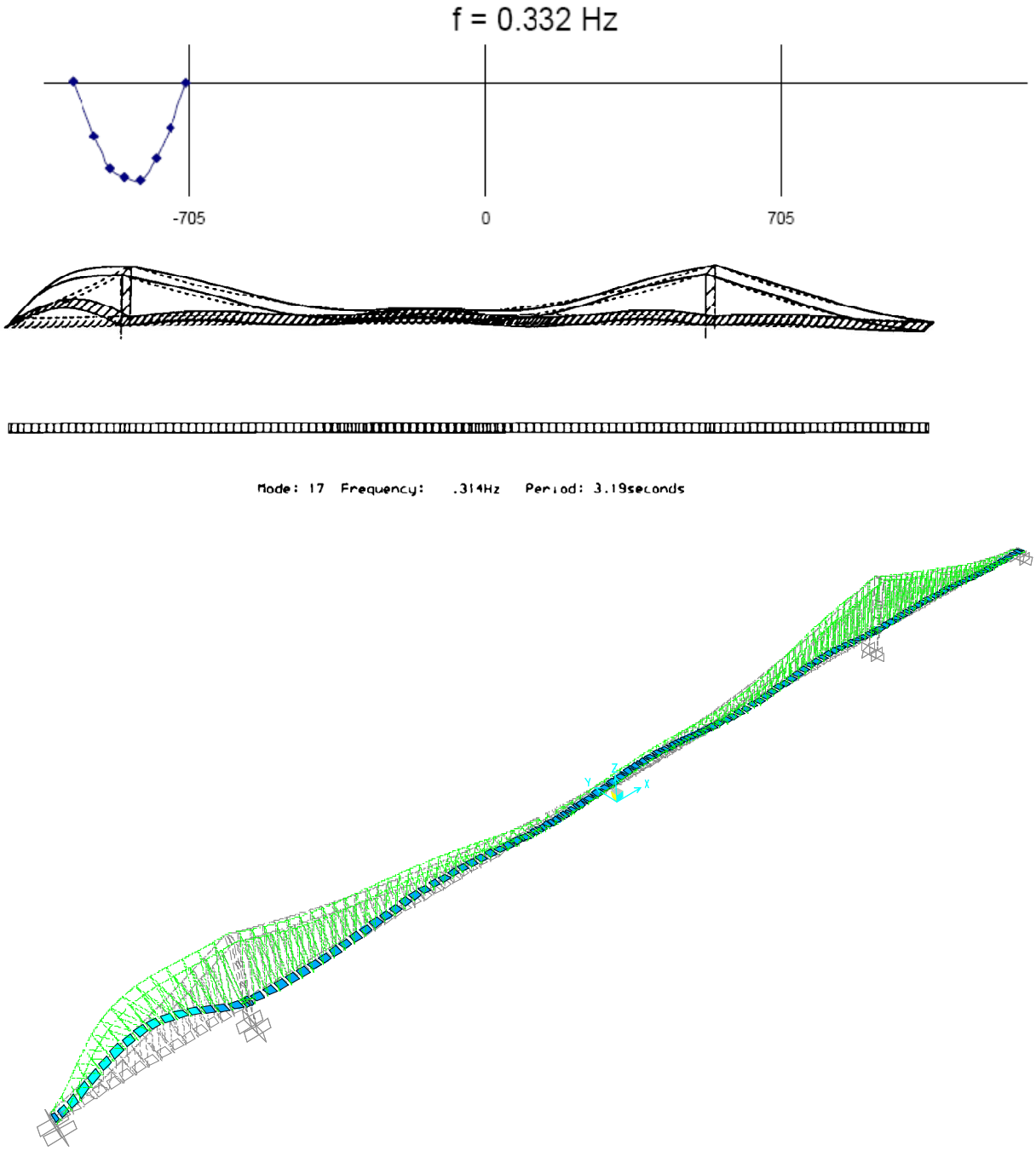

F = 0,34924 Hz

MODE 14 HORIZONTAL

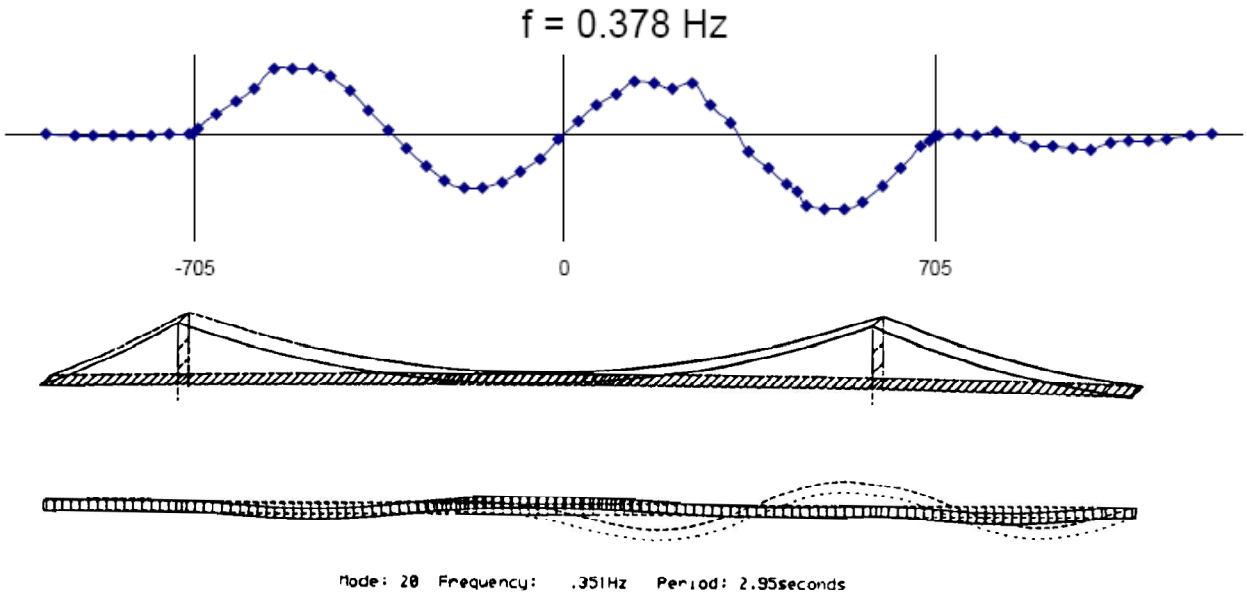

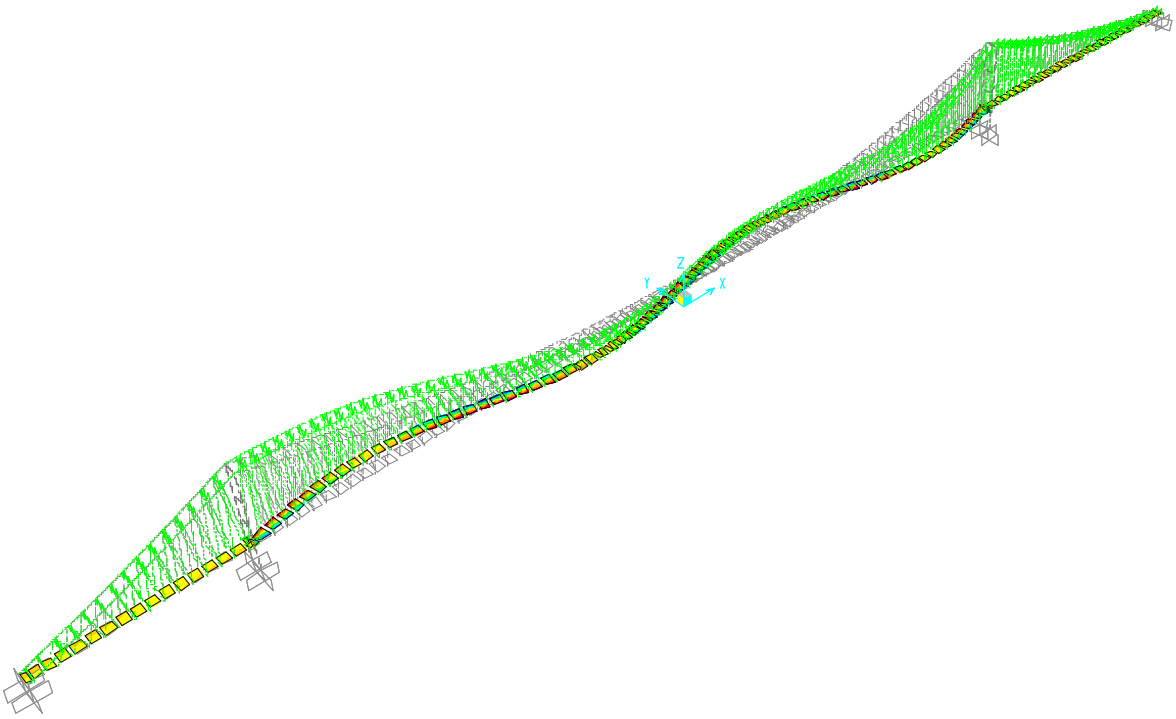

F = 0,36746 Hz

MODE 15 VERTICAL

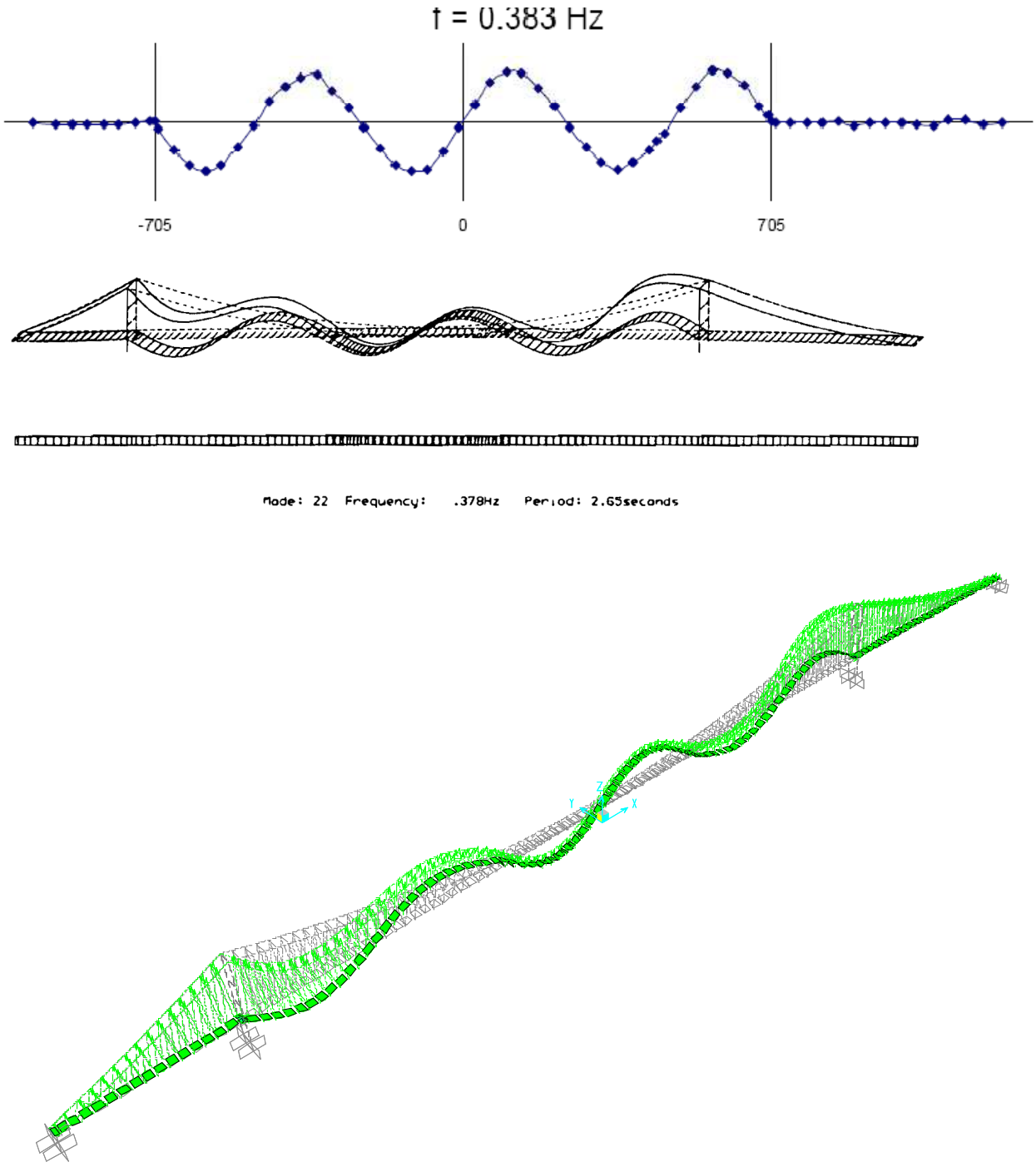

F = 0,37064 Hz

MODE 16 HORIZONTAL

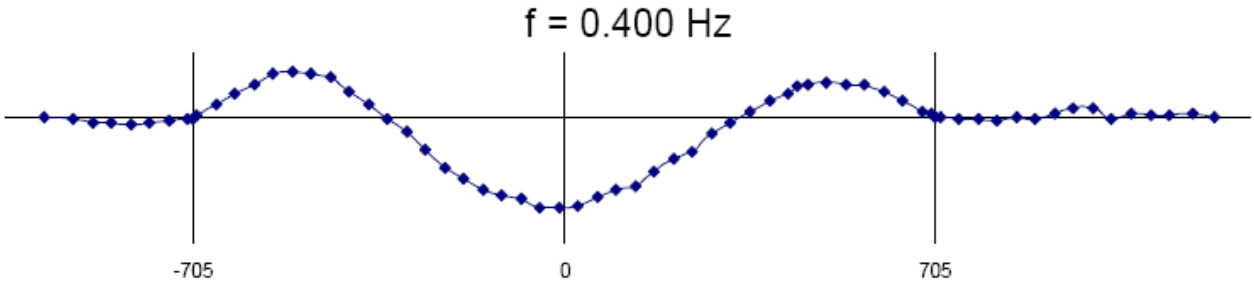

MODE 17 HORIZONTAL

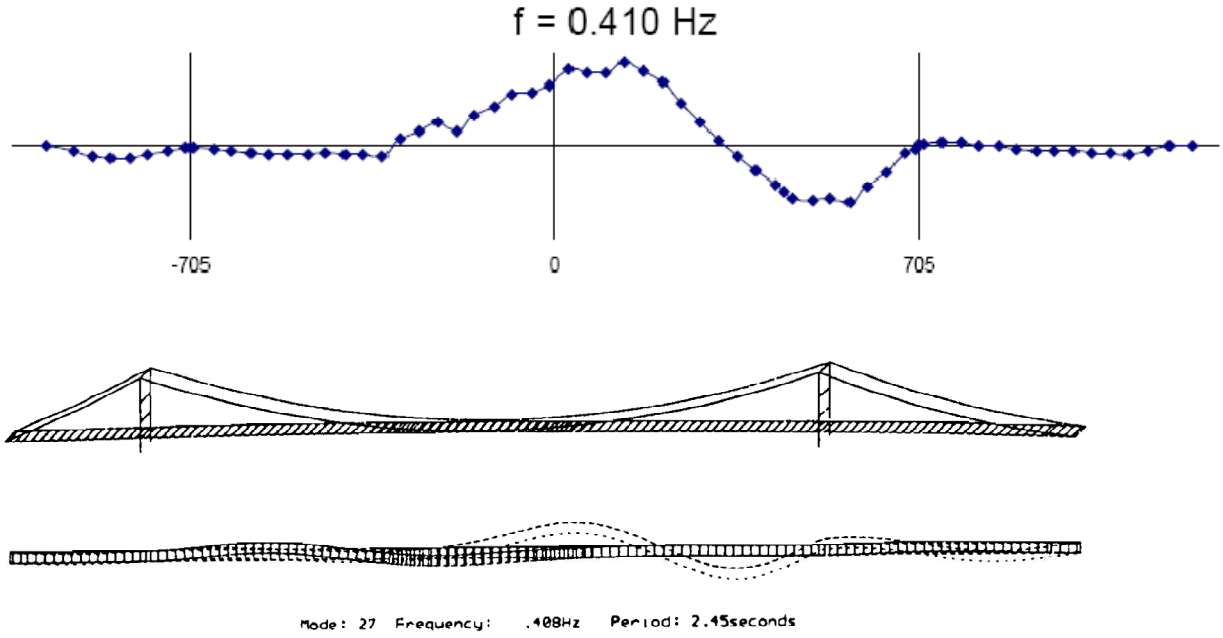

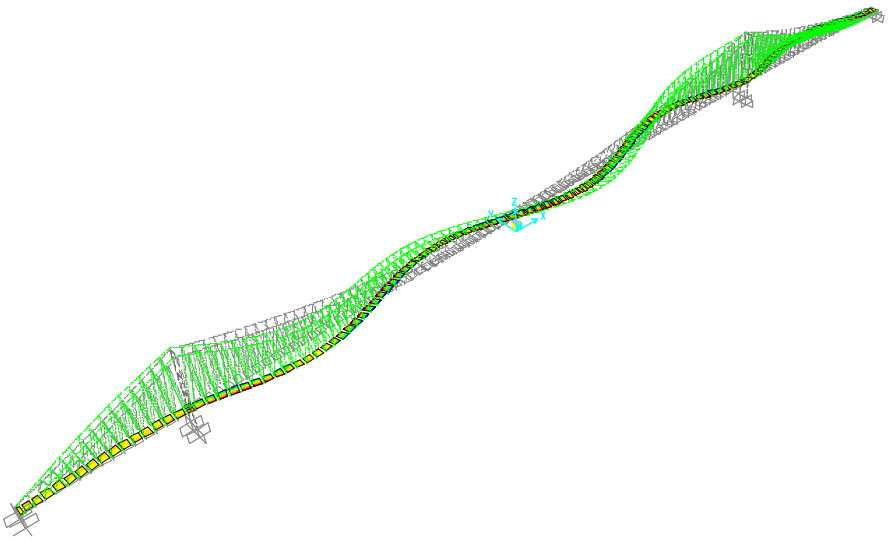

F = 0,38796 Hz

MODE 18 VERTICAL

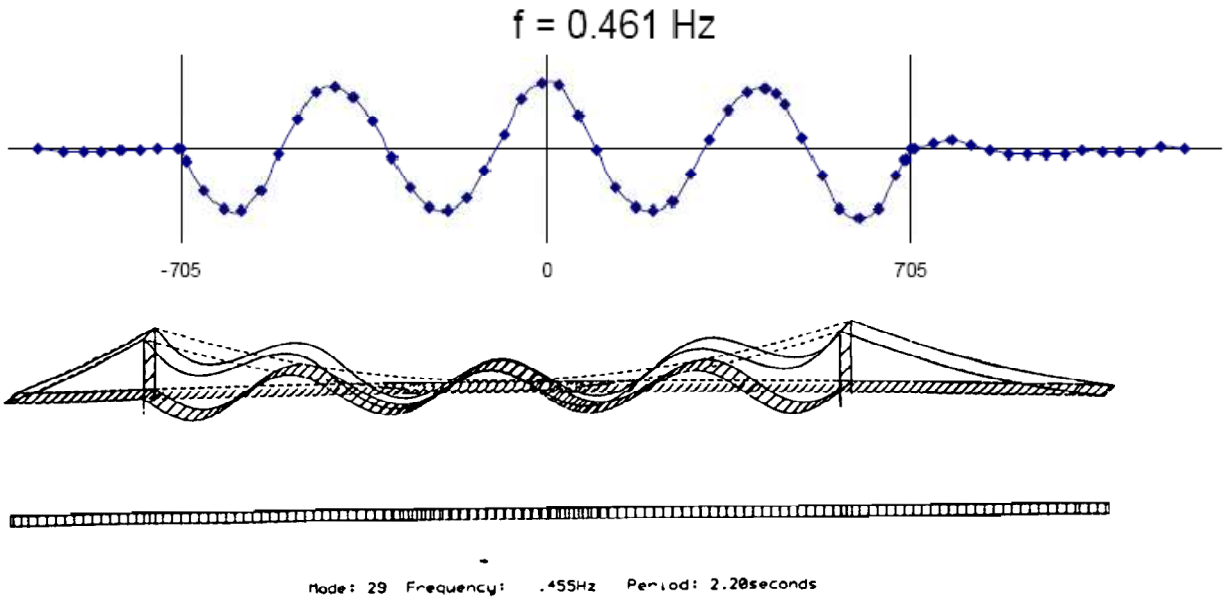

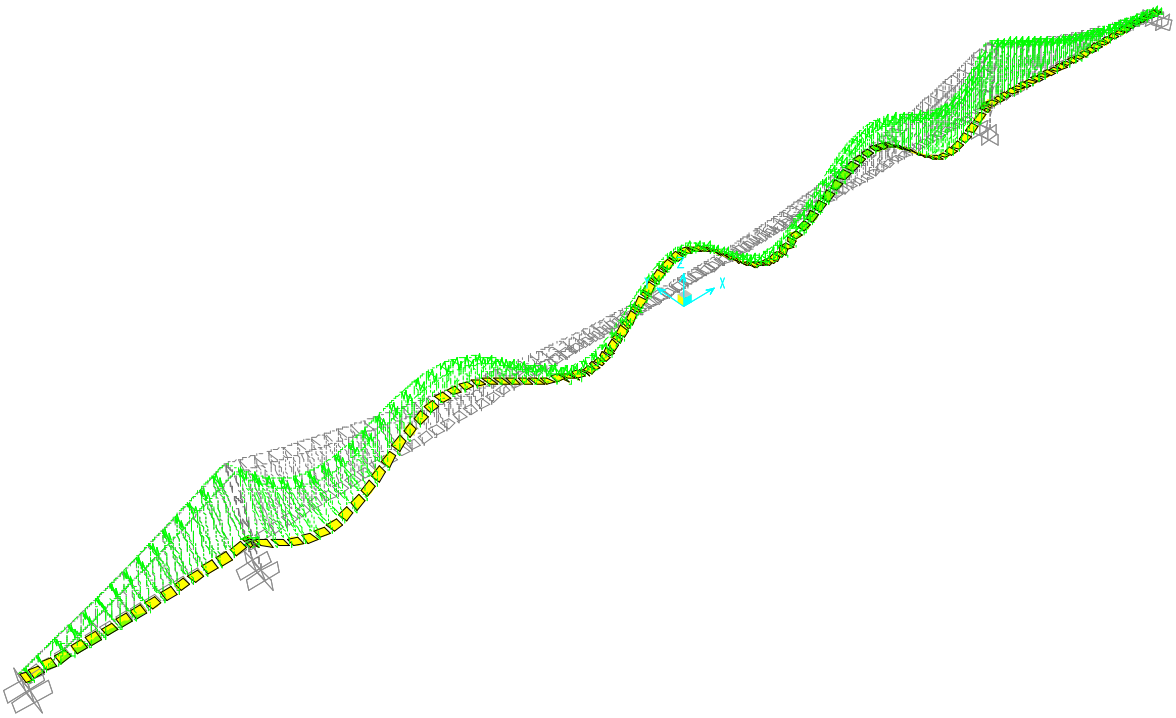

F= 0,44191 Hz

MODE 19 HORIZONTAL

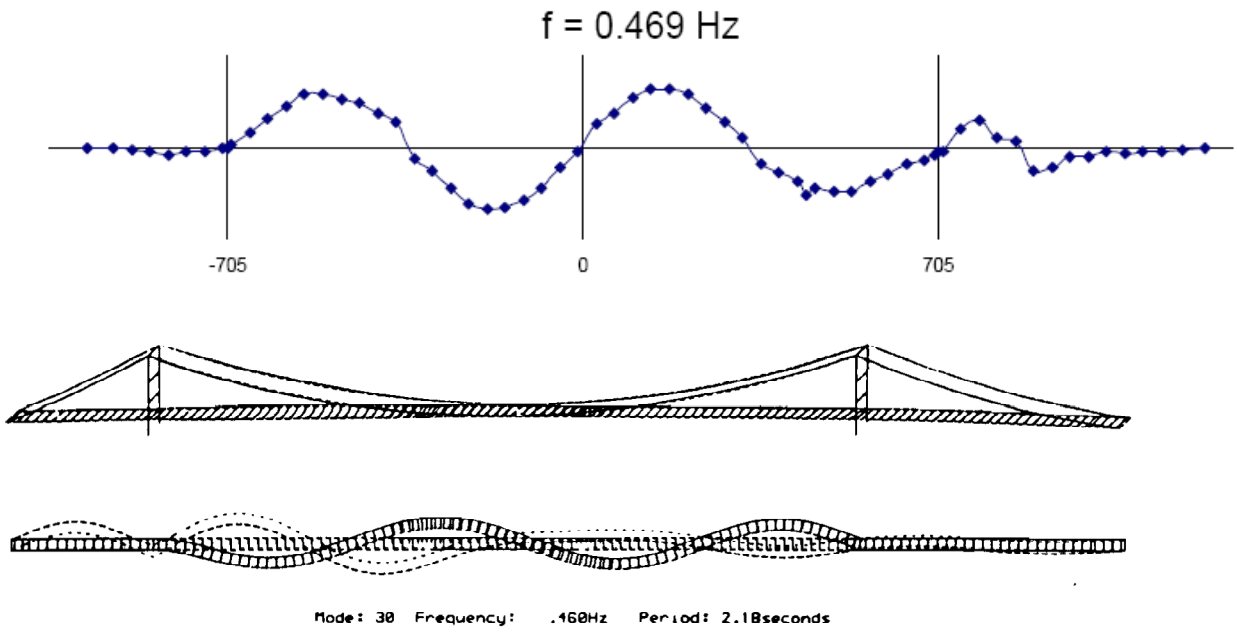

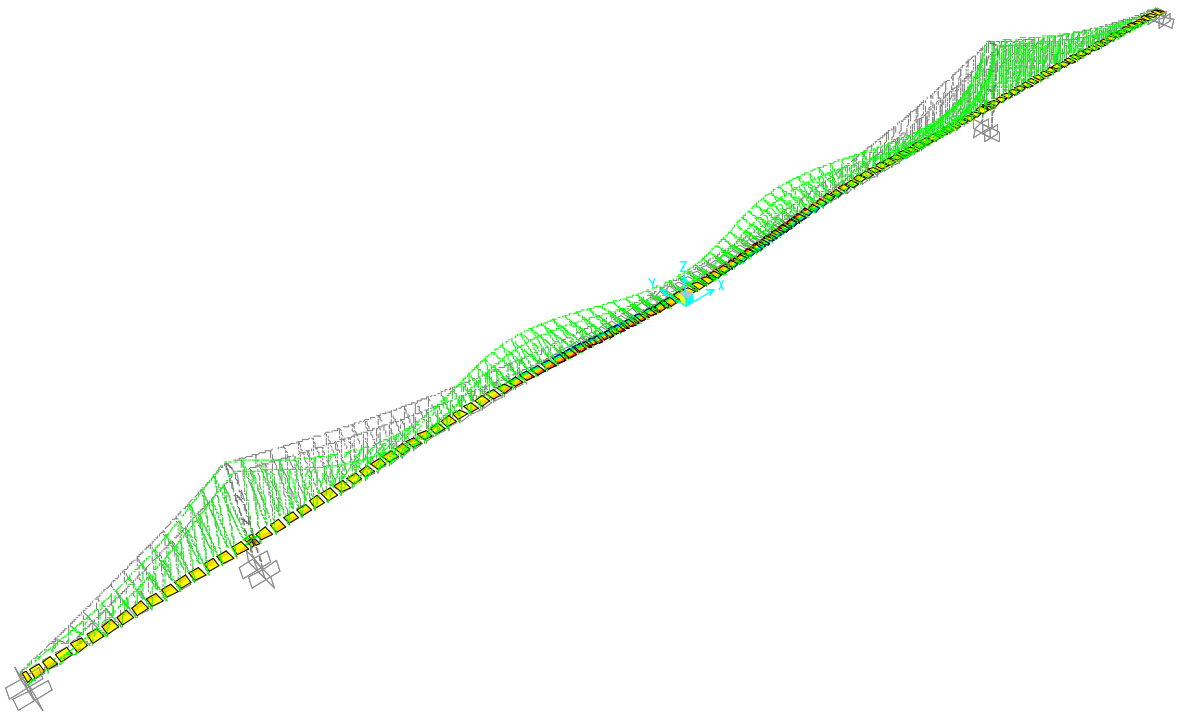

F = 0,45821 Hz

MODE 20 HORIZONTAL

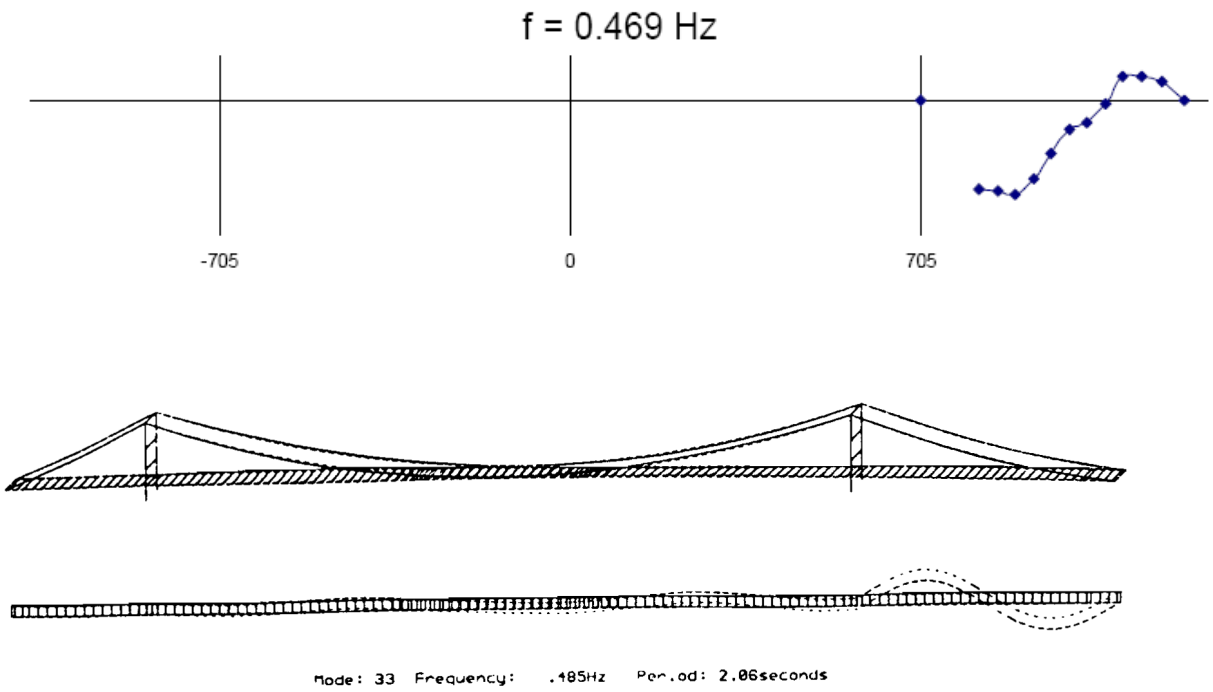

MODE 21 HORIZONTAL

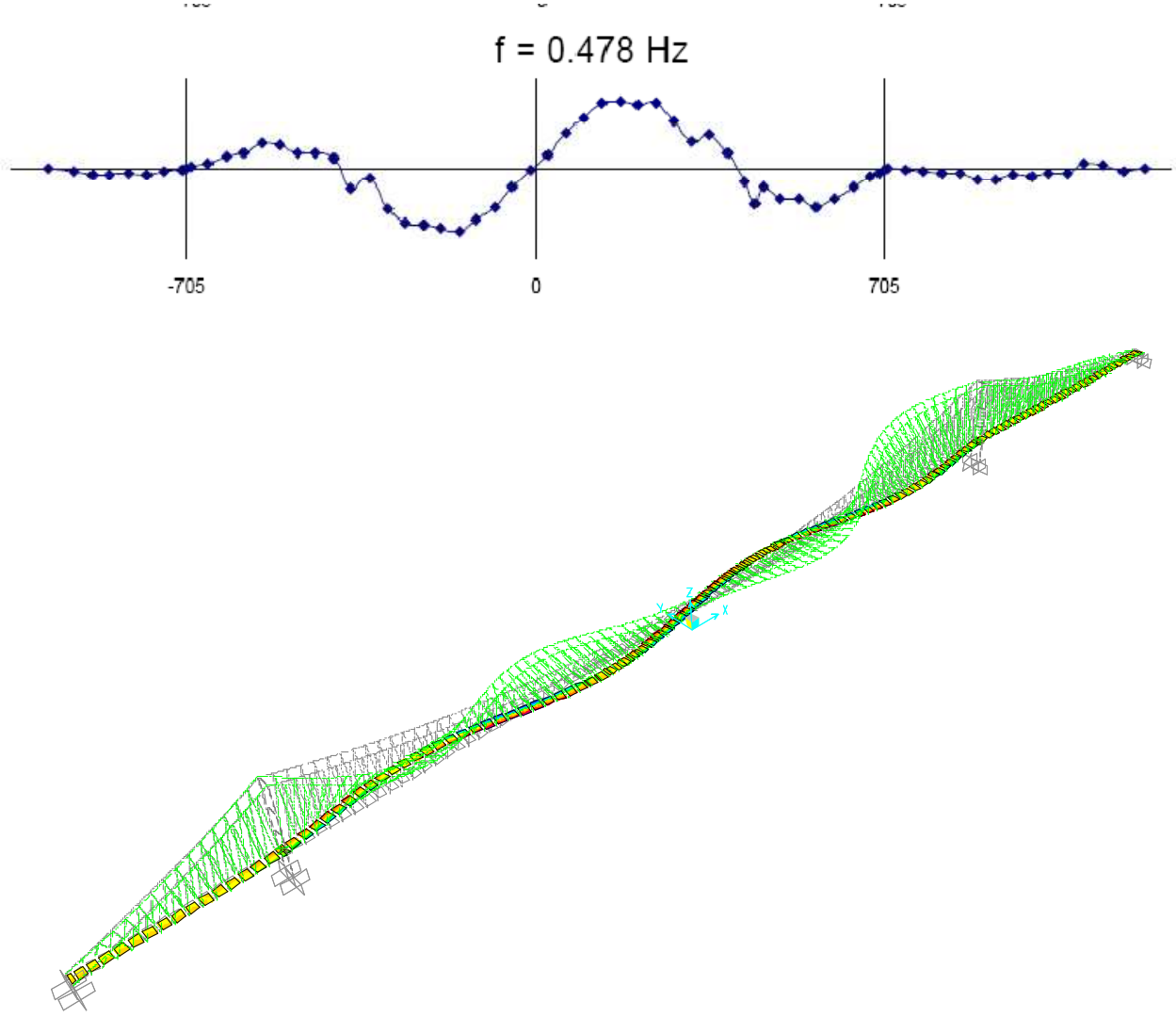

F = 0,49111 Hz

MODE 22 HORIZONTAL

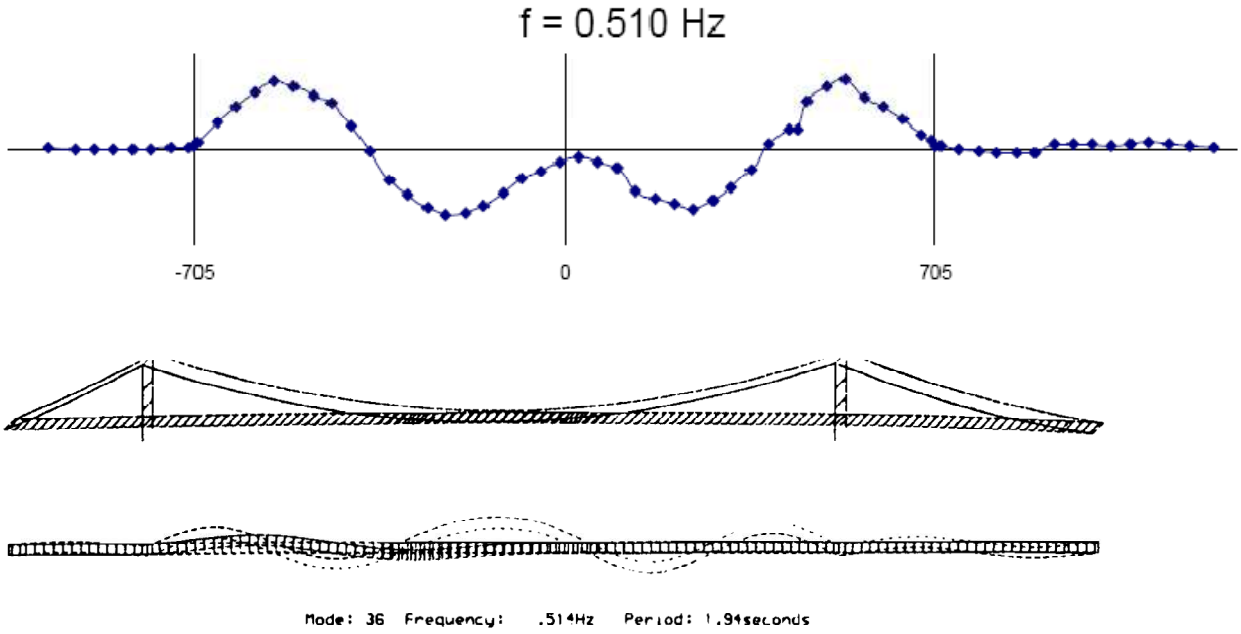

MODE 23 VERTICAL

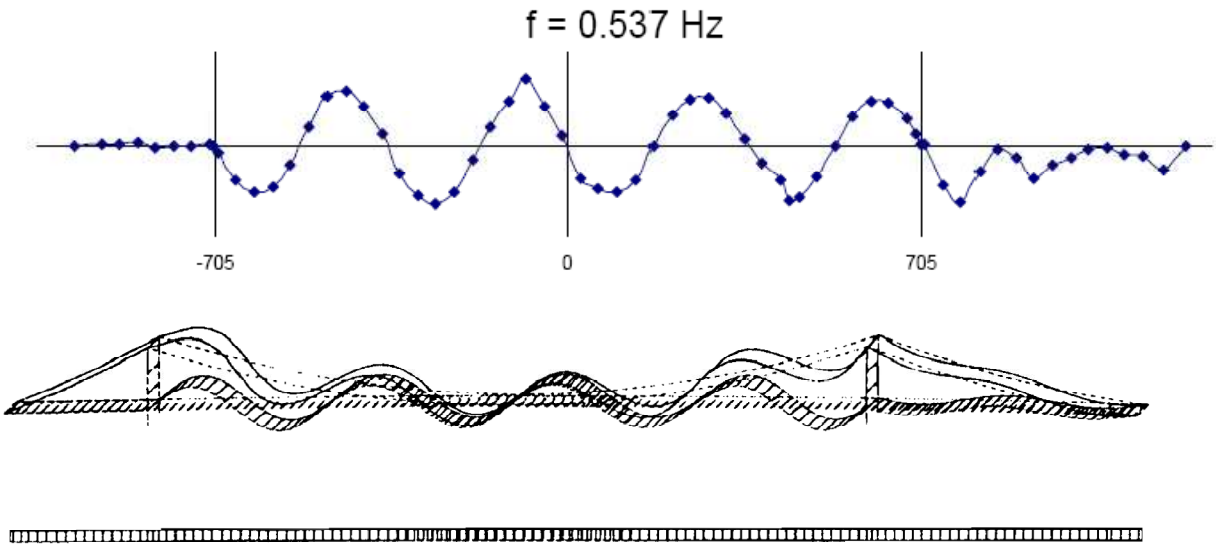

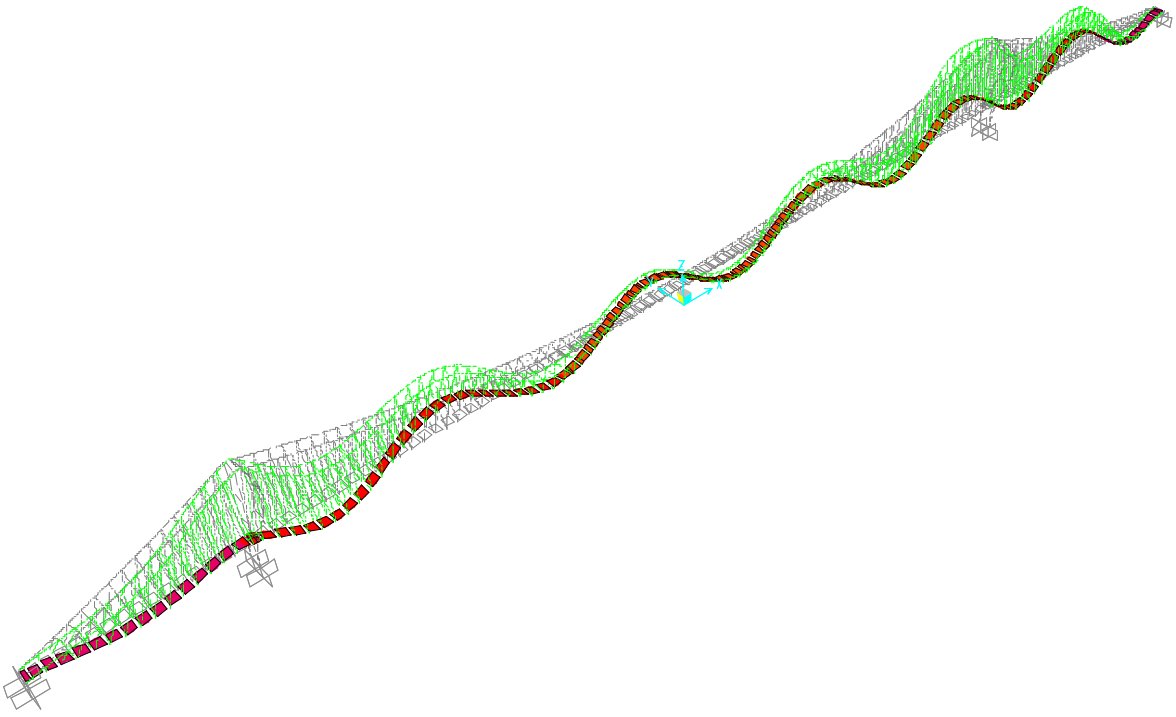

F = 0,50538 Hz

MODE 24 VERTICAL

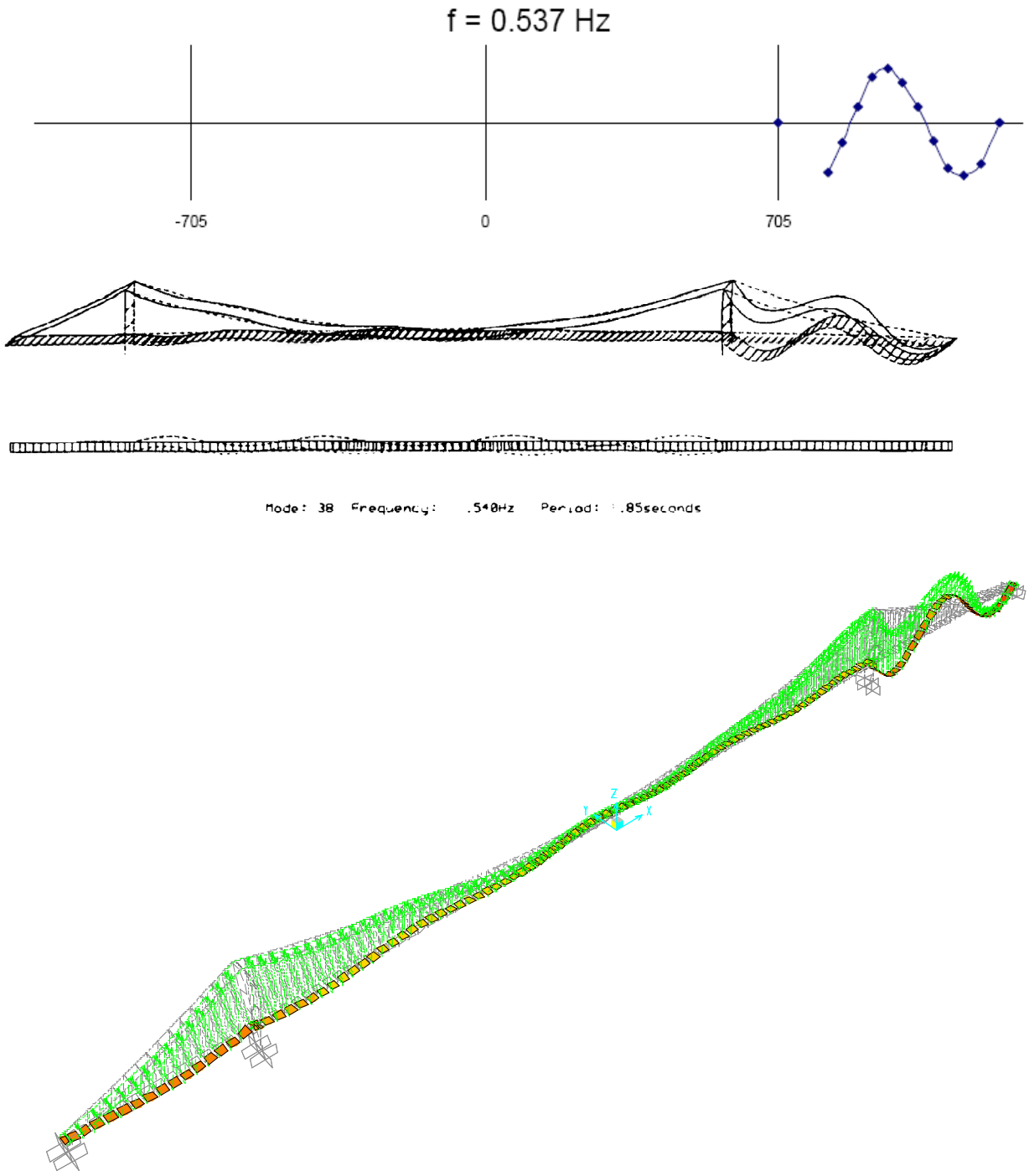

F = 0,55971Hz

MODE 25 HORIZONTAL

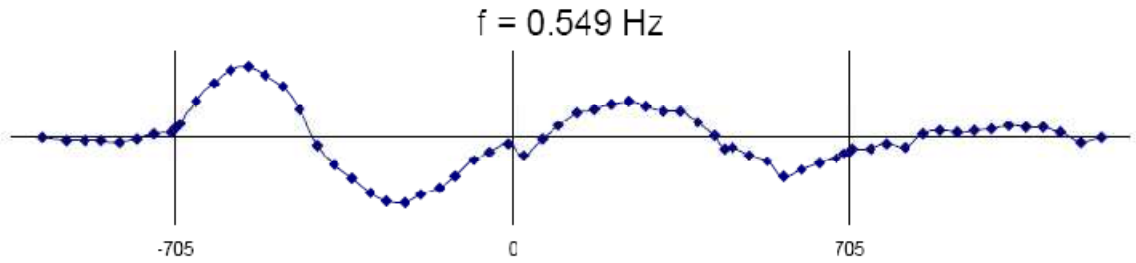

MODE 26 HORIZONTAL

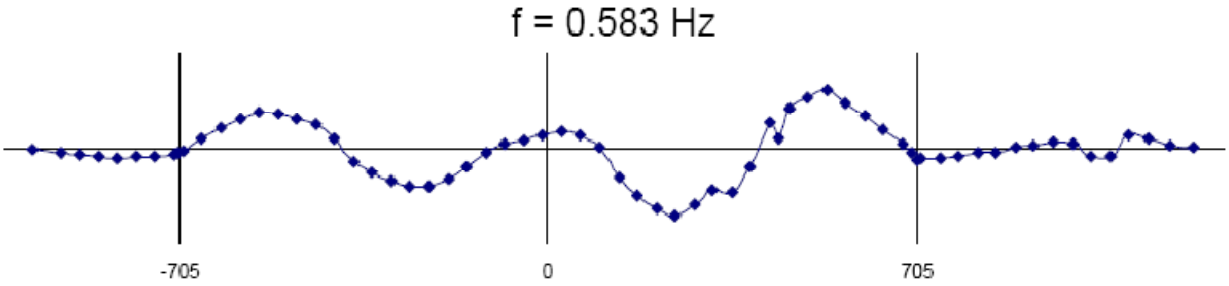

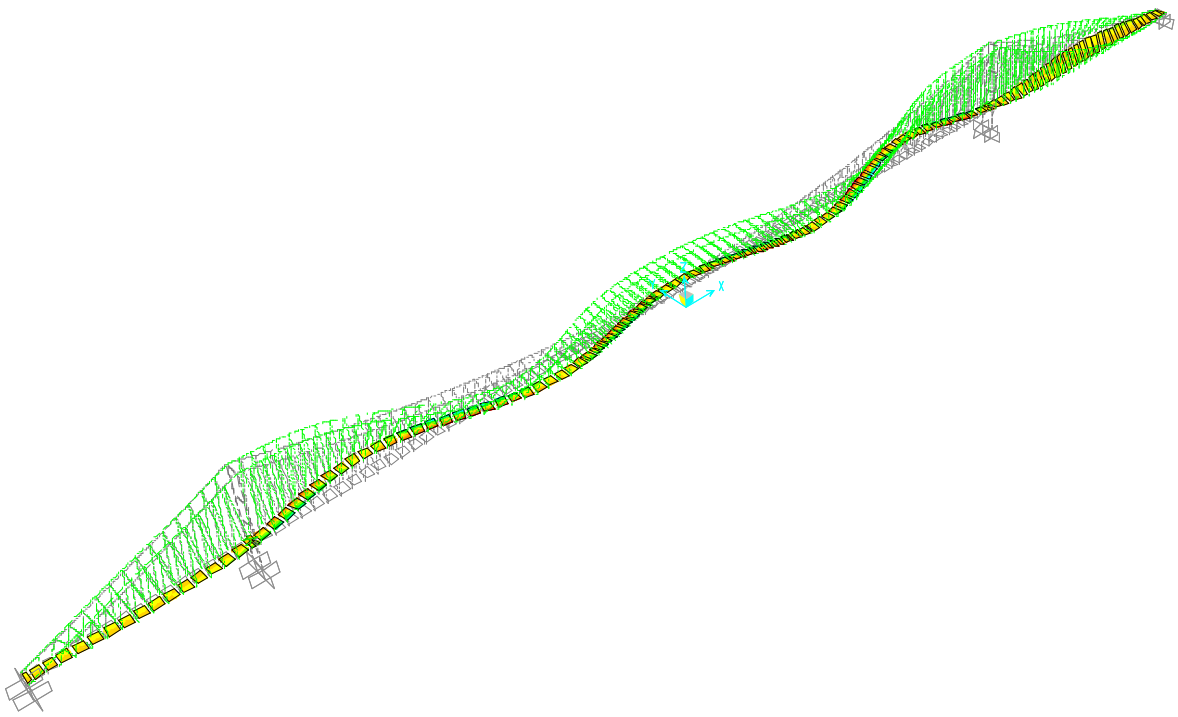

F = 0,54355 Hz

MODE 27 VERTICAL

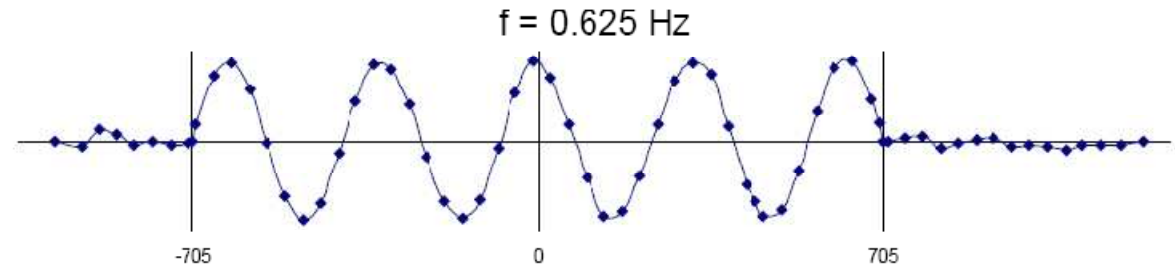

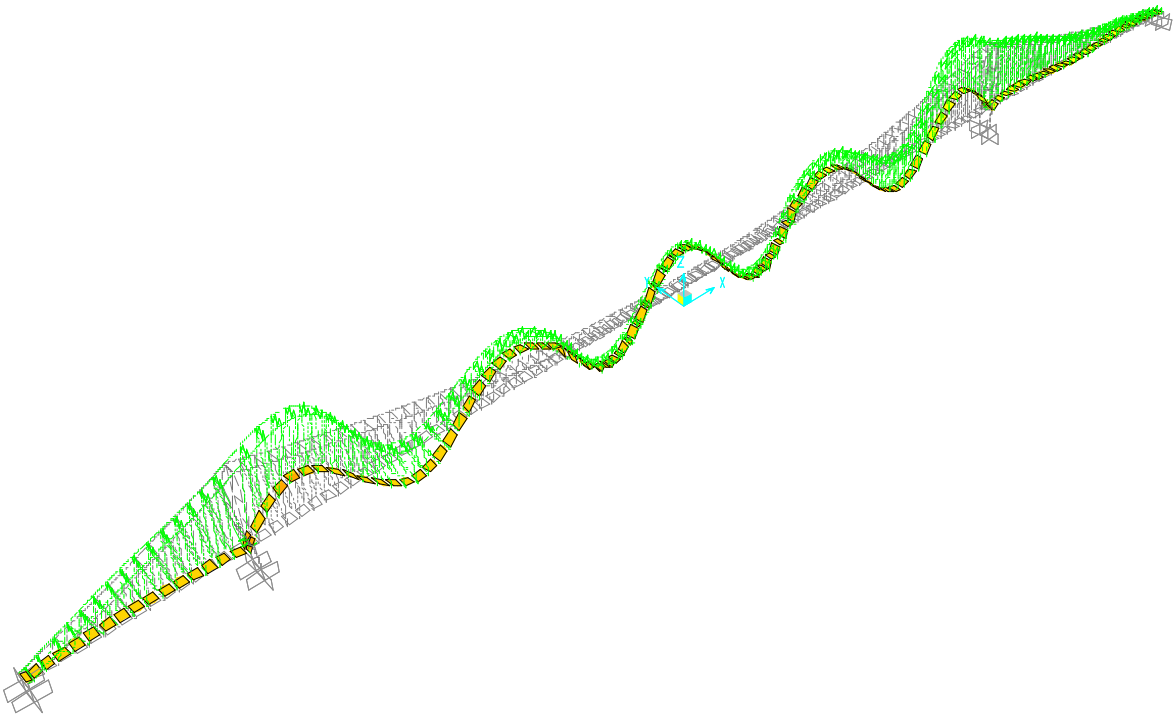

F = 0,60219 Hz

MODE 28 HORIZONTAL

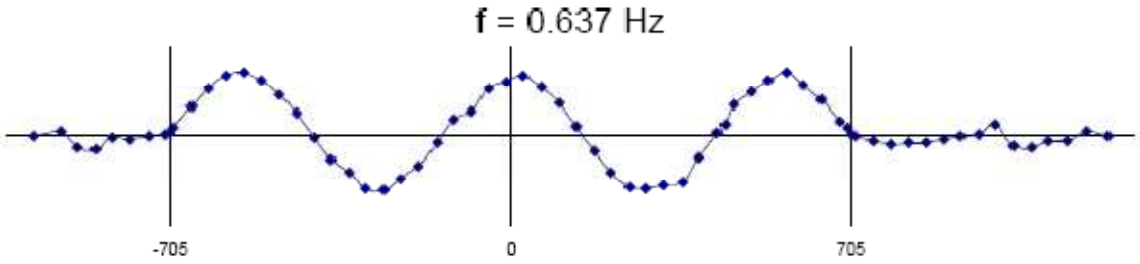

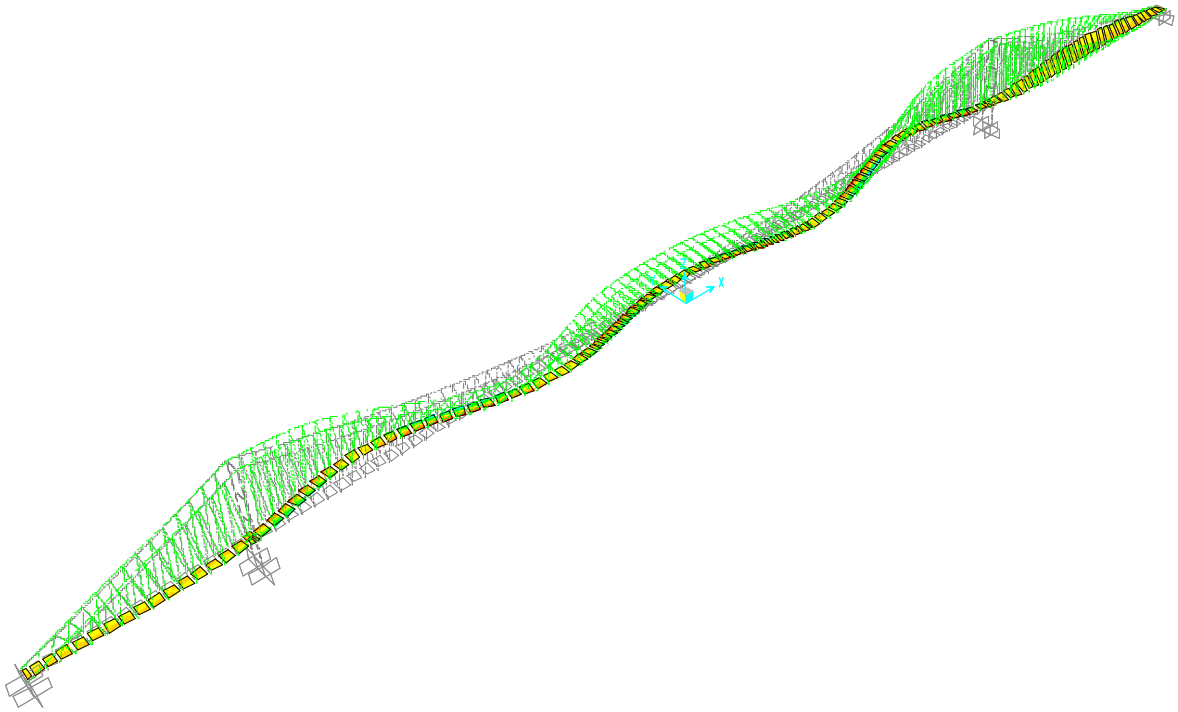

F = 0,63069 Hz

Torsional mode 1

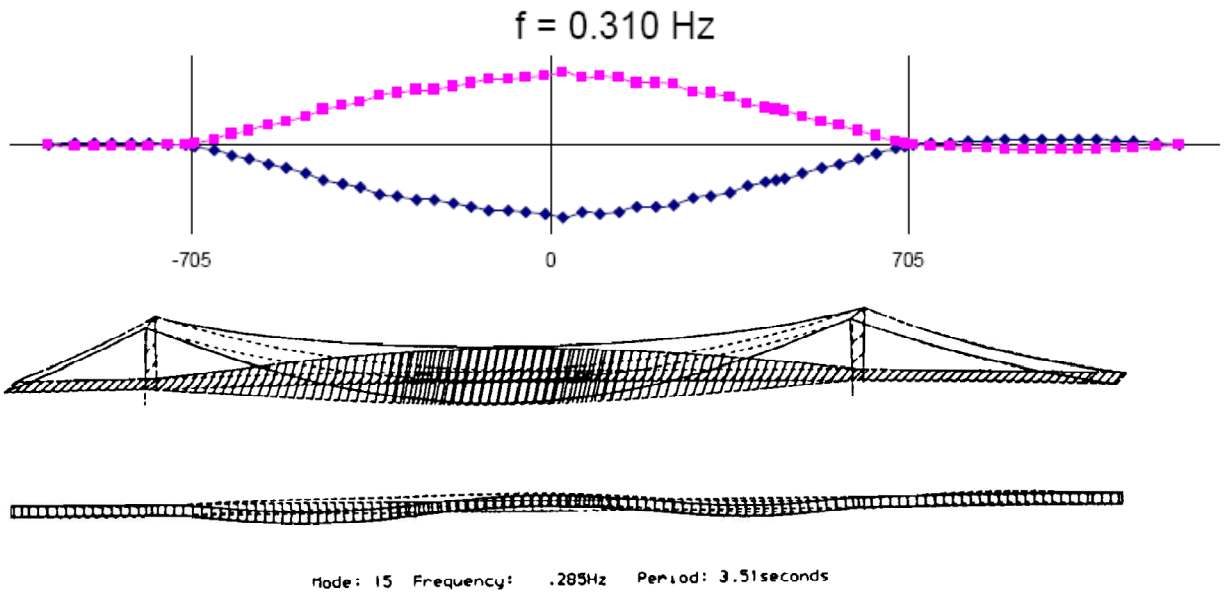

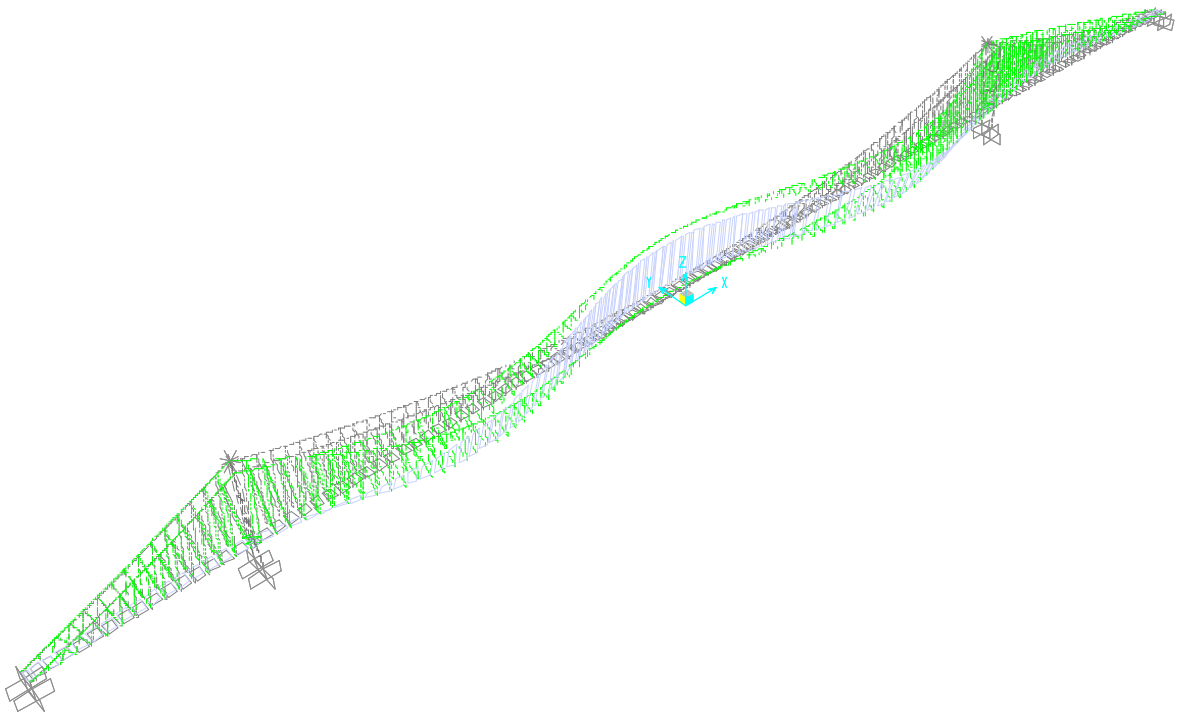

F = 0,3249 Hz

Torsional MODE 2

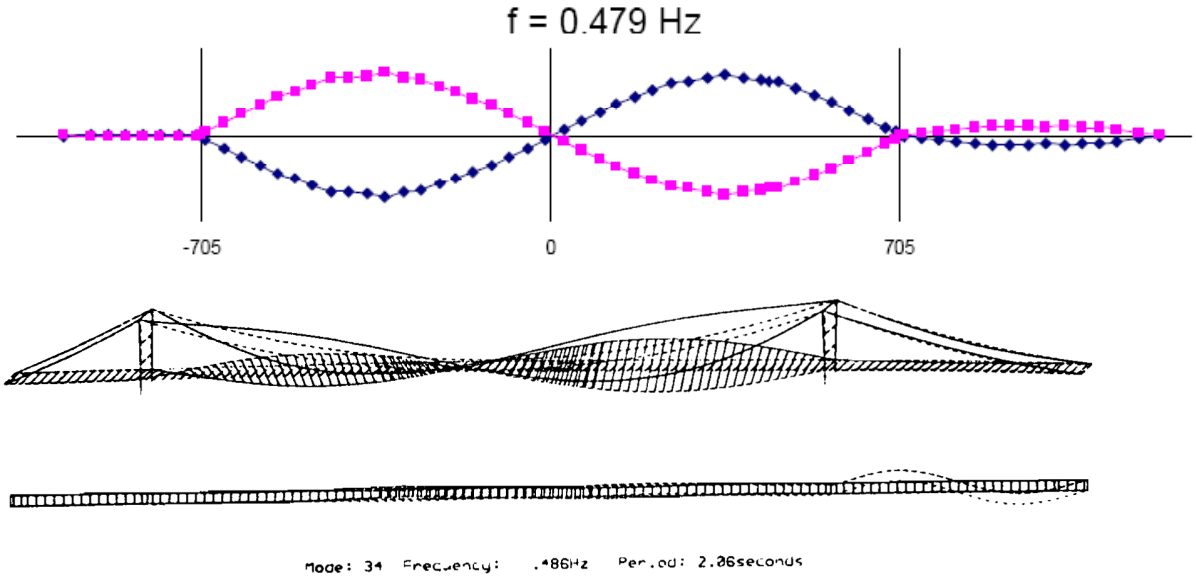

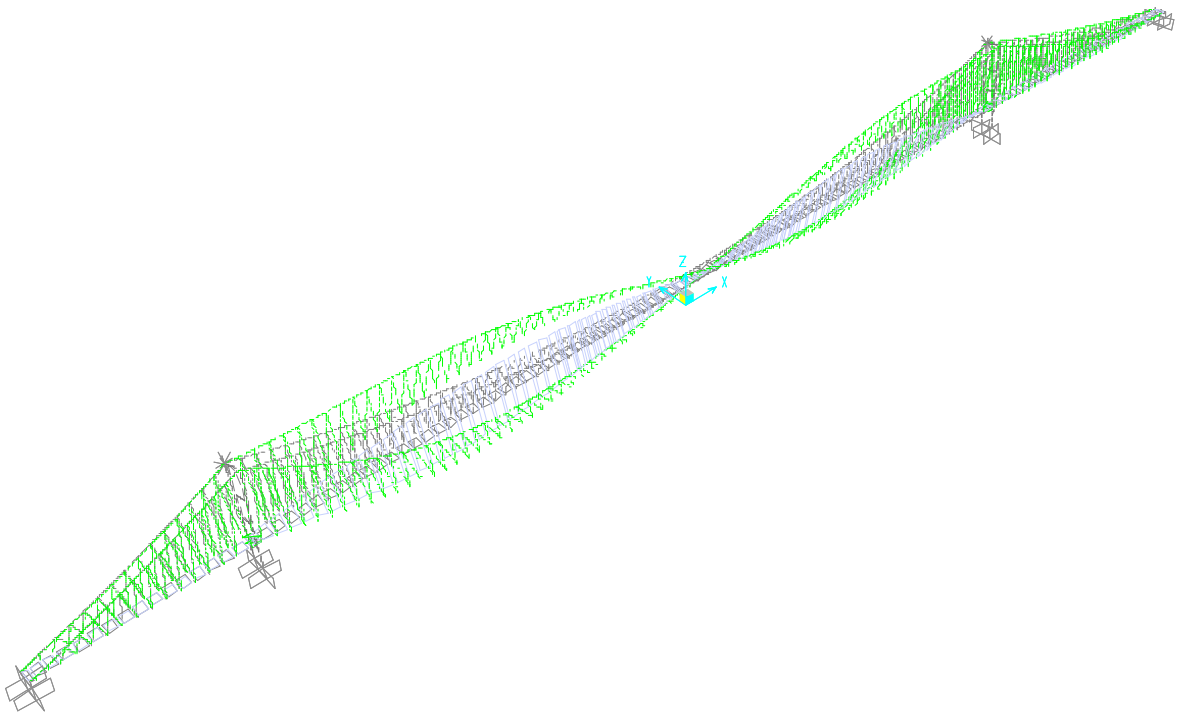

F = 0,4359 Hz

Torsional MODE 3

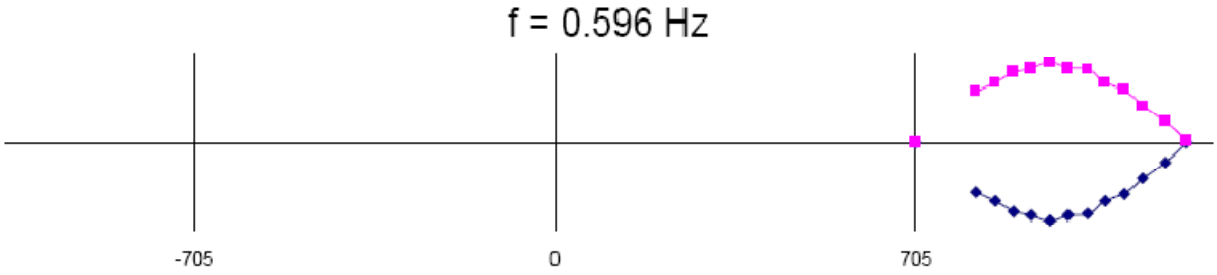

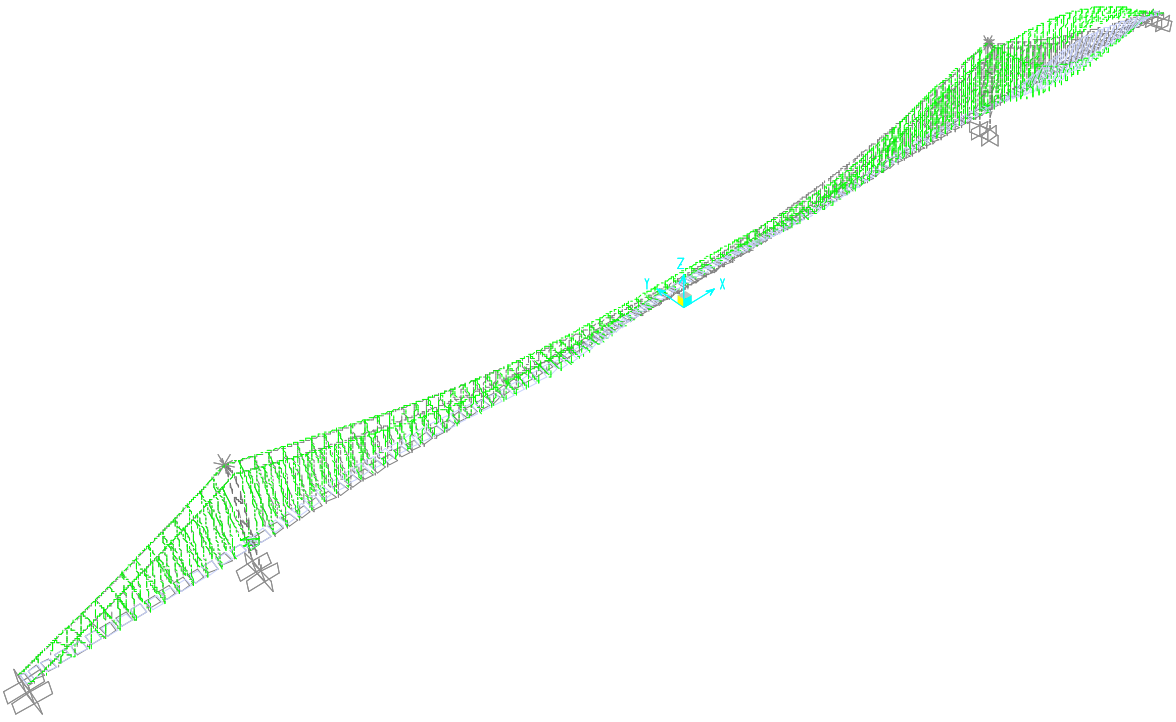

F = 0,5256 Hz

Torsional MODE 5

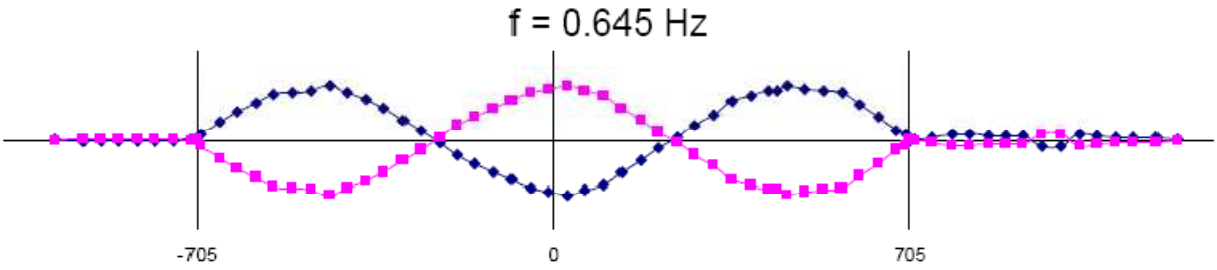

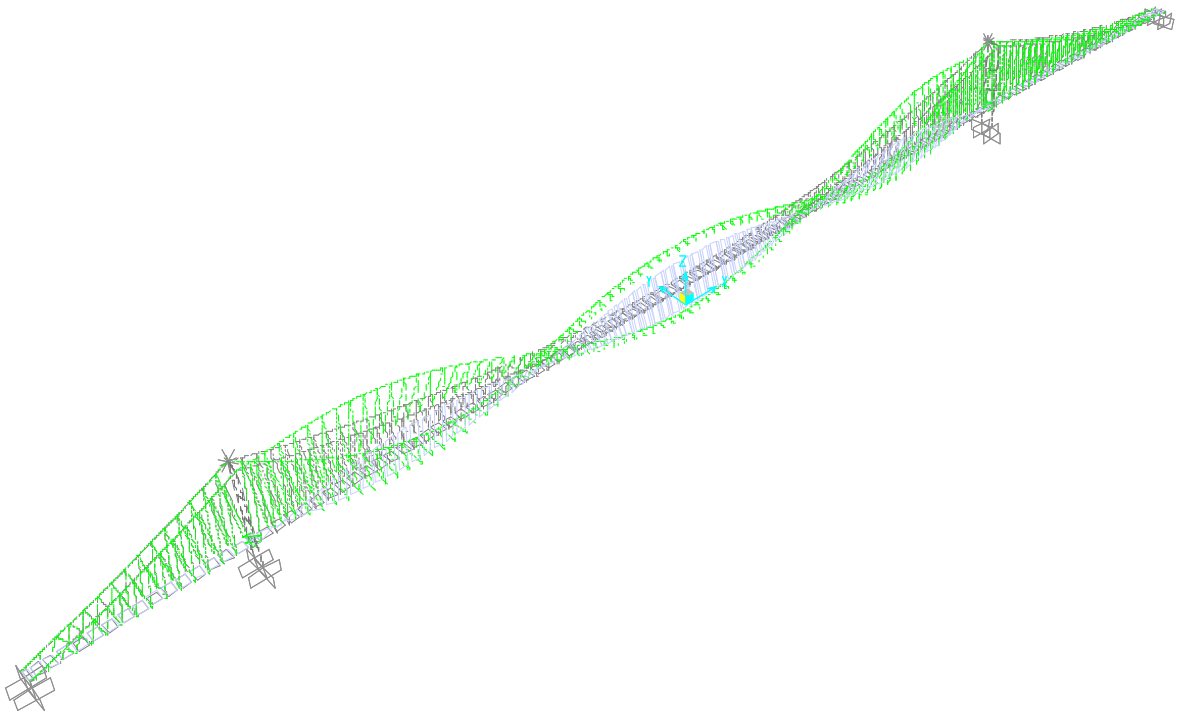

F = 0,5815 Hz

The model, presented in this chapter, is characterized by natural frequencies very proximal to that one obtained experimentally through the ambient test on it performed. In particular, the following table summarizes the comparison between

the frequency obtained by dynamic test in situ and the frequency obtained by the proposed model. For each one the error is computed.

Table 1 Natural frequencies: comparison between experimental and numerical results

Mode	Type of mode	Frequency model	Experimental frequency	Error
1	horizontal	0,06199	0,056	9,66
2	vertical	0,11485	0,115	0,13
3	horizontal	0,14	0,132	5,71
4	vertical	0,15047	0,156	3,68
5	vertical	0,17476	0,176	0,71
6	vertical	0,21525	0,217	0,81
7	vertical	0,23235	0,239	2,86
8	horizontal	0,23711	0,239	0,80
9	horizontal	0,25586	0,269	5,14
10	vertical	0,29894	0,308	3,03
11	horizontal	0,30261	0,31	2,44
12	torsional	0,3249	0,31	4,57
13	vertical	0,3428	0,317	7,53
14	vertical	0,34924	0,332	4,94
15	horizontal	0,36746	0,378	2,87
16	vertical	0,37064	0,383	3,33

17	horizontal	-	0,4	-
18	horizontal	0,38796	0,41	5,68
19	vertical	0,44191	0,461	4,32
20	horizontal	0,45821	0,469	2,35
21	horizontal	-	0,469	-
22	horizontal	0,49111	0,478	2,67
23	torsional	0,4359	0,479	9,89
24	horizontal	-	0,51	-
25	vertical	0,50538	0,537	6,26
26	vertical	0,555971	0,537	3,41
27	horizontal	-	0,549	-
28	horizontal	0,54355	0,583	7,26
29	torsional	0,5256	0,596	13,39
30	vertical	0,60219	0,625	3,79
31	horizontal	0,63069	0,637	1,00

The table 2 shows that good results are obtained for high modes too. The mean error is about 4%, and it is maximum for the 29th torsional mode. An error of about 10% occurs for the first horizontal mode, but the first model confirms this result. Some horizontal modes are not present in the model, but they are high modes, difficult to define. A good agreement is in general obtained in term of frequencies and mode shapes.

The figures below shows some of the local mode obtained through the implemented model

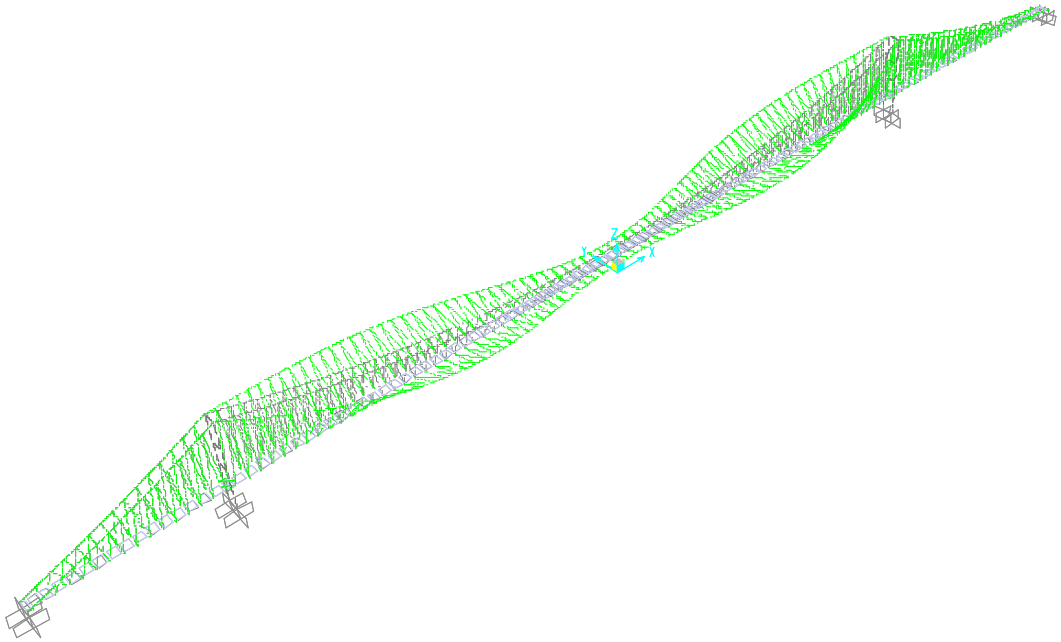

Figure 5.5.1 Local mode at frequency 0,306 Hz

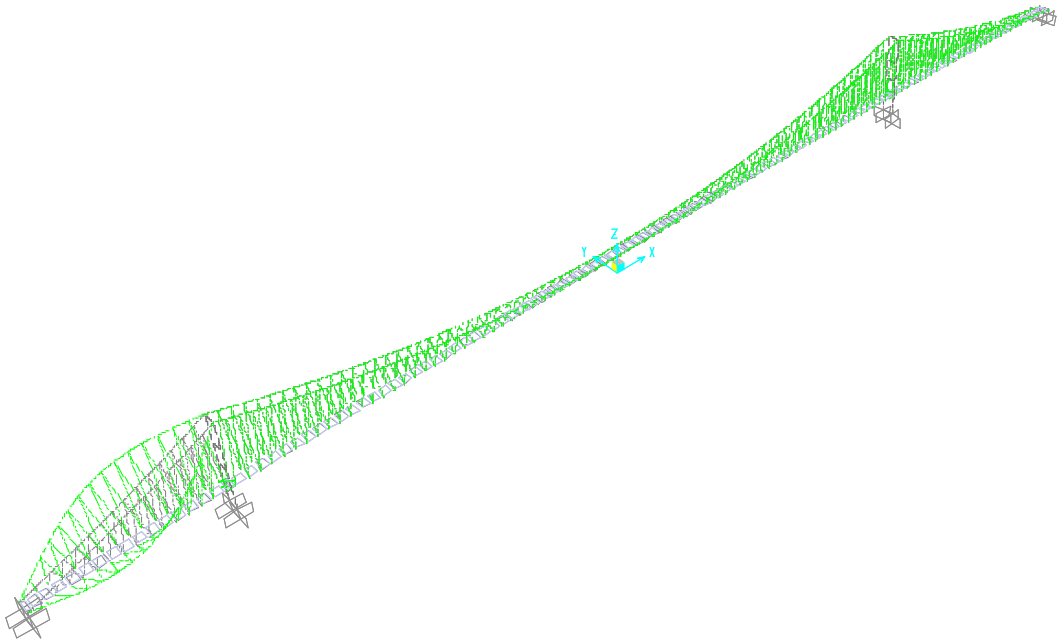

Figure 5.5.2 Local mode at frequency 0,435 Hz

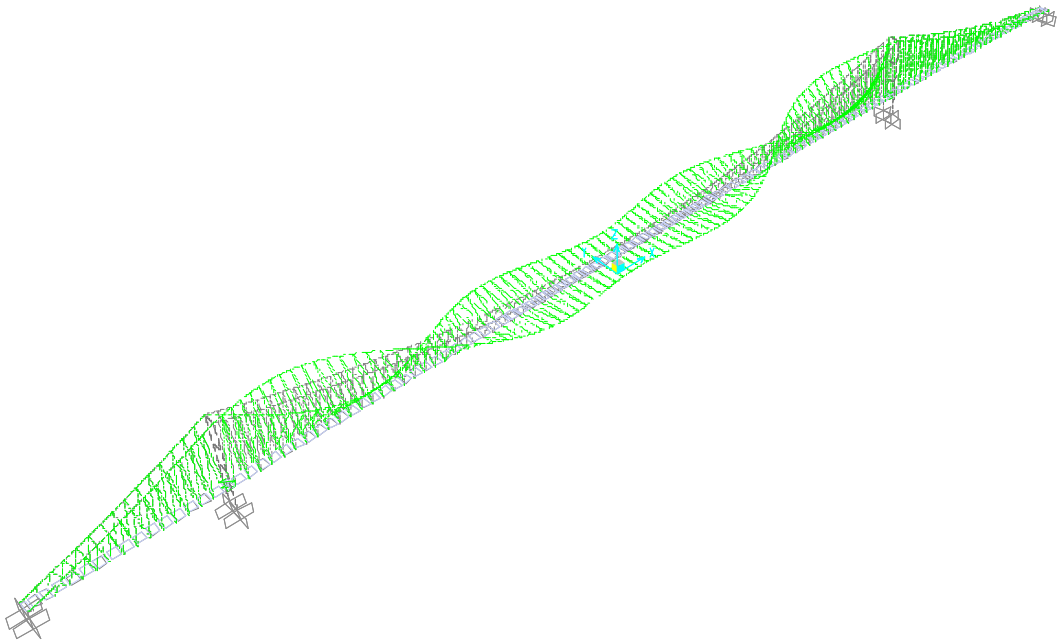

Figure 5.5.3 Local mode at frequency 0,436 Hz

The presence of local mode, where only the cables are involved, cannot be in anyway identified through a dynamic test. The numerical model, constructed on real data collected by an experimental test, is able to define all the structural behavior and this is the principal reason of this kind of study. We would like to underline how an easy model is able to check the experimental natural frequencies but it able to define local modes at the same time. The proposed model is until now object of some improvements, to obtain results more accurate. In particular, a more sophisticated model of the deck is in progress.

CHAPTER SIX

Concluding remarks

6.1. Overview

In this thesis the complex problem of the dynamic identification of an existent structure has been discussed. The goal of dynamic identification is the computation of the modal parameters of a system, i.e. natural frequencies, modal damping and mode shapes, through a post-processing of the signal acquired during a test in situ. The procedures applied to extract the modal parameters are various and they are different for the different way, used to excite the structure. In particular in the thesis three different dynamic tests have been considered: forced vibration tests in the first part and free and ambient test in the second part. The main difference between them is that in the first one it is possible to control the force applied to the system in the other one the excitation is unknown. Thus entails different kind of acquired signal: stationary in the first case, unstationary in the second case. The procedures applied in the two contests are methods in frequency domain (FRF through FTT and Lissajous Diagrams) and method in time-frequency domain (CWT and DWT), respectively.

The extracted modal parameters are important and efficient estimators of the dynamic behaviour of a structure. They can be used in different way, for example, if a dynamic test is performed on the same structure in different time of its life, the comparisons of the modal parameters can be an index of how the stiffness is changed during the time (see chapter 2). They can be used to update a FE model of the structure, due to remove some uncertainties, for example about the behaviour of material used (see chapter 2, uncertainty about Young module of laminated timber). In general the experimental modal parameters are used to obtain a FE model, able to reproduce the real dynamic behaviour of a complex structure. This aspect of the identification process is discussed in the last chapter, where an implemented 3-D model of a suspended bridge is implemented,

beginning from experimental data acquired during an ambient test carried out on it.

6.2. Principal results

6.1.1. Forced vibration test

The modal parameters of a laminated timber footbridge are obtained by the application of two methods, both in frequency domain and for forced vibration test. From what has been said, the FRF can be constructed through classical FFT or the geometric characteristics of an ellipse and the same results can be reached. The proposed method allows on the one hand the construction point by point of the FRF, by which the modal parameters can be extracted through PP method or circle-fit; on the other hand it is a way to define the correlation between the signal that excites the structure and the response acquired as its acceleration. In particular, the ellipse construction can be a good way to test, from the direct comparison between input-output signals, to test the goodness of the signal recorded during the dynamic test. In general, a high dispersion of the points around the ellipse that better approaches them means that the response of the system is not coherent with the force, which excites the structure. Thus is very evident for the low frequency, where the sinusoidal force is so low that it not able to excites strongly the structure. Often in this case we have very bad recorded signal and the constructed FRF could not detect by its peaks the real resonances. The goal is to define which is the natural frequency without considering another kind of test, using only the data collected during the forced vibration test. To understand which frequency between them can be the real natural frequency of the system, the correlation between the structure reply registered in correspondence of each accelerometer and the perfectly sinusoidal force applied by the vibrodyna can be observed for both the tests. The assumption is that, for the real resonance frequency, the structure reply will be almost sinusoidal and will be greater than the applied force.

Then, this correlation can be computed for each accelerometer using the r^2 correlation index. In particular, the computation of r^2 defines the distance between the points, relating to the real case, and the ellipse that better approaches their distribution (the best fit is obtained through the minimum least squares method).

Of course, the r^2 index varies more as the structure reply becomes less sinusoidal (the distance of the points, which directly represent the comparison input-output, from the LS ellipse increases as the structure reply becomes less sinusoidal). If the signal input and the signal output are two sinusoids, the points describe a perfect ellipse and $r^2 = 1$. Then in the real case the maximum r^2 defines the most probable natural frequency, detected through the FRF.

6.1.2. Free and ambient vibration test

The unstationary signals, acquired during an impact test or an ambient vibration test, cannot be analysed through the methods proposed in chapter two, because they work only if the force, that excites the structure is known. In this contest a method, able to investigate the time behaviour of the signal, is necessary. The aim of the second part of the thesis is the application of the CWT due to define the modal parameters of a structure, when the force is in general unknown. The validation of this procedure is obtained through the comparisons between the results obtained by classical methods, like PP or FDD, and the results obtained through CWT.

The comparison between the modal parameters extracted by Peak-Picking method and Wavelet Transforms shows in general a good agreement both in ambient and impact tests. In the free vibration test on the Vasco da Gama Bridge the modal parameters are very similar, only the modal damping at frequency 0.591 Hz is different and a possible interpretation of this important variation is the presence of very close torsional mode around that frequency and the interaction of local cable modes. The CWT defines good results in the definition of mode shapes.

In the ambient vibration test the procedure is able to define easily and accurately the natural frequencies of the system, some difficulties occur in the computation of the modal damping. The signal acquired during an ambient test is constituted by different track, for example corresponding to the crossing of various vehicles. Each track is characterized by different time trend and then by different modal damping. In chapter three a correlation between the amplitude of the track and the value of the modal damping is defined. In particular, as expected, the modal damping increases when the amplitude of the track increases. The identification of the modal damping through the WT is obtained considering always the trend in the time domain of the acquired signal in correspondence of its maximum amplitude. This choice is made from the comparison of the modal dampings to the dampings obtained by EFDD. Similar mode shapes are also obtained, sometimes there is only an inversion of the sign of the vibration mode.

To minimize the computational time of the procedure in chapter four the Discrete Wavelet Transform was applied. The results were not so accurate, as that one obtained by CWT, for each modal parameters. The conclusion is that, when the signal analysed is acquired during an ambient test, then the sample time it is not so long, the CWT is computationally efficient and the results are very accurate. If the signal is acquired during a monitoring of a generic structure, then the sample points of the acquired signal are a lot, the algorithm is not even efficient and it is necessary to apply the DWT. Then, in the contest of modal parameters extraction the CWT is the best way.

The DWT is a very interesting and efficient way to filter a noisy signal. The procedure, easy to implement and very flexible, was applied to the signal acquired during an ambient test on a very stiff bridge, characterized by the presence of a lot of noise. The algorithm works well and good results are obtained.

6.1.3. Model updating

In the last chapter another important aspect of the experimental modal analysis, the model updating, is discussed. In order to obtain a FE model, able to define the real behaviour of a complex structure, a dynamic test is performed on the building, object of study. The experimental modal parameters are then extracted and a FE model, characterized by very similar modal parameters, is after implement. This procedure is often applied for very complex structures, the experimental survey is necessary to check if the numerical model of the system works and it is able to describe how dynamically the realized structure behaves. The model updating is applied on the Humber Bridge, characterized by a span of 1.4 Km. The goal of the model is the possibility to find the local modes, where only the cables are involved.

The first finite element model of the Humber Bridge was realized in 1981, when the bridge was ended (in 1985), by Prof Brownjonh, of the University of Bristol. The model was defined in order to obtain modal parameters similar to that one defined by an ambient vibration test, carried out on the bridge when it was opened. The main objective of the test was to check the accuracy of the mathematical model developed for asynchronous excitation analyses

Starting from the John Brownjonh's model defined in 1985, the goal of this chapter is an improving of the original model in order to obtain the natural frequencies, extracted through the ambient vibration test carried out on the Humber Bridge in 2008 by the University of Porto, previously described.

The model implemented is very easy, it is in fact characterized by frame element for all the towers; shell for the deck and cable for all the cables present. The attach of the deck to the tower is modeled by two rigid links, which permit only longitudinal movement and rotation around lateral and vertical axes. The model reproduces almost the same natural frequencies obtained by the post-processing of the data collected during the ambient test. The trend of the mode shape is almost

the same also. Then, the implemented model is able to describe the dynamic behavior of the real structure.

This model detects some local modes, which cannot be in anyway identified through a dynamic test. This is the principal futures of the numerical model, because the interaction cable-structure, critical point in the study of a suspended bridge, cannot study easily experimentally. The model, if well constructed, can give some important information about the cable behavior, missed in the experimental survey.

6.3. Limitations and future works

The research presented in this thesis has tried to describe the dynamic identification problem in all its various aspects. The first part is focused on the modal parameters extraction from a forced vibration test. In this context a different method in frequency domain has been applied. The goal of the method is the possibility to define a correlation between the known force and the recorded response of the structure. In fact, the idea comes from a particular situation, occurred during the processing of some data acquired from a forced vibration test. As it was explained in chapter two, an FRF characterized by two very proximal peaks in correspondence of the first natural frequency was obtained. It was necessary to define a methodology able to predict which one is the more probable resonance. Of course, only a specific case was analyzed; to ensure that the procedures work, it is necessary to apply it to more tests.

The third chapter is focused on the processing of signals acquired during ambient or free vibration test. The application of the CWT is proposed, and it is shown that it works well in both the case. Some special considerations are necessary, when an ambient test is considered to obtain good results in terms of modal damping and mode shapes. The procedure is based on the application of the Morlet as mother wave, the limit of the CWT is that the results can be influenced by the choice of the mother. A possible improvement of the

methodology can be a studied choice of the wave aimed to obtain better results, or an investigation to understand how the mother wave influences the computed CWT. A limit of the CWT is the computational time, which tends to increases when a good time-frequency resolution would be reached. For this reason it cannot be an efficient way to process data collected from direct monitoring of structure, because the length of the signal makes the computational time too much long.

For this reason in the chapter four a procedure based on the application of DWT was applied. It was shown that the approximation caused by the discretization entails not accurate results, when a short time signal is analyzed, like that one acquired during a dynamic test. A possible development can be the application of the DWT on signals acquired during a structural monitoring, where its short computational time can be an important feature.

The last chapter concerns the model updating, starting from an experimental survey, development by the staff of ViBest, University of Porto. The FE model of the Humber bridge is a work in progress. Until now a very easy 3D-model has been implemented, to check the presence of some local modes, unavailable by a dynamic test in situ. The FE model, although it has reached good results in terms of natural frequencies, needs of various improvements. For example, the deck is modeled as a simple 4-points shell element; another model, where the real trapezoidal shape is modeled, is under study. The attach deck-towers, modeled by two rigid links, can be too object of deeper investigation.

REFERENCES

Abdel-Ghaffar, A.M. 1978. Vibration Studies and Tests of a Suspension Bridge, *Earthquake Engineering and Structural Dynamics*, Vol.6, p.473-496.

Abdel-Ghaffar, A. M. & Khalifa, M. A. 1991. Importance of Cable Vibration in Dynamics of CableStayed Bridges. *Journal of Engineering Mechanics, Vol.* 117, *No.* 11: 2571-2589. ASCE.

Ali, H. 1991. Nonlinear Seismic Analysis of Cable-Stayed Bridges With Passive Energy Dissipation Devices. *Ph.D. Thesis, University of Southern California. USA.*

Alvin, K. F., Robertson, A. N., Reich, G. W. & Park, K. C. 2003. Structural system identification:Fromreality tomodels, *Computers and Structures*, vol. 81(12), pp. 1149–76.

Andersen, P. 1997. Identification of civil engineering structures using ARMA models, *PhD. Thesis*, Department of Building Technology and Structural Engineering, Aalborg University, Denmark.

Asmussen, J.C. 1997. Modal Analysis based on the Random Decrement Technique. Application to Civil Engineering Structures, *Ph.D. Thesis, Univ. Aalborg.*

Balmes, E. 1997. New results on the identification of normal modes from experimental complex modes. *Mechanical Systems and Signal Processing* Vol 11(2): pp. 229-243.

Bendat, J. S. & Piersol, A. G. 1980. Engineering Applications of Correlation and Spectral Analysis, *Wiley-I nterscience.*

Brincker, R., Krenk, S., Kirkegaard, P.H. & Rytter, A. 1992. Identification of the Dynamical Properties from Correlation Function Estimates, *Bygningsstatiske Meddelelser, Danish Society for Structural Science and Engineering*, Vol.63, N.1, p.1-38.

Brincker, R., Ventura, C. & Andersen, P. 2000. Damping Estimation by Frequency Domain Decomposition, *Proc. 19thInt. Modal Analysis Conference*, San Antonio, USA.

Brincker, R., Zhang, L. and Andersen, P. 2000. Modal identification from ambient responses using frequency domain decomposition, *Procceedings of IMAC-XVIII, International Modal Analysis Conference*, pp.625-630, San Antonio, Texas, USA.

Brincker, R., Zhang, L. & Andersen, P. 2001. Modal Identification from Ambient Responses using Frequency Domain Decomposition, *Proc. 18thInt. Modal Analysis Conference*, Kissimmee, USA.

Brownjohn, J. M. W., Dumanoglu A.A., Severn R.T. & Taylor C.A. 1986. Ambient vibration survey of the Humber Suspension Bridge. University of Bristol, Department of Civil Engineering, *Research Report* UBCE EE-86-2.

Brownjohn, J. M. W., Dumanoglu A.A., Severn R.T. & Taylor C.A. 1987. Ambient vibration measurements of the Humber Suspension Bridge and comparison with calculated characteristics, *Proc. Instn Civ. Engrs,* Part 2, vol. 83, pp. 561-600.

Caetano, E. (2000). Dynamics of cable-stayed bridge: experimental assessment of cable-structure interaction, *PhD thesis*, University of Porto.

Causevic, M. S. & Sreckovic, G. 1987. Modelling of Cable-Stayed Bridge Cables: Effects on Bridge Vibrations. In W. Kanok-Nukulchai (ed), *Cable-Stayed Bridges: Experience & Practice, Vol.* 1: 407-420. AlT.

Chopra A. 1995. Dynamic of structures: Theory and application to Earthquake Engineering, *Prentice Hall.*

Clough W, Penzien J. 1993. Dynamic of structures, *Mc Graw Hill.*

Cooley J. & Tuckey J. 1965. An Algorithm for the Machine Calculation of Complex Fourier Series.

Corrêa, M.R. & Campos Costa, A. 1992. Ensaios Dinâmicos da Ponte sobre o Rio Arade, in Pontes Atirantadas do Guadiana e do Arade (in Portuguese), ed. by LNEC.

Crawford, R. & Ward, H.S. 1964. Determination of the Natural Period of Buildings, *Bulletin of the Seismological Society of America*, Vol.54, No.6, p.1743-1756.

Cunha, Á., Caetano, E., & Delgado, R., 2001. Dynamic Tests on a Large Cable-Stayed Bridge. An Efficient Approach, *Journal of Bridge Engineering*, ASCE, Vol. 6, No.1, pp.54-62, 2001.

Cunha, A., Caetano, E., Brincker, R. & Andersen, P. 2004. Identification from the Natural Response of Vasco da Gama Bridge, *Proc. 22nd Int. Modal Analysis*

Daubechies, I. 1990. The wavelet transform time-frequency localization and signal analysis, *IEEE Trans. Inform. Theory*, vol 36, pp. 961–1004.

Daubechies, I., Mallat, S., and Wi II sky, A. S.. 1992. Wavelet transforms and multiresolution signal analysis-special issue. *IEEE Trans. Information Theory*, vol. 38(2).

Daubechies, I., 1993, Ten lectures on Wavelet, SIAM

Diotallevi, P. P., Paladin, A., Tralli, A. and Tullini, N. 1999 Identificazione strutturale di un edificio di muratura sottoposto a prove di vibrazione forzata, *IX Convegno Nazionale "L'ingegneria sismica in Italia"*, Torino, 1999, on CD.

Diotallevi, P.P., Manfroni, O. and Tullini, N. 2000. On site dynamic test of a long span timber footbridge, *Footbridge 2000,* Paris.

Donoho, D. L. 1993. Nonlinear Wavelet Methods for Recovery of Signals, Densities, and Spectra from Indirect and Noisy Data, *Different Perspectives on Wavelets, In Proceedings of Symposia in Applied Mathematics Daubechies, I., Ed.; American Mathematical Society: Providence, RI.* pp 173-205.

Ewins D.J. 2000. Modal Testing: Theory, practice and application, *Research Studies Press Ltd.*, Hertfordshire, England.

Felber, A. 1993. Development of a Hybrid Bridge Evaluation System, *Ph.D. Thesis, University of British Columbia* (UBC), Vancouver, Canada.

Friswell M. I. and Mottershead J. E. 1995. Finite Element Model Updating and Structural Dynamics, *Kluwer*, Dordrecht p. 158–282

Fujino, Y., Warnitchai, P. & Pacheco, B. 1993. An Experimental and Analytical Study of Autoparametric Resonance in a 3DOF Model of a Cable-Stayed-Beam. *Nonlinear Dynamics, No.4:* 111-138. Kluwer Academ ic Publishers.

Gambhir, M. & Batchelor, B. 1977. A Finite Element for 3D Prestressed Cablenets. *International Journal of Numerical Methods in Engineering, Vol.* 11: 1699-1718.

Gao, H. 1997. Threshold Selection, in WaveShrink, *SoftMath, Inc..*

Garibaldi, L., Marchesiello, S. & Bonisoli, E. 2003. Identification and up-dating over the Z24 benchmark, *Mechanical Systems and Signal Processing.* Vol 17(1), pp. 153-161.

Gimsing, N.J. 1983. Cable Supported Bridges: Concept and Design. *Wiley Interscience.*

Gimsing, N.J. 1991. Design of a Long-Span Cable-Supported Bridge across the Great Belt in Denmark- 25 years of Experience and Evolution. In M. Ito, Y. Fujino, T. Myiata & N. Narita (eds), *Cable-Stayed Bridges: Recent Developments and their Future:* 279-298. Elsevier.

Giordano, G. 1993. Tecnica delle Costruzioni in legno, *Hoepli*, Milan.

Gouttebroze S. and Lardies J. 2001. On using the wavelet transform in modal analysis, *Mechanics Research Communications* **28** (2001) (5), pp. 561–569

Heath, S., 2000. A new technique for identifying synchronous resonances using tip-timing, *Int. Gas Turbine and Aero Engine Congress and Exhibition*, Indianapolis, Indiana, ASME 99-GT-402

Huang C.S., Su W.C. 2007. Identification of modal parameters of a time invariant linear system by continuous wavelet transformation, *Mechanical Systems and Signal Processing*, 21 (4), pp. 1642-1664

Hubbard, B. B. 1998. The World According to Wavelets, 2nd ed. *A. K. Peters, Ltd*, Wellesley, MA.

Inman D.J. 1994. Engineering Vibration, *Prentice Hall.*

Jayaraman, H. & Knudson, W. 1981. A Curved Element for the Analysis of Cable Structures.

Johnstone, I. M.; Silverman, B. W. Wavelet Threshold Estimators for Data with Correlated Noise, Available at http://playfair.stanford.edu.

Kajita, T. & Cheung, Y. 1973. Finite Element Analysis of Cable-Stayed Bridges. *International Association of Bridge and Structural Engineering, Publication* 33 *II.*

Kanok-Nukulchai, W. & Hong, G. 1993. Nonlinear Modelling of Cable-Stayed Bridges. *Journal of Constructional Steel Research, Vol.* 26: 249-266. Elsevier.

Kanok-Nukulchai, W. , Yiu, P. & Brotton, D. 1992. Mathematical Modelling of Cable-Stayed Bridges. *Structural Engineering International, Vol.* 2: 108-113. IABSE.

Kennedy, C. & Pancu, C. 1947. Use of Vectors in Vibration Measurement and Analysis. Journal of the Aeronautical Sciences, Vol. 14, No. 11:603-625.

Klosterman, A. 1971. On the Experimental Determination and Use of Modal Representation of Dynamic Characteristics. Ph.D. Thesis, University of Cincinnati. USA.

Kovacs, I. 1982. *Zur Frage der Seilschwingungen und der Seildampfung. Die Bautechnik, October:* 325-332.

Lardies, J. & Gouttebroze, S. 2002. Identification of modal parameters using the wavelet transform, *International Journal of Mechanical Sciences* vol. 44, pp. 2263–2283

Leonhardt, F. & Zellner, W. 1970. Cable-Stayed Bridges- Report on Latest Developments.

Lin, T. Y. & Chow, P. 1991. Gibraltar Strait Crossing- A challenge to Bridge and Structural Engineers. *Structural Engineering International, Vol* 1 (2): 53-58. IABSE.

Link M. 1999. Updating of analytical models—review of numerical procedures and application aspects. *Proceedings of the Structural Dynamics Forum SD2000,* Los Alamos.

Lotfollahi-Yaghin M.A. and Hesari M.A., 2008. Using Wavelet Analysis in Crack Detection at the Arch Concrete Dam under Frequency Analysis with FEM, *World Applied Sciences Journal* 3 (4): pp. 691-704.

Maeda, Y., Maeda, K. & Fujiwara, K. 1983. System Damping Effect and its Application to Design of Cable-Stayed Bridge. *Technology reports of the Osaka University, Vol.* 33, *No.* 1699: 125- 135.

Magalhães, F., Caetano E. & Cunha, A. 2008, Ambient Vibration Test of the Humber Bridge, *Preliminary Report*, ViBest, University of Porto.

Magalhães, F., Costa, B., Cunha, A. & Caetano E. 2006. Experimental validation of the Finite Element Modelling of Pinhão Bridge, *III European Conference on Computational Mechanics Solids, Structures and Coupled Problems in Engineering*, Lisbon, Portugal.

Mathivat, J. 1994. Les ponts a cables. Des Origines a la Conqu8te des Grandes Portees, *Proc.*

MATLAB 2007, *Matlab Wavelet Toolbox User's Guide.*
http://www.mathworks.com.

Maya N.M.M. and Silva J.M.M. 1998. Theoretical and experimental modal analysis, *Research Studies Press Ltd.*, Hertfordshire, England.

Mazzotti C., Vincenzi L., Savoia M., e Poluzzi R., 2004. Identificazione di una struttura da ponte acciaio-calcestruzzo mediante prove di vibrazione forzata, *XI Convegno ANIDIS*, Genova, Italy.

Mc Lamore, V.R., Hart, G. & Stubbs, I.R. 1971, Ambient Vibration of Two Suspension Bridges, *Journal of the Structural Division*, ASCE, Vol.97, N.ST10, p.2567-2582.

Menn, C. 1998. Functional Shaping of Piers and Pylons. *Structural Engineering International, Vol. 8, no.* 4, *November:* 249-251. IABSE.

Meyer, Y. 1993. Wavelets: Algorithms and Applications, S.I.A.M.

Peeters, B., De Roeck, G., Caetano, E. & Cunha, A. (2002). Dynamic study of the Vasco da Gama Bridge, *International Conference on Noise and Vibration Engineering*, ISMA, Leuven, Belgium

Prevosto, M. 1982. Algorithmes d'Identification des Caractéristiques Vibratoires de Structures Mécaniques Complexes, *Ph.D. Thesis, Univ. de Rennes I*, France,

Rioul, O. & Vetterli, M. 1991. Wavelets and signal processing, *IEEE Signal Processing Magazine.*

Robertson, A.N., Park, K.C. & Alvin, K. F. 1998a. Extraction of impulse response data via wavelet transform for structural system identification, *Journal of Vibration and Acoustics*, Transactions of the ASME, vol. 120(1), pp. 252–60.

Robertson, A.N., Park, K.C. & Alvin, K. F. 1998b. Identification of structural dynamics models using wavelet-generated impulse response data, *Journal of Vibration and Acoustics*, Transactions of the ASME, vol. 120(1), pp. 261–6.

Ruzzene M., Fasana A., Garibaldi L., Piombo B. 1997. Natural frequencies and dampings identification using wavelet transform: application to real data, *Mechanichal and systems signal processing* Vol.11(2) pp.207-218

Saito, N. 1994. Simultaneous Noise Suppression and Signal Compression Using A Library of Orthonormal Bases and the Minimum Description Length Criterion, *WaVelets in Geophysics*, Academic Press: San Diego, CA, pp 299-324.

Schoenwald, D. A. 1993, System identification using a wavelet-based approach, in *Proceedings of the 32nd IEEE Conference on Decision and Control*, San Antonio, TX, pp. 3064–5.

Strang G. and Nguyen T. 1996. Wavelets and Filter Banks, *Wellesley-Cambridge Press*, Wellesley, MA 490 p.

Su H. and Chong, K. T. 2004. An Efficient Method for the Mass Unbalance Analysis of a Rotor System Using FFT and Lissajous Diagram, *International Conference of Control, Automation and Systems*, Bangkok, Thailand.

Su H., Huang L., Chong, K. T. 2005. A Real-Time DSP-Based Imbalance Analysis System for Rotating Machine with Vibration Signal, *Journal of Mechanical Science and Technology,* Vol 19, No. 6, pp. 1243-1252,

Tang, Y.Y., Wickerhauser, V., Yuen, P.C., Li C. 2001. Wavelet Analysis and Its Applications, *Proceedings of Second International Conference*, WAA 2001 Hong Kong, China.

Taylor, P. R. 1991. Precast and Composite Concrete Cable-Stayed Bridges. In M. Ito, Y. Fujino, T.

Trifunac, M.D. 1972. Comparison Between Ambient and Forced Vibration Experiments, *Earthquake Engineering and Structural Dynamics*, Vol.1, p.133-150.

Tuladhar, R., Dilger, W. & Elbadry, M. 1995. Influence of Cable Vibration on Seismic response of Cable-Stayed Bridges. *Canadian Journal of Civil Engineering, No.* 22: 1001-1020.

Walczak, B.; Massart, D. L. 1997. TRAC vol. 16, pp. 451-463.

RINGRAZIAMENTI

L'identificazione strutturale, e più in generale la dinamica delle strutture, è sicuramente un filone della ricerca tanto complesso quanto affascinante. Ringrazio innanzitutto il Prof. Pier Paolo Diotallevi, advisor di questa tesi, che per primo mi ha dato la possibilità e il privilegio di conoscere questo importante aspetto dell'ingegneria strutturale. Ha sempre saputo stimolare il mio interesse; il suo intuito e la sua preparazione sono stati fondamentali ed indispensabili negli inevitabili scogli che si incontrano mentre si fa un lavoro di ricerca.

Ringrazio la Prof. Elsa Caetano, co-advisor di questo lavoro, ed il Prof. Alvaro Cunha che mi hanno permesso di approfondire le conoscenze maturate nel campo. Sono state persone, oltre che altamente preparate, molto disponibili. Il loro incoraggiamento e la loro conoscenza hanno inciso in modo importante nella redazione di questo lavoro. Esprimo quindi tutta la mia gratitudine.

Un ringraziamento particolare va al Prof. Erasmo Viola, che mi ha sempre supportato e incoraggiato in questo percorso. Per primo mi ha appassionato al mondo della ricerca nel campo della meccanica della frattura, argomento diverso ma altrettanto affascinante. Egli ha saputo sempre, con le sue parole, infondere in me serenità e fiducia.

Ringrazio infine il Prof. Giovanni Ricci Bitti e il Prof. Luca Landi, che mi hanno sempre sostenuto ed aiutato in questo percorso.

Non posso dimenticare tutti i dottorandi e collaboratori di Tecnica delle Costruzioni che ho avuto il piacere di incontrare e conoscere in questi anni.

Il ringraziamento più sentito va alla mia famiglia, a mio padre che fin da piccola mi ha trasmesso la passione per la ricerca e che mi ha sempre fatto capire che la forza di volontà vale su tutto; a mia madre che invece mi ha lasciato conoscere la parte più emozionale ma non meno importante della vita; a nonna Pina, la mia seconda madre e nonna Giulia che non dimenticherò mai. Un grazie ancora più speciale va a mia sorella Irene, che in tutti questi anni è stato il mio costante

punto di riferimento, che mi ha bacchettato quando necessario e consolato quando ne avevo bisogno.

Un grazie a Ciccio che con la sua infinita pazienza e amore mi è sempre stato vicino, sebbene lontanissimo, in questo percorso.

Come non ringraziare Astra, che mi ha saputo donare in ogni momento e in ogni situazione la voglia di lottare per i propri obiettivi.

Grazie a Marcello e Claudietta, colleghi ma soprattutto amici sinceri e fidati che mi hanno regalato sicuramente i momenti più belli durante questo dottorato.

Grazie a Marta, alle nostre passeggiate la domenica pomeriggio a Porto e alle escursioni periodiche al Piolho, fondamentale presenza in una delle esperienze più importanti della mia vita.

A Nata e Stè, che anche dopo il percorso universitario, continuano a regalarmi la loro amicizia.

Grazie infine a Marika, che con il suo spirito e la sua ilarità, ridimensiona ogni problema in un attimo.